BIOCHEMICAL, BIOPHYSICAL, AND CELLULAR INVESTIGATIONS OF THE INTERACTIONS OF TRANSFERRIN RECEPTOR WITH TRANSFERRIN AND THE HEREDITARY HEMOCHROMATOSIS PROTEIN, HFE

Thesis by

Anthony Michael Giannetti

In Partial Fulfillment of the Requirements for the degree of

Doctor of Philosophy

CALIFORNIA INSTITUTE OF TECHNOLOGY

Pasadena, California

2004

(Submitted May 18, 2004)

ABSTRACT

Hereditary hemochromatosis (HH) is a prevalent genetic disorder that results in the daily excess absorption of dietary iron. If untreated this disease leads to systemic organ failure and death. HH is caused by mutations to the gene coding for a protein called HFE, a type I transmembrane glycoprotein with a demonstrated role in regulating cellular iron homeostasis. HFE binds to the cell-surface receptor transferrin receptor (TfR), a dimeric type II transmembrane glycoprotein responsible for iron uptake into most mammalian cell types. TfR binds iron-loaded transferrin (Fe-Tf) from the blood and transports it to acidic recycling endosomes where iron is released from Fe-Tf in a TfR-facilitated process. Iron-free transferrin (apo-Tf) remains bound to TfR and is recycled to the cell surface, where apo-Tf rapidly dissociates from TfR upon exposure to the basic pH of blood. HFE and Fe-Tf can bind simultaneously to TfR to form a ternary complex, but HFE binding to TfR lowers the apparent affinity of the Fe-Tf/TfR interaction. This reduction could result from direct competition between HFE and Fe-Tf for receptor binding sites, from negative cooperativity, or both. We sought to understand the mechanism of HFE, Fe-Tf, and apo-Tf binding by TfR to help define HFE's role in iron homeostasis. We determined the binding constants for HFE, Fe-Tf, and apo-Tf to an extensive set of site-directed TfR mutants and discovered that HFE and Tf bind to an overlapping site on TfR, indicating the two proteins compete with each other for receptor binding. The mutagenesis results also identified differences in the contact points between TfR and the two forms of Tf, Fe-Tf and apo-Tf. By combining the mutations that are required for apo-Tf, but not Fe-Tf, binding we find that a highly conserved hydrophobic patch on the TfR surface is required for the receptor-mediated stimulation of iron release

from Fe-Tf. From these data we propose a structure-based model for the mechanism of TfR-assisted iron release.

To explore the mechanism of the HFE-induced affinity reduction for Fe-Tf binding by TfR, we engineered a heterodimeric TfR (hdTfR) that contains mutations such that one TfR chain binds only HFE and the other binds only Fe-Tf. Competition binding experiments using hdTfR demonstrate that TfR does not exhibit cooperativity in heterotropic ligand binding, suggesting that some or all of HFE's effects on iron homeostasis result from competition with Fe-Tf for TfR binding. Using transfected cell lines we show that HFE is dependent on its interactions with TfR for transport to endosomal compartments and that competition with extracellular Fe-Tf can alter HFE trafficking patterns. These data suggest that HFE's role in iron homeostasis is as a sensor of body iron status.

ACKNOWELDGEMENTS

Graduate school has been a unique and wonderful experience. It wasn't easy and a lot of people have contributed to the quality of my life during the last six years. At the risk of this exceeding Renée Zellweger's Oscar acceptance speech. . .here we go:

Firstly, I'd like to acknowledge my thesis advisor, Pamela. From experimental design to coloring of figures, you set the standard of quality for everything at the highest level and accepted only the best. You also gave me the freedom to explore my wacky ideas (see Chapter 4) as well as my new found loves of figure design and animation. For all this I am thankful. Well, that and the trip to Australia for the BioIron 2001 meeting. . .that trip is one of the highlights of my life. I'd also like to thank Doug Rees, David Chan, and Rich Roberts, the members of the advisory committee. I appreciate all the input you've given me over the years.

I am especially indebted to my wonderful collaborators. Caroline Enns spent an enormous amount of time teaching me all things TfR during her sabbatical in our lab in the Spring of 2000. This coincided with my candidacy exams and she was instrumental in helping me prepare for them. Over the years she has answered countless e-mails and phone calls and I consider her both colleague and friend. Anne Brown-Mason has been a joy to work with and is always on the spot with 10-15 milligrams of whatever transferrin construct my heart desired. I've really enjoyed our collaborations and am thankful to you, and Peter Halbrooks, for supporting my wacky hypothesis and performing the iron release experiments.

My labmates, or Björkies as they're often called, have been a central part of my time in the lab. I thank Jose Lebrón for all his groundbreaking work on HFE and TfR. Everything was in place when I began my dissertation, which greatly enhanced my ability to get started. Melanie Bennett was my rotation advisor in the Björkman lab and was one of the best mentors I've ever had. She really took the time to teach me careful crystallography, critical data analysis, use of extra controls, and imparted to me some of her secrets of figure making. Anthony West has always been there for helpful discussion about biophysics, crystallography, and all things in general and I've always appreciated his insights. Ben Willcox and Chris O'Callghan, in addition to adding that certain British flair to the lab that I've missed since their departure, helped a lot in the early stages of my Biacore experience and spent hours discussing theory, design and analysis of biosensor data. Andy Herr was instrumental in teaching me rigorous data analysis and for spending hours pouring through Biacore data, and teaching me how to use the analytical ultracentrifuge. I can't believe how tolerant you were of all that a capella pop-music...what WAS I thinking! Zsuzsi, thanks for setting the standard of Photoshop projects so high. Silvia, thanks for being there and listening. Libby, I really appreciate all the help you gave me early on with molecular biology and construct design. Mindy, thanks for keeping me sane these last couple of years and always having a good story to share. I especially appreciate Noreen's work to produce the vast amount of HFE supernatants that I needed. Marta...you were always so wonderful and helpful with everything and I especially thank you for fulfilling all those last minute requests I had while finishing my thesis. Beth, you always have that big smile, even when we moved

across campus and it fell to you to organize everything. Thanks for always being cheerful and helpful through these years.

Life in the lab has been especially enhanced since the arrival of Devin "Kid-Fantastic" Tesar and Adrian Rice. Devin, when I first met you I thought, "Gee, the lab is about to change." Was I ever right! The humor, constant harassment, and sincere friendship have meant more than you'll know. And Adrian fit right in and helped create the most humorous research bay in history! (Yes Devin, I am given to hyperbole) Our friendship and verbal sparring sessions have meant so much through these last years. I want to thank Rich Olson for being the most easy-going person I have ever met. You are a great friend and thank you for routinely getting me out of lab for late night runs to the wine bar during the writing of the heterodimer paper and dissertation.

Of course, not all my time in grad school was spent in the lab (sorry Pamela). In the last couple of years I've been developing a yoga practice that has changed my life in so many ways. A number of the 'yoga people' have been a big part of my time in grad school. I especially want to thank my primary teachers, Tatiana Urquiza, who taught me how to breathe again, and Scott Lewicki for insisting I strive to go further than I thought I could. You both let me hang out in your classes even when I wasn't ready for them and encouraged me to grow, and for that I'm grateful. Marni Greer has been an awesome teacher and friend and the game nights were so helpful for getting me out from under the paperwork while writing up everything. Alicia Pal, Krista Holland, Todd Tesen, Fiona Cole, Stacee Raber, Angela Raskin, Andrea Call, Jeanne Heilman, Susan Priver, Lucy

Bivens, Anne Bosi, Purvi Ghandi, Joan Stevens, Vanessa Ferandell, and Tania Nasir, have all been wonderful teachers and friends. I also want to thank Desiree Rumbaugh for being a constant embodiment of inspiration of both yoga and life. Your friendship and teaching inspires me daily. Without Lorenzo and Antonella I would've never tried yoga in the first place, and I want to thank Anne Knecht for being my first yoga buddy. Without you I don't know if I would've kept up with it.

A few years back I started singing again and had the fortune of joining the Occidental-Foothill Master Chorale. Jeff...you, without a doubt, the most insightful, and certainly most fun, conductor I've ever worked with. I'm going to miss you and all the great friends I made in the group. Ann. . .what can I say, I'll never be able to throw a 'Pointless Party' of the same caliber without you. I hope I can continue to find people to draw funny cartoons with during serious concerts. Corrine, you can always telephone me...ON THE TELEPHONE! I will miss Pei-Yun Lee, Alex Fergusson, Djuna Copley-Woods, Anne Mallek, Ashley Borders, Adam Driscoll, Diane Waggoner, Christina Sheldon, and Caleb Meurer, Anita Gould, Susan Aldrich, Gabe Niles, and Jeff Stone. Those nights out after rehearsal meant a lot.

I also had the fortune of meeting many non-Caltech, non-yoga, non-master chorale friends who supported me through grad school. Kat-n'-Rus™, you were the best neighbors I could've hoped for. Siobhan, thanks for listening to everything and for the creative nicknames and gifts.

Various social groups helped me keep my sanity through the last few years. I want to thank the awesome Silverlake Dinner Club and associated "Bob's-BBQ" group, especially Liza Simone. In the early years there was also the infamous "Friday night social club." I sincerely miss seeing Chris Hart, Eliot Bush, Daw-An Wu, Susan Chen, Erik Read, Colette Wilklow, Lucas Scharenbroich, Lucas Silacci, Jim Carrol, and the many people I'm forgetting at the moment who passed through the group. I also miss all my racquetball buddies including Michael van Dam and most of all, Jackie Kessler. Jax was there from the very beginning and will forever be an integral part of my grad school experience.

There have also been numerous close friendships that I will always cherish. Ted and Micheline. . .y'all were awesome for sticking to the rigorous Sunday Noah's bagels run schedule. We were all at Caltech about the same time and I'm glad we could share our time here together. Best of luck with Alea and Kayley. Tim McGarvey has been one of the closest friends I've ever had and I want to thank him for everything over the last three years. One of the most fun groups was the "Buffy Night" crowd based mostly out of the Bronner-Fraser lab. I miss Anne Knecht, Mike Albrecht, Sarah Ahlgren, Helen McBride, Laura Gammill, Claire Baker, and the good Chinese and Thai food we would order while watching Buffy engage in battle against vampires, demons, gods, monsters, and making us feel a little bit better about our battles with molecules, eggs, gels, and the like in lab (at least our mutants stay in their test tubes).

And most of all I want to thank my parents. You have been so loving and supportive in countless ways, and it is to you that I dedicate this work.

TABLE OF CONTENTS

Chapter 1:

Introduction

INTRODUCTION

Iron is Required to Sustain Life

During the pre-biotic age of our planet there was very little oxygen in the atmosphere, and free iron was abundant. The concentration of the ferrous ion (Fe^{2+}) in the oceans was 50 μM (Holland, 1984) compared with only ~20 nM today (Silver, 1993). About 3 billion years ago photosynthetic cyanobacteria began producing di-oxygen as a metabolic waste product, thereby increasing the level of atmospheric oxygen close to its present level (~23%) (Allegre & Schneider, 1994). This resulted in massive amounts of iron precipitation as magnetite (Fe_3O_4) and hematite (Fe_2O_3), which are the modern commercial iron ores (Holland, 1984).

Since the days of cyanobacteria, life has continued to depend on the versatile chemistry of iron to sustain biological reactions, such that iron is required to sustain almost all life on Earth (Stamatoyannopoulos, 1994). The only identified exceptions are the soil bacteria *Lactobacillus plantarum* (Archibald, 1983) and the Lyme disease-causing bacteria *Borrelia burgdorferi* (Posey & Gherardini, 2000). Biological systems have numerous uses for iron. Many enzymes coordinate it directly using sidechains to create a reactive center for chemical reactions (e.g., ribonucleotide reductase (Jordan & Reichard, 1998) or 5-lipoxygenase (Lange & Que, 1998)), as part of a cofactor such as the iron-sulfur cluster found in many metabolic proteins, electron transfer as in the respiratory complexes, bound to heme either for oxygen binding and transport, as in myoglobin and hemoglobin, or in enzymes such as the cytochromes (reviewed in Groves, 2003). However, in every case the

iron is sequestered to prevent the biologically dangerous products of the Fenton reaction, which can be described as

$Fe^{3+} + O_2^- \rightarrow Fe^{2+} + O_2$

$Fe^{2+} + H_2O_2 \rightarrow Fe^{3+} + OH^- + OH^\cdot$

In the absence of free superoxide in cells, other molecules such as ascorbate can substitute for the reducing agent in the above reaction (Halliwell & Gutteridge, 1990). *In vivo* the resultant hydroxy radical will abstract a hydrogen atom from almost any organic molecule to generate an organic radical that can react to form various end products such as lipid peroxides, modified DNA bases, broken DNA strands, or radial cascade reactions (Halliwell & Gutteridge, 1990).

Iron sequestration serves another purpose in addition to preventing free radical cascades. Since iron is required to sustain most organisms, successful colonization of a host by a pathogen requires that iron be taken from the host. In humans the level of free iron is ~10^{-18} M (Bullen, 1981), which is well below the concentration required for bacterial growth (~10^{-6} to 10^{-7} M) (Weinberg, 1978). As part of the primary immune response to bacterial infection, host cells produce excess lactoferrin, a potent iron-binding protein, to limit available iron in an attempt to slow bacterial growth (Jurado, 1997). Bacteria have evolved numerous ways of abstracting host iron, including secretion of siderophores (small molecule iron sequestering agents) and expression of receptors capable of binding and taking up iron-containing host proteins (Jurado, 1997).

Iron Balance in the Human Body

In order to exploit the advantages of utilizing iron, mammals have overcome the issues involved in working with this inherently toxic element. Iron must be absorbed from dietary sources and then sequestered to prevent oxidative damage or uptake by adventitious organisms. However, this sequestration must be reversible so the element can be used, recycled, and be transported throughout the body to adequately supply every tissue and cell type with the appropriate amount. Additionally, sufficient iron must be stored in case of nutritional deficiency. The average adult human has 3-4 grams of this potentially hazardous substance iron in his/her body and possesses no regulated mechanism for iron excretion, creating the possibility of iron overload if there is a defect in the checkpoints regulating dietary absorption (Andrews, 1999). Thus, the processes of iron uptake, transport, storage, and recycling are performed by a variety of proteins. Some of these proteins, such as hemoglobin, have been studied for over a century, whereas others, such as hemojuvelin reported in January of this year (Papanikolaou *et al.*, 2004), were discovered only recently. Because of the large number of molecules involved in mammalian iron homeostasis, and the even larger number of interactions between them, various environmental and genetic disturbances to the balance maintained by these proteins leads to a myriad of diseases characterized by iron deficiency, overload, and sometimes both (Andrews, 1999).

Imbalance of Iron Handling Leads to Anemia

In 1713 Lemery and Geoffroy demonstrated that iron is transported in the blood. Today we know that approximately 66% of iron in an adult human is bound to hemoglobin in red blood cells for the purpose of oxygen transport through the bloodstream (Beutler, 2002). Because iron is often the limiting factor in hemoglobin production, and because of the fundamental role of hemoglobin in sustaining cellular respiration, many conditions that perturb iron homeostasis result in anemia, a condition in which red blood cells are not properly oxygenating tissue (Schrieber, 1989). Anemia is most commonly the result of internal bleeding, but an iron-poor diet, and other environmental factors can play a role (Schrieber, 1989). Dietary iron deficiency used to be relatively common in the United States until the fortification of foods with various vitamins and minerals, such as iron in 1938, ameliorated many cases of nutrition-related anemia (Junod, 2001). However many environmental factors other than diet can lead to deficient iron delivery to red blood cell precursors. In the simplest case, continuous internal bleeding will deplete iron stores eventually leading to iron deficiency and anemia (Schreier *et al.*, 1994). Another example of deficiency is the anemia of chronic disease, also called anemia of inflammation. This is an acquired condition brought on by a variety of persistent inflammatory disorders resulting in an attenuated response to red blood cell-stimulating factors, such as erythropoietin, decreasing red blood cell production. Additionally, iron availability for erythropoeisis is lowered, possibly because of a defect in the iron recycling pathway of macrophages, which provide the bulk of the iron for red blood cell production (reviewed in Weinstein *et al.*, 2002). Anemia can also be a secondary result of other nutritional disorders. For example, pernicious anemia, a form of megaloblastomic anemia, results from a lack of vitamin B-12, which is necessary in part for healthy red blood cell

production (Cohen, 2004). The B-12 deficiency can arise from poor diet, as in the case of strict vegans who do not supplement with B-12, or a loss of intrinsic factor, which is required for B-12 absorption. Loss of intrinsic factor can result from surgical removal of the stomach, and most commonly from atrophic gastric mucosa, autoimmunity against gastric parietal cells, autoimmunity against intrinsic factor, triggered by other autoimmune endocrine disorders, or very rarely by a genetic deficiency for factor expression (Cohen, 2004). These examples show that iron homeostasis is complicated by the influence of other nutrients in the body.

There are also numerous genetic causes of anemia. Sickle cell anemia results from a genetic mutation in hemoglobin that causes it to aggregate and distort the shape of the red blood cell impairing its function (Schreier *et al*., 1994). Other examples of genetic anemia are the thalassemias, which result from deletions and mutations in the genes coding for hemoglobin causing the production of cells with insufficient oxygen transport activity (Olivieri, 1999). Although thalassemias are characterized by anemia and the inability to effectively transport oxygen throughout the body, they also result in the second consequence of perturbing the iron-homeostatic balance: iron overload. The lack of efficient erythropoesis is interpreted by the body as an iron deficiency and it responds by increasing dietary iron absorption and expanding the erythroid marrow by nearly 30-fold (Olivieri, 1999). This results in the uptake of an additional iron burden of 2 to 5 grams of iron per year (Olivieri, 1999). The anemia accompanied with iron overload puts the thalessemias in a disease class called secondary iron overload disorders. Secondary iron

overload disorders are often side effects of other problems such as liver disease, environmental iron overload, or difficulty with erythropoesis. When iron overload has progressed to the point where iron is deposited into tissues, the patient is said to have hemochromatosis (Schreier *et al*., 1994).

Imbalance of Iron Handling Leads to Toxic Iron Overload: Hemochromatosis

The thalassemias, in addition to the sideroblastic and congenital dyserthropoetic anemias, are diseases that disturb red blood cell production, resulting in excessive iron uptake and iron deposition in erythropoetic tissue in an attempt to ameliorate the lack of functional red blood cell production by providing more iron (Olivieri, 1999). While these diseases are generally genetic in nature, iron overload can be caused by environmental factors. It is difficult, though possible, to induce an overloaded state through the ingestion of excess iron, but more common in modern day is the case of transfusional iron overload (Bottomley, 1998). One milliliter of packed red blood cells contains approximately 1 milligram of iron. Therefore, each transfused unit incorporates approximately 200 mg of unexcreteable iron into a patient (Bottomley, 1998). An individual receiving regular transfusions, for example, to treat any refractory anemia, requires chelation therapy to prevent progressive iron overload and subsequent damage to parenchymal tissues. Another environmentally induced iron overload results from excessive alcohol consumption (Bottomley, 1998). It is thought that damage to the liver induced by chronic drinking leads to the excessive absorption of iron by the liver while other organs are spared (Bottomley, 1998). A rare secondary iron overload disorder called atransferrinemia, or hypotransferrinemia (Hayashi *et al.*, 1993), is characterized by splicing defects that result

in little to no expression of transferrin, a serum protein responsible for shuttling iron atoms through the circulatory system. In the absence of transferrin, erythroid tissues do not receive the iron they need to produce red blood cells. In this case, patients present with extreme siderosis of parenchymal tissues. The anemia is corrected upon administration of plasma or transferrin injections (Bottomley, 1998). Hereditary ceruloplasmin deficiency is characterized by iron deposition in various tissues leading to neurological symptoms, cerebellar ataxia, diabetes mellitus, retinal pigment degeneration, and involuntary movements (reviewed in Sheth & Brittenham, 2000). Ceruloplasmin is a copper-containing serum protein with ferroxidase and is involved in the release of iron from tissue stores (Osaki & Johnson, 1969). Clinical symptoms do not occur until late in life, possibility because hephaestin, a copper-containing membrane bound protein with high sequence similarity to ceruloplasmin, can also function in the export of iron from cells (Sheth & Brittenham, 2000).

Types of Hereditary Hemochromatosis

In recent years several new forms of hereditary hemochromatosis, also called primary iron overload, and their causes have been identified. The first gene to be linked to hereditary hemochromatosis was HFE (Feder *et al.*, 1996), a class I MHC homolog that binds to transferrin receptor 1 (TfR) (Parkkila *et al.*, 1997; Feder *et al.*, 1998). Mutations in HFE result in type I hemochromatosis (Feder *et al*., 1996). HFE and TfR are the focus of this thesis and their interactions and role in iron overload are discussed later. Type II hemochromatosis is clinically and genetically different than type I hemochromatosis (Cazzola *et al.*, 1998) and is characterized by the onset of iron loading resulting in diabetes,

and hypogonadism during the teens and early 20s. If untreated, type II hemochromatosis leads to early death from cardiac dysfunction (Cazzola *et al.*, 1983). The defect was initially mapped to the centromeric region of chromosome 1q, which is incomplete in the human genome assembly (Roetto *et al.*, 1999), but subsequent studies identified the gene whose product is called hemojuvelin (Papanikolaou *et al*., 2004). While mutations to the protein are linked to disease (Lanzara *et al.*, 2004; Lee *et al.*, 2004), the function of hemojuvelin is currently unknown (Brissot *et al.*, 2004). Type III hemochromatosis, which is characterized by severe iron loading and clinical complications that are phenotypically indistinguishable from type I hemochromatosis (Camaschella *et al.*, 2000), results from mutations to a protein called transferrin receptor 2 (TfR2) (Kawabata *et al.*, 1999; Fleming *et al.*, 2002). TfR2 is expressed mainly by hepatocytes and has high sequence and functional similarity to TfR1 (Kawabata *et al*., 1999). The role of TfR2 in acting as a regulator of iron homeostasis is not clear at this time. The cause of type IV hemochromatosis has been mapped to mutations to a recently identified protein called ferroportin (Fpn) (Abboud & Haile, 2000; Donovan *et al.*, 2000; McKie *et al.*, 2000; Fleming & Sly, 2001; Montosi *et al.*, 2001; Roetto *et al.*, 2002; Jouanolle *et al.*, 2003; Rivard *et al.*, 2003). Fpn is a membrane protein capable of transferring ferrous iron from the interior to exterior of the cell. Iron release from cellular warehouses is an important first step in mobilization and defects in ferroportin result in iron loading (Brissot *et al*., 2004).

The Identification of HFE as a Regulator of Iron Homeostasis

The most common form of hemochromatosis is primary, or type I hemochromatosis, also known as idiopathic hemochromatosis, primary iron overload, or hereditary hemochromatosis (HH) (Feder *et al*., 1996). The result of HH is the excess deposition of iron in liver, pancreas, and heart leading to cirrhosis, cancer, myocardial failure, arrhythmias, type II diabetes, arthritis, hypogonadism, and an iron-induced melanin over-expression that can lead to bronzing of the skin, which earned it the name "the bronze killer" (reviewed in Hanson *et al.*, 2001). Individuals afflicted with HH absorb 1 to 3 mg of iron per day in excess of their body's needs. Small amounts of excess iron are well tolerated and can be stored. However, this daily excess iron absorption occurs throughout a lifetime and eventually exceeds the body's iron storage capacities, resulting in the circulation of iron not tightly bound to protein cofactors (Schrieber, 1989). The liver is responsible for clearing this form of iron and so it is often the first target of iron-mediated tissue damage, soon followed by other organs (Craven *et al.*, 1987). At the onset of systemic disease, an affected individual may have an iron load of 20-40 grams, many times that found in a healthy adult (3-5 grams) (reviewed in Schrieber, 1989). While the disease was recognized and carefully documented in the 19th century, the exact cause was not identified until nearly a hundred years later (reviewed in Beutler, 2002). In the late 1970s the gene responsible for HH was shown to be linked the major histocompatibility complex (MHC) and eventually mapped to the short arm of chromosome 6. In the mid 1990s, John Feder and colleagues at Mercator Genetics utilized positional cloning during a proof-of-principle pilot experiment that sought to identify genes linked to disease (Feder *et al*., 1996). Their work identified a gene, now called *HFE*, that codes for a type I transmembrane glycoprotein homologous to the heavy chain of class I MHC molecules. In

their original study of patients identified with hemochromatosis, 83% were homozygous for a mutation converting guanosine 845 to adenosine and resulting in a tyrosine substitution for a cysteine at position 260 (C260Y) in the HFE protein (Feder *et al*., 1996).[1] A second mutation (H41D) was found in some HH patients. Subsequent population studies indicate that H41D hetero- and homozygotes are more common than C260Y hetero- and homozygotes, though the degree of iron loading associated with H41D is not as great compared with C260Y (Waalen *et al.,* 2002). The role of H41D in primary hemochromatosis is less clear, but a recent study utilizing transgenic mice demonstrates that H41D homozygotes have an increased iron load compare to wild-type littermates (Tomatsu *et al.*, 2003). H41D/C260Y compound heterozygous mice are significantly less iron loaded that C260Y homozygotes, but have a much greater hepatic iron load than wild-type mice, H41D/C260Y mice, or H41D homozygotes (Tomatsu *et al*., 2003). These data indicate that the H41D substitution leads to a partial loss of HFE function.

HFE Binds the Transferrin Receptor, a Protein Central to Iron Regulation

The discovery that HFE binds to the transferrin receptor (TfR) linked it to one of the most central proteins in iron metabolism (Parkkila *et al*., 1997; Feder *et al*., 1998). TfR is a dimeric type II transmembrane glycoprotein expressed on virtually all mammalian cell types and serves as the primary entry point for iron into cells (Enns, 2002). The central role of TfR in maintaining iron balance is illustrated by a study of TfR knockout mice (Levy *et al.*, 1999). Homozygous TfR negative animals do not develop beyond embryonic

[1] There is a discrepancy in the HFE field in terms of numbering systems. Here I use the numbering convention for MHC molecules and other cell surface proteins that begins with the first residue of the mature protein after the hydrophobic signal sequence has been removed. Many reports on HFE begin numbering from the start of the signal sequence and differ by 22 residues.

day E12.5 and exhibit extreme anemia and defects in neural tube formation (Levy *et al*., 1999). That the embryos develop this far indicates that there must be another route for iron delivery at the early stages of development, and there is evidence this role is played by a siderophore-binding lipocalin (Yang *et al.*, 2002). Therefore, unlike most of the proteins already discussed, there are no known alleles of TfR associated with any kind of iron overload or deficiency, as an inactive form of TfR would likely be lethal before the end of the gestation period.

Transferrin Receptor Binds Transferrin, an Iron Transport Protein

As its name implies, TfR is a receptor for transferrin (Tf) (Leibman & Aisen, 1977). Serum Tf takes advantage of the circulatory system to fulfill the requirement of iron transport and delivery to tissues throughout an organism (Schade, 1946). Tf is an ~80 kDa soluble glycoprotein and is the third most abundant protein in blood after albumin and immunoglobulin (Schrieber, 1989). Tf was the first identified protein to evolve from ancestral gene duplication and fusion: each Tf molecule is composed of two lobes related by high structural and sequence similarity (Park *et al.*, 1985) (Fig 1A). Each lobe comprises two smaller domains, N-I and N-II in the N-lobe and C-I and C-II in the C-lobe (Anderson *et al.*, 1987). The transferrin superfamily comprises numerous homologs and orthologs such as the ovotransferrins, melanotransferrins, and lactoferrins (Nakamasu *et al.*, 1999). Members of the transferrin family are found throughout eukarya with more recently identified molecules in the hemolymph of the tobacco hornworm (*Manduca sexta*) (Bartfeld & Law, 1990), the cockroach (*Blaberus discoidalis*) (Jamroz *et al.*, 1993), and even in the unicellular green algae *Dunaliella salina* (Fisher *et al.*, 1997). Each lobe of

transferrin binds a single ferric (Fe^{3+}) ion and coordinates it with two tyrosine resides, one histidine, one aspartate, and the synergistic anion bicarbonate (Anderson *et al*., 1987) (Fig 1A). The mechanisms of iron binding and release are complicated and involve multiple protonation steps, the presence of helper ions, chelators, interactions between Tf lobes, and local and large-scale structural changes (reviewed in He, 2002). The most striking structural feature of transferrin is the large conformation change induced by the loss of iron. Upon loss of iron, there is a 54-63º rotation between the domains that comprise each lobe and a repacking of the interface between each lobe, burying previously exposed residues and exposing previously buried residues (Gerstein *et al.*, 1993; Kurokawa *et al.*, 1999) (Fig 1B). Mechanisms of iron release are discussed in more detail in Chapter 4.

While only about 0.1% of the total iron in a healthy adult human is loaded on transferrin, there is significant flux of iron through this member of the iron-transport compartment. The reticuloendothelial system alone requires about 24 mg of iron for the daily production of about 200 billion new erythrocytes (Knutson & Wessling-Resnick, 2003). Transferrin mitigates the inherent danger in transporting potentially reactive iron through an oxygenated aqueous solution, such as blood, by binding the ferric ion with extremely high affinity ($K_A \sim 10^{22}$ M) (Aisen *et al.*, 1978). The spontaneous release of iron from transferrin at basic pH is extremely slow with a half-life of days to weeks. Acidic pH destabilizes iron binding, however even at pH 5.5 the half-life of bound iron is greater than three hours (reviewed in He and Mason, 2002). There are four iron-binding states for the transferrin molecule. Since each lobe can bind an iron atom, and binding of iron in one lobe is not

requisite for binding in the other lobe, then Tf may exist in the diferric state (here referred to as Fe-Tf), monoferric with the C-lobe loaded (Fe_C-Tf), monoferric with the N-lobe loaded (Fe_N-Tf), or iron free (apo-Tf). All of these forms of Tf can be found in the blood with ~70% of the total protein in the apo-Tf form (Aisen *et al*., 1978; Leibman & Aisen, 1979).

Transferrin and Transferrin Receptor Work Together to Deliver Iron to Cells

When circulating Fe-Tf encounters TfR the two proteins bind with high affinity (~1 nM) (Dautry-Varsat *et al.*, 1983). TfR is a dimeric protein and can accommodate two Tf molecules (Enns & Sussman, 1981). The cytoplasmic domain of TfR contains a YTRF sequence that directs it to clathrin-coated pits for endocytosis into the tubulo-vesicular endosomal system. TfR is transported through an acidic compartment and then sorted back to the cell surface (reviewed in Schmid, 1992). When Fe-Tf is bound to TfR during its journey, the exposure to the low pH compartment stimulates the removal of iron from Tf such that release is complete within 2-3 minutes (Aisen & Leibman, 1973). The released iron is then shuttled, presumably through the divalent metal transporter DMT1, to the cytosol where it is picked up for use by the cellular machinery, or incorporated into the iron-storage protein ferritin (Richardson & Ponka, 1997). At acidic pH, apo-Tf and TfR still have a high affinity for each other (~5 nM) and the two proteins stay together through sorting back to the cell surface. Upon exposure to the slightly basic pH of blood (pH~7.4), apo-Tf rapidly dissociates due to its barely detectable affinity for TfR at this pH and renters the circulation (reviewed in Enns, 2002). The amount of TfR-mediated iron uptake is regulated at the translational level such that when iron is low, the translation rate of TfR

mRNA is increased, and when iron is high, TfR translation is decreased (reviewed in Theil, 1994).

HFE Modulates Iron Homeostasis

The interaction between HFE and TfR has been characterized by biochemical and cellular methods (Feder *et al*., 1998; Gross *et al.*, 1998; Riedel *et al.*, 1999; Roy *et al.*, 1999; Salter-Cid *et al.*, 1999; Roy *et al.*, 2000; Davies *et al.*, 2003). HFE binds to TfR with an equilibrium dissociation constant of ~50 nM at the basic pH of the cell surface (pH~7.4) (Lebrón *et al.*, 1998; Lebrón & Bjorkman, 1999; Lebrón *et al.*, 1999; West *et al*., 2000; West *et al.*, 2001; Giannetti *et al.*, 2003; Giannetti & Bjorkman, 2004). This is significantly weaker than the binding of Fe-Tf at the same pH (~1 nM) (Lebrón *et al*., 1998). However, HFE binding does not occur at acidic pH (<6.3) (Lebrón *et al*., 1998). This pH dependence is opposite that of apo-Tf, which binds to TfR at acidic but not basic pH (Paterson *et al*., 1984; Lebrón *et al*., 1998). Early cellular studies on HFE-transfected HeLa cells indicated that expression of HFE lowered the observed affinity of the cells for Tf suggesting an activity for HFE in modulating the binding properties of TfR (Feder *et al*., 1998; Riedel *et al*., 1999; Roy *et al*., 1999; Salter-Cid *et al*., 1999). Subsequent *in vitro* studies using soluble versions of HFE and TfR reported the same result (Lebrón *et al*., 1999; Roy *et al*., 2000). This lead to an initial hypothesis that HFE lowers the amount of endocytosed iron by reducing TfR's ability to bind and transport iron-loaded transferrin. Indeed, some of the early cellular studies noted a marked decrease in cellular iron content of HFE-transfected cells (Gross *et al*., 1998). These experiments have been repeated using various cell lines. Not all studies are in agreement and virtually every possible result has

been reported, including increased iron uptake, decreased transferrin cycling, altered receptor trafficking rates, identical transferrin uptake but lower iron donation by transferrin, and reduced iron export (Gross *et al*., 1998; Corsi *et al.*, 1999; Riedel *et al*., 1999; Roy *et al*., 1999; Salter-Cid *et al*., 1999; Roy *et al*., 2000; Feeney & Worwood, 2001; Drakesmith *et al.*, 2002; Waheed *et al.*, 2002; Wang *et al.*, 2003). Emerging from the aggregate of these results is the awareness that HFE may have differential effects on iron levels depending on cell type. Since almost all cells express TfR, this would suggest that HFE has an alternate binding partner, though TfR binding may be a prerequisite for recognition by this as yet unidentified protein. Hypotheses regarding the identity of this mystery receptor are discussed at the end of this chapter and in chapter 3.

The Molecular Structures of HFE and TfR

HFE and TfR have been structurally characterized alone and in complex (Lebrón *et al*., 1998; Bennett *et al.*, 2000). As predicted from sequence homology, HFE is structurally similar to the class I major histocompatibility complex (MHC) molecules (Lebrón *et al*., 1998), which present antigenic peptides to T lymphocytes (Garcia *et al.*, 1999) (Fig 2). In addition to the characteristic long α–helices, the β–sheet platform, and the α3 domain that are found in class I MHC proteins, HFE also binds the class I MHC light chain β_2-microglobulin (Feder *et al.*, 1997). The significance of the similarity between HFE and class I MHC molecules is unclear since HFE has no known function in the immune response. In fact, the HFE counterpart of the class I MHC peptide-presenting groove is closed in HFE as the result of sidechain substitutions and a 4 Å translation of the α1 domain helix towards the α2 domain helix (Lebrón *et al*., 1998). Cysteine 260, which is

mutated to tyrosine in individuals with hereditary hemochromatosis, is part of a disulphide bridge in the α3 domain. This bridge is highly conserved in MHC molecules and disruption, as in the common HH mutation C260Y, prevents proper folding, β_2-microglobulin binding, and cell surface expression, effectively abrogating HFE function (Feder *et al*., 1997; Waheed *et al.*, 1997).

Transferrin receptor is also a transmembrane glycoprotein. As previously discussed, the N-terminal tail, which is exposed to the cytosol, contains an endocytic motif (Enns, 2002) in addition to a cysteine-linked palmitate (Adam *et al.*, 1984) and a serine residue that can be phosphorylated by protein kindase C (Rothenberger *et al.*, 1987). The extracellular domain of TfR begins with an ~33 residue stalk domain that contains two cysteines that form disulphide bonds to their counterparts on the second chain of the obligate TfR dimer (Enns, 2002). The stalk also contains the only site of O-linked glycosylation and serves a protective role by preventing proteolytic cleavage of TfR near the plasma membrane (Rutledge, Green *et al.*, 1994; Rutledge, Root *et al.*, 1994; Rutledge & Enns, 1996). Despite the covalent linkage of the two TfR chains by cysteines in the stalk region, the dimeric nature of TfR is maintained by the remaining ~640 residues that make up the remainder of the ectodomain (Turkewitz *et al.*, 1988; Lebrón *et al*., 1998). The crystal structure of TfR ectodomain dimer shows that each monomer is formed from three domains (Lawrence *et al.*, 1999) (Fig 3A). The first domain is called the protease-like domain because of its high sequence and structural similarity to carboxypeptidases. The capacity for peptide hydrolysis has been eliminated by substitution of three of the residues

that would coordinate the active site zincs (Lawrence *et al*., 1999). Inserted between the first and second strands of the central β-sheet of the protease-like domain is the apical domain. The physiological function of the apical domain is unknown; however, it is recognized by parvoviruses making TfR the point of cellular entry for those pathogens (Palermo *et al.*, 2003). The third domain of TfR is a large four-helix bundle that comprises a significant fraction of the dimerization surface and contacts all three domains on the partnered monomer (Lawrence *et al*., 1999).

The crystal structure of HFE bound to TfR has also been reported (Bennett *et al*., 2000) (Fig 3B). The complex is formed from associations between the helical domain of TfR and the α1 helix of HFE to form a 3-helix bundle and burying ~2,000 $Å^2$ of total surface area. There are additional contacts from the α2 helix of HFE with TfR's helical domain that are not part of the 3-helix bundle. Before the structure of this complex was solved, it was not clear if HFE molecules would preferentially interact with TfR molecules on the same membrane, or perhaps bind TfR on an adjacent cell. To form the structure observed in the crystal, HFE molecules would only be able to interact with TfR molecules on a common membrane, and in fact would have to "lie down" relative to the orientation commonly associated with class I MHC molecules (Bennett *et al*., 2000) (Fig. 3).

The Mechanism by Which HFE Regulates Iron Metabolism Is Not Known

The observation that HFE binds to TfR circumstantially involves HFE in an important system for iron transport and uptake. However, TfR binding does not explain HFE's role

as a modulator of iron homeostasis. Over the last eight years, hundreds of biochemical, cellular, and physiological studies have been reported in an attempt to understand the role of HFE in maintaining iron balance, and to develop an understanding of the molecular pathology of hereditary hemochromatosis. Theories and models continue to be proposed, but each is confounded either by conflicting reports or the continuous discovery of new proteins involved in maintaining iron balance. Therefore, my approach to studying this system was to focus on the structural and chemical aspects of the HFE/TfR/Tf system and attempt to relate those findings to the cellular case. The dimeric nature of TfR coupled with its ability to bind two ligands, each with different dependency on pH for binding, and one of which (transferrin) has multiple structural and chemical configurations, results in a complex chemical equilibrium, aspects of which may have significant consequences for the mechanism of HFE action (Fig 4).

Thus, I undertook a careful examination of the structural and biochemical interactions between HFE and TfR, Fe-Tf and TfR, and apo-Tf and TfR. The early cellular and biochemical studies involving HFE indicated that HFE lowered the observed affinity of TfR for Tf (Feder *et al*., 1998; Gross *et al*., 1998), and competition binding experiments suggested that HFE and Tf shared the same or similar binding footprint on the receptor surface (Lebrón *et al*., 1999). While the HFE binding footprint on TfR had been characterized by crystallography (Bennett *et al*., 2000), there were only two studies mapping the Tf binding site. Using human/chicken TfR chimeras the binding site for Tf had been mapped to the C-terminal 192 amino acids of TfR (Buchegger *et al.*, 1996), while

a small qualitative mutagenesis study indicated that residues in a conserved Arg-Gly-Asp (RGD) motif (Dubljevic *et al.*, 1999), also in the TfR helical domain, were important. Together all of these data suggested that HFE and Tf have an overlapping binding site on TfR, but more functional information would be required to understand the significance of this overlap to TfR ligand binding.

A Mutagenesis Study Reveals the Binding Footprints of HFE, Fe-Tf, and apo-Tf on the Surface of TfR

While a co-crystal structure of two proteins identifies the interaction surface, it does not reveal which interactions are most functionally relevant. Only by systematically mutagenizing residues in an interface can a map of the functional epitope (those residues contributing at least 2 kcal/mol of free energy of binding) be defined (Cunningham & Wells, 1993). Utilizing the crystal structure of HFE/TfR and the results of a mutagenesis study of HFE that identified some functionally important residues, I began working with Dr. Anthony West in our laboratory to mutate residues in TfR to identify what residues were important for binding HFE. Our hypothesis was that if the binding sites for HFE and Tf overlap, then mapping the HFE interface would reveal some residues responsible for Tf binding. It was initially noted that one of the TfR mutations, L619A, eliminates detectable HFE binding and affects a concomitant drop in Fe-Tf affinity providing the first functional evidence of overlapping binding sites. Another mutation, Y643A, had a similar effect (West *et al*., 2001). The results of this early mutagenesis work are described in Appendix I. However transferrin is a large molecule about the same size as a TfR monomer (~90Å x 50Å x 40 Å; measured using the structure of iron-bound ovotransferrin (Kurokawa *et al.*,

1995), suggesting that Tf could contact multiple domains of TfR. For example, an early modeling study indicated that Tf possesses sufficient surface area to contact all three TfR domains at once (Lawrence *et al.*, 1999). Therefore, I expanded the mutagenesis screen to include residues from disparate parts of the receptor within a radius defined by the long axis of Tf. The search for functional residues mostly involved identifying exposed hydrophobic sidechains, although substitution of some charged residues also significantly affected binding. The results of the mutagenesis study are described in Chapter 2 (Giannetti *et al*., 2003), along with a description of technical improvements in screening and methodology. One development was the use of binding models that better describe the TfR system. A second was the redesign of the assay methodology to develop a new protocol that has higher throughput, requires $1/1000^{th}$ of the amount of starting material, and eliminates the need to purify the TfR before the binding analysis.

Mutagenesis Reveals a Mechanism for TfR-Assisted Iron Release from Tf

The mutagenesis screen revealed several features of HFE, Fe-Tf, and apo-Tf binding, including the observation that Fe-Tf and apo-Tf have differential binding footprints on the TfR surface (Giannetti *et al*., 2003). While most of the residues that affect binding of one form of Tf also affect binding of the other form, there are key functional differences. From the comprehensive mutagenesis study of TfR we identified residues that are specific for binding apo-Tf (Giannetti *et al*., 2003). Chapter 4 describes experiments that reveal that these conserved residues, which form a hydrophobic patch on the TfR surface, are required for TfR to stimulate the release of iron from Fe-Tf at acidic pH. We hypothesize that this

patch facilitates the opening of the Tf molecule to expose the iron atom, thereby enhancing the efficiency of iron removal by cellular chelators.

Biochemical and Biophysical Studies Using an Engineered Transferrin Receptor

We also sought to understand the molecular mechanism for the observed decrease in Tf binding affinity by cells expressing HFE (Feder *et al*., 1998; Riedel *et al*., 1999; Roy *et al*., 1999) by investigating the possibility of cooperativity in ligand binding to TfR. This requires measurement of the formation of the HFE/TfR/Tf ternary complex, which is impossible given the complex equilibrium between HFE, Fe-Tf, and TfR when all three proteins are mixed. In Chapter 3, I describe how this problem was solved by creating a heterodimeric transferrin receptor (hdTfR) in which one chain of the dimer is able to bind HFE but not Tf, and the other chain can bind Tf but not HFE. Characterization of the ligand-binding stoichiometries of hdTfR using sedimentation velocity analytical ultracentrifugation revealed that the hdTfR forms 1:1 complexes with HFE and Fe-Tf according to its design. I also designed and developed a competition assay that allowed the potential for cooperativity to be assessed. Binding studies performed with this assay demonstrate that TfR does not exhibit cooperativity in heterotropic ligand binding, suggesting that some or all of HFE's effects on iron homeostasis result from competition with Fe-Tf for TfR binding. Additionally, we showed that soluble HFE is incapable of competing with Fe-Tf for binding to TfR at any physiologically relevant concentration of Fe-Tf. If HFE competes with Fe-Tf for TfR binding *in vivo*, then the tethering of HFE and TfR to a common membrane, which increases their effective local concentration, may be an important feature of HFE's role in iron homeostasis.

Biochemical Competition Alters HFE's Cellular Trafficking

Given that the concentration of iron-loaded transferrin in blood fluctuates with body iron status (Schrieber, 1989), and that these fluctuations should affect HFE binding to TfR since Fe-Tf and HFE compete for binding to TfR, we sought to test this prediction by investigating the biological relevance of this competition. In Chapter 3, I describe how I used cell lines that either lack TfR expression, or express human TfR (McGraw *et al.*, 1987), to demonstrate that HFE is dependent on TfR binding to traffic from the cell surface to TfR positive endosomes (schematically diagrammed in Fig 5). I then showed that at physiologically-relevant concentrations of Fe-Tf, HFE is able to compete for TfR binding sites and is transported to endosomes. However, at concentrations exceeding those of a healthy individual and approaching those of someone with a high body iron load (Henry, 1991), HFE cannot compete against the high concentrations of Fe-Tf and becomes localized to the cell membrane.

Theories about HFE's Action in Iron Homeostasis

Since the description of HFE as the protein mutated in patients with hereditary hemochromatosis (Feder *et al*., 1996), much has been learned about HFE and other proteins involved in iron homeostasis that will not be discussed at length here (e.g., hepcidin (Nicolas *et al.*, 2001), hemojuvelin (Papanikolaou *et al*., 2004), TfR2 (Kawabata *et al*., 1999), hephaestin (Vulpe *et al.*, 1999), ceruloplasmin (Gitlin, 1998), SFT-1 (Yu & Wessling-Resnick, 1998), frataxin (Radisky *et al.*, 1999), ABC7 (Savary *et al.*, 1997; Allikmets *et al.*, 1999), ALAS2 (Cotter *et al.*, 1994), DcytB (McKie *et al.*, 2001), pantothenate kinase (Zhou *et al.*, 2001), CD163 (Knutson & Wessling-Resnick, 2003),

ferritin (Beaumont *et al.*, 1995), DMT1 (Gunshin *et al.*, 1997), ferroportin (Abboud & Haile, 2000; Donovan *et al*., 2000; McKie *et al*., 2000), and the entire network of iron response proteins that regulate the translational rates of some proteins such as TfR and ferritin (reviewed in Theil, 1994)). The complexity of iron handling by the body is illustrated by considering that in the above list of nearly 20 proteins, none actually use the iron directly for chemical reactions or oxygen binding, but act to manage the problem of iron absorption, transport, and regulation so that other proteins, such as hemoglobin, lipoxygenase, and ribonucleotide reductase have the metal they need to carry out their functions. Considering that most of the proteins listed here and elsewhere in this work were only discovered in the last 10 years, and considering that there are probably more to be discovered, one realizes that developing a model explaining HFE's function in iron homeostasis is challenging.

Currently there are several hypotheses for the function of HFE (Drakesmith *et al*., 2002; Frazer & Anderson, 2003). One proposal is that at the cell surface, free HFE can act as a regulator of iron export, possibly through interactions with the iron export protein ferroportin (Drakesmith *et al*., 2002). Two studies have noted that HFE expression decreases iron export rates from cells, though there is as yet no evidence that this results from direct interactions with ferroportin (Drakesmith *et al*., 2002; Davies & Enns, 2004). In another hypothesis (Frazer & Anderson, 2003), the amount of free HFE at the cell surface may act as a regulator for the expression of hepcidin, a peptide hormone that regulates body iron load (Nicolas *et al*., 2001; Weinstein *et al*., 2002). Expression of

hepcidin results in lower body iron, whereas elimination of hepcidin function, for example, by mutation or transgenic knockout, leads to iron overload (Fleming *et al.,* 2001). In this model, free HFE stimulates the production of hepcidin, thereby down-regulating iron levels. Loss of HFE function, as in hereditary hemochromatosis, would result in down-regulated hepcidin expression and subsequent iron overload. The commonality of both models is that competition between HFE and Fe-Tf for TfR modulates the amounts of free HFE and HFE that is bound to TfR. Therefore, we believe that competition is central both to HFE's role in maintaining iron homeostasis, and key to understanding the molecular basis for the iron overload disorder hereditary hemochromatosis.

References

Abboud, S., & Haile, D. J. (2000). A novel mammalian iron-regulated protein involved in intracellular iron metabolism. *J. Biol. Chem., 275*, 19906-19912.

Adam, M., Rodriguez, A., Turbide, C., Larrick, J., Meighen, E., & Johnstone, R. M. (1984). In vitro acylation of the transferrin receptor. *J. Biol. Chem., 259*(24), 15460-15463.

Aisen, P., & Leibman, A. (1973). The role of the anion-binding site of transferrin in its interaction with the reticulocyte. *Biochim. Biophys. Acta, 304*(3), 797-804.

Aisen, P., Leibman, A., & Zweier, J. (1978). Stoichiometric and site characteristics of the binding of iron to human transferrin. *J. Biol. Chem., 253*(6), 1930-1937.

Allegre, C. J., & Schneider, S. H. (1994). - The Evolution of the Earth. *Sci. Am. 271*(4).

Allikmets, R., Raskind, W. H., Hutchinson, A., Schueck, N. D., Dean, M., & Koeller, D. M. (1999). Mutation of a putative mitochondrial iron transporter gene (ABC7) in X-linked sideroblastic anemia and ataxia (XLSA/A). *Hum. Mol. Genet., 8*(5), 743-749.

Anderson, B. F., Baker, H. M., Dodson, E. J., Norris, G. E., Rumball, S. V., Waters, J. M., & Baker, E. N. (1987). Structure of human lactoferrin at 3.2 Å resolution. *Proc. Natl. Acad. Sci. U SA, 84*(7), 1769-1773.

Andrews, N. C. (1999). Disorders of iron metabolism. *N Engl J Med, 341*(26), 1986-1995.

Archibald, F. (1983). - Lactobacillus-Plantarum, an Organism Not Requiring Iron. *Fems. Microbiol. Lett. 19*(1), 29- 32.

Bali, P. K., & Aisen, P. (1991). Receptor-modulated iron release from transferrin: differential effects on N- and C-terminal sites. *Biochemistry, 30*(41), 9947-9952.

Bartfeld, N. S., & Law, J. H. (1990). Isolation and molecular cloning of transferrin from the tobacco hornworm, Manduca sexta. Sequence similarity to the vertebrate transferrins. *J. Biol. Chem., 265*(35), 21684-21691.

Beaumont, C., Leneuve, P., Devaux, I., Scoazec, J. Y., Berthier, M., Loiseau, M. N., Grandchamp, B., & Bonneau, D. (1995). Mutation in the iron responsive element of the L ferritin mRNA in a family with dominant hyperferritinaemia and cataract. *Nat. Genet., 11*(4), 444-446.

Bennett, M. J., Lebrón, J. A., & Bjorkman, P. J. (2000). Crystal structure of the hereditary haemochromatosis protein HFE complexed with transferrin receptor. *Nature, 403*, 46-53.

Beutler, E. (2002). History of iron in medicine. *Blood. Cells. Mol. Dis., 29*(3), 297-308.

Bottomley, S. S. (1998). Secondary iron overload disorders. *Semin. Hematol., 35*(1), 77-86.

Brissot, P., Troadec, M. B., & Loreal, O. (2004). The clinical relevance of new insights in iron transport and metabolism. *Curr. Hematol. Rep., 3*(2), 107-115.

Buchegger, F., Trowbridge, I. S., Liu, L.-F. S., White, S., & Collawn, J. F. (1996). Functional analysis of human/chicken transferrin receptor chimeras indicates that the carboxy-terminal region is important for ligand binding. *Eur. J. Biochem., 235*, 9-17.

Bullen, J. J. (1981). The significance of iron in infection. *Rev. Infect. Dis., 3*(6), 1127-1138.

Camaschella, C., Roetto, A., Cali, A., De Gobbi, M., Garozzo, G., Carella, M., Majorano, N., Totaro, A., & Gasparini, P. (2000). The gene TfR2 is mutated in a new type of haemochromatosis mapping to 7q22. *Nat. Genet., 25*, 14-15.

Cazzola, M., Ascari, E., Barosi, G., Claudiani, G., Dacco, M., Kaltwasser, J. P., Panaiotopoulos, N., Schalk, K. P., & Werner, E. E. (1983). Juvenile idiopathic haemochromatosis: a life-threatening disorder presenting as hypogonadotropic hypogonadism. *Hum. Genet., 65*(2), 149-154.

Cazzola, M., Cerani, P., Rovati, A., Iannone, A., Claudiani, G., & Bergamaschi, G. (1998). Juvenile genetic hemochromatosis is clinically and genetically distinct from the classical HLA-related disorder. *Blood, 92*(8), 2979-2981.

Cohen, E. W. E. (2004, 11/7/02). *Pernicious anemia*, 2004, from http://www.nlm.nih.gov/medlineplus/ency/article/000569.htm

Corsi, B., Levi, S., Cozzi, A., Corti, A., Altimare, D., Albertini, A., & Arosio, P. (1999). Overexpression of the hereditary hemochromatosis protein, HFE, in HeLa cells induces an iron-deficient phenotype. *FEBS Lett., 460*, 149-152.

Cotter, P. D., Rucknagel, D. L., & Bishop, D. F. (1994). X-linked sideroblastic anemia: identification of the mutation in the erythroid-specific delta-aminolevulinate synthase gene (ALAS2) in the original family described by Cooley. *Blood, 84*(11), 3915-3924.

Craven, C. M., Alexander, J., Eldridge, M., Kushner, J. P., Bernstein, S., & Kaplan, J. (1987). Tissue distribution and clearance kinetics of non-transferrin-bound iron in the hypotransferrinemic mouse: a rodent model for hemochromatosis. *Proc. Natl. Acad. Sci. USA, 84*(10), 3457-3461.

Cunningham, B. C., & Wells, J. A. (1993). Comparison of a structural and a functional epitope. *J. Mol. Biol., 234*, 554-563.

Dautry-Varsat, A., Ciechanover, A., & Lodish, H. F. (1983). pH and the recycling of transferrin during receptor-mediated endocytosis. *Proc. Natl. Acad. Sci. USA, 80*(8), 2258-2262.

Davies, P. S., & Enns, C. A. (2004). Expression of the hereditary hemochromatosis protein, HFE, increases ferritin levels by inhibiting iron export in HT29 cells. *J. Biol. Chem.*

Davies, P. S., Zhang, A. S., Anderson, E. L., Roy, C. N., Lampson, M. A., McGraw, T. E., & Enns, C. A. (2003). Evidence for the interaction of the hereditary haemochromatosis protein, HFE, with the transferrin receptor in endocytic compartments. *Biochem. J., 373*(Pt 1), 145-153.

Donovan, A., Brownlie, A., Zhou, Y., Shepard, J., Pratt, S. J., Moynihan, J., Paw, B. H., Drejer, A., Barut, B., Zapata, A., Law, T. C., Brugnara, C., Lux, S. E., Pinkus, G. S., Pinkus, J. L., Kingsley, P. D., Palis, J., Fleming, M. D., Andrews, N. C., & Zon, L. I. (2000). Positional cloning of zebrafish ferroportin1 identifies a conserved vertebrate iron exporter. *Nature, 403*, 776-781.

Drakesmith, H., Sweetland, E., Schimanski, L., Edwards, J., Cowley, D., Ashraf, M., Bastin, J., & Townsend, A. R. (2002). The hemochromatosis protein HFE inhibits iron export from macrophages. *Proc. Natl. Acad. Sci. USA, 99*(24), 15602-15607.

Dubljevic, V., Sali, A., & Goding, A. (1999). A conserved RGD (Arg-Gly-Asp) motif in the transferrin receptor is required for binding to transferrin. *Biochem. J., 341*, 11-14.

Enns, C. A. (2002). The Transferrin Receptor. In D. M. Templeton (Ed.), *Molecular and Cellular Iron Transport* (pp. 71-94). New York, Basel: Marcel Dekker, Inc.

Enns, C. A., & Sussman, H. H. (1981). Physical characterization of the transferrin receptor in human placentae. *J. Biol. Chem., 256*, 9820-9823.

Feder, J. N., Gnirke, A., Thomas, W., Zsuchihashi, Z., Ruddy, D. A., Basava, A., Dormishian, F., Domingo, R., Ellis, M. C., Fullan, A., Hinton, L. M., Jones, N. L., Kimmel, B. E., Kronmal, G. S., Lauer, P., Lee, V. K., Loeb, D. B., Mapa, F. A., McCellland, E.,

Meyer, N. C., Mintier, G. A., Moeller, N., Moore, T., Morikang, E., Prass, C. E., Quintana, L., Starnes, S. M., Schatzman, R. C., Brunke, K. J., Drayna, D. T., Risch, N. J., Bacon, B. R., & Wolff, R. K. (1996). A novel MHC class I-like gene is mutated in patients with hereditary haemochromatosis. *Nature Genetics, 13*, 399-408.

Feder, J. N., Penny, D. M., Irrinki, A., Lee, V. K., Lebrón, J. A., Watson, N., Tsuchihashi, Z., Sigal, E., Bjorkman, P. J., & Schatzman, R. C. (1998). The hemochromatosis gene product complexes with the transferrin receptor, and lowers its affinity for ligand binding. *Proc. Natl. Acad. Sci. USA, 95*, 1472-1477.

Feder, J. N., Tsuchihashi, Z., Irrinki, A., Lee, V. K., Mapa, F. A., Morikang, E., Prass, C. E., Starnes, S. M., Wolff, R. K., Parkkila, S., Sly, W. S., & Schatzman, R. C. (1997). The hemochromatosis founder mutation in HLA-H disrupts ß2-microglobulin interaction and cell surface expression. *J. Biol. Chem., 272*, 14025-14028.

Feeney, G. P., & Worwood, M. (2001). The effects of wild-type and mutant HFE expression upon cellular iron uptake in transfected human embryonic kidney cells. *Biochim. Biophys. Acta, 1538*(2-3), 242-251.

Fisher, M., Gokhman, I., Pick, U., & Zamir, A. (1997). A structurally novel transferrin-like protein accumulates in the plasma membrane of the unicellular green alga Dunaliella salina grown in high salinities. *J. Biol. Chem., 272*(3), 1565-1570.

Fleming, R. E., Ahmann, J. R., Migas, M. C., Waheed, A., Koeffler, H. P., Kawabata, H., Britton, R. S., Bacon, B. R., & Sly, W. S. (2002). Targeted mutagenesis of the murine transferrin receptor-2 gene produces hemochromatosis. *Proc. Natl. Acad. Sci. USA, 99*(16), 10653-10658.

Fleming, R. E., & Sly, W. S. (2001). Ferroportin mutation in autosomal dominant hemochromatosis: loss of function, gain in understanding. *J. Clin. Invest., 108*(4), 521-522.

Frazer, D. M., & Anderson, G. J. (2003). The orchestration of body iron intake: how and where do enterocytes receive their cues? *Blood Cells Mol. Dis., 30*(3), 288-297.

Garcia, K. C., Teyton, L., & Wilson, I. A. (1999). Structural basis of T cell recognition. *Annu. Rev. Immunol., 17*, 369-397.

Gerstein, M., Anderson, B. F., Norris, G. E., Baker, E. N., Lesk, A. M., & Chothia, C. (1993). Domain closure in lactoferrin. Two hinges produce a see-saw motion between alternative close-packed interfaces. *J. Mol. Biol,. 234*(2), 357-372.

Giannetti, A. M., & Bjorkman, P. J. (2004). HFE and transferrin directly compete for transferrin receptor in solution and at the cell surface. *J. Biol. Chem.*, M401467200.

Giannetti, A. M., Snow, P. M., Zak, O., & Bjorkman, P. J. (2003). Mechanism for multiple ligand recognition by the human transferrin receptor. *PLoS Biol., 1*(3), 341-350.

Gitlin, J. D. (1998). Aceruloplasminemia. *Pediatr. Res., 44*(3), 271-276.

Gross, C. N., Irrinki, A., Feder, J. N., & Enns, C. A. (1998). Co-trafficking of HFE, a non-classical major histocompatibility complex class I protein, with the transferrin receptor implies a role in intracellular iron regulation. *J. Biol. Chem., 273*, 22068-22074.

Groves, J. T. (2003). The bioinorganic chemistry of iron in oxygenases and supramolecular assemblies. *Proc. Natl. Acad. Sci. USA, 100*(7), 3569-3574.

Gunshin, H., Mackenzie, B., Berger, U. V., Gunshin, Y., Romero, M. F., Boron, W. F., Nussberger, S., Gollan, J. L., & Hediger, M. A. (1997). Cloning and characterization of a mammalian proton-coupled metal ion transporter. *Nature, 388*, 482-488.

Halliwell, B., & Gutteridge, J. M. (1990). Role of free radicals and catalytic metal ions in human disease: an overview. *Methods Enzymol., 186*, 1-85.

Hanson, E. H., Imperatore, G., & Burke, W. (2001). HFE gene and hereditary hemochromatosis: a HuGE review. Human Genome Epidemiology. *Am J Epidemiol, 154*(3), 193-206.

Hayashi, A., Wada, Y., Suzuki, T., & Shimizu, A. (1993). Studies on familial hypotransferrinemia: unique clinical course and molecular pathology. *Am. J. Hum. Genet., 53*(1), 201-213.

He, Q.-Y., Mason, A.B. (2002). Molecular aspects of release of iron from transferrin. In D. M. Templeton (Ed.), *Molecular and Cellular Iron Transport* (pp. 95-124). New York, Basel: Marcel Dekker.

Henry, J. B. (1991). *Clinical Diagnosis and Management by Laboratory Methods*. Philadelphia: W.B. Saunders Co.

Holland, H. D. (1984). *The chemical evolution of the atmosphere and oceans*. Princeton, N.J.: Princeton University Press.

Jamroz, R. C., Gasdaska, J. R., Bradfield, J. Y., & Law, J. H. (1993). Transferrin in a cockroach: molecular cloning, characterization, and suppression by juvenile hormone. *Proc. Natl. Acad. Sci. USA, 90*(4), 1320-1324.

Jordan, A., & Reichard, P. (1998). Ribonucleotide reductases. *Annu. Rev. Biochem., 67*, 71-98.

Jouanolle, A. M., Douabin-Gicquel, V., Halimi, C., Loreal, O., Fergelot, P., Delacour, T., de Lajarte-Thirouard, A. S., Turlin, B., Le Gall, J. Y., Cadet, E., Rochette, J., David, V., & Brissot, P. (2003). Novel mutation in ferroportin 1 gene is associated with autosomal dominant iron overload. *J. Hepatol., 39*(2), 286-289.

Junod, S. (2001, 2001-Dec-28). *Folic Acid Fortification: Fact and Folly*, 2004, from http://www.fda.gov/oc/history/makinghistory/folicacid.html

Jurado, R. L. (1997). Iron, infections, and anemia of inflammation. *Clin. Infect. Dis., 25*(4), 888-895.

Kawabata, H., Yang, R., Hirama, T., Vuong, P. T., Kawano, S., Gombart, A. F., & Koeffler, H. P. (1999). Molecular cloning of transferrin receptor 2. A new member of the transferrin receptor-like family. *J. Biol. Chem., 274*(30), 20826-20832.

Knutson, M., & Wessling-Resnick, M. (2003). Iron metabolism in the reticuloendothelial system. *Crit. Rev. Biochem. Mol. Biol., 38*(1), 61-88.

Kurokawa, H., Dewan, J. C., Mikami, B., Sacchettini, J. C., & Hirose, M. (1999). Crystal structure of hen apo-ovotransferrin. Both lobes adopt an open conformation upon loss of iron. *J. Biol. Chem., 274*, 28445-28452.

Kurokawa, H., Mikami, B., & Hirose, M. (1995). Crystal structure of diferric hen ovotransferrin at 2.4 Å resolution. *J. Mol. Biol., 254*, 196-207.

Lange, S. J., & Que, L., Jr. (1998). Oxygen activating nonheme iron enzymes. *Curr. Opin. Chem. Biol., 2*(2), 159-172.

Lanzara, C., Roetto, A., Daraio, F., Rivard, S., Ficarella, R., Simard, H., Cox, T., Cazzola, M., Piperno, A., Gimenez-Roqueplo, A. P., Grammatico, P., Volinia, S., Gasparini, P., & Camaschella, C. (2004). The spectrum of hemojuvelin gene mutations in 1q-linked juvenile hemochromatosis. *Blood, 103*(11), 4317-4321.

Lawrence, C. M., Ray, S., Babyonyshev, M., Galluser, R., Borhani, D. W., & Harrison, S. C. (1999). Structure of the ectodomain of human transferrin receptor. *Science, 286*, 779-782.

Lebrón, J. A., Bennett, M. J., Vaughn, D. E., Chirino, A. J., Snow, P. M., Mintier, G. A., Feder, J. N., & Bjorkman, P. J. (1998). Crystal structure of the hemochromatosis protein HFE and characterization of its interaction with transferrin receptor. *Cell, 93*, 111-123.

Lebrón, J. A., & Bjorkman, P. J. (1999). The transferrin receptor binding site on HFE, the class I MHC-related protein mutated in hereditary hemochromatosis. *J. Mol. Biol., 289*, 1109-1118.

Lebrón, J. A., West, A. P., & Bjorkman, P. J. (1999). The hemochromatosis protein HFE competes with transferrin for binding to the transferrin receptor. *J. Mol. Biol., 294*, 239-245.

Lee, P. L., Beutler, E., Rao, S. V., & Barton, J. C. (2004). Genetic abnormalities and juvenile hemochromatosis: mutations of the HJV gene encoding hemojuvelin. *Blood*.

Leibman, A., & Aisen, P. (1977). Transferrin receptor of the rabbit reticulocyte. *Biochemistry, 16*(7), 1268-1272.

Leibman, A., & Aisen, P. (1979). Distribution of iron between the binding sites of transferrin in serum: methods and results in normal human subjects. *Blood, 53*(6), 1058-1065.

Levy, J. E., Jin, O., Fujiwara, Y., Kuo, F., & Andrews, N. C. (1999). Transferrin receptor is necessary for development of erythrocytes and the nervous system. *Nat. Genet., 21*(4), 396-399.

McGraw, T. E., Greenfield, L., & Maxfield, F. R. (1987). Functional expression of the human transferrin receptor cDNA in Chinese hamster ovary cells deficient in endogenous transferrin receptor. *J. Cell. Biol., 105*(1), 207-214.

McKie, A. T., Barrow, D., Latunde-Dada, G. O., Rolfs, A., Sager, G., Mudaly, E., Mudaly, M., Richardson, C., Barlow, D., Bomford, A., Peters, T. J., Raja, K. B., Shirali, S., Hediger, M. A., Farzaneh, F., & Simpson, R. J. (2001). An iron-regulated ferric reductase associated with the absorption of dietary iron. *Science, 291*(5509), 1755-1759.

McKie, A. T., Marciani, P., Rolfs, A., Brennan, K., Wehr, K., Barrow, D., Miret, S., Bomford, A., Peters, T. J., Farzaneh, F., Hediger, M. A., Hentze, M. W., & Simpson, R. J. (2000). A Novel Duodenal Iron-Regulated Transporter, IREG1, Implicated in the Basolateral Transfer of Iron to the Circulation. *Molecular Cell, 5*, 299-309.

Montosi, G., Donovan, A., Totaro, A., Garuti, C., Pignatti, E., Cassanelli, S., Trenor, C. C., Gasparini, P., Andrews, N. C., & Pietrangelo, A. (2001). Autosomal-dominant hemochromatosis is associated with a mutation in the ferroportin (SLC11A3) gene. *J. Clin. Invest., 108*(4), 619-623.

Nakamasu, K., Kawamoto, T., Shen, M., Gotoh, O., Teramoto, M., Noshiro, M., & Kato, Y. (1999). Membrane-bound transferrin-like protein (MTf): structure, evolution and selective expression during chondrogenic differentiation of mouse embryonic cells. *Biochim. Biophys. Acta, 1447*(2-3), 258-264.

Nicolas, G., Bennoun, M., Devaux, I., Beaumont, C., Grandchamp, B., Kahn, A., & Vaulont, S. (2001). Lack of hepcidin gene expression and severe tissue iron overload in upstream stimulatory factor 2 (USF2) knockout mice. *Proc. Natl. Acad. Sci. USA, 98*(15), 8780-8785.

Olivieri, N. F. (1999). The beta-thalassemias. *N. Engl. J. Med., 341*(2), 99-109.

Osaki, S., & Johnson, D. A. (1969). Mobilization of liver iron by ferroxidase (ceruloplasmin). *J. Biol. Chem., 244*(20), 5757-5758.

Palermo, L. M., Hueffer, K., & Parrish, C. R. (2003). Residues in the apical domain of the feline and canine transferrin receptors control host-specific binding and cell infection of canine and feline parvoviruses. *J. Virol., 77*(16), 8915-8923.

Papanikolaou, G., Samuels, M. E., Ludwig, E. H., MacDonald, M. L., Franchini, P. L., Dube, M. P., Andres, L., MacFarlane, J., Sakellaropoulos, N., Politou, M., Nemeth, E., Thompson, J., Risler, J. K., Zaborowska, C., Babakaiff, R., Radomski, C. C., Pape, T. D., Davidas, O., Christakis, J., Brissot, P., Lockitch, G., Ganz, T., Hayden, M. R., & Goldberg, Y. P. (2004). Mutations in HFE2 cause iron overload in chromosome 1q-linked juvenile hemochromatosis. *Nat. Genet., 36*(1), 77-82.

Park, I., Schaeffer, E., Sidoli, A., Baralle, F. E., Cohen, G. N., & Zakin, M. M. (1985). Organization of the human transferrin gene: direct evidence that it originated by gene duplication. *Proc. Natl. Acad. Sci. USA, 82*(10), 3149-3153.

Parkkila, S., Waheed, A., Britton, R. S., Bacon, B. R., Zhou, X. Y., Tomatsu, S., Fleming, R. E., & Sly, W. S. (1997). Association of the transferrin receptor in human placenta with HFE, the protein defective in hereditary hemochromatosis. *Proc. Natl. Acad. Sci. USA, 94*(24), 13198-13202.

Posey, J. E., & Gherardini, F. C. (2000). Lack of a role for iron in the Lyme disease pathogen. *Science, 288*(5471), 1651-1653.

Radisky, D. C., Babcock, M. C., & Kaplan, J. (1999). The yeast frataxin homologue mediates mitochondrial iron efflux. Evidence for a mitochondrial iron cycle. *J. Biol. Chem., 274*(8), 4497-4499.

Richardson, D. R., & Ponka, P. (1997). The molecular mechanisms of the metabolism and transport of iron in normal and neoplastic cells. *Biochim. Biophys. Acta, 1331*, 1-40.

Riedel, H. D., Muckenthaler, M. U., Gehrke, S. G., Mohr, I., Brennan, K., Herrmann, T., Fitscher, B. A., Hentze, M. W., & Stremmel, W. (1999). HFE downregulates iron uptake from transferrin and induces iron-regulatory protein activity in stably transfected cells. *Blood, 94*, 3915-3921.

Rivard, S. R., Lanzara, C., Grimard, D., Carella, M., Simard, H., Ficarella, R., Simard, R., D'Adamo, A. P., De Braekeleer, M., & Gasparini, P. (2003). Autosomal dominant reticuloendothelial iron overload (HFE type 4) due to a new missense mutation in the FERROPORTIN 1 gene (SLC11A3) in a large French-Canadian family. *Haematologica, 88*(7), 824-826.

Roetto, A., Merryweather-Clarke, A. T., Daraio, F., Livesey, K., Pointon, J. J., Barbabietola, G., Piga, A., Mackie, P. H., Robson, K. J., & Camaschella, C. (2002). A valine deletion of ferroportin 1: a common mutation in hemochromastosis type 4. *Blood, 100*(2), 733-734.

Roetto, A., Totaro, A., Cazzola, M., Cicilano, M., Bosio, S., D'Ascola, G., Carella, M., Zelante, L., Kelly, A. L., Cox, T. M., Gasparini, P., & Camaschella, C. (1999). Juvenile hemochromatosis locus maps to chromosome 1q. *Am. J. Hum. Genet., 64*(5), 1388-1393.

Rothenberger, S., Iacopetta, B. J., & Kuhn, L. C. (1987). Endocytosis of the transferrin receptor requires the cytoplasmic domain but not its phosphorylation site. *Cell, 49*(3), 423-431.

Roy, C. N., Carlson, E. J., Anderson, E. L., Basava, A., Starnes, S. M., Feder, J. N., & Enns, C. A. (2000). Interactions of the ectodomain of HFE with the transferrin receptor are critical for iron homeostasis in cells. *FEBS Lett., 484*(3), 271-274.

Roy, C. N., Penny, D. M., Feder, J. N., & Enns, C. A. (1999). The hereditary hemochromatosis protein, HFE, specifically regulates Tf-mediated iron uptake in HeLa cells. *J. Biol. Chem., 274*, 9022-9028.

Rutledge, E. A., & Enns, C. A. (1996). Cleavage of the transferrin receptor is influenced by the composition of the O-linked carbohydrate at position 104. *J. Cell. Physiol., 168*(2), 284-293.

Rutledge, E. A., Green, F. A., & Enns, C. A. (1994). Generation of the soluble transferrin receptor requires cycling through an endosomal compartment. *J. Biol. Chem., 269*(50), 31864-31868.

Rutledge, E. A., Root, B. J., Lucas, J. J., & Enns, C. A. (1994). Elimination of the O-linked glycosylation site at Thr 104 results in the generation of a soluble human-transferrin receptor. *Blood, 83*(2), 580-586.

Salter-Cid, L., Brunmark, A., Li, Y., Leturcq, D., Peterson, P. A., Jackson, M. R., & Yang, Y. (1999). Transferrin receptor is negatively modulated by the hemochromatosis protein HFE: implications for cellular iron homeostasis. *Proc. Natl. Acad. Sci. USA, 96*, 5434-5439.

Savary, S., Allikmets, R., Denizot, F., Luciani, M. F., Mattei, M. G., Dean, M., & Chimini, G. (1997). Isolation and chromosomal mapping of a novel ATP-binding cassette transporter conserved in mouse and human. *Genomics, 41*(2), 275-278.

Schade A.L., C., L.,. (1946). An iron-binding component in human blood plasma. *Science, 104*, 340-341.

Schmid, S. L. (1992). The mechanism of receptor-mediated endocytosis: more questions than answers. *Bioessays, 14*(9), 589-596.

Schreier, H., Moran, P., & Caras, W. I. (1994). Targeting of liposomes to cells expressing CD4 using glycophosphatidylinositol-anchored gp120. *J. Biol. Chem., 269*, 9090-9098.

Schrieber, W. E. (1989). Iron, porphyrin, and bilirubin metabolism. In L. A. K. a. A. J. Pesce (Ed.), *Clinical Chemistry: Theory, analysis, and correlation* (pp. 496-511). St. Louis: The C.V. Mosby Company.

Sheth, S., & Brittenham, G. M. (2000). Genetic disorders affecting proteins of iron metabolism: clinical implications. *Annu. Rev. Med., 51*, 443-464.

Silver, J. (1993). *Chemistry of iron* (1st ed.). London ; New York: Blackie Academic & Professional.

Stamatoyannopoulos, G. (1994). *The molecular basis of blood diseases* (2nd ed. ed.). Philadelphia: W.B. Saunders.

Theil, E. C. (1994). Iron regulatory elements (IREs): a family of mRNA non-coding sequences. *Biochem. J., 304 (Pt 1)*, 1-11.

Tomatsu, S., Orii, K. O., Fleming, R. E., Holden, C. C., Waheed, A., Britton, R. S., Gutierrez, M. A., Velez-Castrillon, S., Bacon, B. R., & Sly, W. S. (2003). Contribution of the H63D mutation in HFE to murine hereditary hemochromatosis. *Proc. Natl. Acad. Sci. USA, 100*(26), 15788-15793.

Turkewitz, A. P., Amatruda, J. F., Borhani, D., Harrison, S. C., & Schwartz, A. L. (1988). A high yield purification of the human transferrin receptor and properties of its major extracellular fragment. *J. Biol. Chem., 263*, 8318-8325.

Vulpe, C. D., Kuo, Y. M., Murphy, T. L., Cowley, L., Askwith, C., Libina, N., Gitschier, J., & Anderson, G. J. (1999). Hephaestin, a ceruloplasmin homologue implicated in intestinal iron transport, is defective in the sla mouse. *Nat. Genet., 21*(2), 195-199.

Waalen, J., Felitti, V., Gelbart, T., Ho., N.J., Beutler, I. (2001). Penetrance of Hemochromatosis. *Blood, Cells, Molecules, and Diseases*, *29(3)*, 118-132.

Waheed, A., Grubb, J. H., Zhou, X. Y., Tomatsu, S., Fleming, R. E., Costaldi, M. E., Britton, R. S., Bacon, B. R., & Sly, W. S. (2002). Regulation of transferrin-mediated iron uptake by HFE, the protein defective in hereditary hemochromatosis. *Proc. Natl. Acad. Sci. USA, 99*(5), 3117-3122.

Waheed, A., Parkkila, S., Zhou, X. Y., Tomatsu, S., Tsuchihashi, Z., Feder, J. N., Schatzman, R. C., Britton, R. S., Bacon, B. R., & Sly, W. S. (1997). Hereditary hemochromatosis: effects of C282Y and H63D mutations on association with b2-microglobulin, intracellular processing, and cell surface expression of the HFE protein in COS-7 cells. *Proc. Natl. Acad. Sci. USA, 94*, 12384-12389.

Wang, J., Chen, G., & Pantopoulos, K. (2003). The haemochromatosis protein HFE induces an apparent iron-deficient phenotype in H1299 cells that is not corrected by co-expression of beta 2-microglobulin. *Biochem. J., 370*(Pt 3), 891-899.

Weinberg, E. D. (1978). Iron and infection. *Microbiol. Rev., 42*(1), 45-66.

Weinstein, D. A., Roy, C. N., Fleming, M. D., Loda, M. F., Wolfsdorf, J. I., & Andrews, N. C. (2002). Inappropriate expression of hepcidin is associated with iron refractory anemia: implications for the anemia of chronic disease. *Blood, 100*(10), 3776-3781.

West, A. P., Bennett, M. J., Sellers, V. M., Andrews, N. C., Enns, C. A., & Bjorkman, P. J. (2000). Comparisons of the interactions of transferrin receptor and transferrin receptor 2 with transferrin and the hereditary hemochromatosis protein HFE. *J. Biol. Chem., 275*, 38135-38138.

West, A. P., Jr., Giannetti, A. M., Herr, A. B., Bennett, M. J., Nangiana, J. S., Pierce, J. R., Weiner, L. P., Snow, P. M., & Bjorkman, P. J. (2001). Mutational analysis of the transferrin receptor reveals overlapping HFE and transferrin binding sites. *J. Mol. Biol., 313*(2), 385-397.

Yang, J., Goetz, D., Li, J. Y., Wang, W., Mori, K., Setlik, D., Du, T., Erdjument-Bromage, H., Tempst, P., Strong, R., & Barasch, J. (2002). An iron delivery pathway mediated by a lipocalin. *Molecular Cell, 10*(5), 1045-1056.

Yu, J., & Wessling-Resnick, M. (1998). Structural and functional analysis of SFT, a stimulator of Fe Transport. *J. Biol. Chem., 273*(33), 21380-21385.

Zhou, B., Westaway, S. K., Levinson, B., Johnson, M. A., Gitschier, J., & Hayflick, S. J. (2001). A novel pantothenate kinase gene (PANK2) is defective in Hallervorden-Spatz syndrome. *Nat. Genet., 28*(4), 345-349.

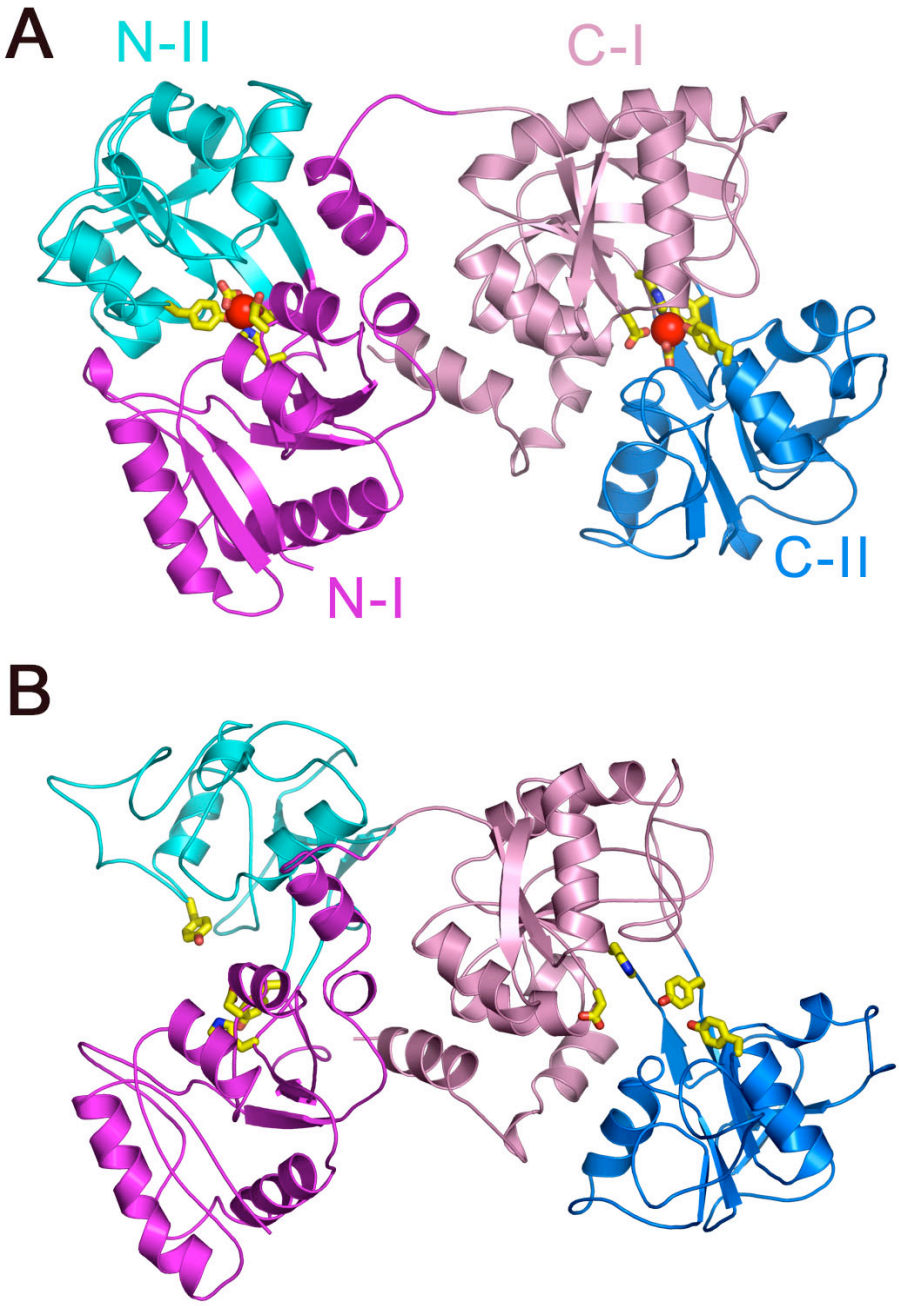

Figure 1. Ribbon diagrams of transferrin. A) Structure of di-ferric ovotransferrin (Kurokawa *et al.*, 1995) colored by domain as shown. Residues coordinating the iron atoms (red spheres) are shown as sticks and colored at atom type (yellow, carbon; blue, nitrogen; red, oxygen). (B) Structure of apo-ovotransferrin (Kurokawa *et al.*, 1999) as in (A) illustrating the large conformational change associated with iron release.

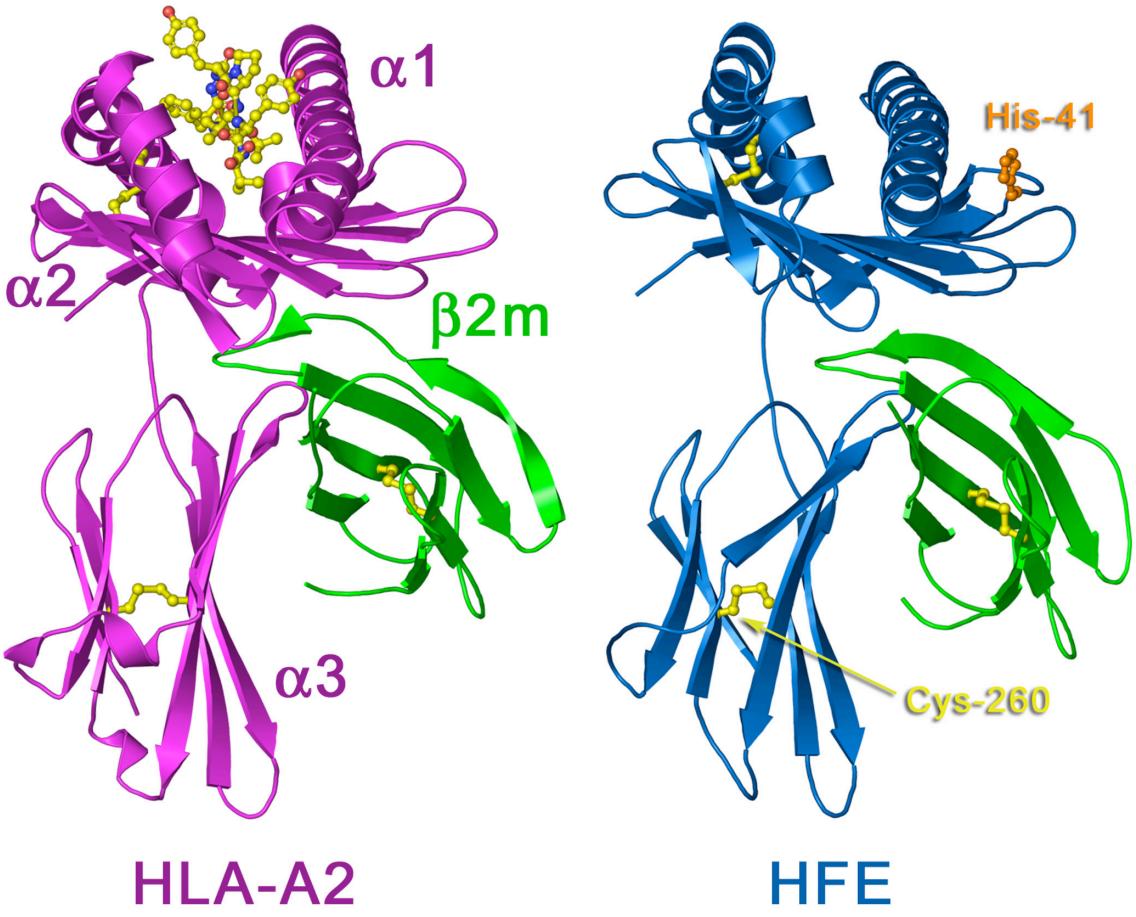

Figure 2: Comparison of the structures of a class I MHC molecule and HFE. HLA-A2 complexed with the tax peptide (Khan *et al.,* 2000) (PDB code: 1DUY) is shown with the various domains and light chain labeled. The peptide is shown as ball-and-sticks. The HFE molecule (Lebron *et al.,* 1998) (PDB code: 1A6Z) is shown for comparison. Residues that are mutated in hemochromatosis patients are indicated.

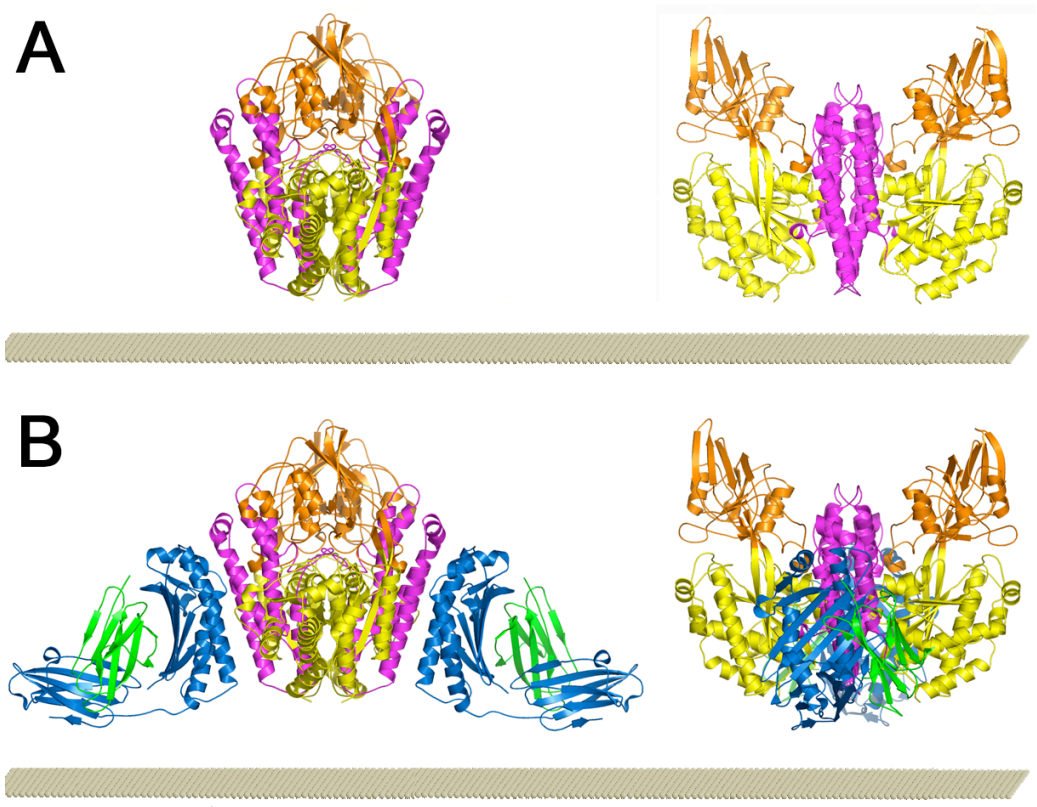

Figure 3. Schematic of the TfR alone (Lawrence *et al.,* 1999) or bound to HFE (Bennett *et al.*, 2000). The soluble domains are shown above a representation of the membrane (yellow). TfR is colored yellow (protease-like domain), orange (apical domain), and magenta (helical domain). The HFE molecules in (B) are colored blue (heavy chain) and green (light chain).

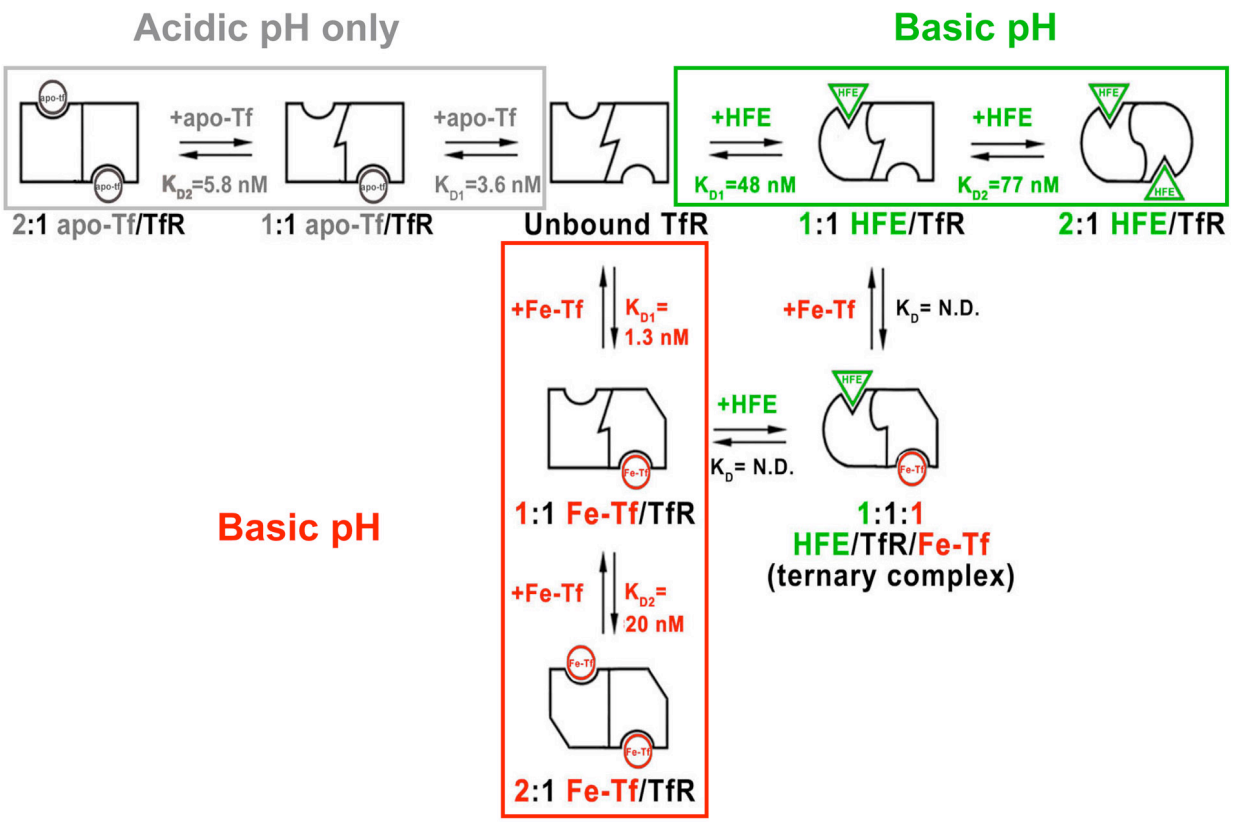

Figure 4: Equilibrium diagram of all possible stoichiometries formed by TfR with apo-Tf, Fe-Tf, and HFE with measured K_D values reported from (Giannetti *et al.,* 2003). HFE and apo-Tf exhibit pH dependence of binding and are colored separately. Fe-Tf binds well at both acidic and basic pH. The ternary complex can only form at basic pH. The K_D values for formation of the ternary complex cannot be determined and are labeled as N.D.

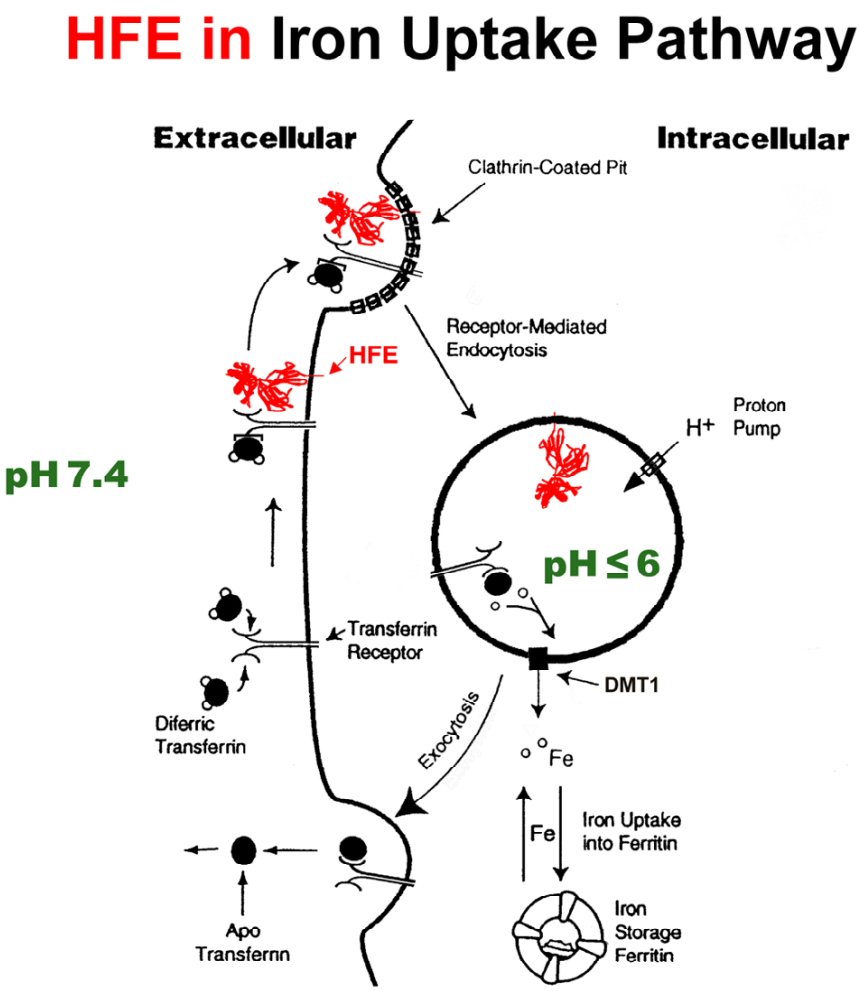

Figure 5: Model of TfR mediated uptake of Fe-Tf and HFE to acidic recycling endosomes. HFE and Fe-Tf can bind to TfR at the basic pH of the cell surface. Receptor mediated endocytosis translocates TfR and its cargo to acidic recycling endosomes where iron is released from Tf, shuttled through DMT1 to the cytosol where it is stored in ferritin. The endosome is recycled to the cell surface where apo-Tf dissociates. The fate of HFE is less clear. HFE is dependent on TfR binding for transport to endosomes (Giannetti and Bjorkman, 2004), but does not bind TfR in biochemical experiments at acidic pH and has been indicated to dissociate within the endosome, though some data suggests the two proteins may remain associated (Davies *et al.,* 2003).

Chapter 2:

The Mechanism for Multiple Ligand Recognition by the Transferrin Receptor

In this paper we report the mapping of the structural and functional binding epitopes for HFE, Fe-Tf and apo-Tf on the surface of TfR, as well as determine the orientation of Tf on the receptor. Peter Snow is director of Caltech's Protein Expression Facility and he generated baculovirus stocks and expressed the wild-type and mutant transferrin recepetors used in this study. Olga Zak produced the recombinant transferrin C-lobe we used to map the site of C-lobe specific contacts to TfR.

PLOS BIOLOGY

Mechanism for Multiple Ligand Recognition by the Human Transferrin Receptor

Anthony M. Giannetti[1], Peter M. Snow[2], Olga Zak[3], Pamela J. Björkman[4*]

1 Graduate Option in Biochemistry and Molecular Biophysics, California Institute of Technology, Pasadena, California, United States of America, **2** Caltech Protein Expression Center, Division of Biology, California Institute of Technology, Pasadena, California, United States of America, **3** Department of Physiology and Biophysics, Albert Einstein College of Medicine, Bronx, New York, United States of America, **4** Division of Biology and Howard Hughes Medical Institute, California Institute of Technology, Pasadena, California, United States of America

Transferrin receptor 1 (TfR) plays a critical role in cellular iron import for most higher organisms. Cell surface TfR binds to circulating iron-loaded transferrin (Fe-Tf) and transports it to acidic endosomes, where low pH promotes iron to dissociate from transferrin (Tf) in a TfR-assisted process. The iron-free form of Tf (apo-Tf) remains bound to TfR and is recycled to the cell surface, where the complex dissociates upon exposure to the slightly basic pH of the blood. Fe-Tf competes for binding to TfR with HFE, the protein mutated in the iron-overload disease hereditary hemochromatosis. We used a quantitative surface plasmon resonance assay to determine the binding affinities of an extensive set of site-directed TfR mutants to HFE and Fe-Tf at pH 7.4 and to apo-Tf at pH 6.3. These results confirm the previous finding that Fe-Tf and HFE compete for the receptor by binding to an overlapping site on the TfR helical domain. Spatially distant mutations in the TfR protease-like domain affect binding of Fe-Tf, but not iron-loaded Tf C-lobe, apo-Tf, or HFE, and mutations at the edge of the TfR helical domain affect binding of apo-Tf, but not Fe-Tf or HFE. The binding data presented here reveal the binding footprints on TfR for Fe-Tf and apo-Tf. These data support a model in which the Tf C-lobe contacts the TfR helical domain and the Tf N-lobe contacts the base of the TfR protease-like domain. The differential effects of some TfR mutations on binding to Fe-Tf and apo-Tf suggest differences in the contact points between TfR and the two forms of Tf that could be caused by pH-dependent conformational changes in Tf, TfR, or both. From these data, we propose a structure-based model for the mechanism of TfR-assisted iron release from Fe-Tf.

Introduction

Transferrin receptor 1 (TfR) is a homodimeric type II membrane protein that plays a critical role in the primary iron acquisition mechanism for all iron-requiring cell types in vertebrates (Enns 2002). TfR binds the serum iron-carrier protein transferrin (Fe-Tf) and imports it to acidic endosomes, where iron is released and transported to the cytosol. The complex between TfR and iron-free transferrin (apo-Tf) is then recycled to the cell surface where apo-Tf dissociates and returns to circulation (reviewed in Enns et al. 1996). TfR also binds the hereditary hemochromatosis protein HFE (Parkkila et al. 1997; Feder et al. 1998). HFE is a class I major histocompatibility complex (MHC)-related protein that is mutated in patients with hereditary hemochromatosis (Feder et al. 1996), an iron-storage disease characterized by excessive iron absorption leading to an accumulation of iron principally in the liver, heart, pancreas, parathyroid, and pituitary gland, leading to tissue damage (Cullen et al. 1999).

The X-ray crystal structures of the human TfR ectodomain, both alone (Lawrence et al. 1999) and in complex with HFE (Bennett et al. 2000), have been reported. The homodimeric TfR ectodomain contains three domains on each polypeptide chain: a protease-like domain resembling amino- and carboxypeptidases (residues 121–188 and 384–606), an apical domain (residues 189–383), and a helical domain involved in TfR homodimerization (residues 607–760). Intact TfR also includes a glycosylated stalk region (residues 90–120), a transmembrane domain (residues 62–89), and an N-terminal cytoplasmic domain (residues 1–61) that includes a tyrosine-based endosomal sorting sequence (YTRF) (Enns 2002). The structure of a 2:1 HFE/TfR complex (two HFEs bound to a homodimeric TfR) shows that each HFE interacts with helices 1 and 3 of the TfR helical domain (Bennett et al. 2000) (Figure 1A and 1B). The central portion of the interface includes a hydrophobic core consisting of TfR residues Leu619, Val622, and Tyr643 packed against hydrophobic residues from the α1 domain helix of HFE.

The structures of various transferrins (Tfs) and related proteins such as lactoferrin have been studied extensively by X-ray crystallography (Bailey et al. 1988; Anderson et al. 1989; Gerstein et al. 1993; Zuccola 1993; Kurokawa et al. 1995, 1999; Baker et al. 1998; Karthikeyan et al. 1999). Tf and its relatives are single-chain molecules consisting of two similarly folded lobes (the N- and C-lobes), each of which contains two domains (NI and NII in the N-lobe; CI and CII in the C-lobe). Diferric Tf (Fe-Tf) contains two iron atoms, each held in a cleft between the domains of each lobe. Transition between the ferric and iron-free states of Tf involves significant conformational changes (Grossmann et al. 1992, 1993). Specifically, loss of iron results in a 54°–63° rotation between the two domains that comprise each lobe (Gerstein et al.

Received July 15, 2003; Accepted September 10, 2003; Published December 22, 2003
DOI: 10.1371/journal.pbio.0000051

Abbreviations: apo-Tf, iron-free transferrin; Fe-C-lobe, iron-loaded transferrin C-lobe; Fe-Tf, diferric transferrin; HFE, hereditary hemochromatosis protein; K_D, equilibrium dissociation constant; MHC, major histocompatibility complex; PIPES, piperazine-1,4-bis(2-ethanesulphonic) acid; RU, resonance unit; Tf, transferrin; TfR, transferrin receptor

Academic Editor: Janet Thornton, European Bioinformatics Institute

*To whom correspondence should be addressed. E-mail: bjorkman@caltech.edu

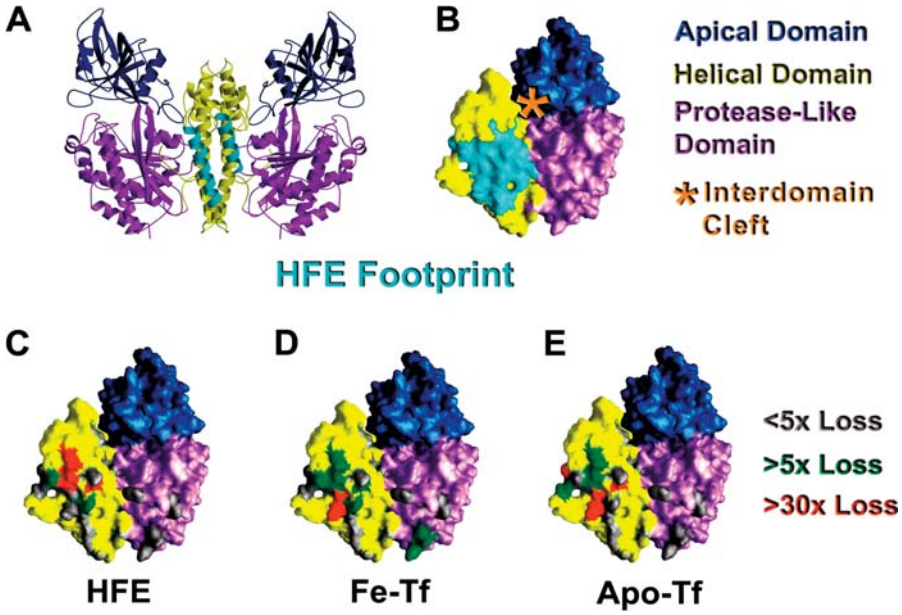

Figure 1. TfR Structure

(A) Ribbon diagram of TfR homodimer derived from the 3.2 Å structure of TfR (Lawrence et al. 1999). The HFE-binding site (deduced from an analysis using the HFE/TfR co-crystal structure [Bennett et al. 2000]) on the TfR helical domain closest to the viewer is highlighted in cyan.

(B) Space-filling representation of one chain from the TfR homodimer, with the HFE structural epitope residues highlighted as in (A). The location of the interdomain cleft is indicated by an orange asterisk.

(C–E) Summary of effects of TfR substitutions for binding HFE (C), Fe-Tf (D), and apo-Tf (E). Color-coding of the TfR sidechains designates the effects of the substitutions on binding affinities as indicated.

Figures were made with Molscript (Kraulis 1991) or GRASP (Nicholls et al. 1993) and rendered with Raster3D (Merritt and Bacon 1997).

DOI: 10.1371/journal.pbio.0000051.g001

1993). Additionally, the interface between the lobes repacks, exposing previously buried residues and burying previously exposed residues (Kurokawa et al. 1999). In vivo, these conformational changes presumably take place while Tf is bound to TfR, as the two proteins remain complexed throughout endocytosis and recycling (Dautry-Varsat et al. 1983).

Free Fe-Tf releases iron at acidic pH, but binding to TfR affects the iron release at both basic and acidic pH (Bali and Aisen 1991, 1992; Bali et al. 1991). At pH 7.4, iron release from Fe-Tf bound to TfR is slower than from free Fe-Tf. At low pH, the opposite effect is observed, such that binding to TfR significantly increases the iron-release rate (Bali and Aisen 1991, 1992; Bali et al. 1991; Sipe and Murphy 1991). Attempts to determine the mechanism by which TfR mediates these effects on the iron release rate have been hampered by a lack of detailed knowledge of the binding footprints of Fe-Tf and apo-Tf on TfR and by the unavailability of crystal structures of Fe-Tf or apo-Tf bound to TfR.

Although the structural details of the interaction between Tf and TfR remain unknown, early studies established that two Tf molecules bind to each TfR homodimer (Enns and Sussman 1981) by primarily interacting with what is now structurally defined as the TfR helical domain (Buchegger et al. 1996). A subsequent mutagenesis study further localized the binding site to include a conserved RGD sequence (residues 646–648) within the TfR helical domain (Dubljevic et al. 1999). The HFE/TfR co-crystal structure revealed that HFE directly contacts TfR residues 646 and 648 (Bennett et al. 2000), which is consistent with biochemical inhibition studies that suggested that HFE and Tf bind to the same or an overlapping site on TfR (Lebrón et al. 1999). As Fe-Tf is a large protein (approximately 90Å × 50Å × 40 Å, measured using the structure of iron-bound ovo-Tf [Kurokawa et al. 1995]), the remainder of the Tf contact site on TfR could include other TfR domains, the TfR interdomain cleft, or both (Figure 1B), as previously suggested (Lawrence et al. 1999). A subsequent mutagenesis study sought to identify other Tf-contacting residues on TfR (West et al. 2001). In that study, residues identified from the HFE/TfR co-crystal structure as involved in contacting HFE were mutated, and their effects on binding to HFE and Fe-Tf were quantitatively evaluated. These experiments identified several residues within the TfR helical domain that are involved in binding to each protein (defined as a substitution producing a greater than or equal to 5-fold reduction in binding affinity) and confirmed that the Fe-Tf- and HFE-binding sites on TfR overlap. However, the larger size of Tf relative to the HFE ectodomain (679 amino acids in Tf compared with 374 for the HFE/β_2-microglobulin ectodomain) suggested that Fe-Tf could contact residues outside of the TfR helical domain. Also, the effects of the TfR substitutions on binding to apo-Tf were not evaluated; thus, the question of whether Fe-Tf and apo-Tf bind differently to TfR was not addressed.

We therefore sought to expand the library of TfR mutants to more extensively map the Fe-Tf interface and to compare the effects of TfR mutants for binding to Fe-Tf versus apo-Tf. Here we report the affinities of 30 mutants of human TfR for binding to HFE and Fe-Tf at pH 7.5 and to apo-Tf at pH 6.3. As expected, the most important residues for Tf binding are located in the center of the TfR helical domain in the vicinity of critical residues for HFE binding. However, we also identified residues within the TfR protease-like domain that make significant contributions to binding of Fe-Tf, but not apo-Tf, to TfR. Conversely, substitution of residues at the edge of the TfR helical domain affects binding of apo-Tf, but not Fe-Tf. This information, together with the identification of common Fe-Tf- and apo-Tf-contacting residues within the helical domain, constrains the possible positions of Fe-Tf and apo-Tf on TfR, allowing for construction of structural models for the placement of the two forms of Tf on TfR. Our data also suggest a structural mechanism to explain TfR's role in the pH-dependent modulation of iron release rates from Fe-Tf.

Table 1. Comparison of the Binding Affinities of TfR Mutants for HFE and Fe-Tf at pH 7.5 and Apo-Tf at pH 6.3

Conservation of Residues in TfR and TfR2 Sequences	HFE Structural Epitope	Class	Mutant	HFE			Fe-Tf			Apo-Tf		
				K_{D1} (nM)	K_{D2} (nM)	K_{D1}, K_{D2} Relative to Wild-type	K_{D1} (nM)	K_{D2} (nM)	K_{D1}, K_{D2} Relative to Wild-type	K_{D1} (nM)	K_{D2} (nM)	K_{D1}, K_{D2} Relative to Wild-type
			Wt-TfR (n = 22)	32.5 ± 12.6	232.7 ± 99.7		0.72 ± 0.6	4.1 ± 1.4		3.6 ± 1.7	5.8 ± 4.3	
YFFYY-FYY	No	Hφ	Y123S	37.4	270.4	1.2, 1.2	6.1	116.2	8.3, 3.9	2.2	3.0	0.6, 0.5
WWWWW-WWW	No	Hφ	W124A	23.5	160.0	0.7, 0.7	11.1	469.5	15.4, 114.5	1.9	3.8	0.5, 0.7
DSTAA-PSS	No		D125K	27.8	176.0	0.9, 0.8	19.8	669.4	27.5, 165.3	2.4	10.2	0.7, 1.8
FFFYYYYYY	No	Hφ	F187A	12.7	122.5	0.4, 0.5	0.6	17.9	0.9, 0.6	1.6	4.7	0.4, 0.8
FFFFYYFRF	No	Hφ	F396A	23.8	105.7	0.7, 0.5	0.9	53.7	1.3, 1.8	1.3	7.8	0.4, 1.4
FSSPSYETT	No	Hφ	F521A	53.3	339.6	1.6, 1.5	0.8	14.3	1.1, 0.5	5.8	3.8	1.6, 0.7
YYYYYYLYY	No	Hφ	Y523S	52.9	386.9	1.6, 1.7	0.6	15.2	0.9, 0.5	4.2	8.5	1.1, 1.5
WWWWWWWDD	No	Hφ	W528A	75.7	411.2	2.3, 1.8	0.7	14.7	1.0, 0.5	4.3	5.9	1.2, 1.0
EEEEEEELL	No		E606K	25.5	208.0	0.8, 0.9	0.9	152.0	1.2, 5.2	2.9	8.7	0.8, 1.5
DNNDDDDDD	No		D610A	60.1	234.5	1.9, 1.0	1.1	68.5	1.5, 2.3	1.6	5.0	0.5, 0.9
LLLLLLLLL	Yes	H1	L619A §	N.B.		>800	9.7	217.0	13.4, 7.4	147.0	118.0	40.5, 20.3
VVVVMMQII	Yes	H1	V622A §	36.9	265.1	1.1, 1.1	0.4	5.6	0.5, 0.2	3.9	4.9	1.1, 0.8
RRRKKKEGG	Yes	H1	R623A §	159.5	1257.2	4.9, 5.4	0.4	9.8	0.5, 0.3	5.7	0.6	1.6, 0.1
RRRRKKISS	Yes	H2	R629A §	1773	29406	54.6, 126.3	3.8	140.0	5.3, 4.7	22.2	10.9	6.1, 1.9
QQQQQQDQQ	Yes	H3	Q640A §	364.5	3519.5	11.2, 15.1	0.7	11.9	0.9, 0.4	11.2	22.9	3.1, 3.9
WWWWWWWWW	Yes	H3	W641A §	127.4	1001.2	3.9, 4.3	0.7	15.6	0.9, 0.5	201.8	345.1	55.5, 59.5
YYYYYYFYY	Yes	H3	Y643A §	N.B.		>800	19.8	428.0	27.5, 14.5	100.9	29.0	27.8, 5.0
SSSSSSFSS	Yes	H3	S644A §	38.3	214.4	1.2, 0.9	2.5	69.9	3.5, 2.4	12.4	17.7	3.4, 3.0
GGGGGGGGG	Yes*	H3	G647A §	85.1	524.7	2.6, 2.3	160.3	2345	222.1, 79.4	1298.4	978.0	357.0, 168.7
FFFFFFQII	Yes	H3	F650A §	450.6	735.0	13.9, 3.2	4.9	109.0	6.8, 3.7	21.1	16.3	5.8, 2.8
RRRRRRRRR	Yes	H3	R651A	33.9	239.8	1.0, 1.0	1800	64800	>2800	N.B.		>3000
SSSSSSTEE	Yes	H3	S654A	25.4	212.0	0.8, 0.9	1.1	18.9	1.5, 0.6	7.5	5.6	2.1, 1.0
TTTTTTRQK	Yes	H3	T658A	53.6	427.6	1.7, 1.8	0.7	10.5	1.0, 0.4	5.1	9.6	1.4, 1.7
NNNNNNNSS	No	H3	N662A	75.1	599.6	2.3, 2.6	0.2	5.4	0.3, 0.2	2.9	0.02	0.8, .003
EEEEEEDEE	No	H3	E664A	51.6	373.2	1.6, 1.6	1.0	22.0	1.4, 0.8	2.4	5.7	0.7, 1.0
WWWWWWFML	No	Hφ	W702A	47.5	313.2	1.5, 1.4	0.4	6.2	0.6, 0.2	1.1	1.7	0.3, 0.3
PSPTSSRGG	No	IDC	P710R	55.9	415.0	1.7, 1.8	0.5	9.1	0.7, 0.3	1.9	5.5	0.5, 1.0
KKKKKRQRR	No	IDC	K717Q	16.9	128.0	0.5, 0.6	0.5	6.4	0.7, 0.2	4.9	18.3	1.3, 3.2
FFFFFFFFF	No	Hφ	F760A	72.8	572.2	2.2, 2.5	1.2	20.7	1.7, 0.7	56.3	183.1	15.5, 31.6
			Y123S/G647A	89.8	775.0	2.7, 3.3	N.B.		>14000	N.B.		>27000

For each substituted position, residues at that position in human and six other species of TfR—feline, canine, hamster, mouse, rat, and chicken—and two species of TfR2 (human and mouse) are listed in the first column.
The second column (HFE Structural Epitope) identifies TfR residues that are part of the crystallographically identified HFE structural epitope. Yes indicates that the residue contains an atom within 4 Å of HFE and No that all atoms of the residue are >4 Å from HFE. The asterisk indicates a glycine residue that is covered by HFE, but which lacks a sidechain and therefore does not contain atoms within 4 Å of HFE (Bennett et al. 2000).
The third column classifies substitutions as to their location or chemical character: HΦ, solvent-exposed hydrophobic residue; H1, H2, or H3, part of the HFE structural epitope on helix 1, 2, or 3 of the TfR helical domain; IDC, part of the TfR interdomain cleft.
The fourth column lists the name of the mutant. The § symbol denotes mutants that were also evaluated for HFE and Fe-Tf binding in previous experiments (West et al. 2001). Current results for these mutants agree closely with those reported previously (West et al. 2001). The K_Ds for wild-type TfR are averages derived from 22 independent measurements, and the numbers after the plus/minus sign represent standard deviations. Mutants with significant relative affinity reductions are highlighted (green, between 5-fold and 30-fold; red, greater than 30-fold). Mutants that showed no binding are labeled N.B. ΔΔG values were calculated from the mutant to wild-type affinity ratios and plotted for each mutant in the form of a histogram, shown in Figure S1.
DOI: 10.1371/journal.pbio.0000051.t001

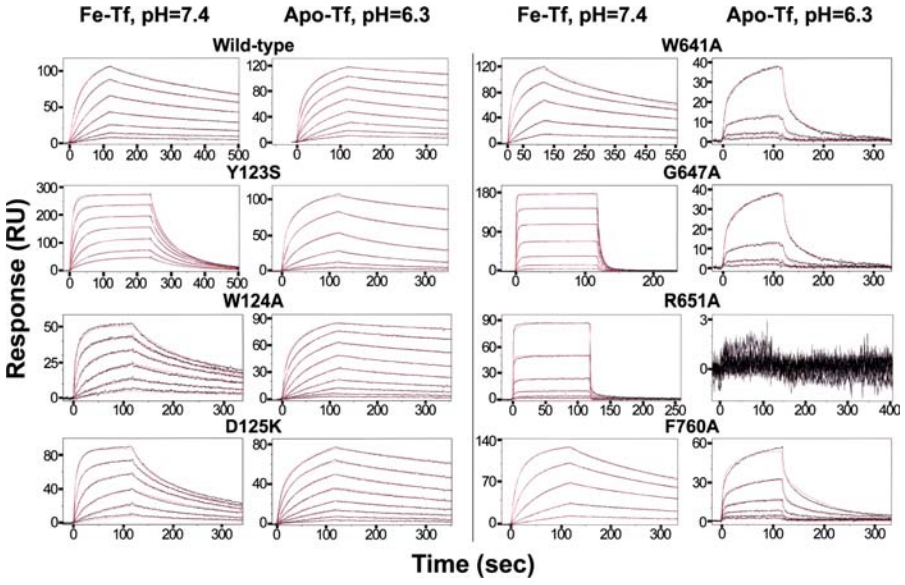

Figure 2. Biosensor Analyses of Tf Binding to Immobilized Wild-Type and Selected Mutant TfR Molecules

Sensorgrams (black lines) of injected Fe-Tf or apo-Tf binding to wild-type TfR (top left) or the indicated TfR mutants are shown with best-fit binding curves (red lines) derived from a bivalent ligand model (see Materials and Methods) superimposed. The sensorgrams demonstrate that the binding responses are concentration dependent, and the superimposed binding curves demonstrate the close fit of the binding model to the experimental data. Concentrations of injected proteins for each sensorgram are given below as two numbers: the first is the highest injected concentration (nM), and the second is the dilution factor, either 2-fold (2×) or 3-fold (3×), that relates successive injections. For each TfR sample, there are two sets of numbers, the first being for Fe-Tf and the second for apo-Tf. Wild-type (31, 2×; 200, 2×), Y123S (250, 2×; 330, 3×), W124A (2,000, 3×; 2,000, 2×), D125K (2,000, 3×; 1,000, 2×), W641A (110, 3×; 1,000, 3×), G647A (6,000, 3×; 780, 3×), R651A (5,000, 3×; 1,000, 3×), F760A (110, 3×; 270, 3×).

DOI: 10.1371/journal.pbio.0000051.g002

Results

Design of TfR Mutants

Our choice of TfR residues to substitute was guided by the crystal structures of TfR alone and bound to HFE (Lawrence et al. 1999; Bennett et al. 2000) and by a previous binding study involving ten TfR point mutants (West et al. 2001) (§ symbol in Table 1). Four substitutions at the HFE-binding site on the TfR helical domain (L619A, R629A, Y643A, and F650A) were found to significantly reduce (greater than or equal to 5-fold) the binding affinity for both HFE and Fe-Tf at pH 7.5, giving a first-order map of the Fe-Tf-binding site on TfR (West et al. 2001). In order to identify additional TfR residues critical for Fe-Tf binding and to evaluate their effects on apo-Tf binding, we extended our TfR mutant library to include an additional 20 mutants. The new set of mutations were chosen using three different strategies: (1) an alanine scan involving solvent-exposed residues on helix 3 of the helical domain (R651A, S654A, T658A, N662A, E664A) (classified as H3 in Table 1); (2) substitution of residues in the TfR interdomain cleft (see Figure 1B), suggested to be part of the Fe-Tf-binding site (Lawrence et al. 1999), for the residues of chicken TfR, which does not bind human Tf (Buchegger et al. 1996) (P710R, K717Q) (classified as IDC in Table 1); (3) mutation of large solvent-exposed hydrophobic residues, which often provide much of the free energy of binding in protein–protein interactions (Jones and Thornton 1996; Tsai et al. 1997; Lo Conte et al. 1999), throughout the remaining TfR surface area (Y123S, F187A, F396A, F521A, Y523S, W528A, W702A, F760A) (classified as Hφ in Table 1). A second generation of mutants was subsequently made to further define newly identified binding sites (W124A, D125K, E606K, D610A) and to test the effect of combining substitutions (Y123S/G647A). Mutants involving TfR residues known from the HFE/TfR crystal structure (Bennett et al. 2000) to contact HFE are denoted as part of the HFE structural epitope in Table 1.

TfR mutants were expressed as N-terminally 6x-His-tagged soluble ectodomains in baculovirus-infected cells, as previously described (Lebrón et al. 1998; West et al. 2001). In a previous TfR mutagenesis study, it was shown that mutants that had a strong effect on binding were properly folded as determined by comparison of their far-UV circular dichroism spectra and gel filtration profiles to that of wild-type TfR (West et al. 2001). In this study, we note that all of the newly made mutants retain wild-type or near wild-type binding affinities for at least one of the three TfR ligands tested (HFE, Fe-Tf, or apo-Tf) (Table 1), confirming their structural integrity.

Affinity Measurements and Analyses

Each of the TfR mutants designed in the current screen, plus the mutants from the previous study (West et al. 2001), were tested in a surface plasmon resonance-based assay for binding to either a soluble form of HFE at pH 7.5, Fe-Tf at pH 7.5, or apo-Tf at pH 6.3 (Table 1; Figure 2). For these experiments, filtered insect cell supernatants containing secreted recombinant TfR mutants were injected over a biosensor chip to which an anti-pentaHis antibody had been immobilized. The antibody captures TfR by binding to its two 6x-His tags, thereby allowing oriented coupling of the receptors to the biosensor chip. HFE, Fe-Tf, or apo-Tf was then injected over the antibody/TfR-coupled sensor chip, and binding data were fit to a bivalent ligand model in which equilibrium dissociation constants (K_{D1} and K_{D2}) were derived for binding to the first and the second binding sites on homodimeric TfR (see Table 1) (West et al. 2001).

Our previous mutagenesis study established that both the HFE- and Fe-Tf-binding sites on TfR include residues within helices 1 and 3 of the TfR helical domain (West et al. 2001) (see Figure 1A and 1B). In the present study, we tested the previously prepared TfR mutants for binding apo-Tf at pH 6.3 and re-evaluated their binding to HFE and Fe-Tf at pH 7.5. In agreement with the previous results, we found that two

mutants, L619A and Y643A, showed no detectable HFE binding and a significant (greater than or equal to 5-fold) decrease in Fe-Tf binding. These substitutions also significantly reduced apo-Tf binding at acidic pH. Two other mutants, R629A and Q640A, were again found to significantly reduce HFE binding and to have a relatively minor effect on Fe-Tf binding (R629A) or no significant effect (Q640A). The effects of these substitutions on apo-Tf binding correlated with their effects on Fe-Tf binding. Likewise, the F650A mutant, which shows a moderate reduction in binding affinity for both HFE and Fe-Tf, also shows a reduced affinity for binding apo-Tf. Only one of the previously analyzed mutants, G647A, exhibited a major (greater than 100-fold) reduction in Fe-Tf binding affinity, and the present analysis reveals that it has a similar effect on apo-Tf binding. Interestingly, one of the previously analyzed mutants, W641A, which does not significantly affect HFE or Fe-Tf binding at pH 7.5, exerted a significant reduction in the binding affinity for apo-Tf at pH 6.3 (see Table 1; Figure 1E; Figure 2), suggesting that it might be possible to find additional substitutions with differential effects on binding of the two forms of Tf.

Our first strategy for finding additional residues critical for Tf binding involved substitution of solvent-exposed residues C-terminal to the Tf-binding epitope residues Gly647 and Phe650 on helix 3 of the TfR helical domain. Of the five new TfR mutants constructed (R651A, S654A, T658A, N662A, E664A), only one (R651A) affected Tf binding, resulting in a greater than 2,800-fold reduction in binding of Fe-Tf and apo-Tf. Having identified a "hot spot" for Tf binding involving TfR helical domain residues Gly647 and Arg651, we then searched for residues affecting Tf binding that were distant from this site, which would allow approximate positioning of the bi-lobed Tf structure on TfR. Two residues within the cleft formed by portions of the three TfR domains were changed to their chicken TfR counterparts to test the prediction that Tf binds to the TfR interdomain cleft (Lawrence et al. 1999). There were no significant differences in Tf binding affinity for either the P710R or the K717Q mutants, suggesting that at least this region of the interdomain cleft is not critical for binding to either form of Tf. Consistent with this interpretation, we found a second binding site at the base of the TfR protease-like domain that is distant from the interdomain cleft (approximately 46 Å). The Y123S mutant, which was constructed as part of a screen to test the effects of changing large solvent-exposed hydrophobic residues, shows a significantly reduced affinity for Fe-Tf, but not to apo-Tf or HFE. To confirm that Tyr123 forms part of the Fe-Tf-binding site, three additional mutants were constructed: the double mutant Y123S/G647A and the two single mutants W124A and D125K. The double mutant showed an increased effect on Fe-Tf binding compared to the G647A alone, consistent with the involvement of Tyr123 in Fe-Tf binding. In addition, the W124A and D125K single mutants, which change residues adjacent to Tyr123, also reduced TfR's affinity for Fe-Tf, but not apo-Tf. Thus, the base of the protease-like domain in the vicinity of Tyr123 is involved in differential binding to the iron-loaded form of Tf, but not apo-Tf. None of the other substitutions constructed in the screen of solvent-exposed hydrophobic residues significantly affected binding to either form of Tf or to HFE.

As Tf is a bi-lobed structure, it should be possible to evaluate the binding of isolated lobes to wild-type and mutant

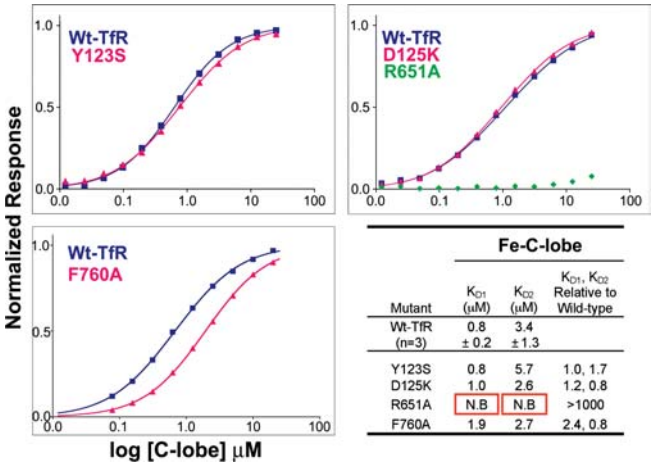

Mutant	Fe-C-lobe K_{D1} (μM)	Fe-C-lobe K_{D2} (μM)	Fe-C-lobe K_{D1}, K_{D2} Relative to Wild-type
Wt-TfR (n=3)	0.8 ± 0.2	3.4 ± 1.3	
Y123S	0.8	5.7	1.0, 1.7
D125K	1.0	2.6	1.2, 0.8
R651A	N.B	N.B	>1000
F760A	1.9	2.7	2.4, 0.8

Figure 3. Biosensor Analyses of Fe-C-Lobe Binding to Immobilized Wild-Type and Selected Mutant TfR Molecules

Plots of the equilibrium binding response, normalized to the R_{max} value (the ligand immobilization value) derived from fitting, versus concentration of injected Fe-C-lobe, are shown for the indicated TfR mutants along with the wild-type TfR control that was present in an adjacent flow cell on the same biosensor chip. Best-fit binding curves derived from a bivalent ligand model are shown as solid lines connecting the datapoints (squares for wild-type TfR and triangles for TfR mutants). The R651A mutant exhibited no binding and was not fit. A summary of derived binding constants is shown in the lower right panel. The K_Ds for wild-type TfR are averages derived from three independent measurements, and the number after the plus/minus sign represents the standard deviation.

DOI: 10.1371/journal.pbio.0000051.g003

TfRs to gain information regarding the positions of the two Tf lobes on TfR. Isolated iron-loaded Tf C-lobe (Fe-C-lobe) binds to TfR with an affinity of approximately 650 nM (Zak et al. 1994; Zak and Aisen 2002). Assuming independent binding of the two Tf lobes without effects of cooperativity, the affinity increase to a K_D of approximately 1 nM for intact Fe-Tf binding to TfR suggests the K_D for binding isolated N-lobe would be approximately 1.5 mM. This affinity is too weak to be detected by most binding assays. Consistent with this assumption, isolated Tf N-lobe neither binds detectably to TfR nor donates iron to TfR-expressing cells (Zak et al. 1994; Mason et al. 1997). We therefore tested purified Fe-C-lobe (Zak and Aisen 2002) for binding to wild-type TfR and selected TfR mutants.

Fe-C-lobe was injected over wild-type TfR and TfR mutants (Y123S, D125K, R651A, F760A) in a biosensor binding assay as described for Fe-Tf above. Binding data were analyzed using an equilibrium-based approach because the rapid kinetics of the Fe-C-lobe interaction with wild-type TfR do not allow accurate derivation of kinetic rate constants (Figure 3). No significant changes in affinity were observed for Fe-C-lobe binding to two mutants in the TfR protease-like domain (Y123S, D125K), but a mutation in the central portion of the Fe-Tf functional epitope on TfR, R651A, eliminated detectable binding (Figure 3). In addition, binding of Fe-C-lobe was not significantly affected by the F760A mutation in the TfR helical domain, which reduces the affinity of apo-Tf, but not Fe-Tf (see Figure 2; Table 1). These results suggest that Tf C-lobe contacts the TfR helical domain, but not the protease-like domain.

Discussion

Despite many years of investigation of the Tf/TfR pathway for iron uptake, molecular details about the interaction between TfR and Tf have been limited largely due to a lack of structural information for a Tf/TfR complex. In the absence of a three-dimensional structure, site-directed mutagenesis can be used to map out a protein–protein interaction. To narrow down a subset of residues for mutageneis from the 639 residues in a soluble TfR monomer, we used the crystal structures of TfR alone (Lawrence et al. 1999) and TfR bound to HFE (Bennett et al. 2000) to locate solvent-exposed residues in the vicinity of the HFE-binding site, which was suggested from competition studies to overlap with the Tf-binding site on TfR (Lebrón et al. 1999). We identified residues within the TfR helical domain whose substitution affected binding of both HFE and Fe-Tf at pH 7.5 in a previous mutagenesis study involving ten human TfR mutants (West et al. 2001). These results established that HFE and Fe-Tf bind to the same or an overlapping site on TfR. In the present study, we have expanded the library of TfR mutants to more precisely map the Tf-binding site on TfR and compared binding of Fe-Tf and apo-Tf to TfR. From a survey of 29 point mutants of human TfR, we identified 11 residues, which, when substituted, reduce the affinity of TfR for either human Fe-Tf, apo-Tf, or both (see Table 1). Six of the 11 residues are completely conserved in different species of TfR and in a more recently identified Tf-binding receptor, TfR2, which shares 45% sequence identity with TfR (Kawabata et al. 1999). Most notably, four of the residues exerting the largest effects on Fe-Tf binding, apo-Tf binding, or both (Leu619, Trp641, Gly647, and Arg651) are completely conserved across all currently known TfR and TfR2 sequences (see Table 1). Others, such as the tyrosines at positions 123 and 643, are either conserved or conservatively substituted for phenylalanine in some TfR species. By contrast, of the 18 positions at which substitutions did not significantly affect Tf binding, 16 are not conserved, and two (Phe187 and Glu664) are conservatively substituted (see Table 1). These results suggest that our conclusions about the mode of binding between human Tf and human TfR can be generalized to include Tf/TfR complexes from other species and the interaction between TfR2 and Tf.

From a quantitative analysis of the affinities of the different TfR mutants for Fe-Tf and apo-Tf, we can classify the residues we mutated using the criteria of Wells and colleagues (Cunningham and Wells 1993), which categorize the structural and functional epitope residues in a protein–protein interaction. The functional epitope is defined as residues exerting a major effect on the binding affinity (a $\Delta\Delta G$ value, $\geq$2 kcal/mol after substitution of a single residue, corresponding to an affinity reduction of at least 30-fold at room temperature). The structural epitope on a protein is all residues at the contact interface with the binding partner, which can be deduced from a co-crystal structure (Cunningham and Wells 1993). Substitution of some, but not all, of the residues at the structural epitope of a protein–protein interface will result in affinity changes (Cunningham and Wells 1993). This is illustrated in our study by comparing the crystallographically-defined structural epitope on TfR for binding HFE (Bennett et al. 2000) (see Figure 1A and 1B; Table 1; Figure S1) with the results of mutagenic mapping of residues affecting HFE binding (see Figure 1C). In the absence of a Tf/TfR co-crystal structure, we can use our mutagenesis results to predict the functional and structural epitope residues (affinity reductions of greater than or equal to 30-fold or between 5- and 30-fold, respectively) on TfR for binding to Fe-Tf and apo-Tf. From the comparison of wild-type and mutant TfR binding affinities, Arg651 was identified as a functional epitope residue for binding both Fe-Tf at pH 7.5 and binding apo-Tf at pH 6.3, as substitution of this single residue to alanine greatly reduces binding to either form of Tf (see Table 1). In combination with the previously studied G647A mutant (Dubljevic et al. 1999; West et al. 2001), which reduces affinity for both Fe-Tf and apo-Tf by over 100-fold, these residues define a functional epitope for Fe-Tf and apo-Tf binding located in the bottom central portion of the TfR helical domain (see Figure 1D and 1E). Two other nearby residues, Leu619 and Trp641, can be considered part of the functional epitope for binding apo-Tf. The HFE/TfR crystal structure shows that these residues are at the contact interface with HFE (see Figure 1A and 1B) (Bennett et al. 2000), but with the exception of Leu619, their substitutions do not significantly affect HFE binding (see Table 1). Instead, the functional epitope for HFE binding is shifted slightly upwards on the TfR helical domain from the Fe-Tf functional epitope to include residues Leu619 and Tyr643 (see Figure 1C). Thus, although most of the functional epitope residues for binding of HFE and Tf are physically separated, they are close enough that binding of either HFE or Fe-Tf to TfR would sterically preclude binding of the other species (see Figure 1C and 1D). In addition, some substitutions in TfR significantly lower the affinity for both HFE and Tf (L619A, R629A, Y643A, and F650A) (see Table 1).

Since Tf is a larger molecule than HFE, we reasoned that Tf could also interact with residues not contained in the HFE binding footprint on TfR. We therefore tested substitutions of residues outside of the TfR helical domain for their effects on binding to Tf. To narrow down the search, we chose to substitute solvent-exposed hydrophobic residues, which are often found in protein–protein interfaces (Jones and Thornton 1996; Lo Conte et al. 1999). We also restricted the search to residues within approximately 90 Å (the longest dimension of Fe-Tf) of the Fe-Tf functional-binding epitope for substitution. Using this strategy, we identified a region at the base of the protease-like domain involving residues Tyr123, Trp124, and Asp125, where substitutions showed significant effects on binding to Fe-Tf at pH 7.5, but not to HFE at pH 7.5 or to apo-Tf at pH 6.3 (see Figure 1D and 1E; Table 1). Having defined two predicted Fe-Tf contact areas on TfR that are separated by approximately 33 Å (measured between TfR residues Arg651 and Tyr123) constrains the ways in which Tf can interact with TfR. In particular, computer modeling suggests that a single Tf lobe cannot make productive contacts with both regions of TfR (A. M. Giannetti, unpublished data); thus both lobes of Fe-Tf are likely to be involved in the interface with TfR. Previous studies of the binding of isolated Fe-N- and Fe-C-lobes of Tf suggested that the majority of the binding energy in the Tf/TfR interaction comes from the C-lobe (Zak et al. 1994; Zak and Aisen 2002). It has also been observed that mixing purified N- and C-lobes results in a significant enhancement of TfR binding over that of C-lobe alone (Mason et al. 1997; Zak and Aisen 2002). These observations are consistent with a

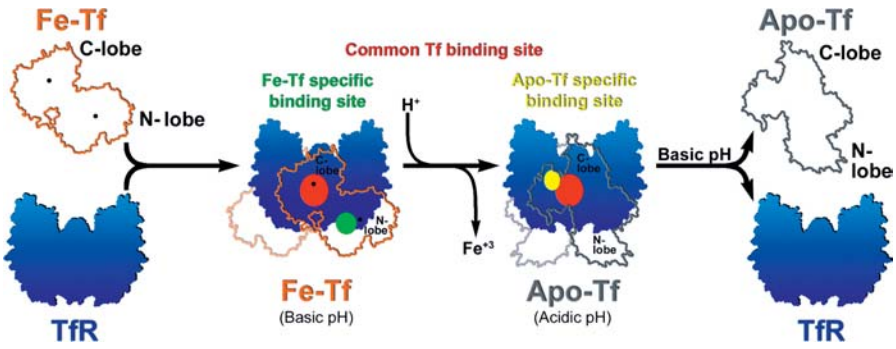

Figure 4. Model for the Binding of Fe-Tf and Apo-Tf to TfR

The figures representing each molecule are drawn to scale as an outline around the known structures of TfR (Lawrence et al. 1999), Fe-ovo-Tf (Kurokawa et al. 1995), and apo-ovo-Tf (Kurokawa et al. 1999). Membrane-bound TfR includes a stalk region that places the TfR ectodomain about 30 Å above the cell surface (Fuchs et al. 1998), which would allow the Tf molecule to extend below the plane of the TfR ectodomain. At basic pH, Fe-Tf (orange, with the iron atom positions shown as black dots) and TfR (blue) associate to make a complex containing one TfR homodimer and two Fe-Tf molecules, one bound to each polypeptide chain of the TfR homodimer. Fe-Tf makes energetically favorable contacts at basic pH to residues identified by mutagenesis in the TfR helical domain (red) and the protease-like domain (green). Acidification results in iron release and large conformational changes in the Tf structure as it becomes apo-Tf (gray). Apo-Tf does not make energetically favorable contacts with the protease-like domain, but retains binding to the helical domain-binding site (red) and makes new contacts to the helical domain (yellow), thereby stabilizing the complex. Upon return to basic pH, the apo-Tf molecules dissociate from TfR. This is also illustrated in Video S1.

DOI: 10.1371/journal.pbio.0000051.g004

Tf orientation on TfR in which the C-lobe contacts the Tf functional epitope on the TfR helical domain and the N-lobe contacts the Tyr123 area at the base of the TfR protease-like domain (Figure 4). In this model, allosteric effects need not be invoked to explain the increased affinity of the N-lobe/C-lobe mixture over C-lobe alone (Zak and Aisen 2002). Instead, the observed increase in affinity is predicted to arise from direct contacts between the N-lobe and TfR. To test the predicted orientation of Tf on TfR (Figure 4), we compared the affinities of isolated Fe-C-lobe (Zak and Aisen 2002) to wild-type TfR and to TfR mutants with substitutions in the helical domain (R651A, F760A) and the protease-like domain (Y123S, D125K) (see Figure 3). As predicted, substitutions in the protease-like domain do not affect binding of Fe-C-lobe, whereas a functional epitope substitution (R651A) in the TfR helical domain eliminates detectable binding of Fe-C-lobe to TfR.

Our binding data also allow us to assess potential differences in the binding of Fe-Tf versus apo-Tf to TfR. Two prior observations are consistent with differences in the binding footprints of Fe-Tf and apo-Tf on TfR. First, Fe-Tf undergoes a large conformational change upon acidification and release of iron, as deduced by comparison of crystal structures of ferric and iron-free forms of Tf and Tf-related molecules such as the lactoferrins (Bailey et al. 1988; Anderson et al. 1989; Gerstein et al. 1993; Zuccola 1993; Kurokawa et al. 1995, 1999; Baker et al. 1998; Karthikeyan et al. 1999) (see Figure 4). Second, TfR has been suggested to undergo a pH-dependent conformational change resulting in aggregation at pH <6 in the absence of Tf (Turkewitz et al. 1988). Our finding of differential effects of TfR substitutions for binding Fe-Tf at pH 7.5 versus apo-Tf at pH 6.3 is consistent with conformational changes in Tf,TfR, or both at acidic pH. We find one TfR region that affects binding of Fe-Tf, but not apo-Tf (the region near Tyr123 involving TfR residues 123–125 at the base of the protease-like domain), and another region that affects binding of apo-Tf, but not Fe-Tf or Fe-C-lobe (the region defined by Trp641 and Phe760, two spatially proximal residues [10.2 Å apart] at the edge of the TfR helical domain) (see Figure 1E and 1F). The apo-Tf-specific binding site may be important for TfR's ability to significantly accelerate iron release from receptor-bound Fe-Tf (Bali and Aisen 1991). Taking all of our data into account, we propose the following structure-based mechanism to explain TfR-assisted iron release from Fe-Tf (see Figure 4; Video S1).

First, Fe-Tf binds to TfR at pH 7.5, with the C-lobe making critical contacts to the TfR region defined by Arg651 in the helical domain and the N-lobe making additional favorable contacts with the second Tf-binding site defined by Tyr123, Trp124, and Asp125. The interaction of the complementary surfaces on each protein presumably limits Fe-Tf's freedom to sample more open states, thereby favoring the closed iron-bound state and lowering the iron release rate from both Tf lobes. This is consistent with the experimental evidence (Navati et al. 2003) suggesting that iron release is reduced by an order of magnitude under conditions favoring a closed Tf conformation relative to conditions favoring an open conformation.

Second, as the pH is lowered, protonation of key residues in Fe-Tf allows it to sample open conformations that facilitate iron release (Navati et al. 2003). A conformational change in Tf, TfR, or both allows additional Tf interactions between Tf and the hydrophobic binding surface defined by TfR residues Trp641 and Phe760. These new interactions stabilize Tf in an open conformation exposing the iron-binding site and thereby enhancing the rate of iron release.

The extensive mutagenic mapping of ligand binding to TfR reported here has revealed residues responsible for functional binding to HFE, Fe-Tf, and apo-Tf. These data confirm that HFE and Tf bind to a physically and functionally overlapping site on the TfR helical domain, although the most important receptor residues for binding are different for the two proteins. Thus, HFE and Fe-Tf must compete with each other for binding to cell surface TfR, which may have functional significance in HFE's role in maintaining iron homeostasis (Townsend and Drakesmith 2002). Additionally, we have found that Fe-Tf makes specific contacts not only to the TfR helical domain through its C-lobe, but also to the TfR protease-like domain, which implies that there are specific N-lobe/TfR contacts contributing to Tf binding. Finally, our demonstration that Fe-Tf and apo-Tf have different binding footprints on the surface of TfR provides insight into the mechanism by which TfR binding differentially affects iron release rates from Fe-Tf at acidic and basic pH.

Materials and Methods

Preparation of TfR ligands. A soluble form of human HFE (residues 1–275 of the mature protein noncovalently associated with the light chain β_2-microglobulin) was expressed and purified as previously described (Lebrón et al. 1998). Human Fe-Tf was prepared from apo-Tf (Sigma, St. Louis, Missouri, United States) by incubation with bicarbonate and excess ferric ammonium sulfate. Free iron was removed by dialysis, and the protein was further purified by gel-filtration chromatography. Iron saturation was 100% as determined spectrophotometrically (A_{465}/A_{280}, ~0.05) (He and Mason 2002). Purified recombinant Fe-C-lobe was cleaved from a full-length Fe-Tf in which the loop that connects the N- and C-lobes was replaced with a Factor X_a site (Zak and Aisen 2002). Concanavalin A chromatography was used to separate the glycosylated C-lobe from unglycosylated N-lobe (Zak and Aisen 2002). Protein concentrations were determined from the A_{280}- value using extinction coefficients of 52,200 M^{-1} cm^{-1} (Fe-C-lobe) (O. Zak, personal communication), 83,360 M^{-1} cm^{-1} (Tf), and 96,570 M^{-1} cm^{-1} (HFE/β_2-microglobulin) (Lebrón et al. 1998).

Production of wild-type TfR and TfR mutants. Soluble human TfR and TfR mutants were expressed in a lytic baculovirus/insect cell expression system as previously described (Lebrón et al. 1998). Mutations were introduced through PCR mutagenesis (Quickchange, Strategene, La Jolla, California, United States) into a baculovirus expression vector (pACGP67A; Pharmingen, San Diego, California, United States) containing a hydrophobic leader sequence, 6x-His tag, Factor X_a site, and residues 121–760 of human TfR. All mutations were confirmed by DNA sequencing of the protein-coding region of the vector. The Y123S mutation was further confirmed by N-terminal sequencing of the purified mutant protein, yielding the sequence ADPHHHHHHSSGIEGRGEFRLSWDD (the serine substitution for tyrosine is underlined), corresponding to residual leader sequence residues (A), vector-encoded sequence (DP), the 6x-His tag, spacer residues (SSG), a Factor X_a site (IEGR), a spacer segment (GEF), and residues 121–126 of the mutant TfR (RLSWDD). The double mutant Y123S/G647A was constructed by introducing the Y123S substitution into the G647A–TfR expression construct, after which the protein-coding region of the expression plasmid was again sequenced. Recombinant viruses were generated by cotransfection of a transfer vector with linearized viral DNA (Baculogold, Pharmingen). Supernatants of baculovirus-infected High 5 cells were used as the source of wild-type TfR and TfR mutants for surface plasmon resonance-based affinity measurements.

Affinity measurements. We used a BIACORE 2000 biosensor system (Pharmacia, LKB Biotechnology, Uppsalla, Sweden) to assay the interaction between TfR and HFE, Fe-Tf, and apo-Tf as described (West et al. 2001). Binding of injected proteins (the analytes were HFE, Fe-Tf, or apo-Tf) to a protein immobilized on the sensor chip (the ligand was TfR) results in changes in surface plasmon resonance that are read out in real time as resonance units (RUs) (Fägerstam et al. 1992; Malmqvist 1993).

For each experiment, the four flow cells of a CM5 biosensor chip (Pharmacia) were prepared by covalently attaching an anti-His-tag antibody (anti-PentaHis; Qiagen, Valencia, California, United States) to a coupling density of 2,000–4,000 RUs through standard amine coupling chemistry (BIACORE manual). Insect cell supernatants (50–300 μl) containing secreted 6x-His-tagged wild-type or mutant TfR were passed through a 0.2 μm filter and injected over one of the four flow cells of a biosensor chip at a flow rate of 30 μl/min, resulting in stable binding of TfR to density of 200–400 RUs. In a typical experiment, a small amount of TfR immediately dissociates from the anti-His antibody, but most TfR protein (>85%) remains bound during the course of the injection of the TfR ligands, resulting in a negligible baseline drift. On each biosensor chip, one flow cell containing only the immobilized antibody was used as the reference cell, one cell containing wild-type TfR served as an internal control for binding of the three TfR binding partners**,** and TfR mutants were coupled to the other two flow cells. HFE or Fe-Tf was injected over the flow cells at 50 μl/min or 70 μl /min, respectively, at 25° C in 50 mM PIPES (pH 7.5), 150 mM NaCl, and 0.005% surfactant P20 (v/v). All analyte injections were made as serial 2- or 3-fold dilutions. The HFE concentration series ranged from 30 nM to 10 μM, and the Fe-Tf and apo-Tf injections typically spanned from 1 nM to 200 nM, except for experiments involving low-affinity mutants requiring higher concentrations to properly derive affinities (see legend to Figure 2). In test experiments, the sensorgrams from duplicate injections could be overlaid to within the experimental noise; thus, single injections were done for each concentration of injected protein in a binding experiment. Between successive injections of analytes, the chips were regenerated to preinjection response levels by either flowing with running buffer until baseline was achieved (in the case of HFE) or by a 12-second injection of the injection buffer containing 0.5 M $MgCl_2$ (in the case of Fe-Tf). This treatment did not cause dissociation of TfR from the anti-His-tag antibody. Apo-Tf was injected in 50 mM PIPES (pH 6.3), 150 mM NaCl, 0.005% surfactant P20 (v/v), including 50 μM desferrioxamine as an iron chelator, and chip regeneration was achieved with an injection of the same buffer at pH 7.5.

Raw sensorgram data were preprocessed using the Scrubber software package (BioLogic Software, Campbell, Australia; www.biologic.com.au). The response from the reference flow cell was subtracted from the experimental flow cells to eliminate bulk refractive index changes. The response from the average of at least three buffer-only injections was then subtracted to correct for potential systematic instrument artifacts. Kinetic constants were obtained by simultaneous fitting of the association and dissociation phases of all curves in the working set using the program Clamp99 (Morton and Myszka 1998). The data were fit to a bivalent ligand model, which describes the two sequential binding events for either Tf or HFE binding to homodimeric TfR. A simple 1:1 binding model did not account for the observed data as judged from large residuals in the fits (data not shown). Equilibrium dissociation constants (K_Ds) were calculated from the ratio of the dissociation and association rate constants, k_{off} (s^{-1}) and k_{on} ($M^{-1}{\cdot}s^{-1}$), respectively, yielding K_Ds for the first and second binding events (K_{D1} and K_{D2}) in the following reaction mechanism:

$$A + TfR \leftrightarrow A{:}TfR \text{ (rate constants: } k_{on,1} \text{ and } k_{off,1})$$
$$K_{D1} = k_{off,1}/k_{on,1}$$
$$A + A{:}\,TfR \leftrightarrow A_2{:}TfR \text{ (rate constants: } k_{on,2} \text{ and } k_{off,2})$$
$$K_{D2} = k_{off,2}/k_{on,2}$$

where A is either HFE, Fe-Tf, or apo-Tf. For independent binding sites, the apparent stepwise equilibrium dissociation constants (K_{D1} and K_{D2}) are related to the intrinsic binding constants for the first and second binding events to TfR ($K_{D,intrinsic}$ and $K_{D,intrinsic}$), as follows:

$$K_{D1,intrinsic} = K_{D1}/2$$
$$K_{D2,intrinsic} = 2K_{D2}$$

Hence, if the binding of a TfR ligand is independent of whether a ligand is bound on the other face of the TfR homodimer, $K_{D2} = 4K_{D1}$.

For each mutant, the relative effect on HFE, Fe-Tf, or apo-Tf binding was calculated as a ratio between the mutant K_D and the average of 22 independent determinations of the wild-type K_D (see Table 1) and as a ratio between the mutant K_D and the wild-type K_D derived from wild-type protein coupled to a flow cell on the same sensor chip as the mutant (data not shown). No significant differences were found for the two methods of calculating the ratios. All mutants were evaluated for HFE and Fe-Tf binding in at least two independent experiments. For apo-Tf binding, those mutants that showed a significant difference in binding compared to wild-type TfR were reevaluated in a separate, independent experiment. No significant differences in K_Ds were observed in independent determinations of mutant affinities. When accurate affinities could not be derived in a duplicate experiment due to problems with baseline drift, visual inspection of the sensorgrams demonstrated that each mutant exerted the same relative effects compared with wild-type TfR in independent binding experiments. Table 1 presents affinities derived from one binding experiment per mutant/ligand pair. The reproducibility of the binding experiments can be assessed by the standard deviation of the wild-type TfR affinity for each of the ligands (derived from 22 independent binding experiments) and from the fact that the affinities of many of the mutants are not significantly changed compared to wild-type TfR.

For binding interactions involving the Fe-C-lobe, which reach equilibrium quickly, we derived K_Ds using an equilibrium-based approach. In these experiments, K_Ds were derived by non-linear regression analysis of plots of R_{eq} (the equilibrium binding response) versus the log of the analyte concentration. The data were fit to a binding model assuming a bivalent ligand in BIAevaluation 3.0 (BIACORE). We were unable to detect significant amounts of binding between apo-C-lobe and wild-type TfR at pH 6.3, presumably due to an intrinsically weak binding affinity.

Supporting Information

Figure S1. ΔΔG for Mutant TfR Binding to HFE, Fe-Tf, and Apo-Tf

Histogram of ΔΔG values for the change relative to wild-type TfR in TfR mutant affinities for HFE (blue), Fe-Tf (pink), and apo-Tf (gray). ΔΔG values (the difference in binding energy for a mutant TfR compared to wild-type TfR) were calculated using the K_{D1} values from Table 1 as $\Delta\Delta G = -RT\ln(K_{D1,mut}/K_{D1,wild\text{-}type})$, where R is the gas constant (1.99×10^{-3} kcal mol^{-1} K^{-1}), and T is the temperature in degrees Kelvin (298 K). The dashed green line represents the cutoff for TfR mutants with a greater than or equal to 5-fold affinity reduction in ligand binding, and the dashed red line indicates a greater than or equal to 30-fold affinity reduction. An orange star indicates non-binding mutants and mutants with a greater than 160-fold affinity reduction whose ΔΔG values exceed the y-axis limit of the histogram (L619A and Y643A, ≥4 kcal/mol; G647A = 3.2 kcal/mol; and R651A, ≥4.6 kcal/mol).

View online at DOI: 10.1371/journal.pbio.0000051.sg001 (1.86 MB TIFF).

Video S1. Model of TfR-Assisted Iron Release from Fe-Tf

View online at DOI: 10.1371/journal.pbio.0000051.sv001 (12 MB MOV).

Accession Numbers

The SwissProt accessions numbers for the proteins discussed in this paper are β_2-microglobulin (P01884), Fe-Tf (P02787), HFE (Q30201), TfR canine (Q9GLD3), TfR chicken (Q90997), TfR feline (Q9MYZ3), TfR hamster (Q07891), TfR human (P02786), TfR mouse (Q62351), TfR rat (Q99376), TfR2 human (Q9UP52), and TfR2 mouse (Q62351).

Acknowledgments

This work was supported by grants from the National Institutes of Health (1-R01-DK60770 to PJB and DK-15056 to Dr. Philip Aisen) and an National Research Service Award predoctoral training grant (5T32-GM-7616 to AMG). We are grateful to Inderjit Nangiana and Cynthia Jones (Caltech Protein Expression Facility) for assistance in expressing TfR proteins and to the Caltech Protein/Peptide Micro-Analytical Laboratory for protein sequencing. We thank Drs. Anthony West, Andy Herr, Caroline Enns, and Anne B. Mason for helpful discussions and members of the Björkman lab for critical reading of the manuscript. We give a special thanks to D. G. Myszka for beta versions of Clamp and Scrubber and discussions of BIACORE experimental details.

Conflicts of interest. The authors have declared that no conflicts of interest exist.

Author contributions. AMG and PJB conceived and designed the experiments. AMG performed the experiments. AMG and PJB analyzed the data. AMG, PMS, and OZ contributed reagents/materials/analysis tools. AMG and PJB wrote the paper. AMG developed and produced the animated figure. ■

References

Anderson BF, Baker HM, Norries GE, Rice DW, Baker EN (1989) Structure of human lactoferrin: Crystallographic structure analysis and refinement at 2.8 Å resolution. J Mol Biol 209: 711–734.

Bailey S, Evans RW, Garratt RC, Gorinsky B, Hasnain S, et al. (1988) Molecular structure of serum transferrin at 3.3 Å resolution. Biochemistry 27: 5804–5812.

Baker EN, Anderson BF, Baker HM, MacGillivray RTA, Moore SA, et al. (1998) Three-dimensional structure of lactoferrin: Implications for function, including comparisons with transferrin. Adv Exp Med Biol 443: 1–14.

Bali PK, Aisen P (1991) Receptor-modulated iron release from transferrin: Differential effects on N- and C-terminal sites. Biochemistry 30: 9947–9952.

Bali PK, Aisen P (1992) Receptor-induced switch in site-site cooperativity during iron release by transferrin. Biochemistry 31: 3963–3967.

Bali PK, Zak O, Aisen P (1991) A new role for the transferrin receptor in the release of iron from transferrin. Biochemistry 30: 324–328.

Bennett MJ, Lebrón JA, Bjorkman PJ (2000) Crystal structure of the hereditary haemochromatosis protein HFE complexed with transferrin receptor. Nature 403: 46–53.

Buchegger F, Trowbridge IS, Liu L-FS, White S, Collawn JF (1996) Functional analysis of human/chicken transferrin receptor chimeras indicates that the carboxy-terminal region is important for ligand binding. Eur J Biochem 235: 9–17.

Cullen LM, Anderson GJ, Ramm GA, Jazwinska EC, Powell LW (1999) Genetics of hemochromatosis. Annu Rev Med 50: 87–98.

Cunningham BC, Wells JA (1993) Comparison of a structural and a functional epitope. J Mol Biol 234: 554–563.

Dautry-Varsat A, Ciechanover A, Lodish HF (1983) pH and the recycling of transferrin during receptor-mediated endocytosis. Proc Natl Acad Sci U S A 80: 2258–2262.

Dubljevic V, Sali A, Goding A (1999) A conserved RGD (Arg–Gly–Asp) motif in the transferrin receptor is required for binding to transferrin. Biochem J 341: 11–14.

Enns CA (2002) The transferrin receptor. In: Templeton DM, editor. Molecular and cellular iron transport. New York: Marcel Dekker. pp. 71–94.

Enns CA, Sussman HH (1981) Physical characterization of the transferrin receptor in human placentae. J Biol Chem 256: 9820–9823.

Enns CA, Rutledge EA, Williams AM (1996) The transferrin receptor. In: Biomembranes. New York: JAI Press. pp. 255–287.

Fägerstam LG, Frostell-Karlsson A, Karlsson R, Persson B, Rönnber I (1992) Biospecific interaction analysis using surface plasmon resonance detection applied to kinetic, binding site and concentration analysis. J Chromatogr 597: 397–410.

Feder JN, Gnirke A, Thomas W, Zsuchihashi Z, Ruddy DA, et al. (1996) A novel MHC class I-like gene is mutated in patients with hereditary haemochromatosis. Nat Genet 13: 399–408.

Feder JN, Penny DM, Irrinki A, Lee VK, Lebrón JA, et al. (1998) The hemochromatosis gene product complexes with the transferrin receptor, and lowers its affinity for ligand binding. Proc Natl Acad Sci U S A 95: 1472–1477.

Fuchs H, Lüchken U, Tauber R, Engel A, Gessner R (1998) Structural model of phospholipid-reconstituted human transferrin receptor derived by electron microscopy. Structure 6: 1235–1243.

Gerstein M, Anderson BF, Norris GE, Baker EN, Lesk AM, et al. (1993) Domain closure in lactoferrin: Two hinges produce a see-saw motion between alternative close-packed interfaces. J Mol Biol 234: 357–372.

Grossmann JG, Neu M, Pantos E, Schwab FJ, Evans RW, et al. (1992) X-ray solution scattering reveals conformational changes upon iron uptake in lactoferrin, serum and ovo-transferrins. J Mol Biol 225: 811–819.

Grossmann JG, Neu M, Evans RW, Lindley PF, Appel H, et al. (1993) Metal-induced conformational changes in transferrins. J Mol Biol 229: 585–590.

He Q-Y, Mason AB (2002) Molecular aspects of release of iron from transferrin. In: Templeton DM, editor. Molecular and cellular iron transport. New York: Marcel Dekker. pp. 95–124.

Jones S, Thornton JM (1996) Principles of protein–protein interaction. Proc Natl Acad Sci U S A 93: 13–20.

Karthikeyan S, Paramasivam M, Yadav S, Srinivasan A, Singh TP (1999) Structure of buffalo lactoferrin at 2.5 Å resolution using crystals grown at 303 K shows different orientations of the N and C lobes. Acta Crystallogr D Biol Crystallogr 55: 1805–1813.

Kawabata H, Yang R, Hirama T, Vuong PT, Kawno S, et al. (1999) Molecular cloning of transferrin receptor 2. J Biol Chem 274: 20826–20832.

Kraulis PJ (1991) MolScript: A program to produce both detailed and schematic plots of protein structures. J Appl Crystallogr 24: 946–950.

Kurokawa H, Mikami B, Hirose M (1995) Crystal structure of diferric hen ovotransferrin at 2.4 Å resolution. J Mol Biol 254: 196–207.

Kurokawa H, Dewan JC, Mikami B, Sacchettini JC, Hirose M (1999) Crystal structure of hen apo-ovotransferrin: Both lobes adopt an open conformation upon loss of iron. J Biol Chem 274: 28445–28452.

Lawrence CM, Ray S, Babyonyshev M, Galluser R, Borhani DW, et al. (1999) Structure of the ectodomain of human transferrin receptor. Science 286: 779–782.

Lebrón JA, Bennett MJ, Vaughn DE, Chirino AJ, Snow PM, et al. (1998) Crystal structure of the hemochromatosis protein HFE and characterization of its interaction with transferrin receptor. Cell 93: 111–123.

Lebrón JA, West AP, Bjorkman PJ (1999) The hemochromatosis protein HFE competes with transferrin for binding to the transferrin receptor. J Mol Biol 294: 239–245.

Lo Conte L, Chothia C, Janin J (1999) The atomic structure of protein–protein recognition sites. J Mol Biol 285: 2177–2198.

Malmqvist M (1993) Biospecific interaction analysis using biosensor technology. Nature 361: 186–187.

Mason AB, Tam BM, Woodworth RC, Oliver RW, Green BN, et al. (1997) Receptor recognition sites reside in both lobes of human serum transferrin. Biochem J 326: 77–85.

Merritt EA, Bacon DJ (1997) Raster3D: Photorealistic molecular graphics. Methods Enzymol 277: 505–524.

Morton TA, Myszka DG (1998) Kinetic analysis of macromolecular interactions using surface plasmon resonance. Methods Enzymol 295: 268–294.

Navati MS, Samuni U, Aisen P, Friedman JM (2003) Binding and release of iron by gel-encapsulated human transferrin: Evidence for a conformational search. Proc Natl Acad Sci U S A 100: 3832–3837.

Nicholls A, Bharadwaj R, Honig B (1993) GRASP: Graphical representation and analysis of surface properties. Biophys J 64: A166–A166.

Parkkila S, Waheed A, Britton RS, Bacon BR, Zhou XY, et al. (1997) Association of the transferrin receptor in human placenta with HFE, the protein

defective in hereditary hemochromatosis. Proc Natl Acad Sci U S A 94: 13198–13202.

Sipe DM, Murphy RF (1991) Binding to cellular receptor results in increased iron release from transferrin at mildly acidic pH. J Biol Chem 266: 8002–8007.

Townsend A, Drakesmith H (2002) Role of HFE in iron metabolism, hereditary haemochromatosis, anaemia of chronic disease, and secondary iron overload. Lancet 359: 786–790.

Tsai CJ, Lin SL, Wolfson HJ, Nussinov R (1997) Studies of protein–protein interfaces: A statistical analysis of the hydrophobic effect. Protein Sci 6: 53–64.

Turkewitz AP, Schwartz AL, Harrison SC (1988) A pH-dependent reversible conformational transition of the human transferrin receptor leads to self-association. J Biol Chem 263: 16309–16315.

West AP Jr, Giannetti AM, Herr AB, Bennett MJ, Nangiana JS, et al. (2001) Mutational analysis of the transferrin receptor reveals overlapping HFE and transferrin binding sites. J Mol Biol 313: 385–397.

Zak O, Aisen P (2002) A new method for obtaining human transferrin C-lobe in the native conformation: Preparation and properties. Biochemistry 41: 1647–1653.

Zak O, Trinder D, Aisen P (1994) Primary receptor-recognition site of human transferrin is in the C-terminal lobe. J Biol Chem 269: 7110–7114.

Zuccola HJ (1993) The crystal structure of monoferric human serum transferrin [dissertation]. Atlanta, Georgia: Georgia Institute of Technology.

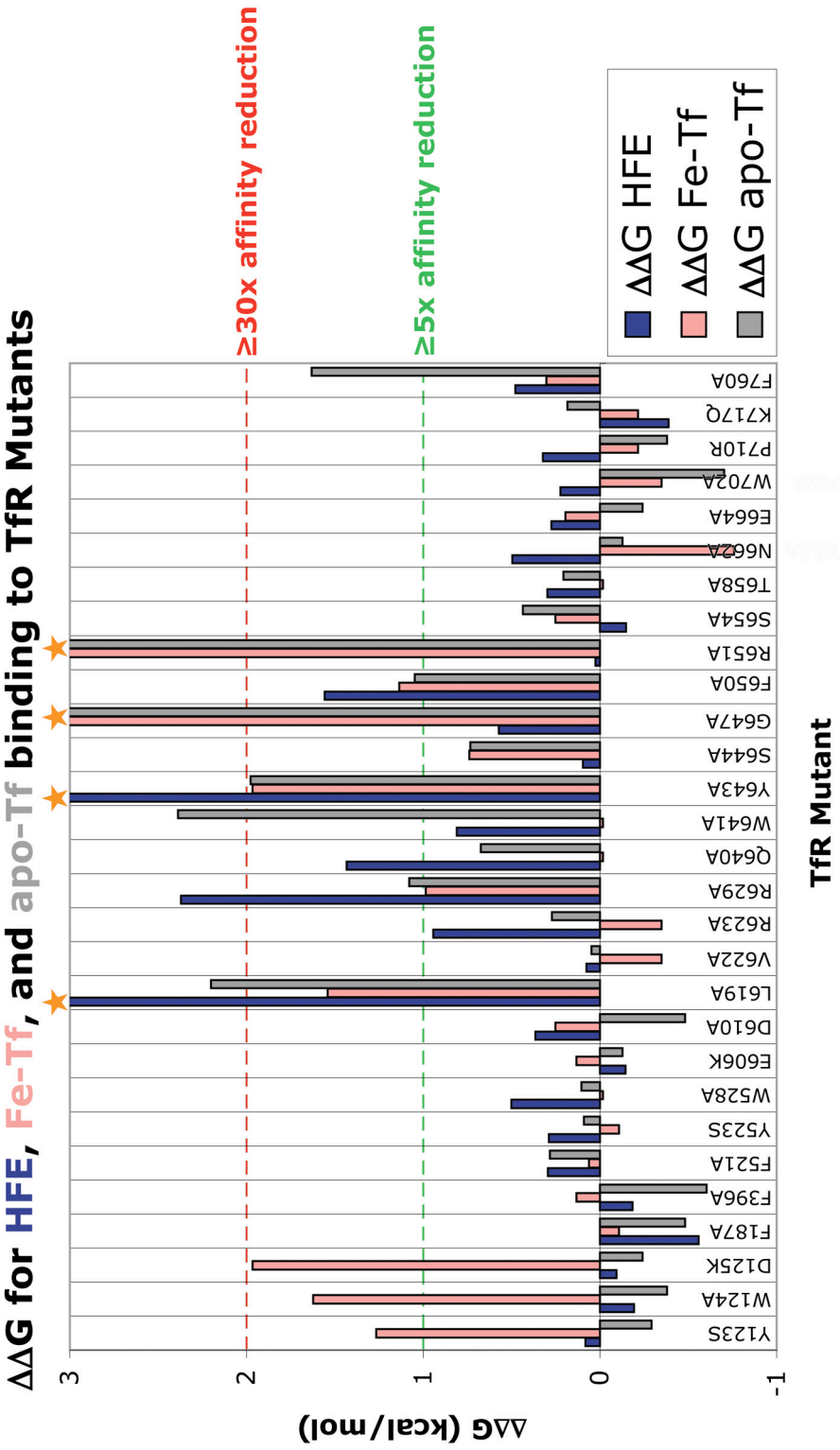
ΔΔG for HFE, Fe-Tf, and apo-Tf binding to TfR Mutants
≥30x affinity reduction
≥5x affinity reduction
ΔΔG HFE
ΔΔG Fe-Tf
ΔΔG apo-Tf
ΔΔG (kcal/mol)
3
2
1
0
-1
TfR Mutant
Y123S
W124A
D125K
F187A
F396A
F521A
Y523S
W528A
E606K
D610A
L619A
V622A
R623A
R629A
Q640A
W641A
Y643A
S644A
G647A
F650A
R651A
S654A
T658A
N662A
E664A
W702A
P710R
K717Q
F760A

Chapter 3:

The Mechanism for Multiple Ligand Recognition by the Transferrin Receptor

This chapter has been published and Giannetti, A.M. and Björkman, P.J. (2004) HFE and Transferrin Directly Compete for Transferrin Receptor in Solution and at the Surface of Cells, Journal of Biological Chemistry, Vol. 279, No. 24, pp. 25866–25875, 2004

ISSN 0021-9258 (print)
ISSN 1083-351x (electronic)
JBCHA3 279(24) 24907–25934 (2004)

The Online Version of This Issue Contains Supplemental Material

The Journal of Biological Chemistry

JUNE 11, 2004 VOLUME 279 NUMBER 24

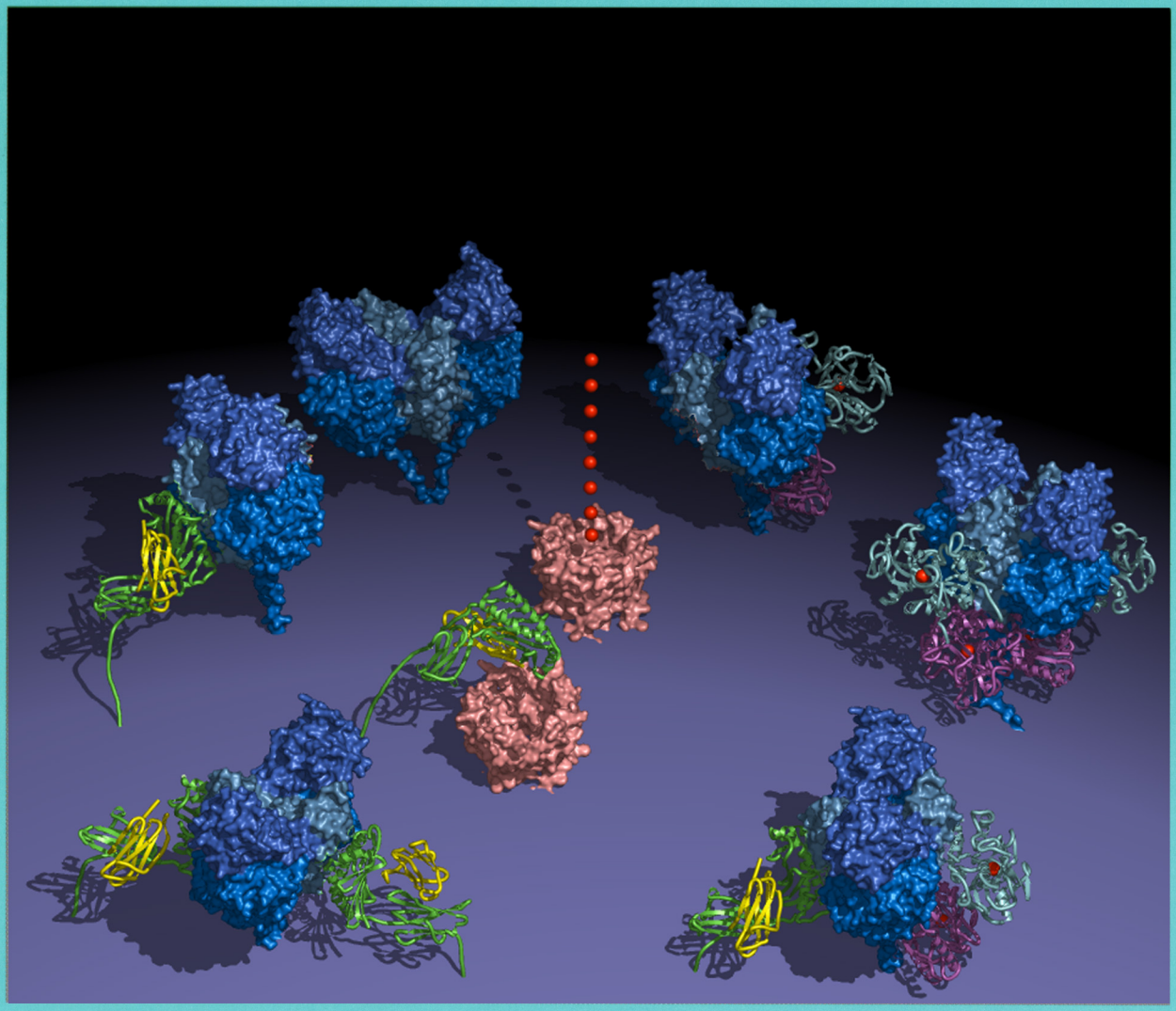

PUBLISHED BY THE AMERICAN SOCIETY FOR BIOCHEMISTRY AND MOLECULAR BIOLOGY

Founded by Christian A Herter and Sustained in Part by the Christian A Herter Memorial Fund

The cover shows a structural view of the interactions of transferrin receptor (TfR) (blue surface) with the hemochromatosis protein HFE (green and yellow ribbon) and the serum iron carrier protein transferrin (Tf) (cyan and magenta ribbon). TfR can bind one or two HFEs, one or two Tfs, or one of each to form the ternary complex (all represented). HFE has been hypothesized to block the function of ferroportin, a transmembrane iron export protein. Two molecules of a ferroportin model are shown in pink surface representation. One is freely exporting iron (red spheres) whereas the other has been blocked by HFE.

THE JOURNAL OF BIOLOGICAL CHEMISTRY
Vol. 279, No. 24, Issue of June 11, pp. 25866–25875, 2004

Printed in U.S.A.

HFE and Transferrin Directly Compete for Transferrin Receptor in Solution and at the Cell Surface*

Received for publication, February 10, 2004, and in revised form, March 30, 2004
Published, JBC Papers in Press, March 31, 2004, DOI 10.1074/jbc.M401467200

Anthony M. Giannetti‡ and Pamela J. Björkman§¶

From the ‡Graduate Option in Biochemistry and Molecular Biophysics and the §Division of Biology and Howard Hughes Medical Institute, California Institute of Technology, Pasadena, California 91125

Transferrin receptor (TfR) is a dimeric cell surface protein that binds both the serum iron transport protein transferrin (Fe-Tf) and HFE, the protein mutated in patients with the iron overload disorder hereditary hemochromatosis. HFE and Fe-Tf can bind simultaneously to TfR to form a ternary complex, but HFE binding to TfR lowers the apparent affinity of the Fe-Tf/TfR interaction. This apparent affinity reduction could result from direct competition between HFE and Fe-Tf for their overlapping binding sites on each TfR polypeptide chain, from negative cooperativity, or from a combination of both. To explore the mechanism of the affinity reduction, we constructed a heterodimeric TfR that contains mutations such that one TfR chain binds only HFE and the other binds only Fe-Tf. Binding studies using a heterodimeric form of soluble TfR demonstrate that TfR does not exhibit cooperativity in heterotropic ligand binding, suggesting that some or all of the effects of HFE on iron homeostasis result from competition with Fe-Tf for TfR binding. Experiments using transfected cell lines demonstrate a physiological role for this competition in altering HFE trafficking patterns.

Hereditary hemochromatosis is a prevalent genetic disorder characterized by a defect in a checkpoint of iron homeostasis resulting in the absorption of dietary iron beyond the body's needs. If left untreated, hereditary hemochromatosis results in the deposit of iron primarily in the liver, heart, pancreas, and parathyroid and pituitary glands, leading to pathologies such as arthritis, liver cancer, diabetes, cardiomyopathy, and bronzing of skin (1, 2). Positional cloning revealed that most hereditary hemochromatosis patients carry mutations in the gene coding for a protein called HFE (3). HFE is a membrane protein homologous to class I major histocompatibility complex proteins (3), which present antigenic peptides to T lymphocytes (4). Like class I major histocompatibility complex molecules and most other class I homologs, HFE is a heterodimer in which a membrane-bound heavy chain associates noncovalently with the light chain β_2-microglobulin (3). Most hereditary hemochromatosis patients are homozygous for a mutation that converts residue 260 of the mature HFE protein from cysteine to tyrosine (3), preventing proper folding, β_2-microglobulin association, and cell surface expression and eliminating its effects on cellular iron levels (5–7).

A potential link between HFE and the regulation of iron homeostasis was established by the observation that HFE binds to transferrin receptor 1 (TfR)[1] (8, 9), a homodimeric cell surface glycoprotein that serves as the receptor for iron-loaded transferrin (Fe-Tf) (10). Each chain of the TfR homodimer contains an ~640-residue ectodomain, a glycosylated stalk region, a membrane-spanning segment, and an N-terminal cytoplasmic domain containing a YTRF endosomal sorting signal. This motif serves as a signal for endocytosis and transport back to the cell surface through recycling endosomes (11–13). The extracellular domain of TfR forms a high affinity complex with circulating Fe-Tf and transports it to acidic endosomes. At the low pH of endosomes (pH ≤6.5), TfR assists in the release of iron from Fe-Tf (14, 15). The iron-free form of Tf (apo-Tf) remains bound to TfR inside acidic endosomes and is recycled to the cell surface, where apo-Tf dissociates at the slightly basic pH of the blood (16).

TfR can form a number of complexes with HFE and Fe-Tf (Fig. 1). TfR homodimers bind two Fe-Tf molecules to form Fe-Tf·TfR complexes with 2:1 ligand/receptor stoichiometry (17, 18). Soluble TfR homodimers also bind two HFE molecules to form 2:1 HFE·TfR complexes (19, 20), although 1:1 HFE·TfR complexes can be found in solution using soluble forms of HFE and TfR (18, 20). When all three proteins are present, HFE·TfR·Fe-Tf ternary complexes are observed in solution (18) and in lysates from HFE-transfected HeLa cells (21, 22). Competition (23), mutagenesis (20, 24), time-resolved x-ray footprinting (25), and electron microscopy studies (26) demonstrate that Fe-Tf and HFE compete for overlapping binding sites on each TfR chain; thus, HFE·TfR·Fe-Tf ternary complexes have a 1:1:1 stoichiometry, such that HFE binds to one TfR polypeptide chain and Fe-Tf binds to the other.

Comparison of the crystal structures of TfR alone (27) and a 2:1 HFE·TfR complex (19) reveals that HFE binding induces changes at the TfR dimer interface that are distant from the HFE binding site, suggesting that HFE binding to one polypeptide chain of the TfR dimer can transmit structural changes to the other TfR chain. These changes could influence the binding of Fe-Tf or another HFE to the other side of the TfR dimer. Indeed, in some studies, Fe-Tf binds with a lower apparent affinity to cell surface TfR in the presence of membrane-bound or soluble HFE (8, 21), and an affinity reduction is also ob-

* This work was supported by the Howard Hughes Medical Institute, by National Institutes of Health Grant 1 R01 DK60770 (to P. J. B.), and by National Research Service Award 5T32-GM-7616 (to A. M. G). The costs of publication of this article were defrayed in part by the payment of page charges. This article must therefore be hereby marked "*advertisement*" in accordance with 18 U.S.C. Section 1734 solely to indicate this fact.

¶ To whom correspondence should be addressed: Division of Biology California Institute of Technology, 1200 E. California Blvd., MC 114-96, Pasadena, CA 91125. Tel.: 626-395-8350; Fax: 626-792-3683; E-mail: bjorkman@caltech.edu.

[1] The abbreviations used are: TfR, transferrin receptor; Tf, transferrin; Fe-Tf, iron loaded transferrin; hdTfR, heterodimeric form of soluble TfR; AUC, analytical ultracentrifugation; SPR, surface plasmon resonance; wtTfR, wild type TfR; GFP, green fluorescence protein; NTA, nitrilotriacetic acid; PIPES, 1,4-piperazinediethanesulfonic acid; EGFP, enhanced green fluorescent protein.

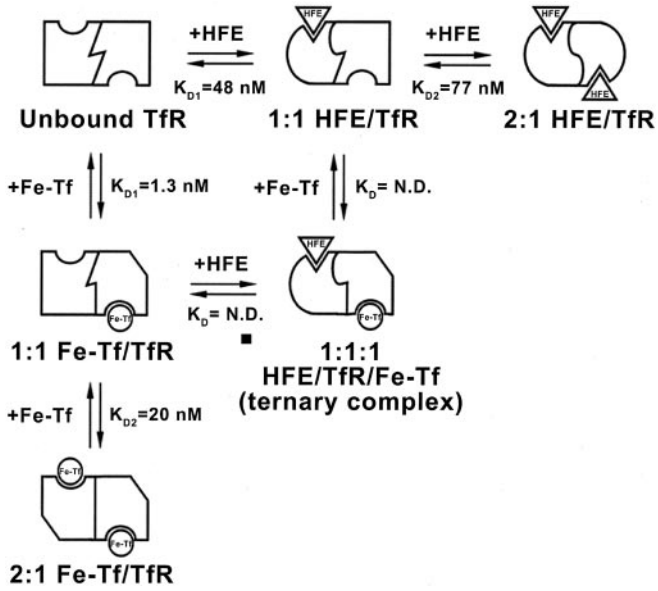

FIG. 1. **Equilibrium relationships for complexes formed by HFE, Fe-Tf, and TfR.** Statistically corrected equilibrium binding constants are shown for binary binding reactions (Table I). *N.D.*, K_D values determined for hdTfR but not wtTfR.

served when Fe-Tf binds to soluble TfR in the presence of soluble HFE (23). The apparent affinity reduction could result from competition between Fe-Tf and HFE for binding to TfR, from negative cooperativity due to structural changes in the unbound TfR chain that are imparted by HFE binding to the other chain, or from a combination of both phenomena.

Investigation of the mechanism by which HFE influences the binding of Fe-Tf to TfR is complicated, because complexes in addition to the HFE·TfR·Fe-Tf ternary complex form in an equilibrium mixture of the three proteins (Fig. 1). Thus, previous quantitative binding studies have derived equilibrium dissociation constants (K_D values) only for binary HFE·TfR and Fe-Tf·TfR complexes (18, 20, 24, 28). Using Fe-Tf, a soluble serum protein, and recombinant soluble forms of HFE and TfR, we previously measured equilibrium dissociation constants (K_D values) for the first (K_{D1}) and second (K_{D2}) binding events to homodimeric TfR, demonstrating that HFE binds with lower affinity to TfR than does Fe-Tf (18, 20, 24) (Fig. 1). In this study, we examine how binding of HFE or Fe-Tf to one side of the TfR dimer affects binding to the other chain in the absence of the competing binary complexes, using a heterodimeric form of soluble TfR (hdTfR) in which one chain can bind HFE and not Fe-Tf and the other chain can bind Fe-Tf but not HFE. Using analytical ultracentrifugation (AUC) and surface plasmon resonance (SPR) binding assays, we verified that hdTfR binds one HFE and one Fe-Tf. We then measured the affinity of the free TfR chain for Fe-Tf (or HFE) when HFE (or Fe-Tf) is bound to the other chain. We found no affinity reduction for Fe-Tf or HFE binding to hdTfR in the presence of saturating amounts of the other ligand, suggesting that direct competition, rather than negative cooperativity, is responsible for the apparent affinity reduction in Fe-Tf binding to cell surface and soluble TfR in the presence of HFE.

Having determined that HFE lowers the apparent affinity for Fe-Tf by directly competing for TfR binding sites rather than through an allosteric mechanism, we evaluated the effects of this competition at physiological concentrations of Fe-Tf using HFE and TfR expressed in transfected cells. We first demonstrate that a green fluorescent protein (GFP)-tagged form of HFE is dependent on its association with TfR for transport to Tf-positive endosomal compartments. We then show that the addition of Fe-Tf to the cellular media induces a redistribution of HFE within the cells, suggesting that fluctuations in serum Fe-Tf concentration can significantly alter the stoichiometric ratios of the possible TfR complexes and free proteins at the cell surface. These results are discussed in terms of the role of HFE in the control of cellular iron homeostasis.

EXPERIMENTAL PROCEDURES

Production of Wild-type Proteins—Soluble wtTfR was produced in a lytic baculovirus/insect cell expression system as previously described (18). Briefly, we used a modified version of the pAcGP67A expression vector (Pharmingen) that codes for the gp67 hydrophobic leader sequence followed by a His_6 tag, factor Xa cleavage site, and residues 121–760 of human TfR. Soluble human HFE/β2-microglobulin heterodimers were expressed in Chinese hamster ovary cells and purified as previously described (18). Human Fe-Tf was prepared from apo-Tf (Sigma) by incubation with bicarbonate and excess ferric ammonium sulfate.

Expression of hdTfR and Homodimeric TfR Mutants—Mutations (L619A/Y643A for the Fe-Tf-binding TfR chain and Y123S/G647A/R651A for the HFE-binding TfR chain) were introduced into the expression vector encoding human wtTfR (wild-type TfR) using the QuikChange™ protocol (Stratagene). Constructs were verified by sequencing of the protein-coding region. His-tagged mutant TfR homodimers were expressed in baculovirus-infected insect cells and purified as described above. For production of hdTfR, the L619A/Y643-TfR construct was mutagenized further to exchange the His_6 tag for the StrepTag II affinity tag (WSHPQEK) (29), a sequence designed to bind to streptactin, a modified form of streptavidin (30). PCR was used to introduce restriction sites and a ribosomal binding sequence (CCTATAAAT) immediately upstream of the start codon and to amplify the coding regions of the L619A/Y643A-TfR and Y123S/G647A/R651A-TfR constructs. The mutant TfR sequences were ligated into the pFastBacDUAL (Invitrogen) dicistronic baculovirus expression vector. The gene encoding Y123S/G647A/R651A-TfR was ligated 3′ to the p10 promoter site using SphI and XhoI restriction sites, and the gene encoding L619A/Y643A-TfR was ligated downstream of the polyhedron promoter using BssHII and NotI restriction sites. Recombinant viruses were generated by co-transfection of a transfer vector with linearized viral DNA (Baculogold, Pharmingen) for TfR homodimers or by use of the Bac-to-Bac® system (Invitrogen) for hdTfR.

Purification of hdTfR—Separation of the three species of TfR produced by insect cells expressing both mutant TfR chains (HFE-binding homodimers, Fe-Tf-binding homodimers, and hdTfR) was achieved using sequential affinity chromatography steps. Infected insect cell supernatants containing the secreted TfR species were concentrated and exchanged into 50 mM Tris, pH 7.4, 300 mM NaCl, 10% glycerol, and 15 mM imidazole. Supernatants were passed over a Ni^{2+}-NTA Superflow agarose column (Qiagen), and the two His-tagged species (Fe-Tf-binding homodimers and hdTfR) were eluted from the column with 250 mM imidazole. The eluted peak was loaded onto a 15-ml streptactin-Sepharose column (Sigma-Genosys). After washing with a buffer containing 50 mM PIPES, pH 7.4, and 150 mM NaCl, the column was eluted by the addition of the same buffer with 3 mM desthiobiotin to obtain hdTfR. The column was regenerated by the addition of 1 mM 4-hydroxyazobenzene-2-carboxylic acid, which was removed by washing the resin according to the manufacturer's instructions. Due to low levels of nonspecific binding of the different TfRs to the Ni^{2+}-NTA and streptactin resins, the columns were washed extensively after loading (>20 column volumes for Ni^{2+}-NTA superflow and >5 column volumes for streptactin superflow), which eliminated homodimer carry-through. The purity of hdTfR was monitored throughout the purification process by reverse-phase fast protein liquid chromatography using a Resource Phe column (Amersham Biosciences). $(NH_4)_2SO_4$ was added to protein samples to a concentration of 850 mM prior to loading on the column, and proteins were eluted by a gradient from 850 to 0 mM $(NH_4)_2SO_4$ over 20 column volumes. The two contaminating homodimers resolve into well separated peaks with the hdTfR appearing as a peak between them, as verified by Western blotting using the anti-penta-His antibody (Qiagen) and alkaline phosphatase-conjugated streptactin (IBA) (data not shown). After elimination of detectable contaminating TfR homodimers, hdTfR samples were passed over a Superdex-200 column (Amersham Biosciences) to remove aggregates and exchanged into 50 mM PIPES, pH 7.4, 150 mM NaCl, and 0.05% NaN_3.

Circular Dichroism—CD spectra and thermal denaturation profiles were obtained using an Aviv 62A DS spectrometer with a thermoelec-

tric cell holder and cuvette with a 1-mm path length. Measurements were recorded using samples containing 5 μM TfR protein in 20 mM PIPES, pH 7.4, and 80 mM NaCl. Wavelength scans were collected from 200 to 250 nm in 1-nm increments. For thermal melts, the CD signal at 220 nm was recorded every 1 °C from 4 to 99 °C with an equilibration time of 2 min and an averaging time of 1 min.

Biosensor Analyses—All biosensor experiments were carried out using a BIACORE 2000 instrument (Amersham Biosciences). Interactions between a protein immobilized on the sensor chip (the "ligand") and a protein injected over the sensor surface (the "analyte") are monitored in real time as a change in surface plasmon resonance as measured in resonance units (31, 32). Sensor chips were prepared using standard primary amine coupling chemistry to attach 2000–4000 resonance units of the anti-penta-His antibody (Qiagen) (BIACORE manual), which was used to capture wtTfR and homodimeric TfR mutants (two His tags) directly from insect cell supernatants as described (24). hdTfR was covalently immobilized using primary amine chemistry (BIACORE manual). In each experiment, one of the four flow cells of a CM5 biosensor chip (Amersham Biosciences) was mock-coupled with antibody but no TfR for use as a reference cell. Binding data were collected as previously described (24).

Kinetic sensorgram data were pre-processed using Scrubber (BioLogic Software Pty. Ltd.; available on the World Wide Web at www.biologic.com.au), and kinetic constants were determined by simultaneously fitting the association and dissociation phases of all curves using the Clamp99 program (33) to either a 1:1 model or a bivalent ligand (2:1) model. The 1:1 model describes a simple bimolecular interaction and yields single association (k_{on}) and dissociation (k_{off}) values. The bivalent ligand model describes the sequential binding of two analyte molecules to a homodimeric ligand. This two-step process yields apparent association ($k_{1on,app}$, $k_{2on,app}$) and dissociation ($k_{1off,app}$, $k_{2off,app}$) values for each of the two reactions as follows,

$$A + TfR \leftrightarrow A{:}TfR \text{ (rate constants: } k_{1on,\,app} \text{ and } k_{1off,\,app})$$

REACTION 1

$$K_{D1,\,app} = k_{1off,\,app}/k_{1on,\,app} \quad \text{(Eq. 1)}$$

$$A + A{:}TfR \leftrightarrow A_2{:}TfR \text{ (rate constants: } k_{2on,app} \text{ and } k_{2off,app})$$

REACTION 2

$$K_{D2,app} = k_{1off,app}/k_{1on,app} \quad \text{(Eq. 2)}$$

where A represents either HFE or Fe-Tf. The apparent rate constants can be converted to intrinsic rate constants (k_{1on}, k_{2on}, k_{1off}, and k_{2off}) by applying statistical factors to account for the two potential binding sites on a homodimeric TfR to which the first analyte molecule can bind and the two sites on the fully bound TfR from which the first dissociation event can occur. Thus, the intrinsic rate constants are related to the apparent rate constants such that $k_{1on} = k_{1on,app}/2$ and $k_{2off} = k_{2off,app}/2$ for independent binding sites. Apparent and intrinsic rates and their relative dissociation constants are reported in Table I to facilitate comparison with our previous studies (20, 24).

To evaluate cooperativity in ligand binding, both hdTfR and wtTfR were chemically coupled because of the requirement for base line stability over the period of 2 days. A concentration series of HFE or Fe-Tf was injected to determine binding affinities in a buffer of 50 mM PIPES, pH 7.4, 150 mM NaCl, 0.005% (v/v) surfactant P-20. The concentration series was then repeated with the analyte diluted into a buffer to which 50 μM Fe-Tf or 10 μM HFE had been added. Equilibrium binding data were collected and processed as previously described (24).

Analytical Ultracentrifugation—Sedimentation velocity experiments were performed at 25 °C in a Beckman XL-I Ultima analytical ultracentrifuge using absorbance optics. Protein concentrations were determined spectrophotometrically at 280 nm using extinction coefficients of 187,199 M^{-1} cm^{-1} (wtTfR dimer), 190,230 M^{-1} cm^{-1} (hdTfR), 89,120 M^{-1} cm^{-1} (HFE/β_2-microglobulin), and 111,399 M^{-1} cm^{-1} (Fe-Tf). The concentrations of wtTfR and hdTfR were fixed at 2.5 μM for all experiments. HFE and Fe-Tf were added at the indicated relative molar ratios to TfR (see Fig. 4). Samples were brought to a final volume of 350–420 μl and loaded into two-sector, charcoal-filled epon centerpieces with quartz windows and placed in a four-hole An-60 titanium rotor. Samples were spun at 32,000, 34,000, or 36,000 rpm. Individual scans were collected at 250 or 280 nm with a step size of 0.005 cm until samples reached the bottom of the cell. Data were fit with the program SEDFIT 8.7 (34) using the $c(s)$ analysis routine, which calculates the differential distribution of sedimentation coefficients with an explicit treatment of sample diffusion. The reported apparent sedimentation coefficients (s^*) values are not corrected to standard conditions because of difficulties obtaining partial specific volumes of the glycosylated HFE, TfR, and Fe-Tf proteins.

Generation of HFE-GFP-expressing TRVb and TRVb-1 Cells—PCR was used to amplify the enhanced green fluorescent protein (EGFP) gene in the pEGFP-1 vector (Clontech) to remove the start codon and introduce a 5′ in-frame XhoI site and 3′ HindIII site. The modified gene was subcloned into pBluescript II SK$^-$ (Stratagene). PCR was used to introduce a 5′ Asp718 site and an in-frame 3′ XhoI site at the 3′-end of the human *HFE* gene, which was then introduced into the EGFP Bluescript vector. The resulting open reading frame encoded the entire HFE amino acid sequence, a leucine-glutamate linker region, and EGFP without its N-terminal methionine. The HFE-EGFP chimeric gene was subcloned after sequencing into the mammalian cell expression vector pCB6-HindIII (gift of Ira Mellman, Yale University), which carries a neomycin resistance gene for G418 selection (35).

TRVb and TRVb-1 cell lines were a generous gift from Dr. Timothy McGraw (Cornell University) (36). Both cell lines were maintained in Ham's F-12 medium (Sigma) supplemented with 10% fetal bovine serum, 2 mM glutamine, 12 mM glucose, and 400 μg/ml G418 (TRVb-1 and transfected cells only). Cells were grown to >90% confluence prior to transfections, which were performed using the HFE-GFP expression vector, a human β_2-microglobulin expression vector (18), and the LipofectAMINE 2000 kit (Invitrogen) according to the manufacturer's directions. Clones exhibiting green cell surface fluorescence were isolated using limiting dilution 2 days after transfection. Cells were sorted for GFP fluorescence using a Coulter Elite flow cytometer (Beckman Coulter Inc.) to isolate cells with a medium level of GFP fluorescence.

Confocal Microscopy—Cells were dissociated using trypsin-free dissociation buffer (Invitrogen), seeded onto glass coverslips in 6-well plates, and grown to confluence. For redistribution experiments, the culture medium was removed and replaced with medium containing varying concentrations of human Fe-Tf (Sigma) or chicken iron-loaded ovo-transferrin (Sigma), and cells were incubated at 37 °C in a 5% CO_2 incubator for 1 h. The culture dishes were then placed on ice and washed three times with ice-cold phosphate-buffered saline. Cells were then fixed at 4 °C for 30 min in 4% paraformaldehyde in phosphate-buffered saline, washed in cold phosphate-buffered saline, and mounted on glass slides using Vecta Shield mounting media (Vector Laboratories, Burlingame, CA). For Tf colocalization experiments, cells were incubated for 1 h at 37 °C with 15 μg/ml Alexa-546-conjugated human Fe-Tf (Molecular Probes, Inc., Eugene, OR) in growth medium and processed as above.

Cells were imaged on a Zeiss LSM Pascal Inverted confocal microscope using a × 63 oil immersion Apochromat objective (numerical aperture 1.4). GFP was excited by the 488-nm line from an argon/krypton laser, and Alexa-546-labeled human Fe-Tf was imaged using the 543-nm line from a helium/neon laser. Two-color data were collected in multitracking mode to prevent fluorophore cross-talk. Images were collected and processed with a Zeiss LSM image examiner. Reported images are 1-μm sections collected 2–3 μm above the basal side of the cell.

RESULTS

Production of a Heterodimeric Transferrin Receptor—To construct a TfR heterodimer (hdTfR) in which one chain only binds HFE and the other chain only binds Fe-Tf, we first identified mutations in human TfR homodimers that eliminate binding of one TfR ligand while having a minimal effect on binding of the other ligand. The choice of residues to substitute was complicated by the fact that the HFE and Fe-Tf binding sites overlap on the surface of TfR; thus, many residue substitutions that reduce binding of one ligand also reduce binding of the other (20, 24). We therefore sought to identify mutations that keep the K_D value for binding the desired ligand within the micromolar to nanomolar range while reducing the affinity for binding to the undesired ligand to a >10 μM or higher K_D. Our choice of TfR substitutions was based on results from previous measurements of the affinities of mutant TfRs for Fe-Tf and HFE (24). To create a TfR chain that binds Fe-Tf but not HFE, we combined substitutions L619A and Y643A, each of which eliminates detectable HFE binding but has a more limited effect on Fe-Tf binding (13- and 27.5-fold affinity reductions,

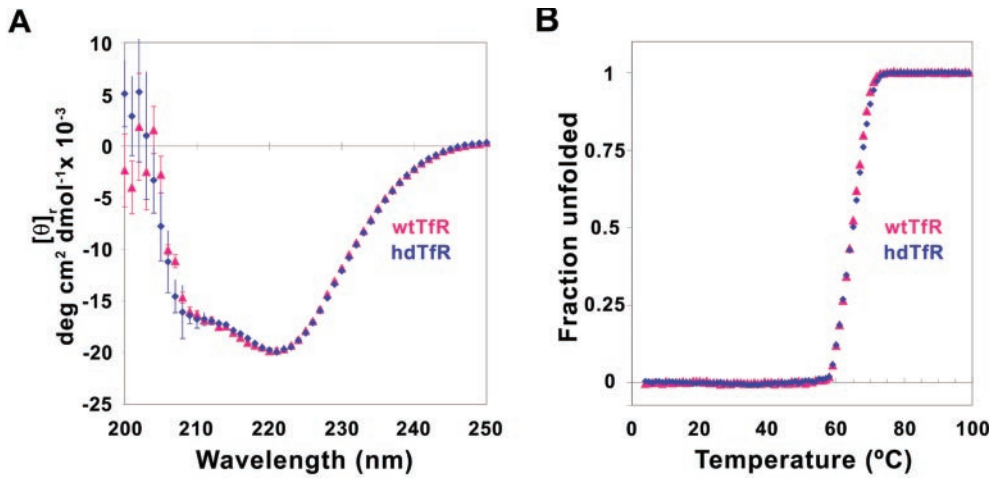

FIG. 2. **Circular dichroism spectra and thermal denaturation profiles of wtTfR (*pink triangles*) and hdTfR (*blue diamonds*).** *A*, far-UV CD spectra of wtTfR and hdTfR. The measured CD signal is given as $[\theta]_r$, the molar ellipticity per residue. Data points represent the average and standard deviation of three (wtTfR) or five (hdTfR) replicate scans. *B*, comparison of thermal denaturation profiles for wtTfR and hdTfR. The CD signal at 220 nm was monitored as a function of increasing temperature and plotted as fraction unfolded after normalization. The transition midpoints derived from a plot of $d[\theta]_r/dT$ *versus* T are 64.8 °C for wtTfR and 65.0 °C for hdTfR.

respectively) (20, 24). To create a TfR mutant that binds HFE but not Fe-Tf, we combined three substitutions: Y123S, G647A, and R651A. Each of these mutations has a significant effect on Fe-Tf binding (8.3-, 222-, and >2,800-fold affinity reductions, respectively) (20, 24). Of these, only one substitution (G647A) exhibits any measurable effect on HFE binding (2.6-fold affinity reduction) (20, 24).

An hdTfR composed of one non-HFE binding and one non-Fe-Tf binding chain was produced by co-expression of the two mutant TfR chains in baculovirus-infected cells. To aid in purification, the Fe-Tf-binding TfR chain contained an N-terminal StrepTagII sequence (29), and the HFE-binding TfR chain contained a His_6 tag. Expression in infected insect cells yields three TfR dimers: HFE- but not Fe-Tf-binding homodimers, Fe-Tf- but not HFE-binding homodimers, and hdTfR. Sequential passage of baculovirus supernatants over a Ni^{2+}-NTA column and a streptactin (30) column resulted in separation of hdTfR from the mutant TfR homodimers and from other proteins in the media. hdTfR appeared to be a stable species, since we found no evidence of homodimers or monomers in hdTfR samples stored for up to 2 months (data not shown). The far UV CD spectra (Fig. 2*A*) and thermal denaturation (Fig. 2*B*) profiles of wtTfR and hdTfR showed no significant differences, demonstrating that the mutations introduced into the hdTfR do not adversely affect its folding or stability.

Binding Affinities of HFE and Fe-Tf to hdTfR and Homodimeric TfR Mutants—Affinities of wtTfR and the mutant TfRs were measured in an SPR-based assay for binding to a soluble form of human HFE or to human Fe-Tf at pH 7.4 (18, 20, 24). Doubly His-tagged wtTfR and homodimeric TfR mutants were captured on biosensor chips using a covalently coupled anti-His tag antibody (20, 24), and the hdTfR was chemically coupled using primary amine chemistry (see "Experimental Procedures"). Either HFE or Fe-Tf was then injected over the TfR-coupled sensor chip. Binding data were fit to a bivalent ligand model in which equilibrium dissociation constants (K_{D1} and K_{D2}) are derived for binding to the first and the second binding sites on homodimeric wild-type and mutant TfRs (Table I and Fig. 3) or to a 1:1 binding model in the case of hdTfR. The Y123S/G647A/R651A mutant homodimer does not detectably bind Fe-Tf at any tested concentration (up to 60 μM) (Fig. 3*B*). Its binding affinity for HFE (Fig. 3*A*) was reduced 2.8-fold relative to wtTfR, consistent with the 2.6-fold reduction observed for the G647A mutant in our previous studies (20, 24). The slight affinity reduction resulted from an increased off-rate compared with wtTfR (Table I). The L169A/Y643A mutant homodimer exhibited no detectable binding to HFE (at concentrations up to 20 μM) (Fig. 3*C*), and its affinity for Fe-Tf was reduced ~500-fold (Fig. 3*D*), again due to an increased off-rate (Table I). We previously demonstrated that the loss in free energy for binding Fe-Tf for the two single mutants that compose the L619A/Y643A mutant is 1.5 kcal/mol (L619A) and 2.0 kcal/mol (Y643A), predicting a $\Delta\Delta G$ value of 3.5 kcal/mol at 25 °C for the double mutant if the two substitutions act independently (24). Consistent with this prediction, the observed 502-fold loss of binding affinity for the L169A/Y643A mutant (Table I) corresponded to a $\Delta\Delta G$ of 3.7 kcal/mol at 25 °C.

The binding data for the mutant TfR homodimers were then compared with binding data for hdTfR. The better fit of the 1:1 binding model to binding reactions involving hdTfR (Fig. 3, *G* and *H*) compared with wtTfR (Fig. 3, *E* and *F*, 1:1 model and residuals) suggests that hdTfR forms 1:1 complexes with Fe-Tf and with HFE. Analysis of the differences in derived binding constants is complicated by the use of different binding models for hdTfR or homodimeric TfRs: a 1:1 binding model for the hdTfR yields a single value for the K_D, whereas the bivalent ligand model describing binding to the homodimeric TfRs yields K_D values describing the first and second binding events (see "Experimental Procedures"). The derived K_D values for the HFE-binding and Fe-Tf-binding chains of the hdTfR are within 3-fold of statistically corrected K_{D1} values for their respective homodimeric mutants (Table I), suggesting that hdTfR does not have significantly altered binding affinities relative to the homodimeric mutants from which it was derived.

Determination of Ligand-binding Stoichiometries of wtTfR and hdTfR—To further compare the ligand-binding properties of hdTfR and wtTfR, we used sedimentation velocity AUC. Velocity AUC data were analyzed using the $c(s)$ size distribution method in the program SEDFIT 8.7 (34). This method fits the data numerically to the Lamm equation and yields a differential distribution of s^* values while explicitly correcting for diffusion of the sedimenting species. The output is displayed as a continuous distribution of s^* values *versus* the $c(s^*)$ function describing the distribution of molecular masses in solution.

We first determined the sedimentation properties of binary HFE·TfR and Fe-Tf·TfR complexes. Each of the individual proteins migrates as a single sharp peak when spun alone (Fig. 4, *dashed black lines labeled HFE*, *Fe-Tf*, *wtTfR*, or *hdTfR*). Fig.

TABLE I
HFE and Fe-Tf binding to TfR constructs at 25 °C

Kinetic and equilibrium constants derived from fitting of the surface plasmon resonance data shown in Fig. 3. Numbers in parentheses are corrected for statistical factors (see "Experimental Procedures"). NB, no binding detected at concentrations of injected analyte up to 80 μM Fe-Tf or 20 μM HFE.

Ligand (immobilized protein)	Analyte (injected protein)	k_{on1}	k_{off1}	k_{on2}	$k_{off}2$	K_{D1}	K_{D2}	K_{D1}, K_{D2} (relative to wild type)
		$M^{-1}s^{-1}$	s^{-1}	$M^{-1}s^{-1}$	s^{-1}	nM	nM	
wtTfR	HFE	3.7×10^6 (1.8×10^6)	0.09	2.6×10^6	0.37 (0.20)	24 (48)	154 (77)	
wtTfR	Fe-Tf	1.7×10^6 (8.3×10^5)	1.0×10^{-3}	1.6×10^5	5.8×10^{-3} (3.2×10^{-3})	0.6 (1.3)	40.6 (20.3)	2.8, 2.5
Y123S/G647A/R651A-TfR	HFE	3.6×10^5 (1.8×10^6)	0.25	2.2×10^6	0.82 (0.41)	67 (134)	384 (192)	
Y123S/G647A/R651A-TfR	Fe-Tf					NB	NB	>27,000
L619A/Y643A-TfR	HFE					NB	NB	>800
L619A/Y643A-TfR	Fe-Tf	5.2×10^5 (2.4×10^5)	0.15	1.5×10^5	0.46 (0.23)	314 (627)	2,940 (1,470)	502, 73
hdTfR	HFE	6.8×10^5	0.27			390		8.1
hdTfR	Fe-Tf	1.9×10^5	0.23			1,210		930

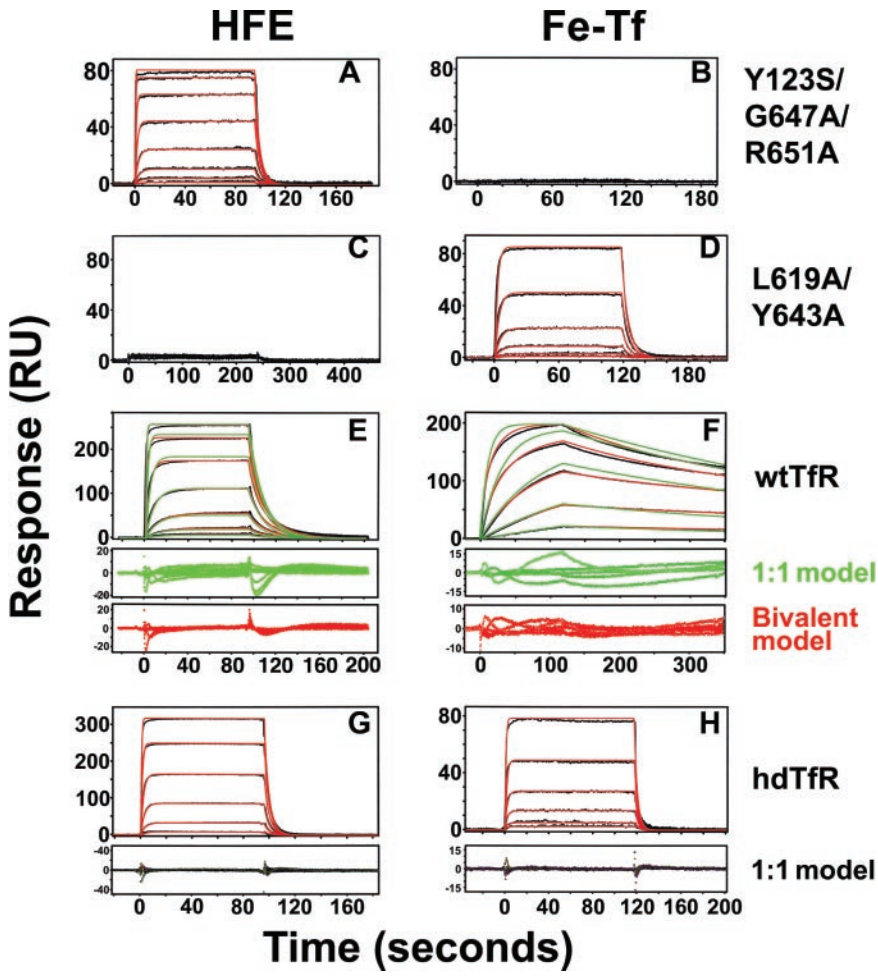

FIG. 3. **SPR analysis of HFE and Fe-Tf binding to TfR proteins.** Experimentally observed response (*black lines*) of HFE or Fe-Tf binding to the indicated TfR molecules is shown with superimposed best fit binding curves (*colored lines*) derived from a bivalent ligand binding model (wtTfR and homodimeric mutant TfRs except where noted) or a 1:1 binding model (hdTfR). Residual plots (difference between the observed and calculated binding data) are shown in *E–H below* the response data. The wtTfR binding data shows fits and residuals for both 1:1 (*green*) and bivalent ligand (*red*) binding models. The highest concentrations in the injection series for each sensorgram are 5 μM (*A*), 60 μM (*B*), 20 μM (*C*), 6 μM (*D*), 2 μM (*E*), 111 nM (*F*), 1.6 μM (*G*), and 10 μM (*H*). Subsequent injections are related by 3-fold dilutions.

4*A* shows the results of mixing HFE and wtTfR in molar ratios of 1:1, 2:1, 4:1, and 6:1, confirming previous findings of both 1:1 and 2:1 HFE/TfR complexes in solution (18, 20), with 2:1 being the terminal stoichiometry as indicated by the presence of excess HFE at the higher mixing ratios. By contrast, mixing excess HFE in the presence of hdTfR resulted in a peak corresponding to a 1:1 HFE·TfR complex, confirming that hdTfR does not readily form 2:1 HFE·TfR complexes (Fig. 4*D*). Analogous experiments were performed to investigate binary interactions of Fe-Tf with wtTfR and hdTfR. Fig. 4*B* shows the results of mixing Fe-Tf and wtTfR at various ratios, confirming previous reports of a 2:1 terminal Fe-Tf/TfR stoichiometry (17, 18). Here we note evidence for formation of a 1:1 Fe-Tf·TfR complex at the 1:1 mixing ratio, which, although predicted to be present in an equilibrium mixture of Fe-Tf and TfR (Fig. 1), has not been previously reported. Mixing Fe-Tf with hdTfR resulted in two connected peaks in the $c(s^*)$ distribution (Fig. 4*E*). The smaller peak represents free hdTfR, and the larger peak is due to the 1:1 Fe-Tf·hdTfR complex. The slightly different position for the 1:1 Fe-Tf·hdTfR peak compared with the position for the 1:1 Fe-Tf·wtTfR peak results from the faster kinetics of complex association and dissociation for hdTfR compared with wtTfR (Table I). We see no evidence of a 2:1 Fe-Tf·hdTfR complex (Fig. 4*E*).

We next used sedimentation velocity AUC to characterize the complexes formed when hdTfR and wtTfR are mixed with both HFE and Fe-Tf. At a mixing ratio of 1:1:1 HFE/wtTfR/Fe-Tf, a broad peak centered at 11.8 S was observed (Fig. 4*C*). The

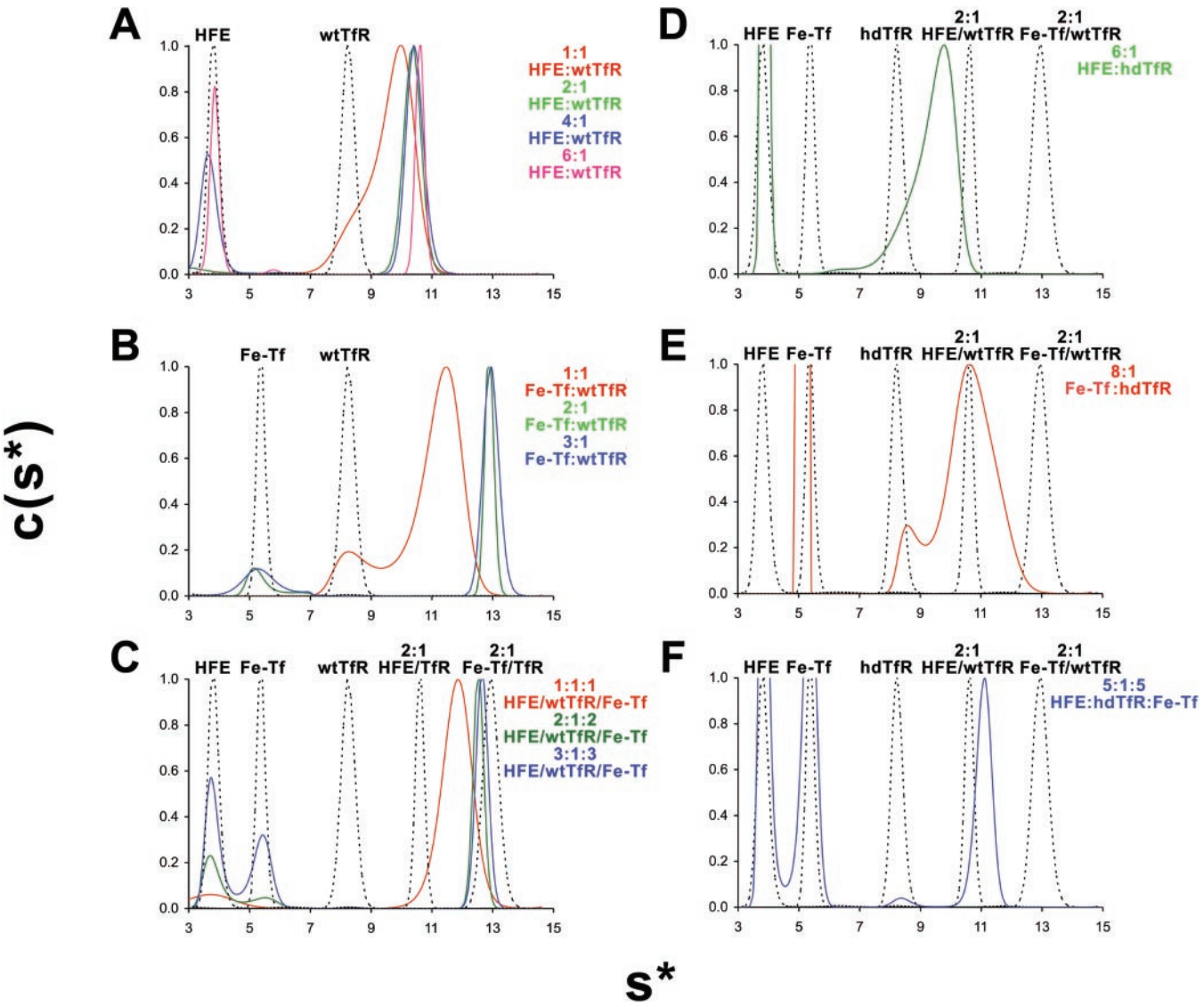

FIG. 4. **Stoichiometries of HFE and Fe-Tf binding to wtTfR and hdTfR from sedimentation velocity ultracentrifugation.** The $c(s^*)$ distribution was determined for each protein alone or in the mixing ratio indicated to the *right* of each *panel*. Reference curves for individual proteins or specific complexes are shown as *dotted black lines*. Peak heights were normalized to the height of the species with the largest s^* value in the distribution.

location of the center of the peak midway between the peaks for the 2:1 HFE·wtTfR and 2:1 Fe-Tf·wtTfR complexes and the fact that the peak spans the positions of the binary complexes are consistent with identification of this peak as a mixture of the 1:1:1 HFE·TfR·Fe-Tf ternary complex with binary 2:1 Fe-Tf·TfR and 2:1 HFE·TfR complexes (Fig. 4*C*, *red curve*). Mixing of the three proteins at higher ligand ratios (2:1:2 and 3:1:3 HFE/TfR/Fe-Tf) resulted in a peak closer to the one observed for 2:1 Fe-Tf/TfR, demonstrating that Fe-Tf effectively competes HFE away from TfR in solution, due to the intrinsically higher TfR binding affinity of Fe-Tf compared with soluble HFE. Mixing of HFE and Fe-Tf with the hdTfR also resulted in a peak between the 2:1 HFE·wtTfR and 2:1 Fe-Tf·wtTfR complexes (Fig. 4*F*). The distribution was more narrow for the ternary complex involving hdTfR, consistent with the expectation that binary complexes with a 2:1 ligand/hdTfR stoichiometry do not form.

Comparison of HFE and Fe-Tf Binding to hdTfR and wtTfR Rules Out Cooperativity in Ligand Binding—Having demonstrated that the engineered hdTfR binds to one HFE and one Fe-Tf to form a ternary complex, we could use the hdTfR to evaluate the potential for heterotropic cooperativity in ligand binding in the absence of the competition observed when using wtTfR. Cooperativity in binding was assessed using an SPR-based binding assay to compare the binding behavior for either HFE or Fe-Tf to hdTfR in the presence and absence of excess Fe-Tf or HFE. If cooperativity is a feature of TfR interactions with HFE or Fe-Tf, then incubation of TfR with saturating amounts of one ligand will perturb the equilibrium binding curve of the second ligand. For these experiments, wtTfR and hdTfR were immobilized on adjacent flow cells of the same sensor chip using primary amine coupling chemistry. We then evaluated the binding of HFE to each TfR in the presence and absence of a saturating concentration of Fe-Tf (50 μM). Binding data were collected using an equilibrium-based approach in which binding reactions reached or closely approached equilibrium. Data for HFE binding to hdTfR in the presence and absence of Fe-Tf (Fig. 5*B*) showed no significant differences, indicating that binding of Fe-Tf to one chain of TfR does not alter the binding properties of the other chain for HFE. Similarly, the binding of Fe-Tf for hdTfR was not altered by the presence of a saturating amount of HFE (10 μM) (Fig. 5*D*). By contrast, when the same binding experiments were performed with wtTfR, we observed competition between HFE and Fe-Tf for binding to TfR. When HFE was injected in the presence of

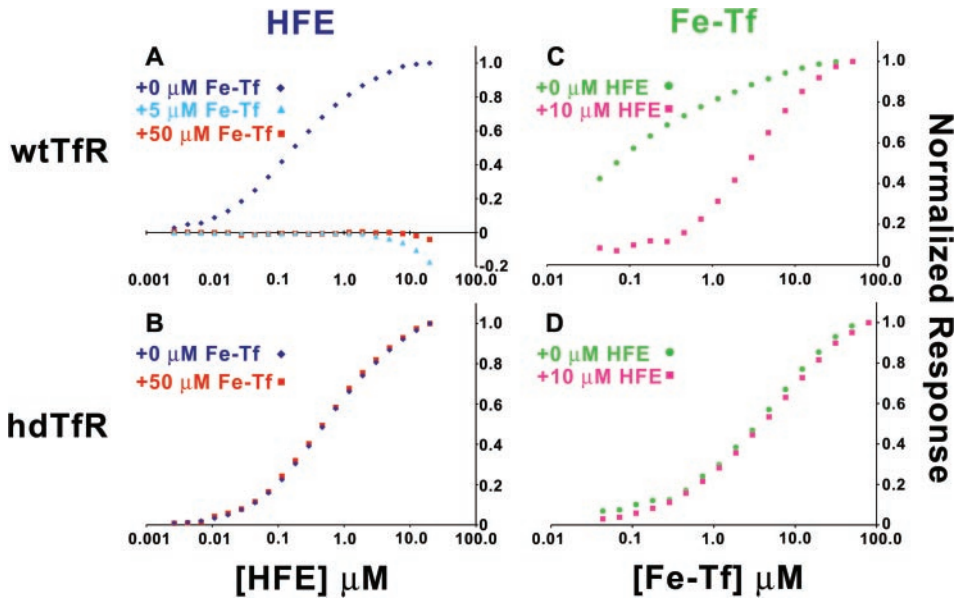

FIG. 5. **SPR assay of competition between HFE and Fe-Tf for binding to wtTfR *versus* hdTfR.** Plots are of the normalized equilibrium biosensor response value *versus* the log of the indicated protein concentration. HFE binding in the absence (*blue diamonds*) or presence of Fe-Tf (50 μM Fe-Tf (*red square*) and 5 μM Fe-T (*cyan triangle*)) to wtTfR (*A*) or to hdTfR (*B*). Fe-Tf binding is shown in the absence (*green circle*) or presence of 10 μM HFE (*magenta square*) to wtTfR (*C*) or to hdTfR (*D*). Data points are related by a 1.6-fold dilution series.

excess (50 μM) or near physiological (5 μM) (37) quantities of Fe-Tf (Fig. 5*A*), only a small amount of HFE binding was observed at the highest concentrations tested (Fig. 5*A*). This binding was observed as a decrease in SPR signal, because the binding of HFE requires the displacement of Fe-Tf, which is 1.8 times heavier than HFE, from its binding site on TfR (20, 24, 25). When Fe-Tf was injected in the presence of saturating amounts of HFE (10 μM), there was a reduction in Fe-Tf binding (Fig. 5*C*), consistent with previous reports that HFE reduces the observed binding affinity of Fe-Tf to TfR (8, 21, 23). Consistent with the lower TfR binding affinity of HFE as compared with Fe-Tf, HFE begins to compete with Fe-Tf for binding wtTfR only when it is present at a 4-fold or higher concentration than Fe-Tf, whereas Fe-Tf begins to compete with HFE for binding wtTfR when it is present at one-tenth the concentration of HFE. Taken together, these experiments confirm that HFE and Fe-Tf compete for TfR binding sites and rule out the effects of negative cooperativity in the HFE/hdTfR/Fe-Tf ternary interaction.

Cell Surface HFE Competes Effectively with Fe-Tf for Binding to Cell Surface TfR—The demonstration that negative cooperativity is not involved in heterotropic interactions between TfR, HFE, and Fe-Tf indicates that direct competition between HFE and Fe-Tf for binding to cell surface TfR is solely responsible for the observation that HFE lowers the affinity of TfR for Fe-Tf (5, 21, 23). Our SPR and AUC experiments demonstrate that soluble HFE competes poorly against Fe-Tf for TfR binding because of its lower affinity for TfR compared with Fe-Tf (Figs. 4*C* and 5*A*). Under physiological conditions, however, HFE and TfR are tethered to the same membrane (19), thereby increasing their effective local concentrations and permitting potential interactions between the HFE and TfR cytoplasmic tails (22). Either or both of these effects could allow HFE to compete more effectively against Fe-Tf for binding to TfR.

To evaluate how the addition of Fe-Tf affects complex formation between full-length HFE and TfR proteins tethered to a common membrane, we first showed that binding to TfR is required for a GFP-tagged form of HFE to traffic to Tf-positive endosomal compartments, and then asked if the addition of Fe-Tf affects endosomal localization of HFE-GFP. For these experiments, we expressed an HFE-GFP chimeric protein, in which GFP was fused to the C terminus of full-length HFE, in two forms of Chinese hamster ovary cells: TRVb cells, which lack expression of endogenous hamster TfR, and TRVb-1 cells, which lack endogenous TfR but stably express human TfR (36). Confocal imaging of HFE-GFP-expressing TRVb-1 (HFE^+/TfR^+) cells reveals primarily intracellular fluorescence (Fig. 6*A*, *middle panel*), which co-localizes with endocytosed Alexa-546-labeled human Fe-Tf (Fig. 6*A*, *right panel*), demonstrating that the HFE traffics to Tf-positive endosomes in cells expressing TfR. By contrast, most of the GFP fluorescence in HFE-GFP-expressing TRVb cells (HFE^+/TfR^-) was primarily localized at the cell surface (Fig. 6*A*, *left panel*), and these cells show no significant intracellular fluorescence in Alexa-546 Fe-Tf uptake experiments (data not shown). These data demonstrate that binding to cell surface TfR is required for HFE localization in Tf-positive endosomes, consistent with the lack of an obvious endocytic signal in the HFE cytoplasmic tail (3, 8, 21). Thus, endosomal localization of HFE-GFP can be used to evaluate competition between Fe-Tf and HFE for binding to cell surface TfR.

Since HFE binding to TfR is required for HFE translocation to Tf-positive endosomes, we investigated whether endosomal localization of HFE could be prevented by the presence of high concentrations of extracellular Fe-Tf. To address this question, we incubated TRVb-1-HFE-GFP (HFE^+/TfR^+) cells in growth medium supplemented with Fe-Tf at concentrations ranging from 0 nM to 50 μM. At relatively low concentrations of extracellular Fe-Tf (500 nM), HFE-GFP fluorescence began to redistribute from intracellular locations to the cell surface (Fig. 6*B*). Upon the addition of micromolar concentrations of Fe-Tf corresponding to serum Fe-Tf levels (37), we saw a substantial reduction of endosomal GFP fluorescence with a concomitant increase in cell surface fluorescence (Fig. 6*B*). At Fe-Tf concentrations exceeding 5 μM, little or no HFE-GFP fluorescence localized to endosomes, indicating that Fe-Tf has competed effectively with HFE to occupy virtually all binding sites on cell surface TfR molecules (Fig. 6*B*). The addition of the same concentrations of iron-loaded ovotransferrin, a transferrin ortholog that does not bind human TfR (38), did not result in detectable redistribution of HFE-GFP from endosomal compartments to the cell surface (Fig. 6*C*), indicating that the HFE

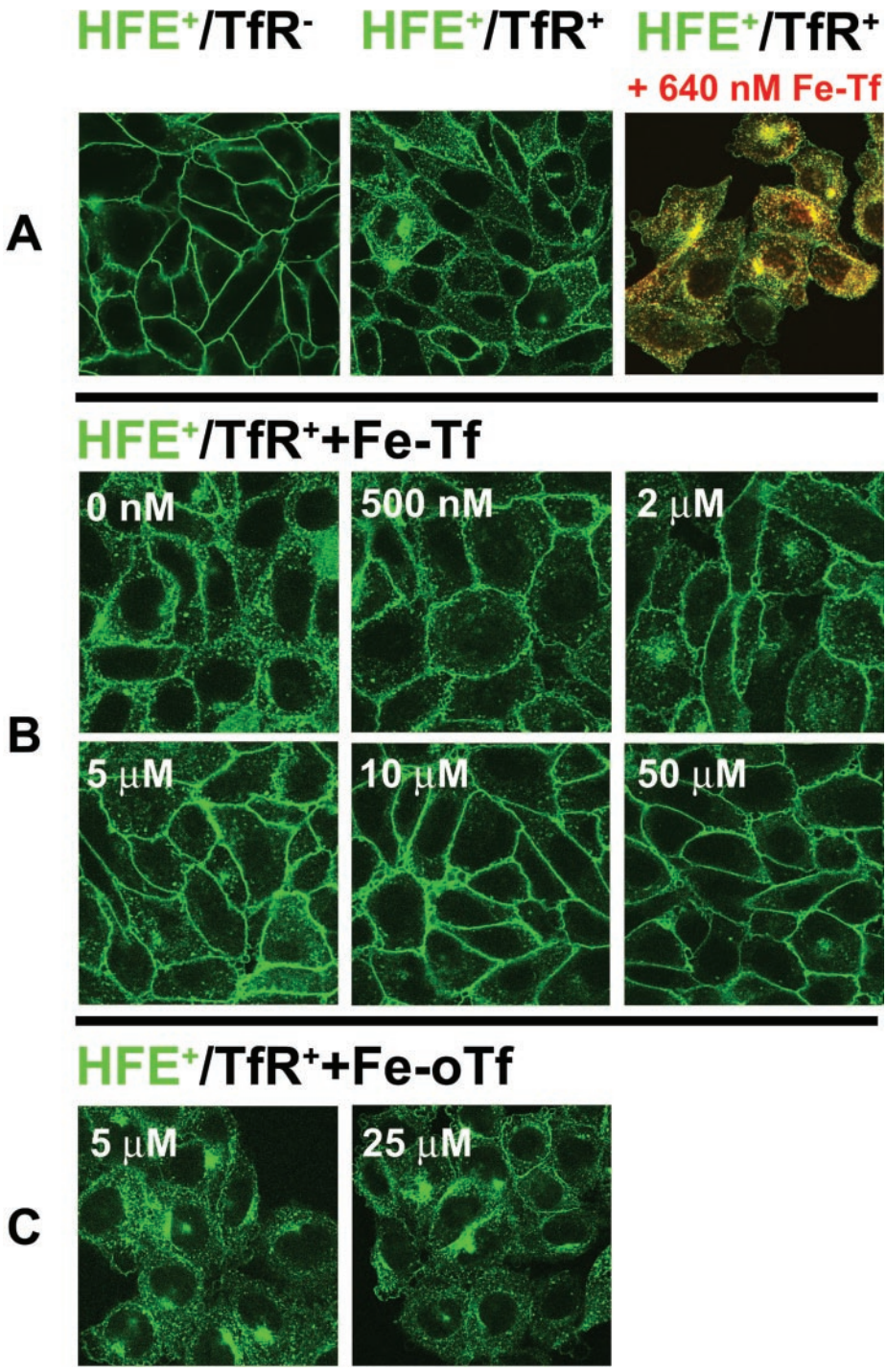

FIG. 6. **Confocal images of HFE-GFP distribution in TRVb (TfR$^-$) and TRVb-1 (TfR$^+$) cells.** *A*, cells expressing HFE-GFP (*green fluorescence*) in the absence (*left*) or presence (*middle*) of co-expressed human TfR. Co-localization of HFE-GFP fluorescence with Alexa-546-labeled human Fe-Tf in TfR$^+$ cells is shown on the *right*. *B*, cells expressing HFE-GFP and human TfR incubated with the indicated concentrations of unlabeled human Fe-Tf in the culture media. *C*, cells expressing HFE-GFP and TfR incubated with the indicated concentrations of chicken Fe-Tf (*Fe-oTf*) in the culture media.

redistribution effect is due to direct competition between HFE and human Fe-Tf for TfR binding sites.

DISCUSSION

TfR is a homodimeric receptor that binds two ligands at neutral or basic pH: Fe-Tf and HFE. TfR can form binary complexes with either HFE or Fe-Tf and can bind both ligands simultaneously to form a 1:1:1 HFE·TfR·Fe-Tf ternary complex (18–20). Characterizing the ternary complex is of interest, because both soluble and membrane-bound HFE reduce the apparent affinity of soluble and membrane-bound TfR for Fe-Tf (8, 21, 23, 39). Since mixtures of binary and ternary complexes form when all three proteins are present (Fig. 1), it has not been possible to determine if HFE reduces the affinity of TfR for Fe-Tf via direct competition for overlapping binding sites on TfR and/or if structural changes induced by HFE binding to one chain of the TfR dimer (19) lowers the binding affinity for ligand on the other TfR chain. Although several studies have demonstrated that HFE and Fe-Tf compete for binding to a common site on TfR (20, 24, 25), the potential role for negative cooperativity in the binding of Fe-Tf to 1:1 HFE·TfR complexes has not been addressed because of complications arising from the competing side reactions that lead to 2:1 HFE·TfR and Fe-Tf·TfR complexes when both HFE and Fe-Tf are incubated with homodimeric wtTfR. To directly evaluate the effects of heterotropic ligand binding to TfR, we constructed a hdTfR in which one chain binds HFE but not Fe-Tf and the other chain binds Fe-Tf but not HFE, such that only ternary complexes can form when hdTfR is incubated with Fe-Tf and HFE.

Although many substitutions in the TfR ligand-binding site affect binding to both ligands (20, 24), we were able to produce an hdTfR in which the HFE-binding chain retains a 390 nM affinity for HFE, but no detectable affinity for Fe-Tf, and the Fe-Tf-binding chain retains a 1.2 μM affinity for Fe-Tf but does not bind detectably to HFE (Fig. 3, *A–D*, Table I). Sedimentation velocity AUC and biosensor binding assays demonstrate that the hdTfR binds only one HFE and only one Fe-Tf and that it forms a 1:1:1 HFE·TfR·Fe-Tf ternary complex when all three proteins are mixed together. Having confirmed that hdTfR does not participate in side reactions leading to binary complexes (Fig. 1), we used it to evaluate whether binding of ligand to one chain of TfR affects the binding affinity of the other ligand for TfR. Biosensor binding assays conducted in the presence and absence of a saturating concentration of Fe-Tf reveal no significant differences in the binding affinity of HFE for hdTfR. Similarly, Fe-Tf binding to hdTfR is not altered by prebinding HFE to one chain of hdTfR. By contrast, when wtTfR is incubated with a saturating amount of HFE, we observe a reduction in the apparent binding affinity for Fe-Tf, as previously reported (23). The experiments using hdTfR demonstrate that there is no cooperativity, either negative or positive, in heterotropic ligand binding by hdTfR, suggesting that the apparent lowering of the Fe-Tf affinity of cell surface and soluble wtTfR by HFE (8, 23, 39, 40) results entirely from competition between HFE and Fe-Tf for overlapping binding sites on the TfR surface. Extending these results to wtTfR requires the assumption that the mutations used to create the hdTfR do not themselves disrupt cooperativity. Because we cannot evaluate cooperativity using wtTfR, we cannot directly address this issue. However, it is unlikely that the mutations themselves disrupt cooperativity, because the substituted residues are on the exterior of the protein in locations that are distant from the TfR dimer interface, across which structural changes would need to be propagated for cooperativity in ligand binding to occur.

Having shown that direct competition rather than allostery affects heterotropic ligand binding by TfR in solution, we next evaluated the effects of competition as a function of ligand concentration. Using wtTfR in a biosensor-based binding assay, we find that HFE shows only minimal binding to wtTfR when Fe-Tf is present at concentrations of 5 μM and above, demonstrating that it can compete with Fe-Tf, but only when it is several times more concentrated. Consistent with this result, sedimentation velocity AUC experiments show that 2:1 Fe-Tf·TfR complexes are the dominant species when HFE, Fe-Tf, and wtTfR are mixed such that the HFE and Fe-Tf are at higher concentrations than wtTfR. Therefore, soluble HFE is a poor competitor for binding to soluble TfR when Fe-Tf is present at high concentrations, including the micromolar concentrations corresponding to physiological levels of Fe-Tf in blood (37).

If TfR binding is required for HFE to act as a regulator of cellular iron homeostasis, then it must compete effectively against physiological levels of Fe-Tf when TfR and HFE are both present at the surface of a cell. Since HFE and TfR are tethered to the same cellular membrane (19), the effective concentrations of both proteins may be much higher than in the biochemical assays involving soluble proteins used here. We therefore developed a cell-based assay to evaluate the effects of the addition of soluble Fe-Tf on the interaction between membrane-bound HFE and membrane-bound TfR. As an indication of HFE·TfR complex formation, we monitored the localization of an HFE-GFP chimeric protein in transfected cells, assuming that HFE-GFP fluorescence in endosomes represents HFE-GFP that trafficked there as a result of binding to cell surface TfR. This assumption was verified by showing that HFE trafficks to Tf-positive endosomes in TfR-positive but not TfR-negative cells; thus, TfR binding is required for HFE to enter endosomes. By incubating the TfR-positive cells with Fe-Tf, we then demonstrated a loss of endosomal HFE-GFP fluorescence at relatively low concentrations of exogenous Fe-Tf (500 nM), with a substantial redistribution of GFP fluorescence to the cell surface at near physiological concentrations of exogenous Fe-Tf (micromolar) (37). Thus, external levels of Fe-Tf can influence both the localization and binding state of HFE in cells. The relatively high concentrations of Fe-Tf required to affect HFE localization and binding to TfR suggest a reevaluation of previous studies using transfected cells in which subphysiological concentrations of Fe-Tf were used as the iron source (7, 21, 22, 39–44). Our data suggest that redistribution of HFE at micromolar concentrations of Fe-Tf in blood has functional consequences that may not be observed in studies using submicromolar levels of Fe-Tf.

Indeed, competition between HFE and Fe-Tf for binding to TfR has been hypothesized to be critical for controlling iron metabolism (45, 46). In one model involving HFE/Fe-Tf competition, the concentration of Fe-Tf controls whether HFE binds to TfR, thereby inhibiting uptake of Fe-Tf, or if HFE binds to another cell surface protein (*e.g.* ferroportin, an iron-export protein (47–49)), thereby inhibiting export of intracellular iron. Although our results show that soluble HFE competes poorly with Fe-Tf for binding to soluble TfR, membrane-bound HFE can compete effectively with physiological concentrations of exogenous Fe-Tf for binding to cell surface TfR. Thus, the amount of cell surface HFE bound to cell surface TfR can be controlled by the concentration of exogenous Fe-Tf, alone or in concert with changes in TfR expression levels, allowing regulation of the binding configuration of HFE at the cell surface. There are three possible binding configurations of HFE at the cell surface (bound to TfR, bound to another protein(s), or free), each of which could be involved in regulation of iron homeostasis. For example, HFE bound to TfR can prevent uptake of iron in the form of Fe-Tf. If Fe-Tf binding to TfR competes away HFE, allowing it to bind to an iron transport protein such as ferroportin or DMT1 (an iron import protein (50)), then fluctuations in the level of free *versus* bound HFE could regulate either the rate of cellular iron export (ferroportin) or import (DMT1). Additionally, if cells can sense the amount of cell surface or endosomally localized HFE, then fluctuations in those levels could affect downstream signaling.

Elucidating the details of the interactions between HFE, TfR, and Fe-Tf will be critical for understanding the mechanisms by which mammals regulate iron levels. We have clarified the interactions between these proteins, demonstrating that several TfR/ligand stoichiometries are possible, that HFE/TfR binding is required for HFE transport to endosomes, and that there is strong allostery-free competition between HFE and Fe-Tf for TfR binding at the cell surface. These results provide experimental support for models of iron regulation in which competition between HFE and Fe-Tf for binding to TfR plays a central role in maintaining cellular iron homeostasis (45).

Acknowledgments—We thank Peter Snow, Inderjit Nangiana, and Cynthia Jones (Caltech Protein Expression Facility) for insect cell expression of TfR constructs; Tim McGraw (Cornell) for providing TRVb and TRVb-1 cells; W. Lance Martin and Jasvinder Nangiana for construction of expression vectors; Rochelle Diamond (Caltech Cell Sorting Facility) for cell sorting; Kirsten Lassila for assistance with CD data collection; the Beckman Imaging Center at Caltech for providing confocal microscopes and support; Andrew Herr, Caroline Enns, Devin Tesar, and Rich Olson for helpful discussions; Dave Myszka for beta versions of Scrubber and Clamp; and members of the Björkman laboratory for critical reading of the manuscript.

REFERENCES

1. Cullen, L. M., Anderson, G. J., Ramm, G. A., Jazwinska, E. C., and Powell, L. W. (1999) *Annu. Rev. Med.* **50,** 87–98
2. Bothwell, T. H., and MacPhail, A. P. (1998) *Semin. Hematol.* **35,** 55–71
3. Feder, J. N., Gnirke, A., Thomas, W., Zsuchihashi, Z., Ruddy, D. A., Basava, A., Dormishian, F., Domingo, R., Ellis, M. C., Fullan, A., Hinton, L. M., Jones, N. L., Kimmel, B. E., Kronmal, G. S., Lauer, P., Lee, V. K., Loeb, D. B., Mapa, F. A., McCellland, E., Meyer, N. C., Mintier, G. A., Moeller, N., Moore, T., Morikang, E., Prass, C. E., Quintana, L., Starnes, S. M., Schatzman, R. C., Brunke, K. J., Drayna, D. T., Risch, N. J., Bacon, B. R., and Wolff, R. K. (1996) *Nat. Genet.* **13,** 399–408
4. Garcia, K. C., Teyton, L., and Wilson, I. A. (1999) *Annu. Rev. Immunol.* **17,** 369–397
5. Feder, J. N., Tsuchihashi, Z., Irrinki, A., Lee, V. K., Mapa, F. A., Morikang, E., Prass, C. E., Starnes, S. M., Wolff, R. K., Parkkila, S., Sly, W. S., and Schatzman, R. C. (1997) *J. Biol. Chem.* **272,** 14025–14028
6. Waheed, A., Parkkila, S., Zhou, X. Y., Tomatsu, S., Tsuchihashi, Z., Feder, J. N., Schatzman, R. C., Britton, R. S., Bacon, B. R., and Sly, W. S. (1997) *Proc. Natl. Acad. Sci. U. S. A.* **94,** 12384–12389
7. Roy, C. N., Carlson, E. J., Anderson, E. L., Basava, A., Starnes, S. M., Feder, J. N., and Enns, C. A. (2000) *FEBS Lett.* **484,** 271–274
8. Feder, J. N., Penny, D. M., Irrinki, A., Lee, V. K., Lebrón, J. A., Watson, N., Tsuchihashi, Z., Sigal, E., Bjorkman, P. J., and Schatzman, R. C. (1998) *Proc. Natl. Acad. Sci. U. S. A.* **95,** 1472–1477
9. Parkkila, S., Waheed, A., Britton, R. S., Bacon, B. R., Zhou, X. Y., Tomatsu, S., Fleming, R. E., and Sly, W. S. (1997) *Proc. Natl. Acad. Sci. U. S. A.* **94,** 13198–13202
10. Leibman, A., and Aisen, P. (1977) *Biochemistry* **16,** 1268–1272
11. Rothenberger, S., Iacopetta, B. J., and Kuhn, L. C. (1987) *Cell* **49,** 423–431
12. Collawn, J. F., Kuhn, L. A., Liu, L. F., Tainer, J. A., and Trowbridge, I. S. (1991) *EMBO J.* **10,** 3247–3253
13. Collawn, J. F., Lai, A., Domingo, D., Fitch, M., Hatton, S., and Trowbridge, I. S. (1993) *J. Biol. Chem.* **268,** 21686–21692
14. Sipe, D. M., and Murphy, R. F. (1991) *J. Biol. Chem.* **266,** 8002–8007
15. Bali, P. K., Zak, O., and Aisen, P. (1991) *Biochemistry* **30,** 324–328
16. Dautry-Varsat, A., Ciechanover, A., and Lodish, H. F. (1983) *Proc. Natl. Acad. Sci. U. S. A.* **80,** 2258–2262
17. Enns, C. A., and Sussman, H. H. (1981) *J. Biol. Chem.* **256,** 9820–9823
18. Lebrón, J. A., Bennett, M. J., Vaughn, D. E., Chirino, A. J., Snow, P. M., Mintier, G. A., Feder, J. N., and Bjorkman, P. J. (1998) *Cell* **93,** 111–123
19. Bennett, M. J., Lebrón, J. A., and Bjorkman, P. J. (2000) *Nature* **403,** 46–53
20. West, A. P., Jr., Giannetti, A. M., Herr, A. B., Bennett, M. J., Nangiana, J. S., Pierce, J. R., Weiner, L. P., Snow, P. M., and Bjorkman, P. J. (2001) *J. Mol. Biol.* **313,** 385–397
21. Gross, C. N., Irrinki, A., Feder, J. N., and Enns, C. A. (1998) *J. Biol. Chem.* **273,** 22068–22074
22. Salter-Cid, L., Brunmark, A., Li, Y., Leturcq, D., Peterson, P. A., Jackson, M. R., and Yang, Y. (1999) *Proc. Natl. Acad. Sci. U. S. A.* **96,** 5434–5439
23. Lebrón, J. A., West, A. P., and Bjorkman, P. J. (1999) *J. Mol. Biol.* **294,** 239–245
24. Giannetti, A. M., Snow, P. M., Zak, O., and Bjorkman, P. J. (2003) *PLoS. Biol.* **1,** 341–350
25. Liu, R., Guan, J. Q., Zak, O., Aisen, P., and Chance, M. R. (2003) *Biochemistry* **42,** 12447–12454
26. Cheng, Y., Zak, O., Aisen, P., Harrison, S. C., and Walz, T. (2004) *Cell* **116,** 565–576
27. Lawrence, C. M., Ray, S., Babyonyshev, M., Galluser, R., Borhani, D. W., and Harrison, S. C. (1999) *Science* **286,** 779–782
28. Lebrón, J. A., and Bjorkman, P. J. (1999) *J. Mol. Biol.* **289,** 1109–1118
29. Schmidt, T. G., Koepke, J., Frank, R., and Skerra, A. (1996) *J. Mol. Biol.* **255,** 753–766
30. Voss, S., and Skerra, A. (1997) *Protein Eng.* **10,** 975–982
31. Fägerstam, L. G., Frostell-Karlsson, A., Karlsson, R., Persson, B., and Rönnber, I. (1992) *J. Chromatogr.* **597,** 397–410
32. Malmqvist, M. (1993) *Nature* **361,** 186–187
33. Morton, T. A., and Myszka, D. G. (1998) *Methods Enzymol.* **295,** 268–294
34. Schuck, P. (2000) *Biophys. J.* **78,** 1606–1619
35. Brewer, C. B., and Roth, M. G. (1991) *J. Cell Biol.* **114,** 413–421
36. McGraw, T. E., Greenfield, L., and Maxfield, F. R. (1987) *J. Cell Biol.* **105,** 207–214
37. Henry, J. B. (1991) *Clinical Diagnosis and Management by Laboratory Methods*, W. B. Saunders Co., Philadelphia
38. Shimo-Oka, T., Hagiwara, Y., and Ozawa, E. (1986) *J. Cell. Physiol.* **126,** 341–351
39. Roy, C. N., Penny, D. M., Feder, J. N., and Enns, C. A. (1999) *J. Biol. Chem.* **274,** 9022–9028
40. Riedel, H. D., Muckenthaler, M. U., Gehrke, S. G., Mohr, I., Brennan, K., Herrmann, T., Fitscher, B. A., Hentze, M. W., and Stremmel, W. (1999) *Blood* **94,** 3915–3921
41. Corsi, B., Levi, S., Cozzi, A., Corti, A., Altimare, D., Albertini, A., and Arosio, P. (1999) *FEBS Lett.* **460,** 149–152
42. Feeney, G. P., and Worwood, M. (2001) *Biochim. Biophys. Acta* **1538,** 242–251
43. Waheed, A., Grubb, J. H., Zhou, X. Y., Tomatsu, S., Fleming, R. E., Costaldi, M. E., Britton, R. S., Bacon, B. R., and Sly, W. S. (2002) *Proc. Natl. Acad. Sci. U. S. A.* **99,** 3117–3122
44. Montosi, G., Paglia, P., Garuti, C., Guzman, C. A., Bastin, J. M., Colombo, M. P., and Pietrangelo, A. (2000) *Blood* **96,** 1125–1129
45. Townsend, A., and Drakesmith, H. (2002) *Lancet* **359,** 786–790
46. Drakesmith, H., Sweetland, E., Schimanski, L., Edwards, J., Cowley, D., Ashraf, M., Bastin, J., and Townsend, A. R. (2002) *Proc. Natl. Acad. Sci. U. S. A.* **99,** 15602–15607
47. McKie, A. T., Marciani, P., Rolfs, A., Brennan, K., Wehr, K., Barrow, D., Miret, S., Bomford, A., Peters, T. J., Farzaneh, F., Hediger, M. A., Hentze, M. W., and Simpson, R. J. (2000) *Mol. Cell* **5,** 299–309
48. Donovan, A., Brownlie, A., Zhou, Y., Shepard, J., Pratt, S. J., Moynihan, J., Paw, B. H., Drejer, A., Barut, B., Zapata, A., Law, T. C., Brugnara, C., Lux, S. E., Pinkus, G. S., Pinkus, J. L., Kingsley, P. D., Palis, J., Fleming, M. D., Andrews, N. C., and Zon, L. I. (2000) *Nature* **403,** 776–781
49. Abboud, S., and Haile, D. J. (2000) *J. Biol. Chem.* **275,** 19906–19912
50. Gunshin, H., Mackenzie, B., Berger, U. V., Gunshin, Y., Romero, M. F., Boron, W. F., Nussberger, S., Gollan, J. L., and Hediger, M. A. (1997) *Nature* **388,** 482–488

Chapter 4:

A Hydrophobic Patch on Transferrin Receptor Regulates the Iron-Release Properties of Receptor-Bound Transferrin

This chapter is being submitted for publication. We test our hypothesis that the transferrin receptor residues required for specifically binding apo-Tf are important in transferrin receptor's role in stimulating iron release from iron-loaded transferrin. I produced the W641A/F760A-TfR mutant described, purified it, and performed the binding analysis. Peter Halbrooks and Anne B. Mason produced the Fe_C-Tf mutant and performed the iron-release experiments.

A hydrophobic patch on transferrin receptor regulates the iron-release properties of receptor-bound transferrin

Anthony M. Giannetti[1], Peter J. Halbrooks[2], Anne B. Mason[2], and Pamela J. Björkman[3*]

[1]Graduate Option in Biochemistry and Molecular Biophysics, MC 114-96
California Institute of Technology
Pasadena, CA 91125

[2] Department of Biochemistry, University of Vermont, College of Medicine
Burlington, VT 05401

[3]Division of Biology 114-96 and Howard Hughes Medical Institute
California Institute of Technology
Pasadena, CA 91125

[*]*Corresponding author*
E-mail: bjorkman@caltech.edu, Telephone: 626-395-8350, Fax: 626-792-3683.

Abstract

The transferrin receptor (TfR), a dimeric membrane glycoprotein, is responsible for iron uptake in most mammalian cells. At the basic pH of blood (pH 7.4), TfR binds iron-loaded transferrin (Fe-Tf) in serum, and transports it to acidic recycling endosomes where iron is released from Fe-Tf in a TfR-facilitated process. Iron-free transferrin (apo-Tf) remains bound to TfR and is recycled to the cell surface, where apo-Tf rapidly dissociates from TfR upon exposure to the basic pH of blood. We previously demonstrated that substitution of either Trp 641 or Phe 760 in the TfR helical domain reduces TfR's binding to apo-Tf but not to Fe-Tf. Studies with a double mutant of TfR, W641A/F760A, substantiate the earlier finding by demonstrating a 300-fold weaker affinity for apo-Tf relative to wild-type TfR. To evaluate the effects of the mutations on TfR-facilitated iron release from Fe-Tf, we measured release rates at acidic pH from a monoferric form of Tf (Fe_C-Tf) alone and when bound to wild-type TfR or W641A/F760A. We find that iron release from Fe_C-Tf is 200-fold slower when it is bound to the mutant TfR than when bound to wild-type TfR. Whereas binding of Fe_C-Tf to the wild-type TfR accelerates iron release rate by 100-fold compared to free Fe_C-Tf, binding to the mutant TfR slows the iron release rate by two-fold as compared free Fe_C-Tf. These findings demonstrate that the conserved hydrophobic patch on TfR that includes W641 and F760 is required for the receptor-mediated stimulation of iron release from the C-lobe of Tf at low pH.

Introduction

Iron is a fundamental nutrient required for sustaining numerous cellular processes in all cell types. The primary pathway for iron uptake by most mammalian cells involves the transferrin receptor (TfR), a dimeric transmembrane glycoprotein that traffics between the cell surface and acidic intracellular compartments (1). At the basic pH of the cell surface (pH 7.4), TfR binds iron-loaded transferrin (Fe-Tf) (2), an iron transport protein present at micromolar concentrations in the blood (3). Fe-Tf binds to the TfR at pH 7.4 with an equilibrium dissociation constant (K_D) of ~1 nM (4). Fe-Tf/TfR complexes enter acidic endosomes through receptor-mediated endocytosis where iron is released from Fe-Tf at acidic pH in a TfR-assisted process (5-10). The resulting iron-free transferrin (apo-Tf) remains bound to TfR at acidic pH (K_D ~5 nM) during recycling of apo-Tf/TfR complexes back to the cell surface, but dissociates from TfR upon exposure to the slightly basic pH of blood (11).

Crystallographic studies have revealed the structures of TfR and several forms of Tf and Tf-related molecules (12). The structure of the soluble ectodomain of TfR has been reported alone (13) and in complex with HFE (14), the protein mutated in patients with the iron-overload disorder hereditary hemochromatosis (15). Each monomer of the TfR ectodomain is comprised of three structural domains: a protease-like domain resembling amino- and carboxypeptidases (residues 121-188 and 384-606), an apical domain (residues 189-383), and a helical domain involved in homodimerization (residues 607-760). Membrane-bound TfR also includes a glycosylated stalk region (residues 90-120),

a transmembrane region (residues 62-89), and an N-terminal cytoplasmic domain (residues 1-61) that contains a tyrosine-based endosomal sorting sequence (YTRF) (1). Transferrin contains two ~40 kDa lobes (the N- and C-lobes), related by sequence and structural homology (Fig. 1A). Each lobe consists of two domains (N-I and N-II in the N-lobe; C-I and C-II in the C-lobe). A single Fe^{3+} atom is held deep within a cleft formed at the interface between the two domains of each lobe. Each iron atom is octahedrally coordinated by four sidechains from Tf (two tyrosine residues, one histidine, and one aspartate) and by a synergistic anion, which is bicarbonate *in vivo* (16). Iron release results in large conformational changes in each lobe and in the interface between lobes (17,18). There is a 54-63º rotation between the domains that comprise each lobe and a repacking of the interface between each lobe, burying previously exposed residues and exposing previously buried residues (19,20) (Fig. 1B). It is presumed that conformational changes resulting from iron loss occur while Tf is bound to TfR inside acidic vesicles, as the two proteins remain complexed throughout endocytosis and recycling (11). Iron release studies have shown that iron dissociates slowly from Fe-Tf at pH 7.4 in the absence of a chelator (half-life >days). The rate is accelerated at the acidic pH of endosomes (half-life >3 hours at pH 5.5), but is still slow compared with the rate observed for iron transfer from Fe_2-Tf/TfR complexes to the cellular interior (2-3 minutes) (21). The discovery that binding to TfR accelerates the release of iron from Fe-Tf at acidic pH by 100- to 300-fold (9,10) suggests that iron is released inside acidic endosomes during a single round of endocytosis and recycling, but the mechanism by which TfR facilitates iron release from Fe-Tf is not known.

Understanding the mechanism by which TfR facilitates iron release from Fe-Tf requires structural information about how TfR binds to both Fe-Tf and to apo-Tf. Despite the lack of a crystal structure for a Tf/TfR complex, competition (22), mutagenesis (23,24), and time-resolved X-ray footprinting (25) studies have mapped the binding site on TfR for Tf, revealing that the Tf C-lobe binds to the central portion of the TfR helical domain and the Tf N-lobe contacts the bottom of the TfR protease-like domain. Consistent with the mutagenesis and mapping results, a recent ~7.5 Å resolution structure of an Fe-Tf/TfR complex derived by cryoelectron microscopy shows the C-lobe contacting the TfR helical domain and the N-lobe making contacts with the TfR protease-like domain (26). Apo-Tf is believed to bind to TfR in a similar manner, based on the fact that most substitutions that strongly reduce Fe-Tf binding to TfR at basic pH exhibit a similar reduction of apo-Tf binding at pH 6.3 (24). However, at least some differences in the specific contacts of apo-Tf versus Fe-Tf to TfR are suggested by two substitutions in TfR (W641A and F760A) (Fig. 1C or 1D), which reduce binding to apo-Tf without significantly affecting binding to Fe-Tf (24). From these mutagenesis results, we suggested that specific contacts at low pH between Tf and the W641/F760 region of TfR stabilize an open conformation of the Tf C-lobe, thereby allowing protons and chelators to more easily access the Fe^{3+} binding site and accelerate iron release from TfR-bound Fe-Tf.

To further evaluate involvement of the apo-Tf-specific region of TfR in affecting iron release from Fe-Tf, we produced a double mutant of TfR that binds Fe-Tf at basic pH

with wild-type affinity, but shows greatly reduced affinity for apo-Tf at acidic pH. This TfR mutant was made by combining the W641A and F760A substitutions and expressed as a recombinant soluble protein for binding and iron release studies in solution. Quantitative binding studies in solution demonstrate that the W641A/F760A mutant retains a wild-type affinity for Fe-Tf at pH 7.4, but binds apo-Tf with an ~300-fold reduced affinity at pH 6.3. Using a fluorescence-based iron release assay we demonstrate that the rate of iron release from the C-lobe of Tf bound to the mutant TfR is 200-fold slower than the rate for Fe-Tf bound to wild-type TfR and two-fold slower than iron release from uncomplexed Fe-Tf. These results suggest a mechanism by which TfR facilitates iron release from Fe-Tf and are relevant to an understanding of the conformational changes in both Fe-Tf and TfR that are necessary for iron release on biological time scales.

Results

Production and Tf-binding properties of wild-type and mutant TfRs

To construct a TfR that binds Fe-Tf but not apo-Tf, we combined two amino acid substitutions previously identified to lower the binding affinity of TfR for apo-Tf at pH 6.3 but not Fe-Tf at pH 7.4: W641A (~56-fold reduction) and F760A (~16-fold reduction) (24). 6x-His tagged soluble wild-type TfR (wtTfR) and W641A/F760A-TfR (hereafter referred to as W641A/F760A) were expressed and purified as previously described (27). To evaluate the binding characteristics of W641A/F760A, we derived equilibrium dissociation constants (K_Ds) for binding to human Fe-Tf at pH 7.4 and to apo-Tf at pH 6.3 using a surface plasmon resonance (SPR) binding assay. His-tagged wtTfR and mutant TfR were captured directly from baculovirus-infected insect cell supernatants on the surface of a biosensor chip using a covalently coupled anti-His tag antibody as previously described (24,28). Experiments involving apo-Tf were done in the presence of 50 μM desferrioxamine, a potent iron chelator (reviewed in 29).

The SPR experiments demonstrate that W641A/F760A exhibits the expected properties, binding to Fe-Tf at pH 7.4 with no reduction in affinity compared to wtTfR, but binding to apo-Tf at pH 6.3 with a significantly reduced affinity (Fig. 2, Table 1). The 4.7 μM K_D for apo-Tf binding to W641A/F760A represents an ~270-fold reduction in affinity compared to wtTfR, which corresponds to a ΔΔG value of 3.3 kcal/mol at 25 ºC. In our previous mutagenesis study, we demonstrated that the loss in free energy for binding apo-Tf for the two single mutants that comprise the W641A/F760A mutant is 2.4 kcal/mol

(W641A) and 1.6 kcal/mol (F760A), predicting a ΔΔG value of 4.0 kcal/mol if the two substitutions act independently. The difference between the predicted and observed ΔΔG values suggests that the two substitutions do not act completely independently, perhaps because the substituted residues are in van der Waals contact (Fig. 1C, 1D, or Fig. 5) (3.3 Å as measured using the structure of free TfR (13), PDB code 1CX8).

Comparison of TfR-facilitated iron release from Fe-Tf bound to wtTfR versus W641A/F760A

We next sought to determine the effects of a reduced binding affinity for apo-Tf at pH 6.3 on the ability of W641A/F760A to facilitate iron release from Fe-Tf. For these experiments, we used a spectrofluorometric assay that yields a rate of iron release as reported by an increase in protein fluorescence due mainly to the release of quenching of tryptophan residues that are exposed as a result of iron loss (there are five Trp residues in the C-lobe of Tf). The kinetics of iron release from diferric-Tf are complicated by different rates of iron release from the N- and C-lobes (30,31) and from the influence of the iron status of the N-lobe on the release rate from the C-lobe (10). Since only the Fe-Tf C-lobe makes significant interactions with the TfR helical domain (24-26), which contains the hydrophobic patch formed by W641 and F760 (13), we conducted iron release assays using a mutant form of Tf capable of binding an iron atom in the C-lobe, but not in the N-lobe (32), referred to here as Fe_c-Tf and in other studies as N-His-Y95F/Y188F hTf-NG. Fe_c-Tf contains an N-terminal His-tag, substitutions in the C-lobe that eliminate N-linked glycosylation sites (N413A and N611D), and substitution of two

of the four ligands to the iron in the N-lobe (Y95F and Y188F) to prevent iron binding. Previous studies demonstrated that the His-tag and the absence of glycosylation do not affect Tf binding to TfR (33,34).

We first verified that Fe_c-Tf forms complexes with wtTfR and W641A/F760A. Each form of TfR was mixed with a molar excess of Fe_c-Tf and passed over a gel filtration column at pH 8.5 to purify the Fe_c-Tf/TfR complex from free Fe_c-Tf (Fig. 3A). SDS-PAGE analysis of the column fractions verified that the slower migrating peak corresponds to a Fe_c-Tf:TfR complex in the case of both wtTfR and W641A/F760A (Fig. 3B).

Measurement of iron removal for Fe_c-Tf alone at pH 5.6 yielded a release rate of $2.6 \pm 0.2 \times 10^{-3}$ s^{-1}. Binding of wtTfR to Fe_c-Tf increases the rate by ~100 to a rate of $270 \pm 46 \times 10^{-3}$ s^{-1}. By contrast, binding of W641A/760A to Fe_c-Tf decreased the iron release rate to $1.3 \pm 0.03 \times 10^{-3}$ s^{-1}, a factor of two slower than free Fe_c-Tf and 200-fold slower than Fe_c-Tf complexed with wtTfR (Fig. 4 & Table I). The assay conditions used here differ from a previous study using a similar methodology to monitor iron release from the C-lobe of transferrin in the presence and absence of TfR (10). Therefore, the comparison of rates may only be made when the experiment was performed under identical assay conditions (34,35). We note that the use of a higher concentration of protein used here eliminates problems with photobleaching described in the earlier work (10).

Discussion

An important aspect of iron homeostasis is the proper transport, delivery, and uptake of iron into cells, since misdirection of toxic iron atoms can result in large-scale oxidative damage (36). In vertebrates, this process is controlled by the interplay of Tf with its cell-surface receptor, TfR. Tf binds iron with a very high affinity ($K_D = 10^{-22}$ M) and exhibits slow release kinetics at pH 7.4 (37). However, when bound to TfR and exposed to acidic pH, iron release is greatly accelerated (9,10,38,39). Within the cell Fe-Tf releases its bound iron to a chelator within 2-3 minutes after TfR-mediated endocytosis (21). The requirement for TfR binding, a low pH environment, possibly reducing agents, and a chelator ensures that iron is not prematurely released from Fe-Tf in the bloodstream or when Fe-Tf is bound to TfR at the cell surface. Instead, these requirements ensure that only when Fe-Tf enters the appropriate endosomal compartment is the iron safely released.

In a previous site-directed mutagenesis study of TfR (24) we noted differences in the binding footprints for Fe-Tf and apo-Tf on the TfR surface. While apo-Tf and Fe-Tf require the same binding determinants in the central region of the TfR helical domain, apo-Tf requires two additional residues in the TfR helical domain: W641 and F760. The sidechains of these two residues are in van der Waals contact with each other and form a hydrophobic patch on the outside edge of the TfR helical domain (Fig. 5). We hypothesize that these residues play a role in TfR-stimulated iron release at low pH by binding to and stabilizing the iron-free form of Tf. We therefore combined the two

substitutions to make a W641A/F760A-TfR and investigated its binding and iron-release stimulating properties.

Using an SPR-based binding assay we demonstrated that W641A/F760A binds Fe-Tf at pH 7.4 with the same affinity as wtTfR. However, its binding to apo-Tf at pH 6.3 is reduced ~300-fold relative to wtTfR. Using a fluorescence-based iron release assay we showed that the W641A/F760A mutant does not stimulate iron release from Fe-Tf at low pH under conditions at which wtTfR accelerates iron release from Fe-Tf by 100-fold relative to unbound Fe-Tf. Instead, the W641A/F760A mutant slows iron release by two-fold relative to free Fe-Tf. W641 and F760 are conserved (24) in all known sequences of TfR and also in sequences of transferrin receptor 2 (TfR2), a recently identified receptor for Fe-Tf (40,41). The conservation of these residues across all known TfR and TfR2 sequences suggests a conserved role for these residues in facilitating iron release from TfR-bound Fe-Tf at acidic pH.

These results, taken together with previous structural and mutagenesis data regarding Tf binding to TfR (23-26), allow speculation on the mechanism of TfR-induced iron release from Fe-Tf at acidic pH. From structural and mutagenesis data we know that Fe-Tf binds to TfR at basic pH with the C-lobe contacting a central region of the TfR domain and the N-lobe contacting residues in the TfR protease-like domain in the vicinity of Tyr 123 (24,26). This binding interaction must stabilize Fe-Tf in a closed conformation as iron release from TfR-bound Fe-Tf is slower than iron release from free Fe-Tf (9,10,38,39).

At basic pH, Fe-Tf does not make functionally important contacts with the hydrophobic patch on TfR that includes W641 and F760 (24). Upon acidification, the Tf molecule makes new contacts on TfR to the hydrophobic patch defined by W641 and F760, and no longer makes significant contacts to the Y123 region of the TfR protease-like domain (24). Our current results demonstrate that the new contacts with TfR residues W641 and F760 are critical for accelerating iron release from Fe-Tf at acidic pH. We therefore suggest that at acidic pH, the sampling rate of the open and closed conformations of Fe-Tf when bound to TfR is slower than that of free Fe-Tf under the same conditions due to constraints imposed by receptor binding. This is consistent with our observation that free Fe_c-Tf spontaneously releases iron more rapidly than Fe_c-Tf bound to the W641A/F760A-TfR. However, we propose that even though the rate of conformational sampling is slowed, that receptor-bound Fe-Tf still samples open conformations and that contacts between Fe-Tf and the W641/F760 hydrophobic patch trap Fe-Tf in an open form. If these contacts are prevented by mutating W641 and F760, as in the W641A/F760A-TfR mutant, then we suggest that the Fe-Tf will rapidly revert to its more closed conformation inhibiting iron release even at the acidic pH. This is consistent with studies showing that conditions favoring the open state of Tf result in accelerated iron release, while conditions that favor the closed conformation inhibit iron release (42).

Our model for TfR-facilitated iron release from Fe-Tf is supported by an examination of the 7.5 Å EM structure of an Fe-Tf/TfR complex (26) (PDB code: 1SUV). The EM structure suggests that TfR residues Trp641 and Phe760 are in close proximity to the C-I

domain of the Tf C-lobe, but are unlikely to make direct contacts, consistent with the Fe-Tf binding data in this and previous studies (24,26). Inspeecttion of the EM model suggests that small structural changes could bring the patch into contact with the Tf. Interestingly, a straight line connecting the sidechains of Trp641 and Phe760 to the Fe^{3+} atom in the C-lobe bisects the C-I/C-II domain interface (Fig. 5A), which must open to expose iron for release. The resolution of the EM model does not allow us to speculate on what specific interactions would be made between TfR and Fe-Tf at this interface, but the placement of the Trp641 Phe760 hydrophobic patch in this proximity and orientation to the C-lobe's cleft and ferric binding site, coupled with its clear activity in binding apo-Tf and stimulating iron release, indicates a functional significance of the interactions in this region. Therefore, we hypothesize that the two residues act on Fe-Tf by stabilizing, and possibly even initiating, an opening in the intralobe cleft that enhances the exposure of the iron atom to protons and chelators for iron removal.

A corollary of this model is that cleft opening is only one step in the iron release process and is not sufficient to release iron as collapse back to the closed state is still possible. However this would require that the iron remain bound to the protein in the open conformation, even though domain opening requires that some of the iron ligands dissociate. From the EM structure of the Fe-Tf/TfR complex it has been noted that the C-I domain is in contact with the TfR helical domain while the C-II domain makes no receptor contacts. Therefore, C-II is free to swing away from the receptor to achieve the open conformation associated with apo-Tf. However, if domain opening is not sufficient for iron release, then the ferric iron must stay associated with one of the

two domains. There is evidence that iron can remain bound to transferrin with only a partial complement of protein ligands. A crystal structure of camel lactoferrin (43) shows both the N- and C-lobes in the open conformation exhibited by other apo-protein structures, except that both lobes contain a bound iron. Both irons are coordinated by bicarbonate and the two tyrosine ligands, whereas the aspartate and histidine ligands normally associated with the iron coordination are distant from the site. Similarly, structures of a fragment of duck ovotransferrin corresponding to the N-II lobe show an iron coordinated by bicarbonate, the two tyrosine ligands, and either an aspartate donated by an adventitiously bound peptide (44) or added nitrilotriacitic acid (NTA) (45). While the iron is octahedrally coordinated, these structures demonstrate that the N-II domain is capable of binding iron without ligand contributions from the N-I lobe. A recent study showed that binding to TfR at acidic pH has the effect of raising the reduction potential of the coordinated Fe^{3+} on Fe-Tf by nearly 200 mV (46), suggesting that the potential for biological reduction to Fe^{+2}, which has a lower affinity for Tf by a factor of 10^{14} (Harris, 1986), is enhanced by TfR binding and precedes iron loss. This elevation of the reduction potential does not occur at basic pH. To evaluate the reduction potential of the bound iron atom, chelators were not used to prevent dissociation of iron from the Tf/TfR complex. It is possible that the reduction potential measured corresponds to the tetrahedral intermediate that we propose forms before cellular reducing agents and chelators abstract the iron from the Tf/TfR complex.

The mechanism for transferrin-mediated iron donation to cells is very complex and exhibits pH dependence, anion and chelator requirements, conformational changes to transferrin, and binding

to TfR. Our model is that at acidic pH, stabilization of the open-form of Tf by interactions with W641 and F760 results in the presentation of an exposed tetrahedrally coordinated iron center from which cellular chelators can remove it from the protein. However, this model relies on observations for lactoferrin and ovotransferrin which, while very similar to human Tf in sequence and structure, may have subtle differences in their modes of iron release. Continued biochemical and structural analysis of this system will be required to develop a comprehensive model of receptor-enhanced iron release.

Materials and Methods

Expression of Soluble TfRs

Soluble wtTfR was produced in a lytic baculovirus/insect cell expression system as previously described (27). Briefly, we used a modified version of the pAcGP67A expression vector (Pharmingen) that codes for the gp67 hydrophobic leader sequence followed by a 6x-His tag, factor Xa cleavage site, and residues 121-760 of human TfR. To make the W641A/F760A mutant, the W641A mutation was introduced into the F760A-TfR expression vector (24) using the Quickchange protocol (Stratagene). The construct was verified by sequencing of the protein-coding region. His-tagged wtTfR and W641A/F760A were expressed in baculovirus-infected insect cells and purified by a combination of Ni-NTA and size exclusion chromatography as previously described (27). Human Fe-Tf was prepared from apo-Tf (Sigma) by incubation with bicarbonate and 3-fold excess of ferric ammonium sulfate.

Biosensor Analyses

All biosensor experiments were carried out using a BIACORE 2000 instrument (Pharmacia, LKB Biotechnology). Interactions between a protein immobilized on the sensor chip (the "ligand") and a protein injected over the sensor surface (the "analyte") are monitored in real time as a change in surface plasmon resonance as measured in resonance units (RU) (47,48). Sensor chips were prepared using standard primary amine coupling chemistry to attach 2000-4000 RU of the anti-pentaHis antibody (Qiagen)

(BIACORE manual), which was used to capture wtTfR and TfR mutants directly from insect cell supernatants as described (24). For each experiment one of the four flow-cells of a CM5 sensor chip (Pharmacia) was coupled with antibody but no TfR to act as a reference cell. Binding data were collected, processed, and the kinetics fit to a bivalent ligand model to derive K_Ds as previously described (24).

Expression of N-HisY95F/Y188F hTf-NG (Fe_c-Tf)

Production and purification of the recombinant Tf containing iron only in the C-lobe has recently been described in detail (49). Both spectral data and urea gel analysis confirm the inability of the N-lobe to bind iron. This authentic monoferric preparation allows assessment of iron release from the C-lobe with no possibility of adventitious iron uptake by the N-lobe due to the strategic mutations of the two liganding tyrosines.

Preparation of Fe_C-Tf/TfR complexes

A molar excess of Fe_c-Tf in 100 mM NH_4HCO_3 pH 8.5 was incubated with wtTfR or the W641A/F760A-TfR for 30 min at room temperature followed by size-exclusion chromatography to separate the Fe_c-Tf/TfR complexes from free Fe_c-Tf. The column was equilibrated and run in 100 mM NH_4HCO_3 at a flow rate of 2 mL/Min using a BioCad Sprint chromatography system.

Measurements of iron release kinetics

The rate of iron release from the recombinant Fe_c-Tf in the presence and absence of the wt and W641A/F760A-TfR was measured by an adaptation of the spectrofluorometric assay previously described (10,50). A QuantaMaster Spectrofluorometer (Photon Technology International, South Brunswick NJ) equipped with a 75 Watt Xenon arc lamp as an excitation source and excitation/emission monochrometers was used to measure steady-state fluorescence. Fluorescence emission spectra were measured by exciting the sample at 280 nm and collecting the emitted fluorescence at 330 nm. Experiments were carried out at ambient temperature with an entry slit of 0.25 nm and an exit slit of 1.0 nm. Data were recorded in 1 second intervals immediately following the addition of 4.8 μL of Fe_c-Tf alone or 9.6 μL of the TfR to a magnetically stirred cuvette containing 1.8 mL of 0.1 M Mes, pH 5.6. The assay conditions were 500 nM Fe_c-Tf in 300mM KCl and 4 mM EDTA.

Acknowledgements

We thank peter Snow, Inderjit Nangiana, and Cynthia Jones (Caltech protein Expression Facility) for insect cell expression of TfR constructs; and members of the Bjorkman and Mason labs for critical reading of the manuscript. This work was supported by the Howard Hughes Medical Institute, the National Institutes of Health grants R01 DK60770 (to P.J.B.), R01 DK21739 (A.B.M.), National Research Service Award 5T32-GM-7616 (to A.M.G) and USDOE DE-FG02-00ER45828 Graduate Assistantship (P.J.H.).

Abbreviations

Tf, transferrin protein; ferric Tf, transferrin in any iron-binding configuration; Fe_C-Tf, N-HisY95F/Y188F hTf-NG; TfR, human transferrin receptor 1; RU, response unit

References

1. Enns, C. A. (2002) in *Molecular and Cellular Iron Transport* (Templeton, D. M., ed), pp. 71-94, Marcel Dekker, Inc., New York, Basel
2. Leibman, A., and Aisen, P. (1977) *Biochemistry* **16**, 1268-1272
3. Henry, J. B. (1991) *Clinical Diagnosis and Management by Laboratory Methods*, W.B. Saunders Co., Philadelphia
4. Enns, C. A., and Sussman, H. H. (1981) *J. Biol. Chem.* **256**, 9820-9823
5. Rothenberger, S., Iacopetta, B. J., and Kuhn, L. C. (1987) *Cell* **49**, 423-431
6. Collawn, J. F., Kuhn, L. A., Liu, L. F., Tainer, J. A., and Trowbridge, I. S. (1991) *EMBO J.* **10**, 3247-3253
7. Collawn, J. F., Lai, A., Domingo, D., Fitch, M., Hatton, S., and Trowbridge, I. S. (1993) *J. Biol. Chem*. **268**, 21686-21692
8. Sipe, D. M., and Murphy, R. F. (1991) *J. Biol. Chem.* **266**, 8002-8007
9. Bali, P. K., Zak, O., and Aisen, P. (1991) *Biochemistry* **30**, 324-328
10. Zak, O., and Aisen, P. (2003) *Biochemistry* **42**, 12330-12334
11. Dautry-Varsat, A., Ciechanover, A., and Lodish, H. F. (1983) *Proc. Natl. Acad. Sci. USA* **80**, 2258-2262
12. Lindley, P. F. (2001) in *Handbook of Metalloproteins* (Messerschmidt, A., Huber, R., Wieghardt, K., and Poulos, T., ed), pp. 793-811, 2 vols., John Wiley and Sons
13. Lawrence, C. M., Ray, S., Babyonyshev, M., Galluser, R., Borhani, D. W., and Harrison, S. C. (1999) *Science* **286**, 779-782
14. Bennett, M. J., Lebrón, J. A., and Bjorkman, P. J. (2000) *Nature* **403**, 46-53

15. Feder, J. N., Gnirke, A., Thomas, W., Zsuchihashi, Z., Ruddy, D. A., Basava, A., Dormishian, F., Domingo, R., Ellis, M. C., Fullan, A., Hinton, L. M., Jones, N. L., Kimmel, B. E., Kronmal, G. S., Lauer, P., Lee, V. K., Loeb, D. B., Mapa, F. A., McCellland, E., Meyer, N. C., Mintier, G. A., Moeller, N., Moore, T., Morikang, E., Prass, C. E., Quintana, L., Starnes, S. M., Schatzman, R. C., Brunke, K. J., Drayna, D. T., Risch, N. J., Bacon, B. R., and Wolff, R. K. (1996) *Nature Genetics* **13**, 399-408

16. MacGillivray, R. T., Moore, S. A., Chen, J., Anderson, B. F., Baker, H., Luo, Y., Bewley, M., Smith, C. A., Murphy, M. E., Wang, Y., Mason, A. B., Woodworth, R. C., Brayer, G. D., and Baker, E. N. (1998) *Biochemistry* **37**, 7919-7928

17. Grossmann, J. G., Neu, M., Pantos, E., Schwab, F. J., Evans, R. W., Townes-Andrews, E., Lindley, P. F., Appel, H., Thies, W. G., and Hasnain, S. S. (1992) *J. Mol. Biol.* **225**, 811-819

18. Grossmann, J. G., Neu, M., Evans, R. W., Lindley, P. F., Appel, H., and Hasnain, S. S. (1993) *J. Mol. Biol.* **229**, 585-590

19. Gerstein, M., Anderson, B. F., Norris, G. E., Baker, E. N., Lesk, A. M., and Chothia, C. (1993) *J. Mol. Biol.* **234**, 357-372

20. Kurokawa, H., Dewan, J. C., Mikami, B., Sacchettini, J. C., and Hirose, M. (1999) *J. Biol. Chem.* **274**, 28445-28452

21. Aisen, P., and Leibman, A. (1973) *Biochim. Biophys. Acta* **304**, 797-804

22. Lebrón, J. A., West, A. P., and Bjorkman, P. J. (1999) *J. Mol. Biol.* **294**, 239-245

23. West, A. P., Jr., Giannetti, A. M., Herr, A. B., Bennett, M. J., Nangiana, J. S., Pierce, J. R., Weiner, L. P., Snow, P. M., and Bjorkman, P. J. (2001) *J. Mol. Biol.* **313**, 385-397

24. Giannetti, A. M., Snow, P. M., Zak, O., and Bjorkman, P. J. (2003) *PLoS Biol* **1**, 341-350

25. Liu, R., Guan, J. Q., Zak, O., Aisen, P., and Chance, M. R. (2003) *Biochemistry* **42**, 12447-12454

26. Cheng, Y., Zak, O., Aisen, P., Harrison, S. C., and Walz, T. (2004) *Cell* **116**, 565-576

27. Lebrón, J. A., Bennett, M. J., Vaughn, D. E., Chirino, A. J., Snow, P. M., Mintier, G. A., Feder, J. N., and Bjorkman, P. J. (1998) *Cell* **93**, 111-123

28. Giannetti, A. M., and Bjorkman, P. J. (2004) *J. Biol. Chem.*, M401467200

29. Templeton, D. M. (2002) *Molecular and cellular iron transport*, Marcel Dekker, New York

30. Bali, P. K., and Harris, W. R. (1989) *Journal of the American Chemical Society* **111**, 4457-4461

31. Bali, P. K., Harris, W. R., and Nessettollefson, D. (1991) *Inorganic Chemistry* **30**, 502-508

32. Huang, C., and Mason, J. T. (1978) *Proc. Natl. Acad. Sci. USA* **75**, 308-310

33. Mason, A. B., Miller, M. K., Funk, W. D., Banfield, D. K., Savage, K. J., Oliver, R. W., Green, B. N., MacGillivray, R. T., and Woodworth, R. C. (1993) *Biochemistry* **32**, 5472-5479

34. Mason, A. B., He, Q. Y., Halbrooks, P. J., Everse, S. J., Gumerov, D. R., Kaltashov, I. A., Smith, V. C., Hewitt, J., and MacGillivray, R. T. (2002) *Biochemistry* **41**, 9448-9454

35. Halbrooks, P. J., He, Q. Y., Briggs, S. K., Everse, S. J., Smith, V. C., MacGillivray, R. T., and Mason, A. B. (2003) *Biochemistry* **42**, 3701-3707

36. Halliwell, B., and Gutteridge, J. M. (1990) *Methods Enzymol* **186**, 1-85

37. Aisen, P., Leibman, A., and Zweier, J. (1978) *J. Biol. Chem.* **253**, 1930-1937

38. Bali, P. K., and Aisen, P. (1991) *Biochemistry* **30**, 9947-9952

39. Bali, P. K., and Aisen, P. (1992) *Biochemistry* **31**, 3963-3967

40. Kawabata, H., Yang, R., Hirama, T., Vuong, P. T., Kawano, S., Gombart, A. F., and Koeffler, H. P. (1999) *J. Biol. Chem.* **274**, 20826-20832

41. Kawabata, H., Germain, R. S., Vuong, P. T., Nakamaki, T., Said, J. W., and Koeffler, H. P. (2000) *J. Biol. Chem.* **275**, 16618-16625

42. Navati, M. S., Samuni, U., Aisen, P., and Friedman, J. M. (2003) *Proc. Natl. Acad. Sci. USA* **100**, 3832-3837

43. Khan, J. A., Kumar, P., Srinivasan, A., and Singh, T. P. (2001) *J. Biol. Chem.* **276**, 36817-36823

44. Lindley, P. F., Bajaj, M., Evans, R. W., Garrett, R. C., Hasnain, S. S., Jhoti, H., Kuser, P., Neu, M., Patel, K., Sarra, R., Strange, R., and Walton, A. (1993) *Acta Crystallographica Section D* **49**, 292-304

45. Kuser, P., Hall, D. R., Haw, M. L., Neu, M., Evans, R. W., and Lindley, P. F. (2002) *Acta Crystallographica Section D* **58**, 777-783

46. Dhungana, S., Taboy, C. H., Zak, O., Larvie, M., Crumbliss, A. L., and Aisen, P. (2004) *Biochemistry* **43**, 205-209

47. Fägerstam, L. G., Frostell-Karlsson, A., Karlsson, R., Persson, B., and Rönnber, I. (1992) *J. Chromatography* **597**, 397-410

48. Malmqvist, M. (1993) *Nature* **361**, 186-187

49. Anne B. Mason, P. J. H., Julia R. Larouche, Sara K. Briggs, Marque L. Moffett, Jon E. Ramsey, Susan A. Connolly, Valerie C. Smith, and Ross T.A. MacGillivray. (2004) *Protein Expression and Purification* ***in press***

50. Egan, T. J., Zak, O., and Aisen, P. (1993) *Biochemistry* **32**, 8162-8167

51. Kurokawa, H., Mikami, B., and Hirose, M. (1995) *J. Mol. Biol.* **254**, 196-207

Table 1. wtTfR and W641A/F760A binding properties and effects on iron release from Fe-Tf

Protein	Fe-Tf pH 7.4 K_{D1} (nM)	Fe-Tf pH 7.4 K_{D2} (nM)	apo-Tf pH 6.3 K_{D1} (nM)	apo-Tf pH 6.3 K_{D2} (nM)	Iron Release $K_{obs}(s^{-1}x\ 10^{3})$
wtTfR	0.90	59	18	39	
W641A/F760A	1.5	53	4,700	56,000	
Tf-Fe_C					2.6 ± 0.2 (n=4)
wtTfR/Tf-Fe_C					270 ± 46 (n=4)
W641A/F760A/Tf-Fe_C					1.3 ± 0.03 (n=3)

Table I: The K_Ds for binding of Fe-Tf at pH 7.4 and apo-Tf at pH 6.3 were derived from fits to the sensorgrams shown in figure 2. Rates for iron release from Tf-Fe_C alone or complexed with wtTfR or W641A/F760A are derived from the fits to release curves in figure 4.

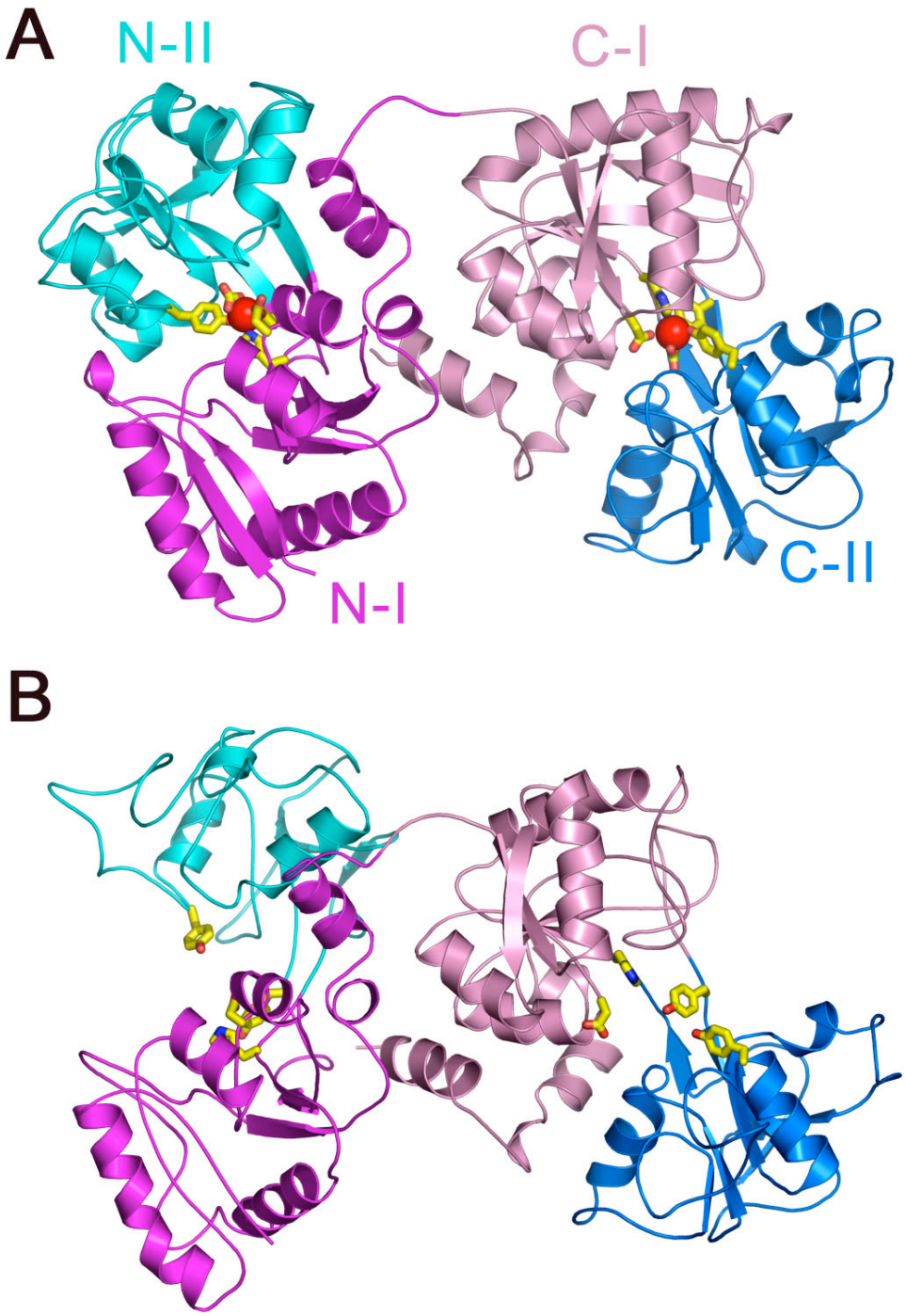

Figure 1. Ribbon diagrams of Fe-Tf, apo-Tf, and TfR. (A) Structure of di-ferric ovotransferrin (51) colored by domain as shown. Residues coordinating the iron atoms (red spheres) are shown as sticks and colored at atom type (yellow, carbon; blue, nitrogen; red, oxygen). (B) Structure of apo-ovotransferrin (20) colored as in (A) illustrating the large structural change associated with iron release.

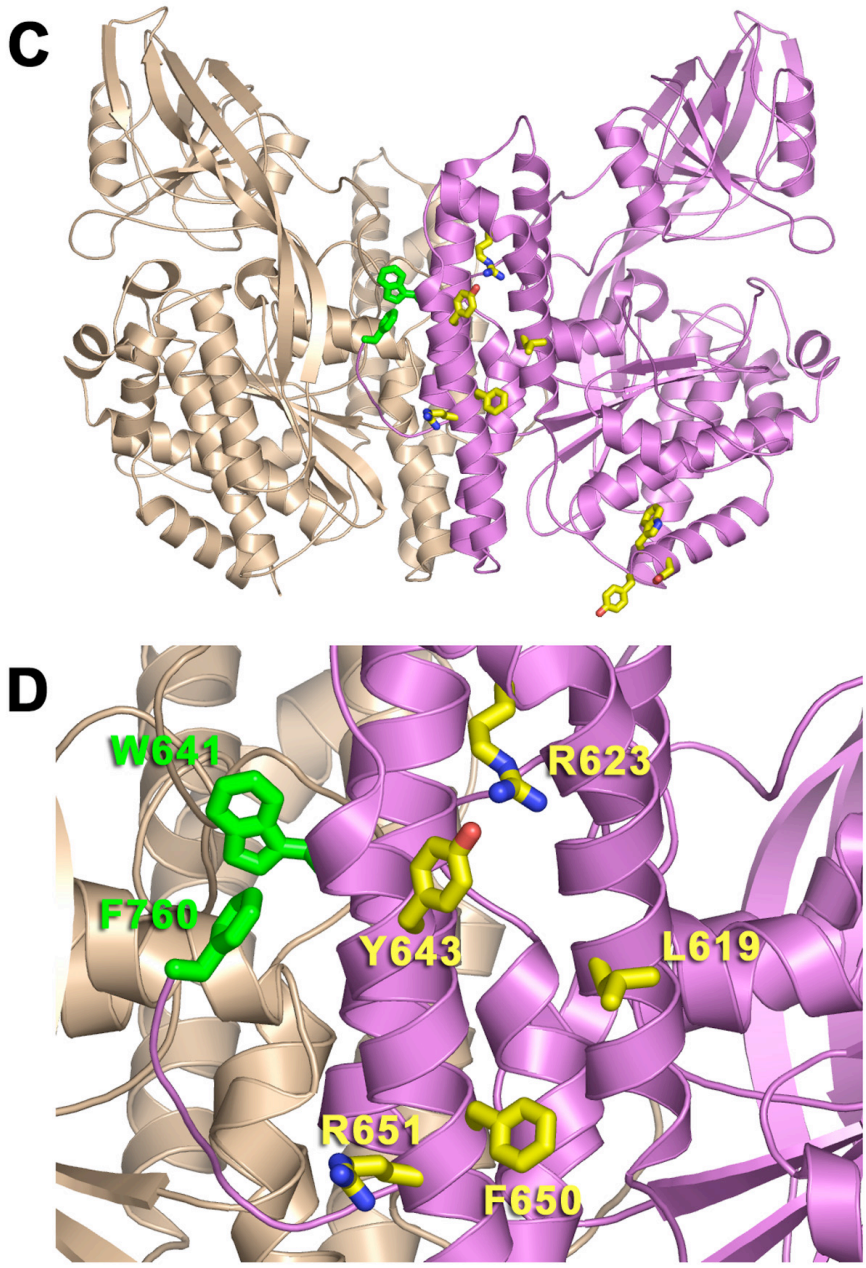

Figure 1 continued: (C) Structure of the TfR dimer with one monomer colored brown and the other magenta. Residues specific for binding apo-Tf (W641 and F760) are highlighted in green. Residues contributing significantly to Fe-Tf binding are shown with carbons yellow, nitrogens blue, and oxygens red. (D) Closeup of the TfR helical domain. Residues are colored as in (C).

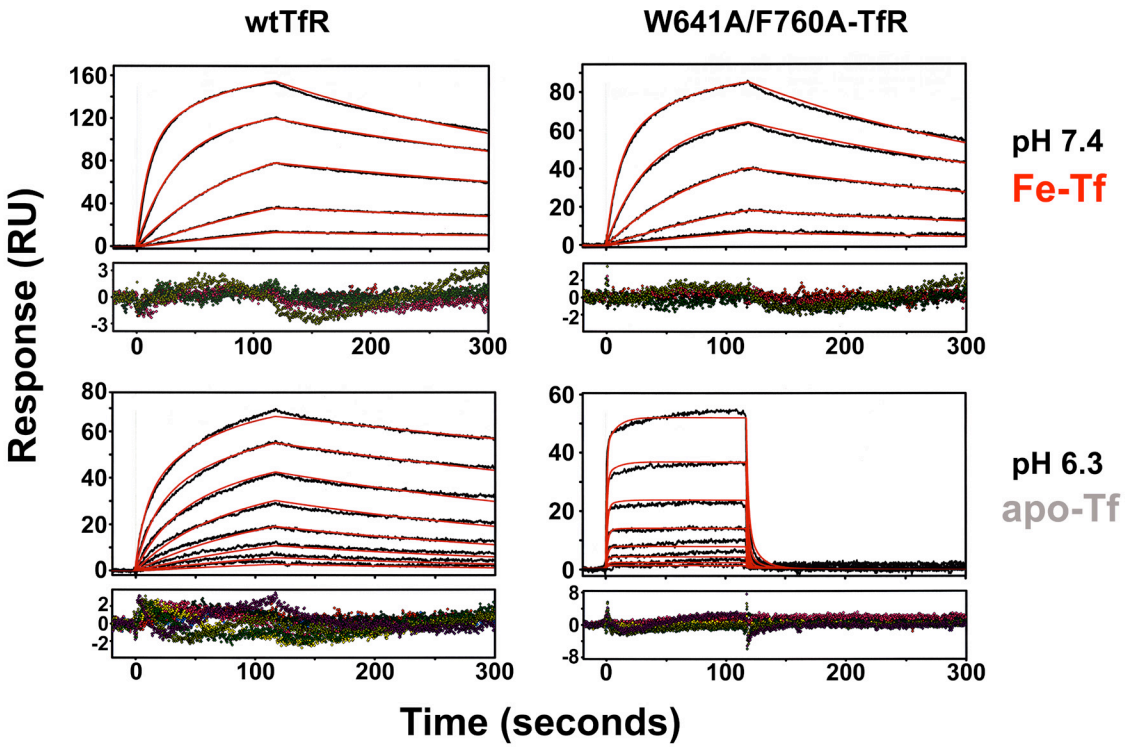

Figure 2. SPR analysis of Fe-Tf and apo-Tf binding to wtTfR and W641A/F760A at pH 7.4 and pH 6.3. Experimentally observed responses are shown as black lines with the best-fit binding curves (red lines) derived from a bivalent ligand model (see Methods and Materials) superimposed. The highest concentration in the injection series for each sensorgram is A, 73 nM; B, 73 nM; C, 625 nM; D, 10 μM. Subsequent injections are related by 3-fold dilutions.

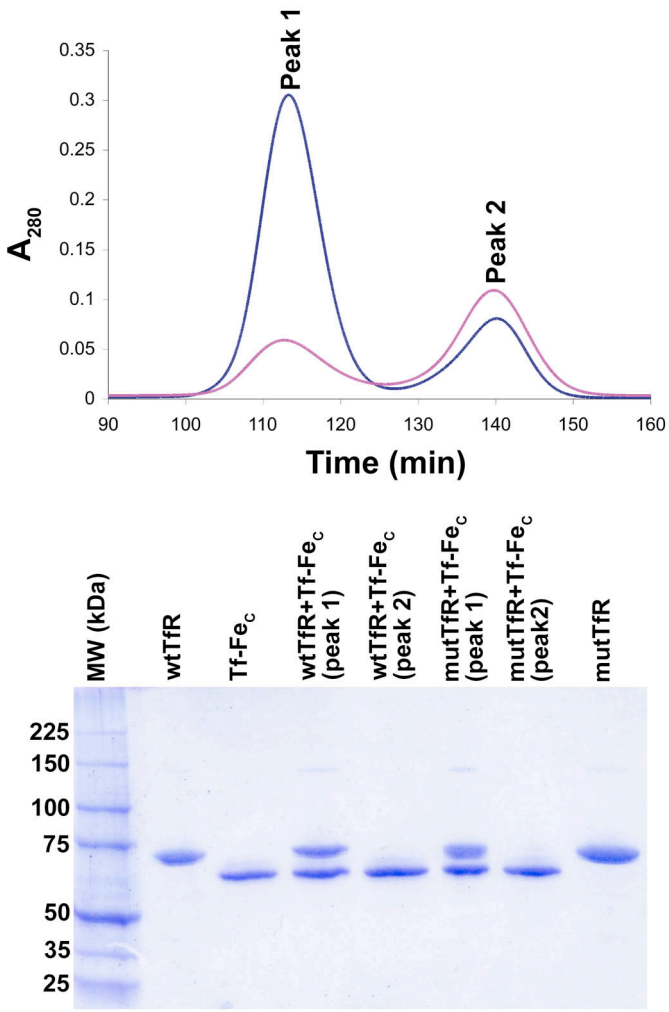

Figure 3. Preparation and purity of TfR proteins, Tf-Fe_c, and their complexes. (A) Size exclusion chromatogram of wtTfR (magenta), W641A/F760A (cyan), and Tf-Fe_c (green). (B) Chromatogram of the Tf-Fe_c/wtTfR (blue) and the Tf-Fe_c/W641A/F760A (green) complexes showing a peak for the complex and a peak for excess Tf-Fe_c. (C) 10% SDS-PAGE gel showing purified wtTfR, W641A/F760A-TfR, Tf-Fe_c and peaks one and two from the sizing column traces showing the presence of Tf-Fe_c/TfR complex in the first peak and only Tf-Fe_c in the second.

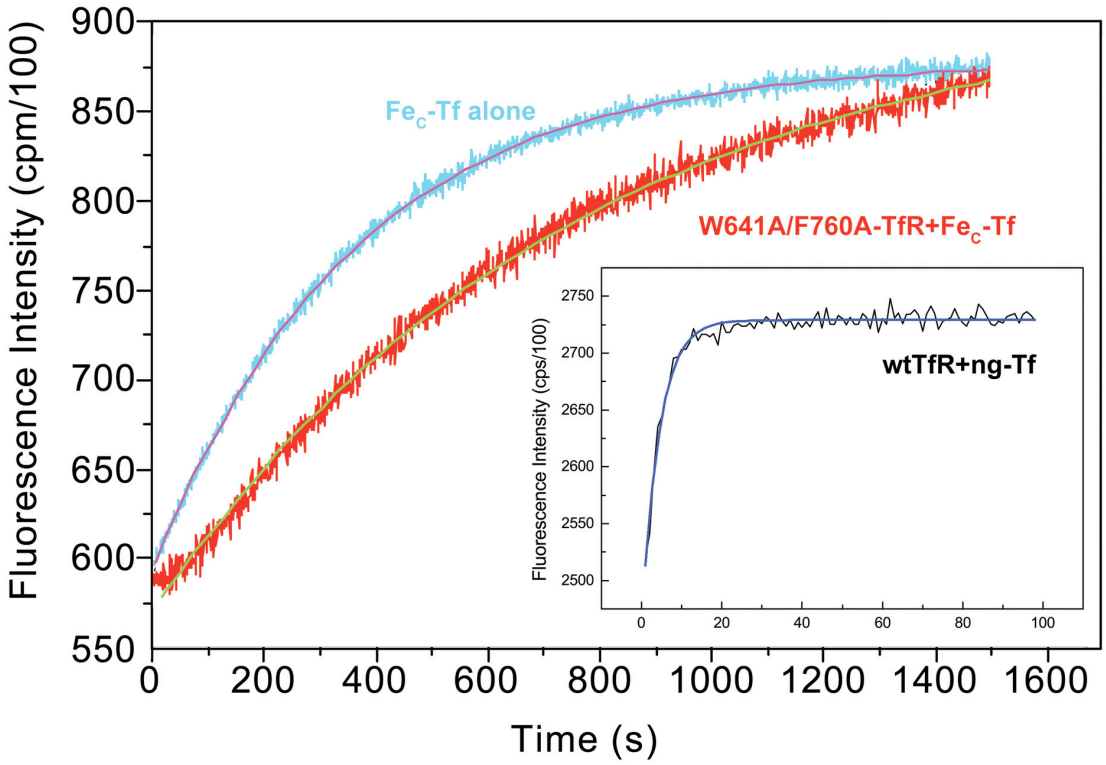

Figure 4. Kinetics of iron release from Tf-Fe$_C$ alone and in complex with TfR proteins. Release was monitored as a change in relative fluorescence intensity versus time. Loss of iron results in an increase in fluorescence signal that was fit to a first order rate equation to derive the rate constants shown in Table I.

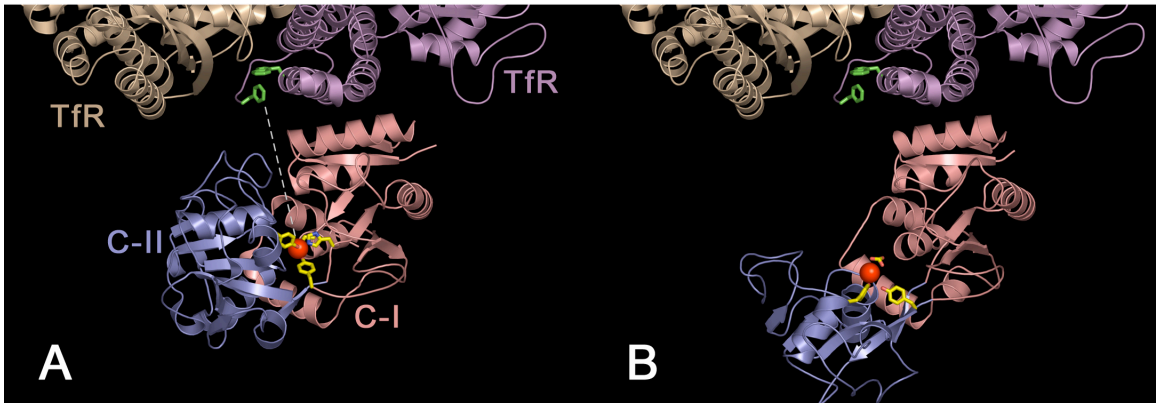

Figure 5. Structure-based hypothesis for the mechanism of TfR accelerated iron release. A) The structure of the Tf/TfR complex based on the 7.5 Å EM model (24). Protein domains are colored as shown. W641 and F760 are shown in green and the residues coordinating the iron (red sphere) are shown in yellow. A line connecting the F760 and the iron atom is shown in white dashes and bisects the C-I/C-II domain boundary. B) Structures as in (A) except that transferrin has been replaced with the structure of camel lactoferrin bound to iron, but in the open conformation (39). Model was made by superimposing the C-I domain of the lactoferrin structure with the C-I domain of the human Tf in the EM model (RMSD 0.77 Å for 470 Cα atoms). The iron is coordinated by two tyrosines and a bicarbonate ion.

Chapter 5:

Crystallographic Studies of the H41D Mutant of the Hereditary Hemochromatosis Protein Alone and in Complex with Transferrin Receptor

This chapter is being prepared for publication and describes the crystallographic structure determination of a mutant form of HFE linked to increased body iron. I performed all the crystal growth, data collection, building, and refinement, with the exception the unliganded H41D-HFE crystal which was grown, and a dataset collected, by Dr. Melanie Bennett.

Crystallographic studies of the H41D mutant of the hereditary hemochromatosis protein HFE alone and in complex with transferrin receptor

Anthony M. Giannetti, Melanie J. Bennett, and Pamela J. Björkman

Abstract.

The iron overload disorder hereditary hemochromatosis (HH) is caused by mutations to the gene coding for the hemochromatosis protein HFE. The most common disease-linked mutation, C260Y, prevents proper folding and cell surface expression of HFE. A second mutation, H41D, correlates with higher body iron levels by exacerbating the iron overload in individuals who are heterozygous for C260Y. H41D-HFE folds, transports to the cell surface, and exhibits wild-type affinity for the only currently documented HFE binding partner, transferrin receptor (TfR), therefore the mechanism by which the substitution affects iron levels is unclear. To assess the potential structural changes caused by the mutation, we determined crystal structures of H41D-HFE alone and complexed with TfR, and compared these structures to their wild-type HFE counterparts. The unliganded H41D-HFE exhibits almost no structural differences from wild-type HFE. However, comparison of the two forms of the protein complexed with TfR reveals structural rearrangement of two loops in the HFE structure. The potential significance of these structural changes as they relate to primary iron overload are discussed.

Introduction.

The identification of mutations to HFE as the causative agent of type I hemochromatosis, also known as hereditary hemochromatosis, implicated HFE as a modulator of mammalian iron homeostasis. Positional cloning of the HFE gene revealed that most hemochromatosis patients carry the mutation C260Y (Feder *et al.*, 1996). This substitution acts as a loss-of-function mutation by eliminating a conserved disulphide bridge in the α3 domain of the protein preventing proper folding, association with the β2-microglobulin light chain, and transported the cell surface (Feder *et al.*, 1996; Feder *et al.*, 1997; Waheed *et al.*, 1997a). Another mutation, H41D, which is found in some hemochromatosis patients who are heterozygous for C260Y, appears to be linked to increased risk for developing iron overload (Feder *et al*., 1996; Risch, 1997). A recent study using transgenic mice demonstrated that mice carrying an H41D-HFE allele exhibit a greater body iron load compared to mice that have at least one wild-type copy of the gene (Tomatsu *et al.*, 2003). A study utilizing macrophages demonstrated that while wild-type HFE (wt-HFE) decreases iron export from cells, H41D-HFE does not (Drakesmith *et al.*, 2002). These results suggest that the H41D substitution impairs HFE's activity in modulating iron homeostasis.

HFE is structurally similar to class I MHC molecules (Lebrón *et al.*, 1998), which present antigenic peptides to T lymphocytes (Garcia *et al.*, 1999). The heavy chain is composed of three domains (α1, α2, α3) and is noncovalently associated with the light chain β2-microglobulin (β2m) (figure 1). His-41 is located on a loop (loop II) connecting ß-

strands 3 and 4 on the outside edge of the α1- α 2 platform, where it forms a salt bridge with Asp-73 (Fig. 1; 4A) (Lebrón *et al.*, 1998). It was originally proposed that substitution of the histidine for a negatively charged residue would disrupt the salt bridge with Asp-73 and juxtapose two negative charges, perhaps leading to a change in loop structure (Lebrón *et al.*, 1998). The loop is potentially mobile as judged from map quality and the crystallographic temperature factors (B-factor) in the unliganded HFE structure. The average B-factor for atoms in loop II is 94.3 $Å^2$ compared to 64.5 $Å^2$ for the entire HFE molecule.

HFE binds to the transferrin receptor (TfR) (Parkkila *et al.*, 1997; Feder *et al.*, 1998), a homodimeric type II membrane glycoprotein found on the surface of most mammalian cell types (Leibman & Aisen, 1977). TfR binds transferrin, a circulating iron transport protein, and transports it to acidic recycling endosomes by receptor-mediated endocytosis (Dautry-Varsat *et al.*, 1983). Iron is removed from transferrin in the endosome (Rothenberger *et al.*, 1987; Bali *et al.*, 1991; J.F. Collawn *et al.*, 1991; Sipe & Murphy, 1991; J. F. Collawn *et al.*, 1993; Zak & Aisen, 2003) and transported to the cytosol where it is used for the metabolic requirements of the cell, or stored in the iron storage protein ferritin (Radisky & Kaplan, 1998). While the mechanism for HFE modulation of iron homeostasis is not known, binding to TfR is most likely an important part of that mechanism.

The X-ray crystal structure an HFE/TfR complex reveals two HFE molecules bound to TfR, one on each side of the obligate dimer (Bennett *et al.*, 2000). The interaction is mediated mostly through the long α1 helix on HFE with some contacts from the α2 helix and the platform domain with the helical domain on TfR (Fig. 3A). Biochemical and biophysical studies using soluble forms of HFE have not demonstrated an effect of the H41D mutation on the stability or binding affinity of HFE to TfR (Feder *et al.*, 1998; Lebrón *et al.*, 1999), but potential structural differences between H41D-HFE and wt-HFE that could affect HFE's activity in TfR-independent functions have not been addressed.

In order to determine the structural consequences of the H41D mutation, we determined the X-ray structures of H41D-HFE alone and complexed with TfR. We find that aside from a slight reorientation of Asp-41 relative to His-41, that there are no structural differences between unliganded H41D-HFE and wt-HFE.

However, comparison of H41D-HFE crystallized while bound to TfR reveals a rearrangement of the loop relative to that of the wt-HFE/TfR structure. By comparing the structures of unliganded HFE, wt-HFE bound to TfR, and H41D-HFE bound to TfR, we find loop II to be a mobile structure and that this mobility may have longer-range effects on other regions of the HFE structure. The potential consequences of this structural variability are discussed in terms of HFE's role in maintaining iron balance.

Results.

Structure of H41D-HFE

Crystals of H41D-HFE were grown as described for wt-HFE (Lebrón *et al*., 1998) in spacegroup $P2_12_12_1$ with two molecules per asymmetric unit. The structure was solved by molecular replacement to 2.9 Å resolution using the 2.6 Å structure of wt-HFE (Lebrón *et al*., 1998). Data collection and refinement results are presented in Table I. Before data processing and rigid-body refinement, the histidine residue at position 41 was converted to an asparate in both molecules of the asymmetric unit. A σ_A-weighted $2F_o$-F_c annealed omit map in the vicinity of Asp-41 after rigid-body refinement shows negative density around the aspartate sidechain with a small peak of positive density nearby (Fig. 2A). This positive peak can be occupied by the aspartate sidechain by a rotation about the Asp-41 $\chi 1$ torsion angle. Rebuilding and refinement produced the model and annealed omit density (entire loop omitted) in figure 2B. The position of the Asp-41 sidechain is not clearly defined as loop II is not well ordered in either this structure or the structure of wild-type HFE, as judged either from the quality of the electron density and comparison of the average B-factors for the loop (94.3 $Å^2$) compared to the entire HFE heavy chain (64.5 $Å^2$) (based on the wt-HFE structure). The map in figure 2B shows residual density for the Asp-41 sidechain in its original position suggesting alternate conformations for the sidechain, but the only moderate resolution of the structure (2.9Å) and the low quality of the electron density in the vicinity of residue 41 did not warrant building alternate sidechain conformations followed by occupancy refinement. Figure 2C shows the superposition of the refined H41D-HFE and wt-HFE structures,

demonstrating that that the H41D mutation does not cause an overall structural rearrangement of the H41-containing loop.

Structure of the H41D-HFE/TfR complex

H41D-HFE/TfR complex crystals formed in space group C2 space group and were isomorphous with wt-HFE/TfR crystals (Bennett *et al*., 2000), but did not diffract beyond 3.5 Å, as compared with the wt-HFE/TfR crystals, from which the crystal structure was determined to 2.8 Å resolution. Coordinates for the wt-HFE/TfR binary structure (PDB code: 1DE4) were used for molecular replacement. Refinement statistics are given in Table 2 and the final model in the vicinity of loop II and σ_A-weighted annealed omit electron density in shown in Figure 2E. Figure 2D shows an initial $F_{O,mut}$-$F_{C,wild\text{-}type}$,ϕ_C difference map with the carbon-α coordinates from the wt-HFE/TfR structure. Positive (blue) and negative (red) 2σ difference density shows that loop II occupies an alternate position in the H41D-HFE/TfR structure. The loop, and all nearby areas, were rebuilt and refined.

Comparison of the backbones of loop II region in the wt-HFE/TfR and H41D-HFE/TfR structures reveals a change in the path of the main chain, with the largest difference being 5.7 Å between the α-carbons of Glu 42 in each structure (Fig. 2F). Figure 3 compares a half-complex of HFE/TfR (one HFE/β2m heterodimer bound to one chain of the TfR dimer) from the wt-HFE/TfR (Bennett *et al*., 2000) and H41D-HFE/TfR structures. Loop

II is near the interface between HFE and TfR but does not directly contact the receptor. The shift in the overall loop position observed in the H41D-HFE/TfR structure flips Asp-41 out of the interior of the protein, relative to His-41 in the wild-type complex, and directs it towards solvent. Interestingly, loop II is not well ordered in the structure of wt-HFE alone or complexed with TfR, but is better ordered in the H41D-HFE/TfR structure (data not shown).

We also note a small amount of change to the loop connecting the first and second ß-strands of the HFE platform (loop I). The position of loop I is constrained because HFE residue Leu-22 makes direct contacts to TfR Leu-619 contributing 140 $Å^2$ of buried surface area (7% of the total buried surface area in the interface (Bennett *et al.*, 2000). This interaction is preserved in the H41D-HFE/TfR structure. The largest change for loop I is the movement of Asp-17 from a buried position, where it forms a hydrogen bond to His-41, to a completely solvent-exposed position in the H41D-HFE/TfR structure (compare Fig. 4B and C). The exposed surface area for this residue increases from 65.3 $Å^2$ to 143.1 $Å^2$. The functional consequences of this transition are not known at this time. Even in this new position Asp-19 is too far from TfR (closest TfR atom is 12 Å away) for the change to be relevant to TfR binding.

Discussion.

HFE has a demonstrated role in maintaining iron homeostasis, yet the mechanism for HFE function in regulating iron homeostasis in unknown. Early cellular and biochemical studies did not demonstrate significant differences between wt-HFE and H41D-HFE in terms of either TfR binding or effects on transfected cells (Waheed *et al.*, 1997b; Lebrón *et al*., 1999; Roy *et al.*, 2000; Feeney & Worwood, 2001). However, a recent study utilizing transgenic 'knock-in' mice shows heightened hepatic iron load in H41D-HFE mice compared to wt-HFE mice (Tomatsu *et al*., 2003). Additionally, H41D-HFE does not inhibit iron release from macrophages to the same degree as wt-HFE (Drakesmith *et al*., 2002). Therefore, characterization of the structure of H41D-HFE may help explain how H41D affects HFE's function. HFE has been proposed to interact with other proteins in the membrane (Townsend & Drakesmith, 2002; Frazer & Anderson, 2003), such as ferroportin, a membrane protein that exports iron from cells (Abboud & Haile, 2000; Donovan *et al.*, 2000; McKie *et al.*, 2000). The proposals suggest that the chemical and/or structural changes induced by the H41D substitution may alter HFE's proposed interactions with these other proteins.

To characterize any potential structural changes caused by the H41D mutation in HFE, we determined the crystal structures of H41D-HFE alone and in complex with TfR to 2.9 Å and 3.5 Å resolution, respectively. Comparison of the unliganded H41D-HFE

structure with unliganded wt-HFE reveals no significant differences, suggesting that the substitution does not lead to major changes in the structure of the protein. However, when H41D-HFE is bound to TfR, we see a rearrangement to the local structure of the loop containing the H41D mutation (loop II) and slight changes to a nearby loop (loop I connecting ß-strands 1 and 2). Loop II is not well ordered in the structures of wt-HFE alone or the wt-HFE/TfR complex, but is better ordered in the H41D-HFE/TfR structure.

It has been hypothesized that HFE functions to regulate iron homeostasis through interactions with other, as yet unidentified, binding partners in addition to TfR (Townsend & Drakesmith, 2002; Frazer & Anderson, 2003). Our crystallographic investigations have revealed that the region around His-41 is flexible and that substitutions could lead to changes in flexibility. Figure 4A shows that His-41 forms a salt bridge with Asp-73 in the structure of wt-HFE alone. In contrast, the structure of wt-HFE bound to TfR exhibits a local rearrangement of loop II that positions His-41 to interact with Asp-19 and Glu-26 (Fig. 4B). Substitution of His-41 to aspartate would create repulsive interactions in this region and indeed, in the structure of H41D-HFE bound to TfR we observe that Asp-19 has moved to a position closer to that observed in the structure of unliganded wt-HFE (Fig. 4C), although motion is constrained in the case of loop I because of the important interactions of Leu-22 with TfR. The H41D-HFE/TfR structure also shows that Asp-41 is pointing away from HFE and into solution. The Asp-41 sidechain is in a position to form hydrogen bonds or salt bridge interactions with Arg-45 on the other side of the loop (Fig. 4C). Additionally, the structural changes in this

region have also moved the sidechain of Asp-40 into a position to interact with R45. It may be these interactions that lead to the decreased flexibility of the loop in this structure relative to that observed in the wt-HFE/TfR complex.

While these data and observations do not directly explain why H41D leads to an increase in body iron load, they demonstrate that the structures of loop I and loop II in HFE can be affected by this mutation. These changes could affect the interaction of HFE with a ligand other than TfR. If HFE can bind this hypothesized ligand by itself, then His-41 might be directly involved in the interaction since substitution of this residue does not lead to large perturbations of the local structure. However, if binding of HFE to TfR is required for binding to this new ligand (such that the HFE/TfR complex forms a receptor for the other protein), then the loop rearrangements observed in the H41D-HFE/TfR structure could reduce or prevent binding. Alternatively, His-41 may not be directly involved in the interaction at all, but may act to stabilize other regions of the structure through longer-range interactions, as in the case of the 10 Å translation of Asp-19 in the H41D-HFE/TfR structure relative to the wt-HFE/TfR structure. New experiments and structures will be necessary to determine if the structural changes induced by H41D observed here play a significant role in the mechanism of H41D-induced iron overload.

Materials and Methods.

Data collection and structure solution

An H41D-HFE crystal was grown as previously described (Lebrón *et al*., 1998). A dataset for a crystal of unliganded H41D-HFE was collected at the Stanford Synchrotron Radiation Laboratory (SSRL) at beamline 7-1 to a resolution of 2.9 Å. The dataset was processed and scaled with the HKL package (Otwinowski, 1993).

Transferrin receptor and H41D-HFE were kindly provided by J.A. Lebrón and were mixed in a ratio of one HFE to one TfR monomer and concentrated to 50 μM 2:1 HFE/TfR complex. Crystals of the H41D-HFE/TfR binary complex were grown in hanging-drops in conditions similar to the wt-HFE/TfR complex (Bennett *et al*., 2000), but with higher concentrations of PEG 8000 (8.4% PEG 8000, 200 mM tris pH 8.0, and 10 mM trimethylamine HCl). Crystals were cryoprotected by stepwise transfer into higher concentration glycerol and PEG concentrations to a final solution of 20% glycerol and 12% PEG 8000 and flash frozen in liquid nitrogen. A dataset complete to 3.5 Å was collected on a Raxis-IV mounted on a Rigaku RU-200 generator. and a 3.7 Å dataset was collected at beamline 7-1 at the Stanford Synchrotron Radiation Laboratory. A combined dataset was used for building but only the higher resolution dataset was used for refinement.

The H41D-HFE and H41D-HFE/TfR complex structures were solved by molecular replacement using the structures of wild-type HFE (Lebrón *et al*., 1998)(PDB code:

1A6Z) or the wild-type HFE/TfR binary complex (Bennett *et al.*, 2000)(PDB code: 1DE4) followed by rigid-body refinement freeing individual protein domains (α1, α2, α3 and β2m for HFE, and the protease-like domain, apical domain, and helical domain for TfR). Models were inspected and rebuilt in O (Jones & Kjeldgaard, 1997) using σ_A-weighted $2F_o$-F_c annealed omit or composite omit density maps. Refinement was performed with CNS (Brünger *et al.*, 1998) using simulated annealing torsional refinement with grouped B factors, bulk-solvent corrections, and tight NCS restraints (300 kcal/mol Å^2) for all residues not involved in crystal contacts. The calcium ions, carbohydrate residues, and tris molecules observed in the wt-HFE/TfR model were eliminated from the H41D-HFE/TfR model due to the lower resolution of the data for the mutant complex (3.5 Å versus 2.8 Å for wt-HFE/TfR). Figures were prepared with Molscript (Kraulis, 1991), Bobscript (Esnouf, 1997), Raster3D (Merritt & Bacon, 1997), Swiss-PDB viewer (Kaplan & Littlejohn, 2001), and PyMol (DeLano, 2002). All surface area calculations were performed with VADAR (Willard *et al.*, 2003).

References

Abboud, S., & Haile, D. J. (2000). A novel mammalian iron-regulated protein involved in intracellular iron metabolism. *J. Biol. Chem., 275*, 19906-19912.

Bali, P. K., Zak, O., & Aisen, P. (1991). A new role for the transferrin receptor in the release of iron from transferrin. *Biochemistry, 30*(2), 324-328.

Bennett, M. J., Lebrón, J. A., & Bjorkman, P. J. (2000). Crystal structure of the hereditary haemochromatosis protein HFE complexed with transferrin receptor. *Nature, 403*, 46-53.

Bjorkman, P. J., Saper, M. A., Samraoui, B., Bennett, W. S., Strominger, J. L., & Wiley, D. C. (1987). Structure of the human class I histocompatibility antigen, HLA-A2. *Nature, 329*, 506-512.

Brünger, A. T., Adams, P. D., Clore, G. M., Gros, P., Grosse-Kunstleve, R. W., Jiang, J.-S., Kuszewski, J., Nilges, M., Pannu, N. S., Read, R. J., Rice, L. M., Simonson, T., & Warren, G. L. (1998). Crystallography and NMR system: A new software system for macromolecular structure determination. *Acta Cryst. D, 54*, 905-921.

Collawn, J. F., Kuhn, L. A., Liu, L. F., Tainer, J. A., & Trowbridge, I. S. (1991). Transplanted LDL and mannose-6-phosphate receptor internalization signals promote high-efficiency endocytosis of the transferrin receptor. *EMBO J., 10*, 3247-3253.

Collawn, J. F., Lai, A., Domingo, D., Fitch, M., Hatton, S., & Trowbridge, I. S. (1993). YTRF is the conserved internalization signal of the transferrin receptor, and a second YTRF signal at position 31-34 enhances endocytosis. *J. Biol. Chem., 268*(29), 21686-21692.

Dautry-Varsat, A., Ciechanover, A., & Lodish, H. F. (1983). pH and the recycling of transferrin during receptor-mediated endocytosis. *Proc. Natl. Acad. Sci. USA, 80*(8), 2258-2262.

Davies, P. S., & Enns, C. A. (2004). Expression of the hereditary hemochromatosis protein, HFE, increases ferritin levels by inhibiting iron export in HT29 cells. *J. Biol. Chem*.

DeLano, W. K. (2002). The PyMOL Molecular Graphics System (Version 0.95). San Carlos, CA, USA: DeLano Scientific.

Donovan, A., Brownlie, A., Zhou, Y., Shepard, J., Pratt, S. J., Moynihan, J., Paw, B. H., Drejer, A., Barut, B., Zapata, A., Law, T. C., Brugnara, C., Lux, S. E., Pinkus, G. S.,

Pinkus, J. L., Kingsley, P. D., Palis, J., Fleming, M. D., Andrews, N. C., & Zon, L. I. (2000). Positional cloning of zebrafish ferroportin1 identifies a conserved vertebrate iron exporter. *Nature, 403*, 776-781.

Drakesmith, H., Sweetland, E., Schimanski, L., Edwards, J., Cowley, D., Ashraf, M., Bastin, J., & Townsend, A. R. (2002). The hemochromatosis protein HFE inhibits iron export from macrophages. *Proc. Natl. Acad. Sci. USA, 99*(24), 15602-15607.

Esnouf, R. M. (1997). An extensively modified version of MolScript that includes greatly enhanced coloring capabilities. *J. Mol. Graph. Model., 15*(2), 132-134, 112-133.

Feder, J. N., Gnirke, A., Thomas, W., Zsuchihashi, Z., Ruddy, D. A., Basava, A., Dormishian, F., Domingo, R., Ellis, M. C., Fullan, A., Hinton, L. M., Jones, N. L., Kimmel, B. E., Kronmal, G. S., Lauer, P., Lee, V. K., Loeb, D. B., Mapa, F. A., McCellland, E., Meyer, N. C., Mintier, G. A., Moeller, N., Moore, T., Morikang, E., Prass, C. E., Quintana, L., Starnes, S. M., Schatzman, R. C., Brunke, K. J., Drayna, D. T., Risch, N. J., Bacon, B. R., & Wolff, R. K. (1996). A novel MHC class I-like gene is mutated in patients with hereditary haemochromatosis. *Nature Genetics, 13*, 399-408.

Feder, J. N., Penny, D. M., Irrinki, A., Lee, V. K., Lebrón, J. A., Watson, N., Tsuchihashi, Z., Sigal, E., Bjorkman, P. J., & Schatzman, R. C. (1998). The

hemochromatosis gene product complexes with the transferrin receptor, and lowers its affinity for ligand binding. *Proc. Natl. Acad. Sci. USA, 95*, 1472-1477.

Feder, J. N., Tsuchihashi, Z., Irrinki, A., Lee, V. K., Mapa, F. A., Morikang, E., Prass, C. E., Starnes, S. M., Wolff, R. K., Parkkila, S., Sly, W. S., & Schatzman, R. C. (1997). The hemochromatosis founder mutation in HLA-H disrupts ß$_2$-microglobulin interaction and cell surface expression. *J. Biol. Chem., 272*, 14025-14028.

Feeney, G. P., & Worwood, M. (2001). The effects of wild-type and mutant HFE expression upon cellular iron uptake in transfected human embryonic kidney cells. *Biochim. Biophys. Acta, 1538*(2-3), 242-251.

Frazer, D. M., & Anderson, G. J. (2003). The orchestration of body iron intake: how and where do enterocytes receive their cues? *Blood Cells Mo.l Dis., 30*(3), 288-297.

Garcia, K. C., Teyton, L., & Wilson, I. A. (1999). Structural basis of T cell recognition. *Annu. Rev. Immunol., 17*, 369-397.

Jones, T. A., & Kjeldgaard, M. (1997). Electron density map interpretation. *Meth. Enzymol., 277*, 173-208.

Kaplan, W., & Littlejohn, T. G. (2001). Swiss-PDB Viewer (Deep View). *Brief Bioinform., 2*(2), 195-197.

Kraulis, P. (1991). MOLSCRIPT: a program to produce both detailed and schematic plots of protein structures. *J. Appl. Crystallogr., 24*, 946-950.

Lebrón, J. A., Bennett, M. J., Vaughn, D. E., Chirino, A. J., Snow, P. M., Mintier, G. A., Feder, J. N., & Bjorkman, P. J. (1998). Crystal structure of the hemochromatosis protein HFE and characterization of its interaction with transferrin receptor. *Cell, 93*, 111-123.

Lebrón, J. A., West, A. P., & Bjorkman, P. J. (1999). The hemochromatosis protein HFE competes with transferrin for binding to the transferrin receptor. *J. Mol. Biol., 294*, 239-245.

Leibman, A., & Aisen, P. (1977). Transferrin receptor of the rabbit reticulocyte. *Biochemistry, 16*(7), 1268-1272.

McKie, A. T., Marciani, P., Rolfs, A., Brennan, K., Wehr, K., Barrow, D., Miret, S., Bomford, A., Peters, T. J., Farzaneh, F., Hediger, M. A., Hentze, M. W., & Simpson, R. J. (2000). A novel duodenal iron-regulated transporter, IREG1, implicated in the basolateral transfer of iron to the circulation. *Molecular Cell, 5*, 299-309.

Merritt, E. A., & Bacon, D. J. (1997). Raster3D: Photorealistic molecular graphics. *Meth. Enzymol., 277*, 505-524.

Otwinowski, Z. (1993). DENZO. New Haven CT 06511 USA: Department of Molecular Biophysics and Biochemistry, Yale University and HHMI.

Parkkila, S., Waheed, A., Britton, R. S., Bacon, B. R., Zhou, X. Y., Tomatsu, S., Fleming, R. E., & Sly, W. S. (1997). Association of the transferrin receptor in human placenta with HFE, the protein defective in hereditary hemochromatosis. *Proc. Natl. Acad. Sci. USA, 94*(24), 13198-13202.

Radisky, D. C., & Kaplan, J. (1998). Iron in cytosolic ferritin can be recycled through lysosomal degradation in human fibroblasts. *Biochem. J., 336 (Pt 1)*, 201-205.

Risch, N. (1997). Haemochromatosis, HFE and genetic complexity. *Nat Genet, 17*(4), 375-376.

Rothenberger, S., Iacopetta, B. J., & Kuhn, L. C. (1987). Endocytosis of the transferrin receptor requires the cytoplasmic domain but not its phosphorylation site. *Cell, 49*(3), 423-431.

Roy, C. N., Carlson, E. J., Anderson, E. L., Basava, A., Starnes, S. M., Feder, J. N., & Enns, C. A. (2000). Interactions of the ectodomain of HFE with the transferrin receptor are critical for iron homeostasis in cells. *FEBS Lett., 484*(3), 271-274.

Sipe, D. M., & Murphy, R. F. (1991). Binding to cellular receptor results in increased iron release from transferrin at mildly acidic pH. *J. Biol. Chem., 266*, 8002-8007.

Tomatsu, S., Orii, K. O., Fleming, R. E., Holden, C. C., Waheed, A., Britton, R. S., Gutierrez, M. A., Velez-Castrillon, S., Bacon, B. R., & Sly, W. S. (2003). Contribution of the H63D mutation in HFE to murine hereditary hemochromatosis. *Proc. Natl. Acad. Sci. USA, 100*(26), 15788-15793.

Townsend, A., & Drakesmith, H. (2002). Role of HFE in iron metabolism, hereditary haemochromatosis, anaemia of chronic disease, and secondary iron overload. *Lancet, 359*(9308), 786-790.

Waheed, A., Parkkila, S., Zhou, X. Y., Tomatsu, S., Tsuchihashi, Z., Feder, J. N., Schatzman, R. C., Britton, R. S., Bacon, B. R., & Sly, W. S. (1997a). Hereditary hemochromatosis: effects of C282Y and H63D mutations on association with β2-microglobulin, intracellular processing, and cell surface expression of the HFE protein in COS-7 cells. *Proc. Natl. Acad. Sci. USA, 94*, 12384-12389.

Waheed, A., Parkkila, S., Zhou, X. Y., Tomatsu, S., Tsuchihashi, Z., Feder, J. N., Schatzman, R. C., Britton, R. S., Bacon, B. R., & Sly, W. S. (1997b). Hereditary hemochromatosis: effects of C282Y and H63D mutations on association with beta2-microglobulin, intracellular processing, and cell surface expression of the HFE protein in COS-7 cells. *Proc. Natl. Acad. Sci. USA, 94*(23), 12384-12389.

Willard, L., Ranjan, A., Zhang, H., Monzavi, H., Boyko, R. F., Sykes, B. D., & Wishart, D. S. (2003). VADAR: a Web server for quantitative evaluation of protein structure quality. *Nucleic Acids Res., 31*(13), 3316-3319.

Zak, O., & Aisen, P. (2003). Iron release from transferrin, its C-lobe, and their complexes with transferrin receptor: presence of N-lobe accelerates release from C-lobe at endosomal pH. *Biochemistry, 42*(42), 12330-12334.

Tables.

Table 1: Data collection and refinement statistics for H41D-HFE

Unit cell dimensions	
a, b, c (Å)	68.8, 100.1, 147.6
Space Group	$P2_12_12_1$
Temp	-150°C
Data Processing	
Resolution (Å)	37-2.9
Observations	165,578
Unique Reflections	22,525
Completeness	99.3% (99.1%)
I/σ	21 (3.6)
Rsym%	6.4/37.4
Refinement	
Reflections in Working set	20,265
Reflections in Test Set	2,250
Rfree%	24.80
Rcryst%	22.35
Rms deviations from ideality	
Bond length (Å)	0.009
Bond Angles (deg)	1.4
Number of protein atoms	6,066

Table 2: Data collection and refinement statistics for H41D-HFE:TfR binary complex.

a, b, c, (Å); β(deg)	110.4, 144.4, 327.1, 93.60
Space Group	C2
Temp	-150C
Data Processing	
Resolution (Å)	25-3.5
Observations	347,353
Unique Reflections	69,418
Completeness	95.0% (95.7%)
I/σ	8.7 (1.9)
Rsym%	8.3/35.2
Refinement	
Reflections in Working set	57,834 (9,642)
Reflections in Test Set	6,180 (1,064)
Rfree%	29.0
Rcryst%	25.4
Rms deviations from ideality	
Bond length (Å)	0.010
Bond Angles (deg)	1.4
Number of protein atoms	24,333

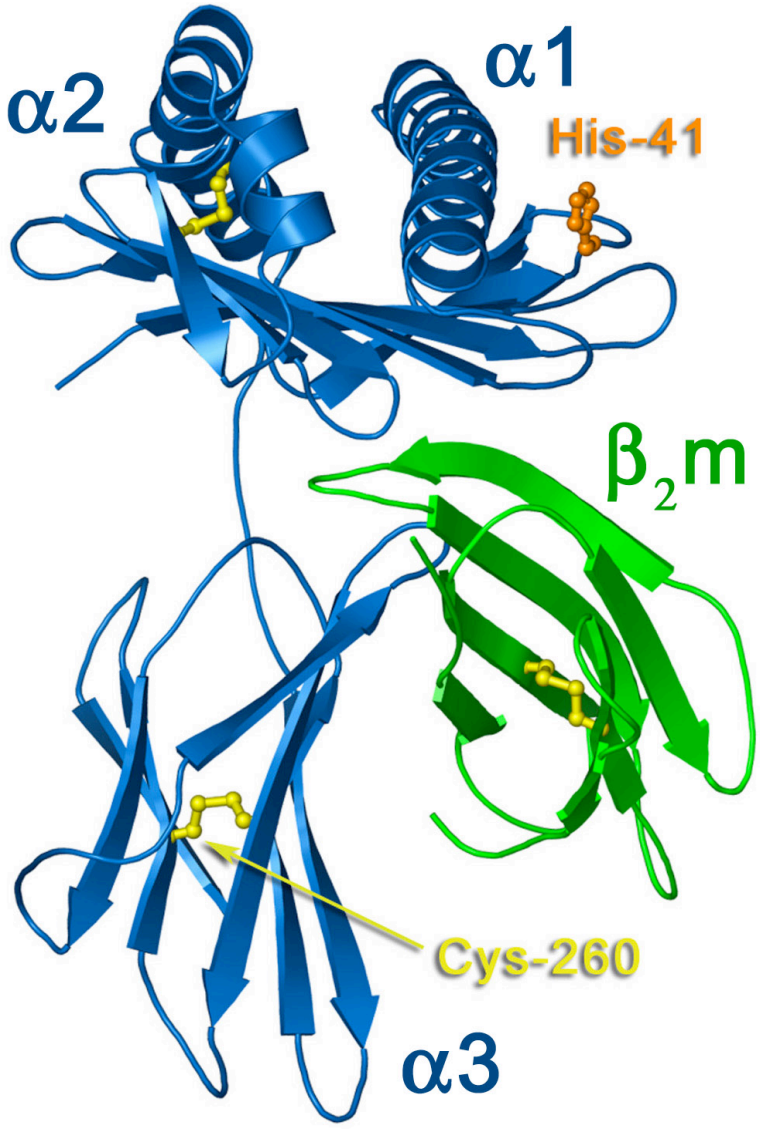

Figure 1. Ribbon diagram of the structure of wt-HFE. The positions of residues mutated in HH are highlighted.

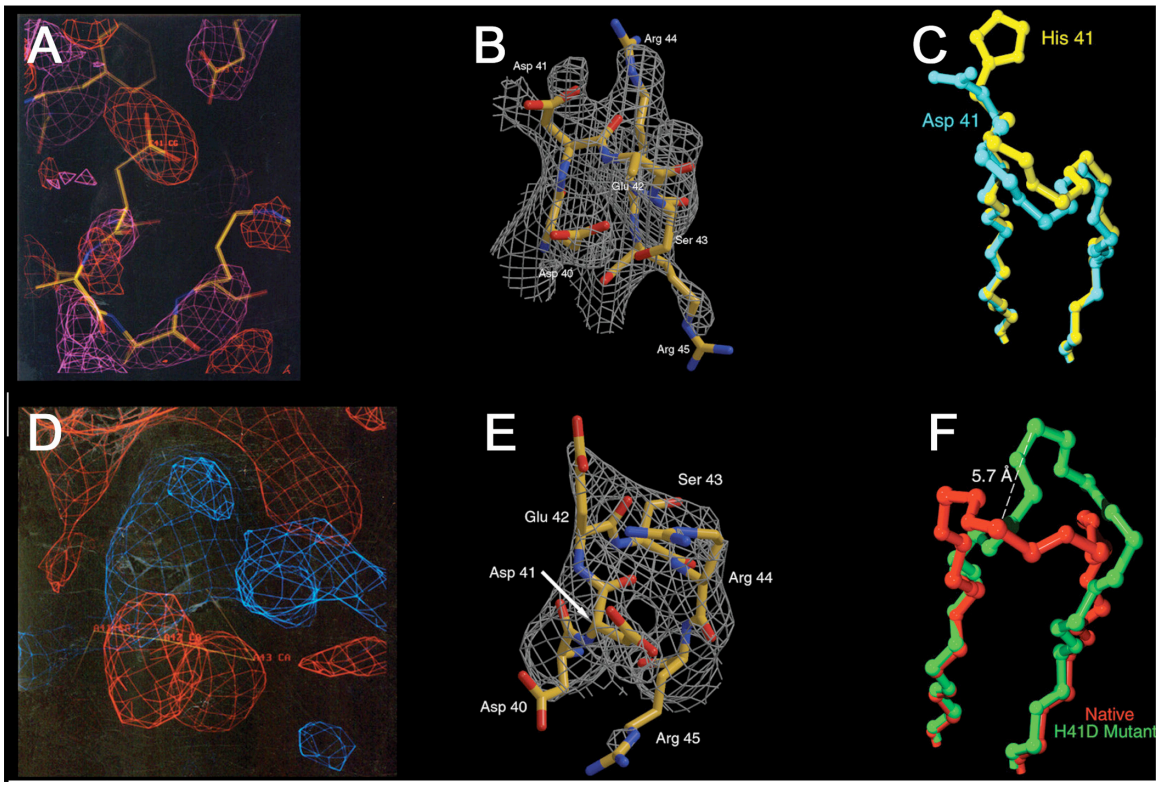

Figure 2. Initial and refined models for loop II in the structures of H41D-HFE and H41D-HFE/TfR. A) Initial model for H41D-HFE in difference density. Red corresponds to F_O-F_C,ϕ_C density contoured at –2σ. Magenta density is annealed omit $2F_O$-F_C,ϕ_C contoured at 1σ. There is a large negative peak near the Asp41 side chain. B) Refined structure of H41D-HFE in annealed omit-type density. C) Superposition of wt-HFE and H41D-HFE loop II showing the sidehchains of His-41 and Asp-41. D) Initial orientation of loop II in wt-HFE/TfR structure superimposed on F_O-F_C,ϕ_C difference density for the H41D-HFE/TfR dataset. Density is contoured +2σ (blue) and –2σ (red). E) Rebuilt and refined model for loop II in annealed omit density. F) Superposition of loop II in wt-HFE/TfR and H41D-HFE/TfR. The largest difference is the atomic shift for the α-carbon of Glu-42 as indicated.

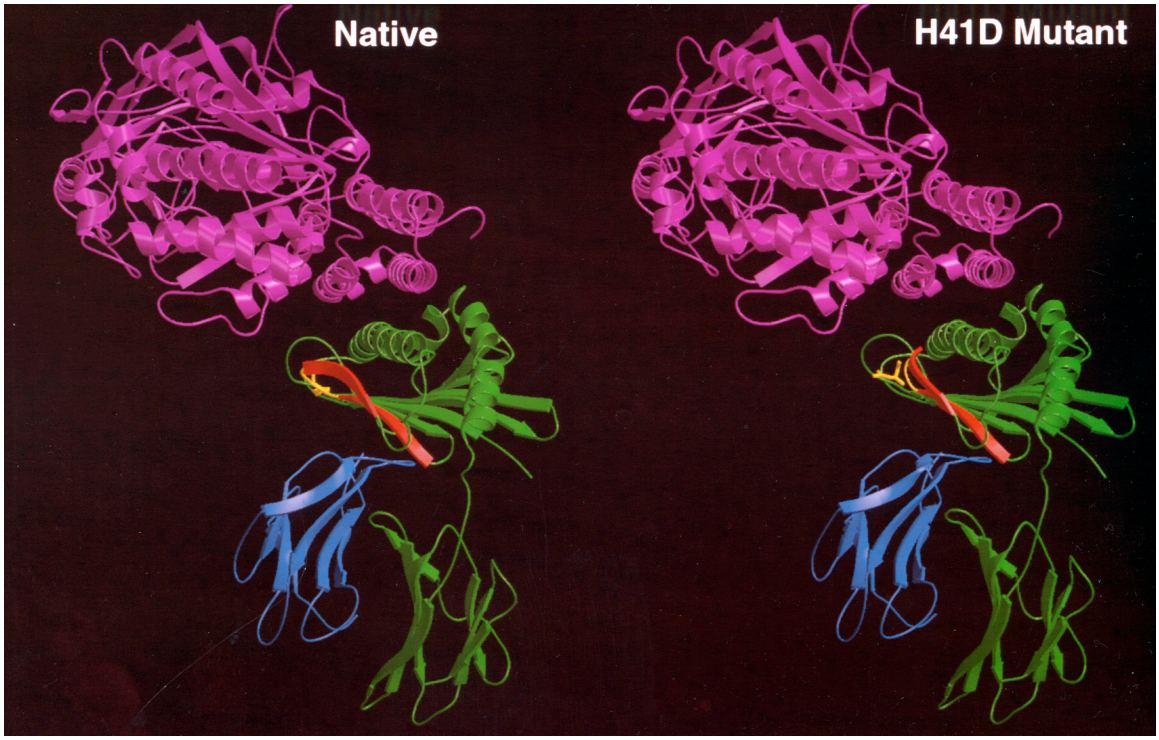

Figure 3. Comparison of wt-HFE/TfR and H41D-HFE/TfR structures. A half complex (one HFE bound to one polypeptide chain of the TfR dimer) is shown for each. The helical domain of TfR (magenta) interacts with the helical regions of HFE. HFE is shown in green, β_2m in blue. β1 and β2 are colored red and loop II is shown in yellow. His-41 and Asp-41 are shown in stick representation.

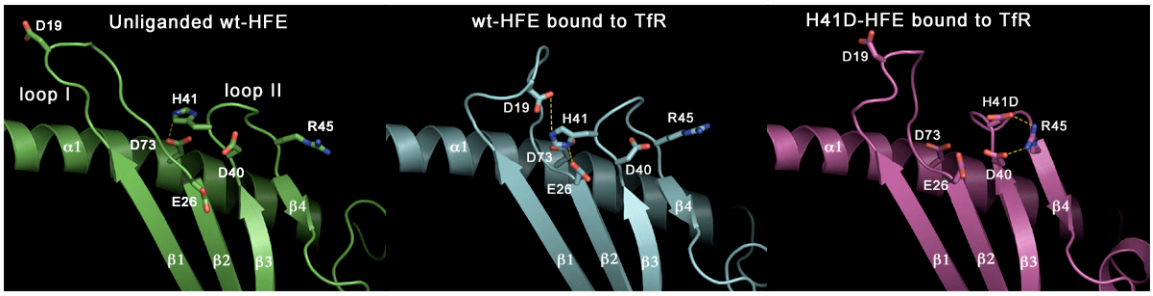

Figrue 4. Comparison of HFE structures in the vicinity of loops I and II. Secondary structural elements and relevant amino acids are labeled. A) The structure of unliganded wt-HFE (PDB code 1A6Z) (Lebrón et al., 1998) is shown in green and the salt bridge between His-41 and Asp-73 is highlighted. B) The structure of wt-HFE bound to TfR (PDB code 1DE4) (Bennett et al., 2000). Hydrogen bonds between His-41 and Asp-19 and Glu-26 are indicated. (C) Structure of H41D-HFE bound to TfR. Loop II has shifted closer to the position observed in (A) with Asp-19 reoriented towards the solvent. Asp-41 is in a different position than His-41 in the other two structures and appears poised to from an H-bond or salt bridge to Arg-45. The structure of this loop also positions Asp-40 for a potential interaction with Arg-45. Exact distance measurements are not provided given the low resolution of the structures. As measured from these models no interaction is longer than 3.4 Å.

Appendix I:

Mutational Analysis of the Transferrin Receptor Reveals Overlapping HFE and Transferrin Binding Sites

This appendix details the characterization of some of the first TfR mutants that were characterized further in Chapter II. I contributed some of the mutants, to the development of surface plasmon resonance methods and data analysis procedures that improved the data, and produced the structure figures in the manuscript.

doi:10.1006/jmbi.2001.5048 available online at http://www.idealibrary.com on IDEAL® *J. Mol. Biol.* (2001) **313**, 385–397

JMB

Mutational Analysis of the Transferrin Receptor Reveals Overlapping HFE and Transferrin Binding Sites

Anthony P. West, Jr[1], Anthony M. Giannetti[2], Andrew B. Herr[1] Melanie J. Bennett[1], Jasvinder S. Nangiana[1], James R. Pierce[1] Leslie P. Weiner[1], Peter M. Snow[1,3,4] and Pamela J. Bjorkman[1,3*]

[1]*Division of Biology 156-29*

[2]*Graduate Option in Biochemistry and Molecular Biophysics*

[3]*Howard Hughes Medical Institute*

[4]*Caltech Protein Expression Center, California Institute of Technology, Pasadena CA 91125, USA*

**Corresponding author*

The transferrin receptor (TfR) binds two proteins critical for iron metabolism: transferrin (Tf) and HFE, the protein mutated in hereditary hemochromatosis. Previous results demonstrated that Tf and HFE compete for binding to TfR, suggesting that Tf and HFE bind to the same or an overlapping site on TfR. TfR is a homodimer that binds one Tf per polypeptide chain (2:2, TfR/Tf stoichiometry), whereas both 2:1 and 2:2 TfR/HFE stoichiometries have been observed. In order to more fully characterize the interaction between HFE and TfR, we determined the binding stoichiometry using equilibrium gel-filtration and analytical ultracentrifugation. Both techniques indicate that a 2:2 TfR/HFE complex can form at submicromolar concentrations in solution, consistent with the hypothesis that HFE competes for Tf binding to TfR by blocking the Tf binding site rather than by exerting an allosteric effect. To determine whether the Tf and HFE binding sites on TfR overlap, residues at the HFE binding site on TfR were identified from the 2.8 Å resolution HFE-TfR co-crystal structure, then mutated and tested for their effects on HFE and Tf binding. The binding affinities of soluble TfR mutants for HFE and Tf were determined using a surface plasmon resonance assay. Substitutions of five TfR residues at the HFE binding site (L619A, R629A, Y643A, G647A and F650Q) resulted in significant reductions in Tf binding affinity. The findings that both HFE and Tf form 2:2 complexes with TfR and that mutations at the HFE binding site affect Tf binding support a model in which HFE and Tf compete for overlapping binding sites on TfR.

Keywords: HFE; iron overload; surface plasmon resonance; functional epitope; class I MHC homolog

Introduction

Mammals possess complex mechanisms to regulate the absorption of iron on both the cellular and organism level. The transferrin receptor (TfR) plays a central role in cellular iron uptake: iron-loaded serum transferrin (Tf) binds to cell surface TfR, which is followed by endocytosis of the TfR/Tf complex (reviewed by Richardson & Ponka[1]). In the acidic endosome environment, iron is released from Tf, transported across the endosomal membrane, and enters a chelatable intracellular pool from which it is utilized for the metabolic needs of the cell or incorporated into the storage protein ferritin. Iron-free Tf (apo-Tf) remains bound to TfR at the low pH of the acidic vesicle ($\leqslant$pH 6.5) and the

Present addresses: J. S. Nangiana, Department of Molecular and Cellular Biology, University of California at Berkeley, Berkeley, CA 94720, USA; J. R. Pierce, Jefferson Medical College, Philadelphia, PA 19107, USA; L. P. Weiner, University of Southern California School of Medicine, Department of Neurology, 2025 Zonal Avenue, Los Angeles, CA 90033, USA.

Abbreviations used: Tf, transferrin; TfR, transferrin receptor; MHC, major histocompatibility complex; β2m, β2-microglobulin; K_D, equilibrium dissociation constant; RU, resonance units.

E-mail address of the corresponding author: bjorkman@its.caltech.edu

0022-2836/01/020385–13 $35.00/0

TfR/apo-Tf complex is then recycled to the cell surface, where apo-Tf dissociates at the higher pH of blood (~pH 7.4). Cellular uptake of iron by TfR and intracellular iron levels are regulated at the translational level by iron-responsive elements in the untranslated regions of mRNA for TfR and ferritin.[1,2]

An additional component of the iron regulatory machinery was recognized from the positional cloning of the gene responsible for hereditary hemochromatosis (HH),[3] a disease characterized by excessive intestinal iron absorption leading to progressive organ failure.[4] The gene mutated in HH encodes a class I major histocompatibility complex (MHC)-related protein called HFE. Like class I MHC molecules, HFE is composed of a heavy chain with three extracellular domains (α1, α2, and α3), a single transmembrane-spanning region, a short cytoplasmic domain, and the non-covalently associated light chain, β2-microglobulin (β2m). Class I MHC proteins bind peptides in a groove within the α1-α2 superdomain and present them to T-cells as part of the adaptive immune response against pathogens.[5] HFE contains a narrowed version of the class I peptide binding groove and does not bind peptides or play any known role in the immune system.[6] Instead, HFE associates with TfR[7,8] in a pH-dependent interaction, such that a nanomolar binding affinity is observed at pH 7.5 with no detectable binding at pH 6 and below.[6] In cell lines and in tissues such as the intestine and placenta, TfR associates with HFE.[7,8] In transfected cell lines, HFE association with TfR negatively regulates Tf-mediated iron uptake.[9–11]

Crystal structures of HFE,[6] TfR,[12] and the HFE/TfR complex[13] reveal the molecular basis for the interaction between TfR and HFE. However, little is known about the binding site on TfR for Tf. Two mutational analyses report localization of the Tf binding site to a region identified from the TfR crystal structure[12] as the helical domain. In the first, Tf binding studies using human/chicken chimeric TfRs suggested that species-specific Tf binding ability is conferred by a region corresponding to the helical domain.[14] In the second, site-directed mutagenesis of an RGD (Arg-Gly-Asp) sequence (residues 646-648) within the TfR helical domain resulted in reduced affinities for Tf binding. HFE binds to the helical domain of TfR and contacts portions of the RGD sequence at residues 646-648,[13] suggesting that the HFE and Tf binding sites on TfR at least partially overlap. Indeed, HFE binding to TfR results in a reduced affinity for Tf, both in transfected cells[7,9] and in a solid-phase assay involving soluble proteins.[15] In principle, the reduction in Tf binding affinity could occur due to direct competition between Tf and HFE for TfR binding caused by overlapping binding sites, or through an allosteric effect.

Understanding the nature of the competitive binding is complicated by the apparent differences between the stoichiometries of TfR/Tf and TfR/HFE complexes observed in solution. In gel-filtration experiments conducted under non-equilibrium conditions, two molecules of Tf bind per TfR homodimer (2:2, TfR/Tf stoichiometry), whereas only one molecule of HFE binds per TfR homodimer (2:1, TfR/HFE stoichiometry)[6] (Figures 1 and 2(a)). In the TfR/HFE co-crystals, however, a 2:2 TfR/HFE stoichiometry was observed.[13] If only 2:1 TfR/HFE complexes form in solution or on cells, Tf affinity reduction would require an allosteric mechanism, since formation of a Tf/TfR/HFE ternary complex, as observed in solution,[6] demonstrates that binding of one HFE molecule does not block both Tf binding sites. If 2:2 TfR/HFE complexes can form in solution, then a pure competition model could explain the observed reduction in Tf affinity. To develop a more detailed microscopic model of the HFE-TfR-Tf system, we have further investigated the TfR/HFE stoichiometry in solution using equilibrium gel-filtration and analytical ultracentrifugation, and verified the overlapping binding site hypothesis by demonstrating that TfR mutations that affect HFE binding also affect Tf binding. We find that several mutations at the crystallographically determined binding site for HFE eliminate HFE binding and reduce Tf affinity. These data confirm that HFE and Tf bind to overlapping sites on TfR and further localize the Tf binding site on TfR.

Results

Stoichiometry of the TfR/HFE complex by equilibrium gel-filtration

To determine the stoichiometry of the TfR/HFE interaction in solution under equilibrium conditions, we performed a series of equilibrium gel-filtration experiments. Conventional gel-filtration experiments are often used to assess the stoichiometry of protein complexes. However, transient dissociation of weak complexes during chromatography can lead to altered stoichiometries.[16] To

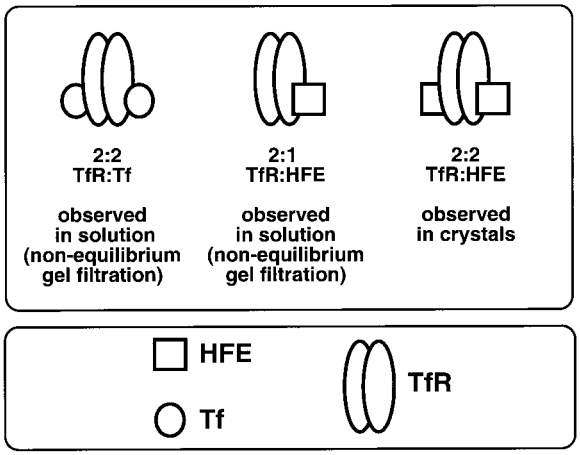

Figure 1. Stoichiometries of the TfR/Tf and TfR/HFE complexes observed in solution or in crystals.

avoid this problem, gel-filtration experiments can be done under equilibrium conditions by including one of the binding partners in the running buffer,[17] as described for previous studies of the interaction between FcRn and its IgG or Fc ligands.[16,18,19]

For our experiments, the gel-filtration column was equilibrated and run using a buffer containing a fixed concentration of HFE (the equilibration buffer). Different ratios of HFE plus TfR were then injected onto the column in equilibration buffer. Although transient dissociation of TfR/HFE complexes occurs as in a conventional gel-filtration experiment, HFE molecules that dissociate from the complex can be replaced by HFE in the equilibration buffer. For each concentration of HFE in the equilibration buffer, there is a ratio of injected proteins such that no peak or trough appears at the elution volume of free HFE (Figure 2(b)-(e)). By determining this ratio at several concentrations of HFE in the equilibration buffer, one can perform a Scatchard analysis yielding both a stoichiometry and a solution phase affinity.[20] The Scatchard analysis in Figure 2(f) shows an x intercept of 2.1, thus the stoichiometry of the TfR/HFE complex is 2:2 (two molecules of HFE bind to each TfR homodimer), in contrast to the 2:1 stoichiometry obtained from non-equilibrium gel-filtration experiments (Figure 2(a)).[6]

Stoichiometry of the TfR/HFE complex by analytical ultracentrifugation

As an independent verification of the solution phase 2:2 TfR/HFE stoichiometry, we examined the sedimentation behavior of TfR/HFE complexes using analytical ultracentrifugation. In a sedimentation equilibrium experiment, the processes of sedimentation and diffusion are allowed to come to equilibrium, at which point a stable concentration gradient is formed. Under these conditions, the observed concentration gradient can be described by either a single-exponential curve (for a single sedimenting species) or a sum of exponentials (for a mixture of species). From these fitted curves, the molecular mass of sedimenting species can be determined.[21]

Soluble forms of HFE and TfR alone each sedimented as a single species, with experimentally derived molecular masses of 48.3 kDa and 150 kDa, respectively, corresponding to an HFE/β2m heterodimer and a homodimeric TfR (Table 1). Fitting the data from centrifugation of TfR/HFE mixtures to a single exponential yields σ_w, the weight-average buoyant molecular mass, which includes information from all species present in solution. The value of σ_w for a TfR/HFE sample loaded at a 2:1 stoichiometry in which the concentration of each TfR polypeptide chain was 0.4 μM was within 1 % of the calculated sum of σ_{HFE} and σ_{TfR}, indicating formation of a 2:1 complex ($\sigma_w = 1.934$, $\sigma_{w,calc} = 1.948$) (Figure 3). The σ_w value for a TfR/HFE sample loaded at a 2:2 stoichiometry (TfR concentration of 0.4 μM) was between the values calculated for the 2:1 and 2:2 complexes, suggesting formation of a mixture of 2:1 and 2:2 complexes ($\sigma_w = 2.157$, $\sigma_{w,calc}$ for the 2:1 complex = 1.948, $\sigma_{w,calc}$ for the 2:2 complex = 2.444). The data for the sample loaded with 2:2 stoichiometry at 0.4 μM TfR can be described as an equilibrium between free TfR, free HFE, 2:1 complex, and 2:2 complex. When the data are analyzed with these assumptions, the 2:1 and 2:2 complexes make up 21 % and 75 %, respectively, of the species in solution at the highest concentrations tested. That the 2:2 complex predominates at 0.4 μM TfR implies that the equilibrium dissociation constant (K_D) for binding the second HFE is submicromolar.

Derivation of stepwise binding affinities for HFE binding to TfR

In a previous surface plasmon resonance-based study,[6] we observed that the apparent affinity of the TfR/HFE interaction depended on the orientation of the binding experiment, such that TfR bound to immobilized HFE with an ~1 nM equilibrium dissociation constant (K_D), whereas HFE bound to immobilized TfR with a 100-600 nM K_D. This difference can now be interpreted in light of the 2:2 TfR/HFE stoichiometry in solution demonstrated by equilibrium gel-filtration and ultracentrifugation (Figures 2 and 3). The higher apparent affinity when TfR is bound to immobilized HFE is due to an avidity effect, in which a TfR molecule in solution can be bound to two HFE proteins on the chip. In the original derivation of the affinity of TfR for immobilized HFE,[6] we used a 1:1 binding model, which does not extract stepwise binding affinities between TfR and HFE. In order to determine the sequential binding affinities between HFE and TfR, we analyzed surface plasmon resonance-

Table 1. Apparent molecular mass (M) of HFE, TfR, and TfR/HFE mixtures as determined by analytical ultracentrifugation (sedimentation equilibrium)

Sample	Concentration (μM)	σ_w (at 9000 rpm)	Apparent M (kDa)	Calculated M[a] (kDa)
HFE	0.4, 6	0.497 (0.474-0.519)	48.3 (46.0-50.4)	44.0
TfR	0.4, 2, 6	1.45 (1.40-1.50)	150 (144-155)	148
2:1 TfR/HFE	0.4	1.93 (1.87-2.00)	196 (190-203)	192
2:2 TfR/HFE	0.4	2.16 (2.08-2.23)	216 (209-224)	236

[a] Calculated from the amino acid sequences of the expressed ectodomains, excluding carbohydrate contributions.

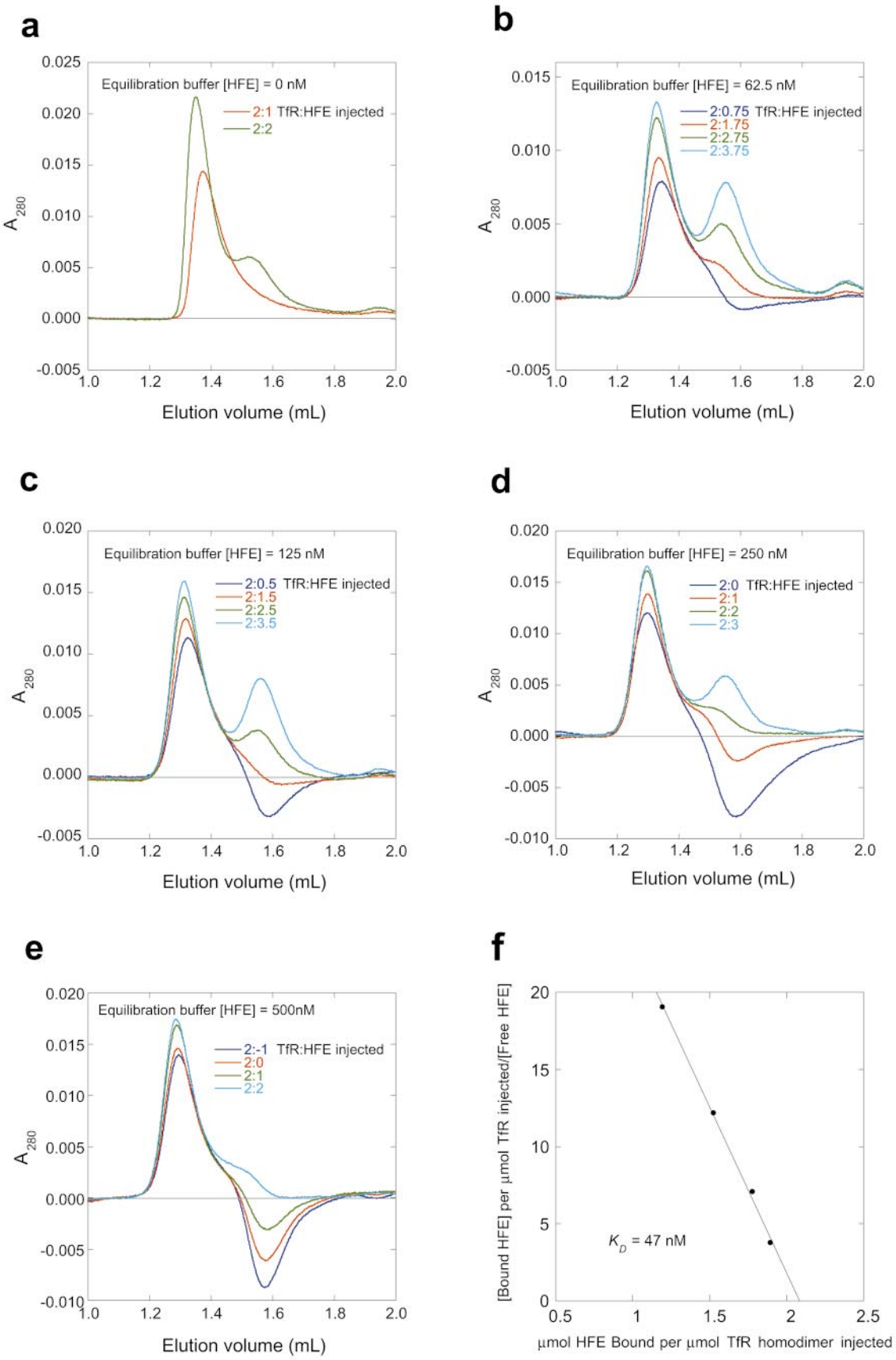

Figure 2 (*legend opposite*)

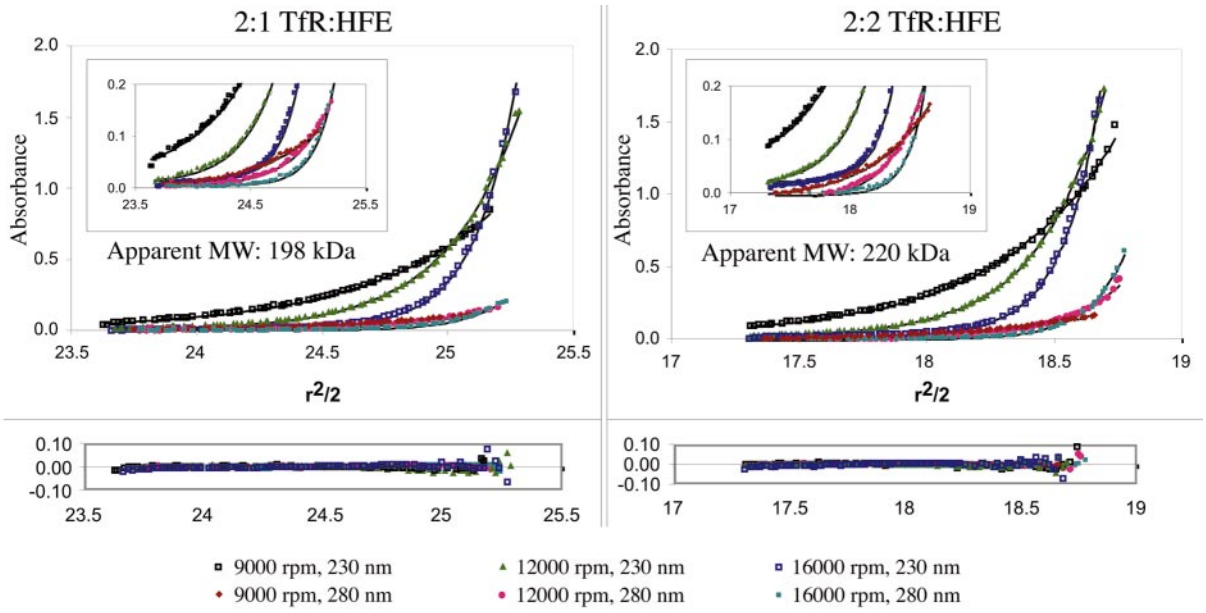

Figure 3. Sedimentation equilibrium data for 2:1 (left) and 2:2 (right) mixtures of wild-type TfR and HFE, both containing 0.40 μM TfR. The inset displays the same data on an expanded *y*-axis. All six curves in each panel were globally fitted, with the residuals for the fit shown below each panel. The 2:1 TfR/HFE sample sedimented as a single species with a molecular mass corresponding to a 2:1 TfR/HFE complex. The 2:2 TfR/HFE sample sedimented as a mixture of 2:1 and 2:2 species, with the 2:2 species predominating.

based binding data for the interaction between TfR and immobilized HFE using a bivalent analyte model. In this model, K_D values are derived for sequential interactions between HFE and TfR, yielding $K_{D1} = 46$ nM and $K_{D2} = 210$ nM (Figure 4). Analysis of the same data using a 1:1 binding model yields a K_D of ~1 nM, consistent with previous results[6] (see Materials and Methods). These results, together with the equilibrium gel-filtration and ultracentrifugation data, give a consistent picture showing that both the first and second HFE binding affinities are submicromolar.

Structure-based design of TfR mutants at the HFE binding site

To test whether the binding sites on TfR for HFE and Tf overlap, we made a series of mutants at the HFE binding site on TfR. Residues at the HFE binding site were identified from the 2.8 Å resolution TfR-HFE co-crystal structure[13] (Protein Data Bank code 1DE4). This structure shows that two helices in the helical domain of TfR (highlighted in green in Figure 5) interact with the HFE α1 and α2 domain helices, forming an extensive interface. The interface includes both apolar and polar interactions and buries 1000 Å^2 of solvent-accessible surface area per subunit. Previous work showed that HFE residues Val78 and Trp81 are critical for TfR binding,[22] hence we chose to mutate TfR residues (Leu619, Val622, Arg623, and Tyr643) that contact these HFE residues. Substitution of TfR residue Gly647, which is within 6.5 Å of HFE but does not form a direct contact, was previously shown to reduce the affinity for Tf,[23] so we generated the G647A mutant to determine its effect on HFE binding. Additional TfR residues that were altered include TfR Arg629, which forms salt-bridges with HFE Glu85 and Glu146, TfR Gln640, which contacts HFE His150 and Arg153, TfR Trp641, which forms a hydrophobic contact with HFE Ile152, TfR Ser644, which contacts HFE

Figure 2. Gel-filtration analyses of TfR/HFE complexes. (a) Non-equilibrium gel-filtration chromatography of 2:1 and 2:2 TfR/HFE mixtures (1.0 μM TfR plus 0.5 or 1.0 μM HFE) demonstrating formation of only the 2:1 complex under these conditions. (b)-(e) Equilibrium gel-filtration of TfR/HFE mixtures. Samples containing 500 nM TfR plus 250, 500, 750, or 1000 nM HFE were injected onto a column equilibrated in a buffer containing (b) 62.5 nM, (c) 125 nM, (d) 250 nM or (e) 500 nM HFE. The peak that elutes first corresponds to a TfR-HFE complex. The second peak or trough is at the elution volume of free HFE (~1.6 ml). From this series of injections, one can calculate the HFE concentration that, when co-injected with 500 nM TfR, yields a free HFE concentration equal to the concentration of HFE in the equilibration buffer (i.e. no HFE peak/trough). The injected TfR/HFE stoichiometries given in the legend account for the baseline unbound HFE in the equilibration buffer. (f) Scatchard plot including data from equilibration buffers containing 62.5, 125, 250, and 500 nM HFE. The best fit line yields a K_D of 47 nM and an *x*-intercept of 2.1.

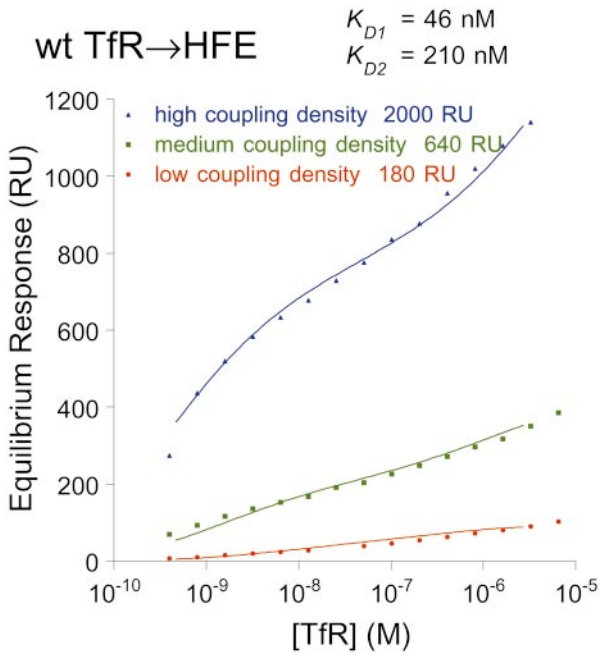

Figure 4. Plots of equilibrium binding responses *versus* the log of the concentration of injected TfR derived from biosensor experiments in which binding responses closely approached or reached equilibrium. TfR was injected over HFE, which was immobilized at low, medium, and high coupling densities to vary the avidity effect on apparent TfR affinity. All three binding curves were globally fit to a bivalent analyte model, yielding affinities that are similar to those obtained in the opposite orientation (HFE injected over TFR).

His150, and Phe650, which contacts HFE Gly71 and His74 (Table 2). All residues chosen for mutagenesis were changed to alanine, with the exception of Phe650. This residue was changed to glutamine, the side-chain found at this position in chicken TfR, which does not bind human Tf.[14]

The soluble ectodomains of TfR mutants were expressed in baculovirus-infected insect cells with polyhistidine tags at their N termini, as described for production of soluble wild-type TfR.[6] Correct folding of mutants that had altered HFE or Tf affinities was verified by gel-filtration elution profiles (ensuring they formed homodimers migrating similarly to wild-type TfR) and by comparing their far-UV circular dichroism spectrum to that of wild-type TfR. All TfR mutants that showed reduced affinities for Tf, HFE, or both showed gel-filtration profiles and circular dichroism spectra similar to those of the wild-type TfR (data not shown).

Measurements of affinities of wild-type TfR and TfR mutants for HFE and Tf

For analyses of the affinities of TfR mutants for HFE and Tf, we also used a surface plasmon resonance-based assay. For these measurements, TfR proteins were coupled to the chip so that the affinities for HFE and Tf could be derived using the same flowcell. Purified His-tagged TfR mutants were immobilized on the sensor chip using an anti-His-tag antibody, and various concentrations of Tf or HFE were injected at pH 7.5. Use of the anti-His-tag antibody allowed oriented coupling of TfR to the biosensor chip, providing a uniform ligand population. All mutant affinities were determined using wild-type TfR coupled to one flowcell as an internal control. Analysis of Tf binding to wild-type TfR (Figure 6(a)) yields two K_D values (calculated from kinetic constants), $K_{D1} = 0.92(\pm 0.17)$ nM and $K_{D2} = 37(\pm 17)$ nM, when the data were fit to a model assuming sequential binding of two molecules of Tf to each TfR homodimer (see Materials and Methods). These results are similar to results

Table 2. Comparison of the Tf and HFE binding affinities of TfR mutants

	HFE			Tf			From TfR-HFE crystal structure	
Mutant	K_{D1} (nM)	K_{D2} (nM)	K_{D1}, K_{D2} Relative to wt	K_{D1} (nM)	K_{D2} (nM)	K_{D1}, K_{D2} Relative to wt	Accessible with HFE (%)	Type of interaction
wt TfR	89 ± 14	650 ± 150		0.92 ± 0.17	37 ± 17			
L619A	**N.B.**		**>500**	**21**	**510**	**23, 14**	**10**	**vdW**
V622A	140	1000	1.6, 1.5	0.38	13	0.41, 0.36	2	vdW
R623A	380	2100	4.3, 3.2	0.15	19	0.16, 0.52	7	vdW
R629A	**2500**	**8700**	**28, 13**	**6.0**	**160**	**6.5, 4.1**	**10**	**H bonds (4)**
Q640A	1200	6800	13, 10	1.3	42	1.4, 1.1	10	H bond (1)
W641A	220	1400	2.5, 2.1	0.42	72	0.46, 1.9	5	vdW
Y643A	**N.B.**		**>500**	**35**	**870**	**38, 23**	**4**	**vdW**
S644A	350	1600	4.0, 2.5	4.0	130	4.3, 3.6	4	vdW
G647A	**300**	**2500**	**3.4, 3.8**	**140**	**950**	**150, 25**		
F650Q	**6200**	**9900**	**70, 15**	**8.2**	**240**	**8.9, 6.5**	**7**	**vdW**

TfR mutant affinities for HFE and Tf were determined by bivalent ligand analysis of biosensor kinetic data. The K_D values for wild-type TfR are averages derived from five independent measurements and the number after the ± sign represents the standard deviation. TfR mutant affinities relative to wild-type derived from independent equilibrium measurements parallel the kinetic-derived values reported here. Mutants with relative TF affinity changes greater than fivefold are shown underlined and in bold.

N.B., no binding detected. Number of hydrogen bonds (in parentheses) and accessible surface area (%) were calculated using the protein-protein interactions server.[44] Accessible surface area (%), percentage of total interface area contributed by each TfR residue; vdW, interactions with HFE involving only van der Waals interactions; H bond, interactions with HFE that include hydrogen bonds.

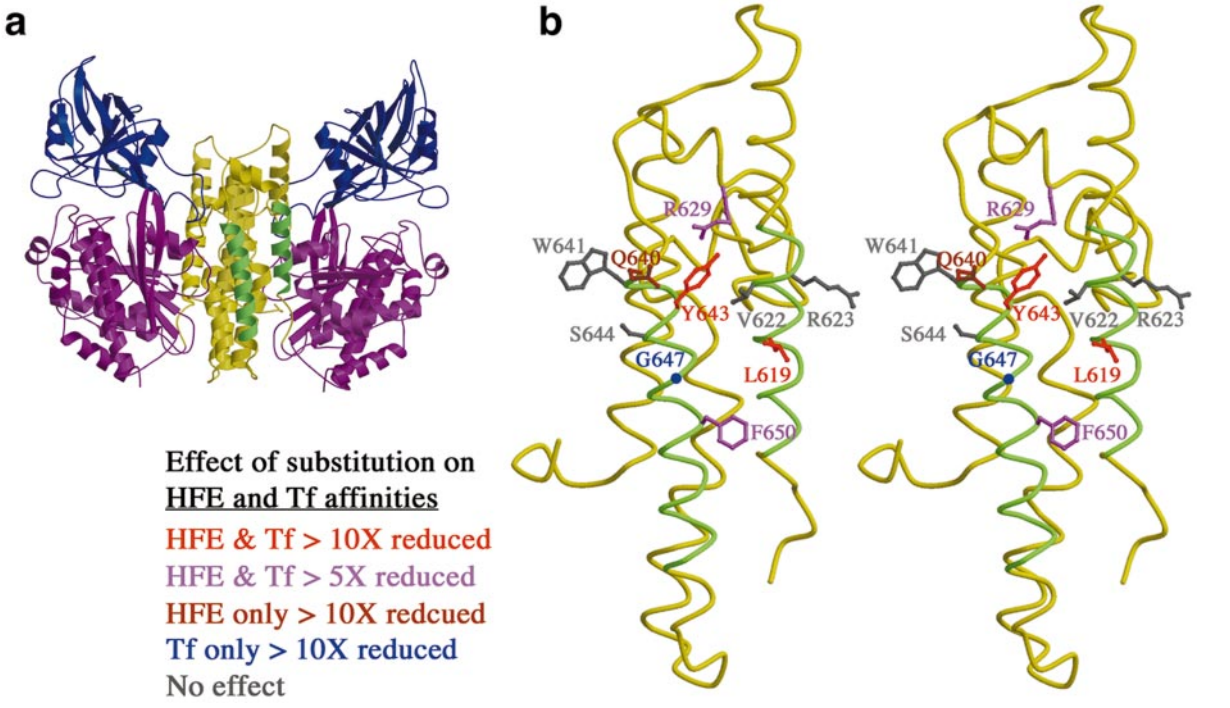

Figure 5. TfR structure. (a) Ribbon diagram of the structure of TfR derived from the 2.8 Å HFE/TfR complex structure.[13] The HFE binding site on the helical domain closest to the viewer is highlighted in green. The HFE binding site on the other helical domain is omitted for clarity. (b) Close-up of the HFE binding site on TfR. The α-carbon trace of one polypeptide chain of the TfR dimer is shown with the side-chains of mutated TfR residues shown in ball and stick representation. Color-coding of the TfR side-chains summarizes the effects of the substitutions as indicated. The Figures were made with MOLSCRIPT[42] and rendered with Raster3D.[43]

obtained from previous biosensor and cell-based measurements of the affinity between TfR and Tf.[1,6] Using the same model for HFE binding to wild-type TfR we calculate $K_{D1} = 89(\pm 14)$ nM and $K_{D2} = 650(\pm 150)$ nM (Figure 6(b)), consistent with values obtained when wild-type TfR interacts with immobilized HFE (Figure 4).

The affinities of ten TfR mutants were measured: L619A, V622A, R623A, R629A, Q640A, W641A, Y643A, S644A, G647A, and F650Q. Residues with significant effects on the affinity between TfR and HFE (Table 2) are highlighted on the TfR structure in Figure 5. Two mutants, L619A and Y643A, had no detectable HFE binding and exhibited over a tenfold decrease in their affinity for Tf. Three other mutants had a greater than tenfold effect on HFE binding: R629A, Q640A, and F650Q. Of these, two (R629A and F650Q) also had a greater than fivefold effect on Tf affinity. The G647A TfR mutant had a large effect on Tf affinity and three- to fourfold effect on HFE binding.

Discussion

Competition studies suggested that HFE and Tf bind to the same or an overlapping site on TfR.[15] Binding to overlapping sites on TfR implies the stoichiometry of the TfR-Tf and TfR-HFE interactions are the same. Both in solution and on the cell surface, TfR homodimers bind two molecules of Tf (2:2 TfR/Tf stoichiometry),[6,24] whereas a 2:1 TfR/HFE stoichiometry was observed by non-equilibrium gel-filtration using soluble forms of TfR and HFE.[6] Since the TfR/HFE co-crystal structure revealed two molecules of HFE bound per TfR homodimer,[13] it was apparent that 2:2 TfR/HFE complexes could form under some conditions. If only 2:1 TfR/HFE complexes can form in solution, however, this would suggest that HFE binds to TfR in a quite different manner from that of Tf, whereby one HFE molecule would prevent binding of Tf or another molecule of HFE through an allosteric effect exerted across the TfR homodimer. In order to ascertain whether TfR can form 2:2 complexes with HFE in solution, we used equilibrium gel-filtration and analytical ultracentrifugation to determine the binding stoichiometry. Both techniques indicate that 2:2 TfR/HFE complexes can form at submicromolar concentrations. This implies that the previously reported 2:1 stoichiometry observed by gel-filtration chromatography (see also Figure 2(a)) resulted from the non-equilibrium nature of the experiment and not from a drastically reduced TfR affinity for binding a second HFE molecule. Indeed, using a sequential binding model to analyze equilibrium binding data, we derived submicromolar K_D values for the first and second binding affinities for the HFE interaction with TfR (Figure 4).

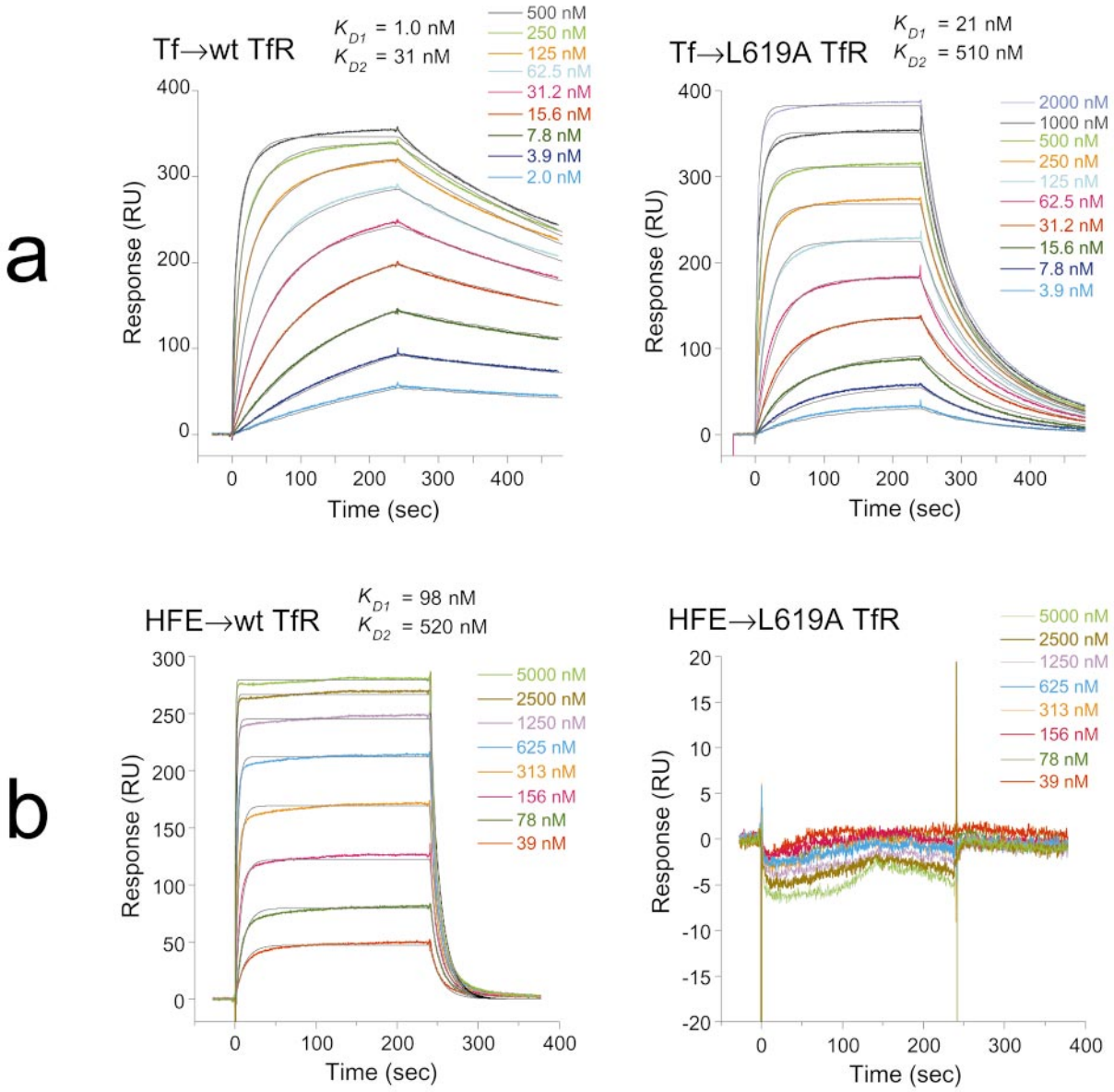

Figure 6. Biosensor analyses of Tf and HFE binding to immobilized wild-type and mutant TfR . (a) Sensorgrams (colored curves) of injected Tf binding to wild-type TfR (left panel) or the L619A TfR mutant (right panel) immobilized using a covalently attached anti-His-tag antibody. Best fit binding curves (assuming a bivalent ligand model) are shown as thin black lines. (b) HFE binding to immobilized wild-type (left panel) or L619A TfR mutant (right panel).

To determine if HFE and Tf compete for TfR binding because they bind at overlapping sites, we characterized the binding properties of a series of soluble TfR proteins with substitutions at the HFE binding site, under the hypothesis that some of the HFE-interacting residues in TfR are likely to contribute to the Tf binding site. A previous study suggested that the RGD sequence in TfR (residues 646-648, a region of TfR that contacts HFE in the co-crystal structure[13]) interacts with Tf, by analogy with fibronectin RGD interactions with integrins.[23] Although a direct structural analogy is unlikely, because RGD sequences that interact with integrins are located on extended loops,[25] whereas the TfR RGD sequence is located within a helix,[12,13] site-directed mutagenesis of the RGD sequence reduced Tf binding to TfR.[23] Consistent with these results, we find that two of our TfR mutants, L619A and Y643A, each altering a residue at the HFE binding site, show no detectable HFE binding and a ~20-fold reduced affinity for Tf. Of three other mutants having a greater than tenfold effect on HFE binding, two (R629A and F650Q) also had a greater than fivefold effect on Tf affinity. The observation that five mutations at the HFE binding site significantly affect Tf affinity (>fivefold reduction) strongly supports a model in which HFE and Tf compete for overlapping binding sites on TfR.

The residues that we have mutated may be classified using the scheme of Wells and colleagues[26] that distinguishes structural and functional epitopes of a protein-protein interaction. Structural epitope residues are defined as all residues at the contact site between two proteins, whereas functional epitope residues are those having a major effect on the binding affinity (defined as $\Delta\Delta G > 2$ kcal/mol for substitution of a single amino acid, which corresponds to an affinity reduction of at least 30-fold). From the crystal structure of the TfR-HFE complex,[13] we have already identified the structural epitope for HFE binding on TfR. The results of this mutagenesis study now identify Leu619, Tyr643, and Phe650 as functional epitope residues for HFE binding. That only a few structural epitope residues are critical for HFE binding is as expected: in mutagenesis studies involving human growth hormone and its receptor, it was found that only ~25% of residues within the structural epitope on the hormone are responsible for the majority of the binding energy between the hormone and receptor.[26] For localization of the Tf binding site, we can provisionally assign structural epitope residues as those that reduce the affinity by 5 to 30-fold when substituted and functional epitope residues as those with a greater than 30-fold effect on the affinity. Thus TfR residues Gly647 and Tyr643 are part of the functional epitope for Tf binding, and TfR Leu619, Arg629, and Phe650 are likely to be at the structural epitope for Tf binding. Because the structures of HFE[6] and Tf[27,28] are very different, the two proteins must therefore bind differently to TfR even though their binding sites overlap. Thus we would not expect the same TfR residues to serve as functional epitope residues for both proteins.

Although Tf and HFE binding appear to be mutually exclusive at their shared binding site on TfR,[15] the homodimeric nature of TfR permits formation of a 1:2:1 Tf/TfR/HFE ternary complex. The observation of ternary complexes in solution using purified proteins,[6] where the stoichiometry was established as 1:2:1,[15] and in HFE-transfected cell lysates[9] raises the possibility that Tf/TfR/HFE ternary complexes may play a role in HFE function. Although we have demonstrated that TfR can readily bind two HFE molecules in solution, the stoichiometry of a TfR/HFE complex on a cell membrane, and how that is influenced by serum Tf, remain to be determined.

What happens when circulating Tf and membrane-bound HFE compete for binding to cell surface TfR? Both Tf and HFE possess advantages for binding TfR that could prevent exclusive formation of either 2:2 TfR/Tf or 2:2 TfR/HFE complexes. In the case of Tf, its presence in micromolar concentrations in serum[29] and its intrinsically higher affinity for TfR compared with HFE make it an effective competitor. In the case of HFE, tethering to a common membrane with TfR facilitates binding of TfR to HFE compared with binding to Tf. The ongoing competition between Tf and HFE for binding TfR and the presence of 2:1 TfR/HFE cell surface complexes may result in formation of Tf/TfR/HFE ternary complexes. Two observations are consistent with ternary complexes being involved in Tf uptake: (i) expression of HFE in transfected cells does not prevent TfR-mediated endocytosis of Tf under conditions in which HFE is associated with TfR at the cell surface, even when HFE is over-expressed and Tf is present at sub-physiological concentrations;[9,11] (ii) HFE is transported to acidic endosomes by TfR in the presence and absence of added Tf.[30] The finding that the HFE and Tf sites on TfR overlap further supports a ternary complex stoichiometry of 1:2:1. Thus HFE-bound TfR should transport only half as much Tf into cells as non HFE-bound TfR, which may explain why ferritin levels are lowered in cells expressing HFE.[9,11,30,31]

Recently, a second receptor for Tf, TfR2, was identified[32] and found to share 45% sequence identity with TfR in its extracellular domain. A surface plasmon resonance-based assay and immunoprecipitation experiments demonstrated that soluble HFE does not bind to soluble TfR2.[33] About half of the TfR residues that form contacts with HFE are replaced by different amino acids in TfR2,[13] suggesting a structural basis for the lack of HFE binding by TfR2. While some critical binding residues are identical (e.g. TfR Leu619 and Tyr643 correspond to TfR2 Leu651 and Tyr675), some substitutions in TfR2 compared to TfR can now be identified that contribute to the inability of TfR2 to bind HFE: TfR residues Arg629 (corresponding to TfR2 residue Ser661) and Phe650 (corresponding to TfR2 residue Ile682) strongly affect HFE binding, and TfR Arg623 (corresponding to TfR2 Gly655) has a moderate effect (Table 2). Together, these differences in TfR2 compared to TfR are expected to strongly destabilize its interaction with HFE. While soluble TfR2 did not bind to HFE in surface plasmon resonance-based experiments, it bound to Tf with ~tenfold weaker affinity than observed for Tf binding to TfR. Of the five TfR residues observed to reduce Tf binding affinity by greater than fivefold when mutated, three are conserved in TfR2: TfR residues Leu619 (TfR2 Leu651), Tyr643 (Tyr675) and Gly647 (TfR2 Gly679).

A key question that remains to be answered is whether HFE has any action besides competing with Tf for binding to TfR and thereby directly reducing Tf-mediated iron uptake. A recent study provides evidence that HFE inhibits apical iron uptake by DMT1,[34] though it remains unclear whether HFE interacts directly with DMT1. Alternatively, HFE that is brought into endosomes while bound to TfR could be the HFE fraction that transmits a signal. We recently tested this second possibility by producing a form of HFE that does not bind to TfR but localizes to endosomes due to addition of a constitutive internalization sequence.[30] This form of HFE did not lead to the reduced ferritin levels observed when wild-type HFE was used in the same assay, thus endosomal

localization of HFE alone is not sufficient for altering iron homeostasis. The stoichiometry of the TfR/HFE complex may critically influence the uptake of iron into cells. Further studies measuring the ratio of HFE to TfR in tissues expressing HFE will be important to determine if HFE regulates iron homeostasis by direct competition with Tf for TfR binding.

Materials and Methods

Protein reagents

Soluble forms of human HFE (residues 1-275 of the mature protein plus β2m) and wild-type human TfR (residues 121-760) were prepared as described.[6] Human Tf (Sigma) was further purified by gel-filtration chromatography. Protein concentrations were determined spectrophotometrically using extinction coefficients at 280 nm of 83,360 M^{-1} cm^{-1} (Tf), 96570 M^{-1} cm^{-1} (HFE), and 93790 M^{-1} cm^{-1} (TfR monomer). Extinction coefficients were calculated as described.[6] All TfR concentrations are reported in terms of a single polypeptide chain of the TfR homodimer.

Equilibrium gel-filtration

The equilibrium column chromatography method of Hummel & Dreyer[17] including Scatchard analysis[20] was used to analyze the association of HFE with TfR. Chromatography was performed at room temperature at a flow-rate of 0.1 ml/minute using a SMART micropurification system (Pharmacia), and the absorbance of the eluant was monitored at 280 nm. A Superdex 200 PC 3.2/30 gel-filtration column was equilibrated with and run in 20 mM Tris (pH 7.4), 150 mM NaCl containing 62.5, 125, 250, or 500 nM HFE (equilibration buffer): 20 μl samples including 500 nM TfR and various concentrations of HFE (250, 500, 750, or 1000 nM) were incubated for 20 minutes at room temperature prior to injection. Relative trough and peak areas were determined by integrating the HFE elution region using the SMART system software. By plotting the area of the trough or peak *versus* the injected HFE concentration, one can derive the concentration of injected HFE that would give a flat baseline with no peak or trough at the position where free HFE elutes. At this injected HFE concentration, the concentration of free HFE is equal to that in the equilibration buffer. The concentration of bound HFE can be determined by subtracting the equilibrium buffer concentration from the injected concentration. Thus each series of injections at a single equilibration buffer concentration gives one datum point (HFE bound, HFE bound/HFE free) for a Scatchard analysis.

Determination of stoichiometry by analytical ultracentrifugation

We analyzed the molecular mass of soluble TfR, soluble HFE, and TfR/HFE complexes by sedimentation equilibrium experiments in a Beckman XL-I Ultima analytical ultracentrifuge. Samples of HFE alone (0.4 and 6 μM), TfR alone (0.4, 2, and 6 μM), and mixtures of TfR and HFE at 2:1 and 2:2 TfR/HFE stoichiometries (0.4 and 6 μM TfR) were spun at speeds of 9000, 12,000, 16,000, and 20,000 rpm at 20 °C. The buffer consisted of 20 mM Tris (pH 7.4) and 150 mM NaCl. Sample volumes of 110 μl were loaded into six-hole, charcoal-filled Epon centerpieces, with 115 μl of matching buffer as reference. Scans were collected at 280, 250, and 230 nm. Samples were judged to be at equilibrium when successive scans collected two hours apart superimposed, typically after 14-16 hours. Data files were trimmed using the program XLAEDIT (D. Yphantis) and analyzed using the program WinNONLIN.[35] Trimmed data sets were globally fitted, using the non-linear least-squares fitting program WinNONLIN, to equation (1):

$$A(r) = e^{\ln A_0} e^{\sigma_w \left(\frac{r^2 - r_0^2}{2}\right)} + \delta \qquad (1)$$

where $A(r)$ is the observed absorbance as a function of radial position, A_0 is the absorbance at reference position r_0, σ_w is the weight-average reduced buoyant molecular mass, r is the radial position (in cm), and δ is the baseline offset. For HFE, data collected at 12,000, 16,000, and 20,000 rpm were globally analyzed, whereas for TfR alone and TfR/HFE mixtures, data collected at 9000, 12,000, and 16,000 rpm were analyzed. Data from TfR alone and the 2:1 and 2:2 TfR/HFE mixtures showed decreasing trends in the weight-average buoyant molecular mass (σ_w) with increasing loading concentration, indicating non-ideal behavior due to glycosylation (data not shown). An estimate of the corrected σ_w was determined by plotting the apparent σ_w at each loading concentration and extrapolating to infinite dilution. These extrapolated values agreed closely with the values of σ_w determined from a global fit in which the non-ideality parameter B was included. For TfR, the corrected value of σ_w determined from the global non-ideal fit is reported in Table 1. For the 2:1 and 2:2 mixtures, the corrected values for σ_w from a global non-ideal fit of both the 0.4 and 3 μM data were within 3 % of the values determined for the 0.4 μM data that is reported in Table 1. Molecular mass was calculated from values of σ_w according to the relation:

$$\sigma_w = \frac{M(1 - \bar{\nu}\rho)\omega^2}{RT} \qquad (2)$$

where $\bar{\nu}$ is the partial specific volume of the macromolecule, ρ is the buffer density, ω^2 is the square of the rotor's angular velocity $(rpm/30)^2$, R is the gas constant (in g/mol K), and T is the absolute temperature. The partial specific volume for each protein was calculated from amino acid sequence information using the program Sednterp[36] and corrected for the estimated level of glycosylation by using a $\bar{\nu}$ of 0.63 for the saccharide moiety as described.[37] The experimentally determined σ_w values for HFE and TfR were consistent with 9 % and 1 % of the total mass being due to glycosylation, respectively; the resulting $\bar{\nu}$ values were 0.719 for HFE and 0.735 for TfR.

Expression and purification of TfR mutants

Soluble human TfR mutants were expressed in a lytic baculovirus/insect cell expression system using the approach described previously for expression of soluble wild-type TfR.[6] A construct encoding residues 121-760 of TfR follows a gene segment encoding the leader peptide from the baculovirus protein GP67, a His_6-tag, and a factor X_a cleavage site in a modified form of the pAcGP67A expression vector (Pharmingen). Mutagenesis of TfR was performed using the Quikchange protocol (Stratagene), and all mutants were verified by DNA sequencing. Recombinant virus was generated by co-transfection of

the transfer vector with linearized viral DNA (Baculogold, Pharmingen). TfR mutants were purified from supernatants of baculovirus-infected High 5 cells using Ni-NTA chromatography (Ni-NTA superflow; Qiagen) followed by gel-filtration chromatography using a Superdex-200 FPLC column (Pharmacia).

Verification of correct folding of TfR mutants

The mutations of TfR were at residues that are solvent-exposed in the TfR crystal structure,[12] and thus would not be expected to influence folding. Correct folding of the mutants was confirmed by verifying homodimer formation by gel-filtration elution profile and by comparing the far-UV CD spectrum of wild-type TfR with the spectra of all mutants having significantly altered HFE or Tf affinities. All mutants migrated on the gel-filtration column in the same position as wild-type TfR (data not shown). CD spectra were obtained by collecting wavelength scans (190-250 nm) at room temperature on an Aviv 62A spectropolarimeter from 1-3 μM protein samples in 25 mM sodium phosphate (pH 7.5) using a 0.1 mm path-length cell. All CD spectra were characteristic of folded proteins with significant α-helical structure. No significant difference was observed between wild-type and mutant spectra (data not shown).

Biosensor-based affinity measurements

A BIACORE 2000 biosensor system (Pharmacia, LKB Biotechnology) was used to assay the interaction of TfR proteins with HFE and human Tf. The BIACORE system includes a biosensor chip with a dextran-coated gold surface to which one protein (referred to as the ligand) is immobilized. Binding of an injected protein (the analyte) to the immobilized protein results in changes in surface plasmon resonance that are directly proportional to the amount of bound protein and read out in real time as resonance units (RU).[38,39]

In our previous analysis of TfR binding to immobilized HFE,[6] a 1:1 binding model was used. Since this model does not take into account the avidity effect of a bivalent analyte, it yields higher apparent affinities than measured when the bivalent protein is coupled to the biosensor chip. In the present experiments, we analyzed equilibrium-based binding data using a bivalent analyte model, which fits binding data to sequential reactions deriving microscopic K_D values for the binding reactions that produce singly and doubly-liganded TfR molecules:

$$\mathrm{HFE} + \mathrm{Tfr} \underset{k_{d1}}{\overset{k_{a1}}{\rightleftharpoons}} \mathrm{HFE/TfR} \quad K_{D1} = \frac{k_{d1}}{k_{a1}}$$

$$\mathrm{HFE} + \mathrm{HFE/TfR} \underset{K_{a2}}{\overset{k_{a2}}{\rightleftharpoons}} \mathrm{HFE/TfR/HFE} \quad K_{D2} = \frac{k_{d2}}{k_{a2}}$$

The intrinsic binding constants for the first and second HFE binding to TfR ($K_{D,first}$ and $K_{D,second}$) are related to the calculated stepwise dissociation constants (K_{D1} and K_{D2}).[40] In the case of independent binding sites:

$$K_{D,first} = 2K_{D1}$$
$$K_{D,second} = K_{D2}/2$$

Hence, if the binding of a TfR ligand was independent of whether a ligand was bound on the other face of the TfR homodimer, we would expect that $K_{D2} = 4\ K_{D1}$ (since our definitions of K_{D1} and K_{D2} do not include statistical factors).

To obtain data exhibiting both weak and strong avidity effects, we immobilized HFE using standard primary amine chemistry (as described in the BIACORE manual) at three different densities (180, 640, and 2000 RU). Varying concentrations of wild-type TfR were injected in 50 mM Pipes (pH 7.5), 150 mM NaCl, 0.005 % (v/v) surfactant P20. Binding reactions were allowed to closely approach or to reach equilibrium by using long injections (48 minutes) with slow flow rates (5 μl/minute), and chips were regenerated after binding reactions by injection of a pH 6.0 buffer. Equilibrium binding responses (R_{eq}) to varying concentrations of injected TfR were derived for the three coupling densities, and data were globally fit to obtain K_{D1} and K_{D2} using the bivalent analyte model as described[19] (Figure 4). The fit values, $K_{D1} = 46$ nM and $K_{D2} = 210$ nM, are consistent with those derived from HFE binding to immobilized TfR (Table 2). Analyzing the medium and high coupling density data with a 1:1 binding model yields high apparent affinities ($K_D < 1$ nM) similar to those reported earlier.[6]

For comparisons of binding by wild-type TfR and TfR mutants, purified TfR proteins were immobilized using an oriented coupling procedure in which an anti-His-tag antibody (anti-pentahis; Qiagen) was covalently attached to the chip surface followed by injection of the His-tagged protein. The anti-His-tag antibody was coupled at 2000-3000 RU to all four flow-cells on a CM5 biosensor chip (Pharmacia) using standard primary amine coupling chemistry (BIACORE manual). His-tagged TfR was then injected in 50 mM Pipes (pH 7.5), 150 mM NaCl, 0.005 % surfactant P20 and allowed to bind to individual flow-cells at levels between 200 and 400 RU. Although a small portion of the bound TfR dissociates within a few minutes of this binding step, the majority (>85 %) remains bound during the course of the experiment. A flow-cell containing only immobilized antibody served as a blank. HFE or Tf was injected over the TfR-coupled flow-cells at 25C° in 50 mM Pipes (pH 7.5), 150 mM NaCl, 0.005 % surfactant P20. Chips were regenerated after analyte binding by injection of 0.5 M $MgCl_2$, 50 mM Pipes (pH 7.5), 150 mM NaCl, 0.005 % surfactant P20, which did not result in dissociation of TfR from the anti-His-tag antibody. Equilibrium dissociation constants (K_D) were calculated from association and dissociation rate constants, which were derived from binding experiments with four minute association and four minute dissociation phases using a flow-rate of 50 μl/minute. Kinetic constants were calculated from sensorgram data using simultaneous fitting of the association and dissociation phases with global fitting to all curves in the working set using CLAMP 99.[41] The data were fit to a bivalent ligand model, i.e. two sequential binding steps for either Tf or HFE binding to TfR.

Acknowledgments

We thank D. G. Myszka, José Lebrón, Caroline Enns and W. Lance Martin for helpful discussions, and members of the Bjorkman laboratory for critical reading of the manuscript. A.P.W. was supported by a grant from the Cancer Research Fund of the Damon Runyon-Walter Winchell Foundation Fellowship, DRG-1445. A.M.G. was supported by NRSA predoctoral training grant 5T32-GM07616. A.B.H. was supported by a grant from the

Cancer Research Fund of the Damon Runyon-Walter Winchell Foundation Fellowship, DRG-1658. This work was supported by the Howard Hughes Medical Institute and a grant from the Arthritis Foundation (to P.J.B.).

References

1. Richardson, D. R. & Ponka, P. (1997). The molecular mechanisms of the metabolism and transport of iron in normal and neoplastic cells. *Biochim. Biophys. Acta,* **1331**, 1-40.
2. De Silva, D. M., Askwith, C. C. & Kaplan, J. (1996). Molecular mechanisms of iron uptake in eukaryotes. *Physiol. Rev.* **76**, 31-47.
3. Feder, J. N., Gnirke, A., Thomas, W., Zsuchihashi, Z., Ruddy, D. A., Basava, A. *et al*. (1996). A novel MHC class I-like gene is mutated in patients with hereditary haemochromatosis. *Nature Genet.* **13**, 399-408.
4. Cullen, L. M., Anderson, G. J., Ramm, G. A., Jazwinska, E. C. & Powell, L. W. (1999). Genetics of hemochromatosis. *Annu. Rev. Med.* **50**, 87-98.
5. Garcia, K. C., Teyton, L. & Wilson, I. A. (1999). Structural basis of T cell recognition. *Annu. Rev. Immunol.* **17**, 369-397.
6. Lebrón, J. A., Bennett, M. J., Vaughn, D. E., Chirino, A. J., Snow, P. M., Mintier, G. A. *et al*. (1998). Crystal structure of the hemochromatosis protein HFE and characterization of its interaction with transferrin receptor. *Cell,* **93**, 111-123.
7. Feder, J. N., Penny, D. M., Irrinki, A., Lee, V. K., Lebrón, J. A., Watson, N. *et al*. (1998). The hemochromatosis gene product complexes with the transferrin receptor, and lowers its affinity for ligand binding. *Proc. Natl Acad. Sci. USA,* **95**, 1472-1477.
8. Parkkila, S., Waheed, A., Britton, R. S., Bacon, B. R., Zhou, X. Y., Tomatsu, S. *et al*. (1997). Association of the transferrin receptor in human placenta with HFE, the protein defective in hereditary hemochromatosis. *Proc. Natl Acad. Sci. USA,* **94**, 13198-13202.
9. Gross, C. N., Irrinki, A., Feder, J. N. & Enns, C. A. (1998). Co-trafficking of HFE, a non-classical major histocompatibility complex class I protein, with the transferrin receptor implies a role in intracellular iron regulation. *J. Biol. Chem.* **273**, 22068-22074.
10. Riedel, H. D., Muckenthaler, M. U., Gehrke, S. G., Mohr, I., Brennan, K., Herrmann, T. *et al*. (1999). HFE downregulates iron uptake from transferrin and induces iron-regulatory protein activity in stably transfected cells. *Blood,* **94**, 3915-3921.
11. Roy, C. N., Penny, D. M., Feder, J. N. & Enns, C. A. (1999). The hereditary hemochromatosis protein, HFE, specifically regulates Tf-mediated iron uptake in HeLa cells. *J. Biol. Chem.* **274**, 9022-9028.
12. Lawrence, C. M., Ray, S., Babyonyshev, M., Galluser, R., Borhani, D. W. & Harrison, S. C. (1999). Structure of the ectodomain of human transferrin receptor. *Science,* **286**, 779-782.
13. Bennett, M. J., Lebrón, J. A. & Bjorkman, P. J. (2000). Crystal structure of the hereditary haemochromatosis protein HFE complexed with transferrin receptor. *Nature,* **403**, 46-53.
14. Buchegger, F., Trowbridge, I. S., Liu, L.-F. S., White, S. & Collawn, J. F. (1996). Functional analysis of human/chicken transferrin receptor chimeras indicates that the carboxy-terminal region is important for ligand binding. *Eur. J. Biochem.* **235**, 9-17.
15. Lebrón, J. A., West, A. P. & Bjorkman, P. J. (1999). The hemochromatosis protein HFE competes with transferrin for binding to the transferrin receptor. *J. Mol. Biol.* **294**, 239-245.
16. Sánchez, L. M., Penny, D. M. & Bjorkman, P. J. (1999). Stoichiometry of the interaction between the MHC-related Fc receptor and its Fc ligand. *Biochemistry,* **38**, 9471-9476.
17. Hummel, J. P. & Dreyer, W. J. (1962). Measurement of protein-binding phenomena by gel-filtration. *Biochim. Biophys. Acta,* **63**, 530-532.
18. Martin, W. L. & Bjorkman, P. J. (1999). Characterization of the 2:1 complex between the class I MHC-related Fc receptor and its Fc ligand in solution. *Biochemistry,* **38**, 12639-12647.
19. West, A. P. & Bjorkman, P. J. (2000). Crystal structure and IgG binding properties of the human MHC-related Fc receptor. *Biochemistry,* **39**, 9698-9708.
20. Gegner, J. A. & Dahlquist, F. W. (1991). Signal transduction in bacteria: CheW forms a reversible complex with the protein kinase CheA. *Proc. Natl Acad. Sci. USA,* **88**, 750-754.
21. Laue, T. M. & Stafford, W. F. (1999). Modern applications of analytical ultracentrifugation. *Annu. Rev. Biophys. Biomol. Struct.* **28**, 75-100.
22. Lebrón, J. A. & Bjorkman, P. J. (1999). The transferrin receptor binding site on HFE, the class I MHC-related protein mutated in hereditary hemochromatosis. *J. Mol. Biol.* **289**, 1109-1118.
23. Dubljevic, V., Sali, A. & Goding, A. (1999). A conserved RGD (Arg-Gly-Asp) motif in the transferrin receptor is required for binding to transferrin. *Biochem. J.* **341**, 11-14.
24. Enns, C. A. & Sussman, H. H. (1981). Physical characterization of the transferrin receptor in human placentae. *J. Biol. Chem.* **256**, 9820-9823.
25. Hynes, R. O. (1992). Integrins: versatility, modulation and signaling in cell adhesion. *Cell,* **69**, 11-26.
26. Cunningham, B. C. & Wells, J. A. (1993). Comparison of a structural and a functional epitope. *J. Mol. Biol.* **234**, 554-563.
27. Bailey, S., Evans, R. W., Garratt, R. C., Gorinsky, B., Hasnain, S., Horsburgh, C. *et al*. (1988). Molecular structure of serum transferrin at 3.3 Å resolution. *Biochemistry,* **27**, 5804-5812.
28. Anderson, B. F., Baker, H. M., Norries, G. E., Rice, D. W. & Baker, E. N. (1989). Structure of human lactoferrin: crystallographic structure analysis and refinement at 2.8 Å resolution. *J. Mol. Biol.* **209**, 711-734.
29. Henry, J. B. (1991). *Clinical Diagnosis and Management by Laboratory Methods*, W.B. Saunders Co., Philadelphia.
30. Ramalingam, T. S., West, A. P., Lebrón, J. A., Nangiana, J. S., Hogan, T. H., Enns, C. A. & Bjorkman, P. J. (2000). Transferrin receptor binding is required for trafficking and function of HFE in duodenal cells. *Nature Cell Biol.* **2**, 953-957.
31. Corsi, B., Levi, S., Cozzi, A., Corti, A., Altimare, D., Albertini, A. & Arosio, P. (1999). Overexpression of the hereditary hemochromatosis protein, HFE, in HeLa cells induces an iron-deficient phenotype. *FEBS Letters,* **460**, 149-152.
32. Kawabata, H., Yang, R., Hirama, T., Vuong, P. T., Kawno, S., Gombart, A. F. & Koeffler, H. P. (1999). Molecular cloning of transferrin receptor 2. *J. Biol. Chem.* **274**, 20826-20832.

33. West, A. P., Bennett, M. J., Sellers, V. M., Andrews, N. C., Enns, C. A. & Bjorkman, P. J. (2000). Comparisons of the interactions of transferrin receptor and transferrin receptor 2 with transferrin and the hereditary hemochromatosis protein HFE. *J. Biol. Chem.* **275**, 38135-38138.
34. Arredondo, M., Muñoz, P., Mura, C. V. & Nuñez, M. T. (2001). HFE inhibits apical iron uptake by intestinal epithelial (Caco-2) cells. *FASEB J.* **15**, 1276-1278.
35. Johnson, M. L., Correia, J. J., Yphantis, D. A. & Halvorson, H. R. (1981). Analysis of data from the analytical ultracentrifuge by nonlinear least-squares techniques. *Biophys. J.* **36**, 575-588.
36. Laue, T. M., Shah, B. D., Ridgeway, T. M. & Pelletier, S. M. (1992). Computer-aided interpretation of sedimentation data for proteins. In *Analytical Ultracentrifugation in Biochemistry and Polymer Science* (Harding, S. E., Rowe, A. J. & Horton, J. C., eds), pp. 90-125, Royal Society of Chemistry, London.
37. Fairman, R., Fenderson, W., Hail, M. E., Wu, Y. & Shaw, S. Y. (1999). Molecular weights of CTLA-4 and CD80 by sedimentation equilibrium ultracentrifugation. *Anal. Biochem.* **270**, 286-295.
38. Fägerstam, L. G., Frostell-Karlsson, A., Karlsson, R., Persson, B. & Rönnber, I. (1992). Biospecific interaction analysis using surface plasmon resonance detection applied to kinetic, binding site and concentration analysis. *J. Chromatog.* **597**, 397-410.
39. Malmqvist, M. (1993). Biospecific interaction analysis using biosensor technology. *Nature,* **361**, 186-187.
40. Wyman, J. & Gill, S. J. (1990). *Binding and Linkage: Functional Chemistry of Biological Macromolecules*, University Science Books, Mill Valley, CA.
41. Morton, T. A. & Myszka, D. G. (1998). Kinetic analysis of macromolecular interactions using surface plasmon resonance. *Methods Enzymol.* **295**, 268-294.
42. Kraulis, P. J. (1991). MOLSCRIPT: a program to produce both detailed and schematic plots of protein structures. *J. Appl. Crystallog.* **24**, 946-950.
43. Merritt, E. A. & Bacon, D. J. (1997). Raster3D: photorealistic molecular graphics. *Methods Enzymol.* **277**, 505-524.
44. Jones, S. & Thornton, J. M. (1996). Principles of protein-protein interaction. *Proc. Natl Acad. Sci. USA,* **93**, 13-20.

Edited by I. A. Wilson

(Received 13 July 2001; received in revised form 28 August 2001; accepted 28 August 2001)

Appendix II:

Heterotypic Interactions Between Transferrin Receptor and Transferrin Receptor 2

This paper describes work I did in collaboration with Caroline Enns' group at the Oregon Health Sciences Institute. They found that TfR and TfR2 heterodimerize in cells. I used sequence alignments, computational contact analysis, and manual graphical inspection of the dimer interface of the known TfR crystal structures. I was able to determine that there would be few, if any differences in a TfR1/TfR2 heterodimer that would prevent the chains from associating.

Heterotypic interactions between transferrin receptor and transferrin receptor 2

Todd M. Vogt, Aaron D. Blackwell, Anthony M. Giannetti, Pamela J. Bjorkman, and Caroline A. Enns

Cellular iron uptake in most tissues occurs via endocytosis of diferric transferrin (Tf) bound to the transferrin receptor (TfR). Recently, a second transferrin receptor, transferrin receptor 2 (TfR2), has been identified and shown to play a critical role in iron metabolism. TfR2 is capable of Tf-mediated iron uptake and mutations in this gene result in a rare form of hereditary hemochromatosis unrelated to the hereditary hemochromatosis protein, HFE. Unlike TfR, TfR2 expression is not controlled by cellular iron concentrations and little information is currently available regarding the role of TfR2 in cellular iron homeostasis. To investigate the relationship between TfR and TfR2, we performed a series of in vivo and in vitro experiments using antibodies generated to each receptor. Western blots demonstrate that TfR2 protein is expressed strongest in erythroid/myeloid cell lines. Metabolic labeling studies indicate that TfR2 protein levels are approximately 20-fold lower than TfR in these cells. TfR and TfR2 have similar cellular localizations in K562 cells and coimmunoprecipitate to only a very limited extent. Western analysis of the receptors under nonreducing conditions reveals that they can form heterodimers. (Blood. 2003;101: 2008-2014)

Introduction

Iron is an essential nutrient required for a variety of biochemical processes such as respiration, metabolism, and DNA synthesis. To maintain intracellular iron levels, cells possess tightly regulated mechanisms for iron absorption and metabolism. Transferrin (Tf), the major iron transport protein in the blood, is taken up into cells by binding to the transferrin receptor 2 (TfR2). This homodimeric membrane receptor binds 2 Tf molecules and is internalized into endosomes that are acidified, resulting in the release of iron from Tf. Iron is transported across the vesicle membrane for utilization and/or storage within the cell, and the TfR-Tf complex recycles back to the cell surface where apo-Tf is released at the higher pH of blood (pH 7.4; reviewed in Aisen et al[1]). The TfR plays a critical role in iron homeostasis. The TfR knock-out mouse results in embryonic lethality.[2]

The recently identified TfR2, a second distinct Tf receptor, is most likely responsible for the non–TfR-mediated uptake of Tf into cells, and it also plays a critical role in iron homeostasis.[3] Mutations in this gene are associated with a rare form of hemochromatosis unrelated to mutations in the hereditary hemochromatosis protein, HFE.[3] TfR2 can support growth of a transfected Chinese hamster ovary cell line lacking endogenous transferrin receptors when given Tf as an iron source.[4] However, TfR2 expression is not sufficient to replace the function of TfR, because mice in which the TfR gene has been deleted die as embryos.[2] TfR2, like TfR, is a type II membrane glycoprotein with a large C-terminal ectodomain and a small N-terminal cytoplasmic domain.[5,6] TfR2 shares 45% amino acid sequence identity with TfR in the extracellular region, contains a cytoplasmic internalization motif similar to TfR, and has 2 cysteines, which form intersubunit disulfide bonds, in the ectodomain proximal to the transmembrane domain.[5,6]

Clear differences exist between the 2 transferrin receptors despite their similarities. Both receptors bind diferric Tf better than apotransferrin at neutral pH, however the affinity of TfR2 for Tf is approximately 25-fold lower than that of TfR.[5] While TfR and HFE are associated in the placenta and transfected cells,[7,8] and in vitro binding assays demonstrate that the ectodomain of TfR binds to HFE with nM affinity,[9-11] the TfR2 ectodomain does not detectably bind to HFE.[12] In humans and mice, TfR2 is expressed predominantly in liver and erythroid cells, while TfR is expressed in a wider range of tissues.[5,6,13] Even though the ectodomains of the 2 TfRs are similar, their cytoplasmic domains share no sequence homology. TfR expression is controlled primarily at the posttranscriptional level in response to cellular iron levels, while TfR2 expression is not influenced by changes in cellular iron levels.[4-6] TfR2 expression is controlled at the transcriptional level by the erythroid transcription factor GATA-1.[14]

Although TfR2 can mediate cellular iron uptake in transfected cells, little is known about its physiologic function and potential interaction with TfR in cell lines that express both receptors. In this study, we investigated the interaction of TfR and TfR2 from the K562 chronic myelogenous cell line with erythrocytic features and from human liver tissue, and we compared the quantities and cellular localization of each receptor. TfR is more abundant than TfR2 in K562 cells while the reverse is true in human liver. We found that in K562 cells TfR and TfR2 colocalize, but coprecipitate to only a limited extent. In liver, only limited coprecipitation of the 2 receptors is detected. These data suggest that homotypic more than heterotypic interactions at the dimer interface are favored.

From the Department of Cell and Developmental Biology, Oregon Health and Science University, Portland OR; Howard Hughes Medical Institute and the Division of Biology, California Institute of Technology, Pasadena, CA.

Reprints: Caroline A. Enns, Department of Cell and Developmental Biology L215, Oregon Health and Science University, 3181 SW Sam Jackson Park Rd, Portland, OR 97201-3098; e-mail: ennsca@ohsu.edu.

Submitted September 9, 2002; accepted October 16, 2002. Prepublished online as *Blood* First Edition Paper, October 24, 2002; DOI 10.1182/blood-2002-09-2742.

Supported by National Institutes of Health grant DK 40608 (C.A.E.) and Howard Hughes Medical Center (P.J.B.).

The publication costs of this article were defrayed in part by page charge payment. Therefore, and solely to indicate this fact, this article is hereby marked "advertisement" in accordance with 18 U.S.C. section 1734.

Materials and methods

Generation of monoclonal antibodies to TfR and TfR2

Soluble versions of human TfR and TfR2 were expressed separately in a lytic baculovirus/insect cell expression system as described previously.[9,12] Briefly, constructs encoding the ectodomain of TfR or TfR2 were joined to a gene segment encoding the leader peptide from the baculovirus protein GP67, a 6xHis-tag, and a Factor Xa cleavage site in a modified form of the pAcGP67A expression vector (Pharmingen, San Diego, CA). Recombinant virus was generated by cotransfection of the transfer vector with linearized viral DNA (Baculogold; Pharmingen). TfR or TfR2 was purified from supernatants of baculovirus-infected High 5 cells using nickel-nitrilotriacetic acid chromatography (Ni-NTA Superflow; Qiagen, Valencia, CA) followed by gel filtration chromatography using a Superdex 200 fast protein liquid chromatography column (Amersham Pharmacia Biotech, Piscataway, NJ). Monoclonal antibodies 3B8 2A1 and 9F8 1C11 were generated against the purified ectodomains of the human TfR and human TfR2, respectively. Female BALB/c mice (aged 5 weeks) were primed and boosted twice (at 2-week intervals) by intraperitoneal injection of 100 μg of the purified ectodomain of TfR2 or TfR in adjuvant. Serum was screened one week after each injection by enzyme-linked immunoassay (ELISA) as described.[15] At 3 days preceding the fusion, one mouse was boosted with 100 μg of purified TfR2 or TfR. Splenocytes from the boosted mouse were fused with HL-1 murine myeloma cells. Media from the hybridoma cultures were tested for antibodies against TfR2 or TfR by ELISA and subsequently by Western blotting. After subcloning positive clones at clonal density, ascites tumors were produced in pristine-primed BALB/c mice. These monoclonals were selected by ELISA assay and then screened for their ability to detect TfR2 or TfR by Western blot analysis. Both antibodies were the immunoglobulin G1 (IgG1), κ subtype. Antibodies to TfR2 did not interact with the ectodomain of TfR by either Western blot or ELISA analysis. The opposite was also true.

Cell lines

HepG2 cells (human hepatocarcinoma) were obtained from the Vollum Institute (Portland, OR), Huh7 cells (human hepatocarcinoma) were kindly provided by Dr Philip Aisen (Einstein University, Bronx, NY). TRVb1 and TRVb cells were gifts of Dr Tim McGraw (Cornell Medical College, New York, NY). The TRVb2 cell line was generated by transfection of TRVb cells with pCDNA 3.1 encoding TfR2 with a FLAG epitope on the N-terminus, selected with G418, and subcloned as described previously.[16] The plasmid was the gift of Drs Koeffler and Kawabata (University of California, Los Angeles). All other cell lines were obtained from the American Type Culture Collection (ATCC; Manassas, VA).

Immunodetection

K562 cells were maintained in RPMI-1640 (Sigma, St Louis, MO) supplemented with 10% fetal bovine serum. Cells were collected and counted on a hemocytometer, washed 3 times with ice-cold phosphate-buffered saline (PBS; pH 7.4) and lysed at a concentration of 1×10^7 cells/mL in NET-Triton buffer (150 mM NaCl, 5 mM EDTA [ethylenediaminetetraacetic acid], 10 mM Tris, pH 7.4, 1% Triton X-100). Cell extracts were incubated with 2 × Laemmli buffer[17] and subjected to electrophoresis on 8% polyacrylamide gels under both reducing and nonreducing denaturing conditions. Separated proteins were transferred to nitrocellulose and blocked overnight at 4°C with 5% milk in 0.01 M Tris-HCl, 0.15 M NaCl, pH 7.4, plus 0.05% Tween-20. Immunoblot analysis was performed using either a sheep anti-TfR serum (1:10 000 dilution)[18] or the monoclonal anti-TfR2 (9F8 1C11) antibody (1:10 000 dilution) followed by the appropriate secondary antibody conjugated to horseradish peroxidase and chemiluminescence (Supersignal; Pierce, Rockford, IL) per the manufacturer's directions.

Immunoprecipitation

K562 cells were washed 3 times with ice-cold PBS and lysed with NET-Triton buffer (0.05 M Tris-Cl, 0.15 M NaCl, 5 mM EDTA, pH 7.4, 1% Triton X-100) followed by centrifugation at 2000*g* for 5 minutes to remove nuclei. Cell lysates were incubated for 60 minutes at 4°C with either 25 μL of protein A–Sepharose (Amersham Pharmacia Biotech) or 25 μL of protein A–Sepharose coated with affinity-purified rabbit anti–mouse IgG (Jackson ImmunoResearch Laboratories, West Grove, PA), and 1.5 μL of either sheep anti-TfR serum or mouse anti-TfR2. The pellet was resuspended into 100 μL NET-Triton buffer, layered on top of 1 mL of the same buffer with 15% sucrose, and pelleted. Samples were eluted in 30 μL of 2 × Laemmli buffer,[17] subjected to sodium dodecyl sulfate–polyacrylamide gel electrophoresis (SDS-PAGE) analysis on an 8% polyacrylamide gel, transferred to nitrocellulose, and immunodetected for either TfR or TfR2.

Quantitation of TfR and TfR2

Subconfluent K562 cells were incubated overnight at 37°C in RPMI-1640 medium without methionine (Life Technologies, Invitrogen, Carlsbad, CA) with 50 μCi (1.85 MBq) of ^{35}S-methionine/cysteine with 10% fetal bovine serum. The cells were then washed 3 times with ice-cold PBS and lysed in NET-Triton, and the nuclei pelleted. Cell extracts were subjected to immunoprecipitation with either sheep anti-TfR or mouse anti-TfR2 antibody as described in "Immunoprecipitation" and analyzed by SDS-PAGE on an 8% acrylamide gel under reducing and denaturing conditions. Gels were fixed, treated with Amplify (Amersham Pharmacia Biotech) for 30 minutes, dried, and exposed to a PhosphorImager screen (Amersham Pharmacia Biotech). Quantitation of the amount of TfR and TfR2 took into account the differences in methionine and cysteine composition of the 2 receptors (22 Met and Cys for TfR and 15, for TfR2).

Interaction of soluble HFE with cell extracts

Cell extracts from K562 cells were incubated with the ectodomain of purified recombinant HFE/β_2 microglobulin (final concentration 1 μM) for 60 minutes at 4°C (K562 + HFE) and immunoprecipitated using sheep anti-TfR serum and *Staphylococcus aureus* (Pansorbin; Calbiochem, San Diego, CA). The ectodomain of purified recombinant HFE/β_2 microglobulin was generated as previously described.[9] Immunoprecipitated proteins were subjected to SDS-PAGE on an 8% acrylamide gel, transferred to nitrocellulose, and immunodetected for TfR2 or TfR.

Immunohistochemistry

K562 cells were fixed in 4% paraformaldehyde, blocked with 2.5 mg/mL bovine serum albumin (BSA), then incubated with sheep anti-TfR (1:50) and mouse anti-TfR2 antibody (1:300) for 1 hour at room temperature. Cells were layered onto 500 μL of fetal bovine serum, centrifuged at 1000*g* for 2 minutes, and resuspended, followed by incubation for 60 minutes with both Alexa 488 conjugated donkey antisheep antibody (1:500) (Molecular Probes, Eugene, OR) and donkey anti–mouse IgG (Jackson ImmnunoResearch Laboratories) conjugated to Alexa 594 using an Alexa Fluor 594 Protein Labeling Kit (1:100) (Molecular Probes). Cells were again layered on top of 500 μL fetal bovine serum, pelleted, washed with PBS, and mounted on slides using Prolong Antifade (Molecular Probes). Images were obtained using a BioRad 1024 ES laser scanning confocal system (Hercules, CA) on a Nikon Eclipse TE300 microscope (Melville, NY) with a × 60 oil immersion Planapo objective. Permeabilized cells were treated with NET-Triton after fixation and prior to incubation with antibodies.

Results

Characterization of TfR2 expression

The relative amounts of TfR2 in a variety of human cell lines were visualized by Western blot analysis using the mouse monoclonal antibody (9F8 1C11) against the ectodomain of human TfR2

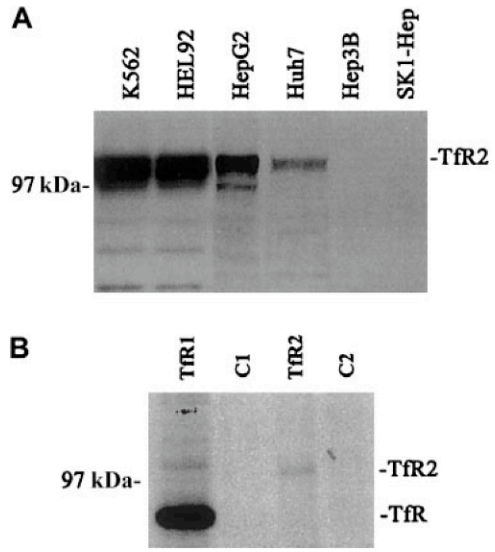

Figure 1. Expression of TfR and TfR2. (A) The relative amounts of TfR2 were visualized in a variety of human cell lines by Western blots. Equal amounts of cell extracts (25 μg) were loaded onto gels and subjected to SDS-PAGE. TfR2 was detected with the mouse monoclonal antibody to human TfR2 (9F8 1C11) followed by a goat antimouse/horseradish peroxidase (HRP) secondary antibody. All blots were developed by chemiluminescence (Pierce): K562, HEL 92 (erythroid leukemia), HepG2, Huh7, Hep 3B, and SK-1 Hep (hepatoma). The TfR2 signal produces multiple bands between 97 and 105 kDa. (B) Quantitative immunoprecipitation of TfR and TfR2. K562 cells were labeled overnight with 50 μCi (1.85 MBq) ^{35}S-methionine, lysed, and quantitatively immunoprecipitated with either a sheep antihuman TfR serum and protein A–Sepharose (Pharmacia) (TfR); cell extract and protein A–Sepharose as a control (C1); the TfR2 monoclonal antibody (9F8 1C11) and rabbit anti–mouse IgG–coated protein A–Sepharose (TfR2); or cell extract and rabbit antimouse coated protein A–Sepharose as a control (C2). Immunoprecipitated proteins were eluted with 2 × Laemmli buffer, run on an SDS-8% polyacrylamide gel, dried, and exposed to film. The relative amount of radioactivity in each band was determined by PhosphorImager analysis correcting for the Met/Cys content of each TfR. Reimmunoprecipitation of the supernatants of the immunoprecipitates showed that all of TfR and TfR2 were bound in the first immunoprecipitation (results not shown).

(Figure 1A). Closely migrating bands (2-3) of between approximately 97 and 105 kDa were observed for TfR2. Multiple bands have been observed previously and have been attributed to heterogeneity in glycosylation.[4] The TfR2 signal was strongest in K562 and HEL 92 cells (erythroleukemia cell lines), moderate in HepG2 and Huh7 cells (hepatoblastoma cell lines), and undetectable in the Hep3B and SK1 Hep cell lines (hepatoblastoma cell lines). These results correlate with previous work, which demonstrated that TfR2 mRNA was expressed strongly in both K562 and HepG2 cells by Northern blot and reverse transcriptase–polymerase chain reaction (RT-PCR) analysis.[5] In contrast, TfR protein levels were strong and uniform in these and other cell lines tested (data not shown).

Quantitation of TfR and TfR2 in K562 cells

To measure the relative amounts of TfR and TfR2 protein, cell lysates from ^{35}S-methionine/cysteine-labeled K562 cells were immunoprecipitated with either a sheep antihuman TfR antiserum or the mouse antihuman TfR2 monoclonal antibody (9F8 1C11), separated on a 8% acrylamide gel under reducing and denaturing conditions, dried, and exposed to a PhosphorImager (Figure 1B). The amount of TfR2 protein is approximately 20 times less than TfR protein. Background of the ^{35}S-labeled immunoprecipitates prevented the quantitation of the amount of each receptor that formed heterodimers. We estimate that if 5% of TfR formed heterodimers with TfR2 then TfR should have been detectable in the TfR2 immunoprecipitates. If less than 25% of the TfR2 coprecipitated with TfR1 then the heterodimers would not be detectable by this method. Thus although the 2 TfR receptors coprecipitate in K562 cells, the coprecipitated material accounts for only less than 5% of the total amount of receptors.

TfR and TfR2 association

A series of immunoprecipitations and Western blots of the immunoprecipitated proteins were performed using TfR and TfR2 antibodies to determine the relative amounts of each protein in this cell line (Figure 2). When TfR was immunoprecipitated from K562 cell lysates followed by Western blotting for TfR2, TfR2 clearly coimmunoprecipitates with TfR (Figure 2A, lane 4). TfR2 also coprecipitates with TfR (Figure 2B, lane 4), as demonstrated by conducting the experiment in the reverse order (immunoprecipitate TfR2 and immunoblot for TfR). The coprecipitation does not result from an artifactual association of TfR or TfR2 with reagents used in the immunoprecipitation, since TfR does not bind protein G–Sepharose in the absence of antibody (Figure 2B, lane 3), TfR2 does not bind *S aureus* in the absence of antibody (Figure 2A, lane 3) and both *S aureus* and protein G–Sepharose contain no

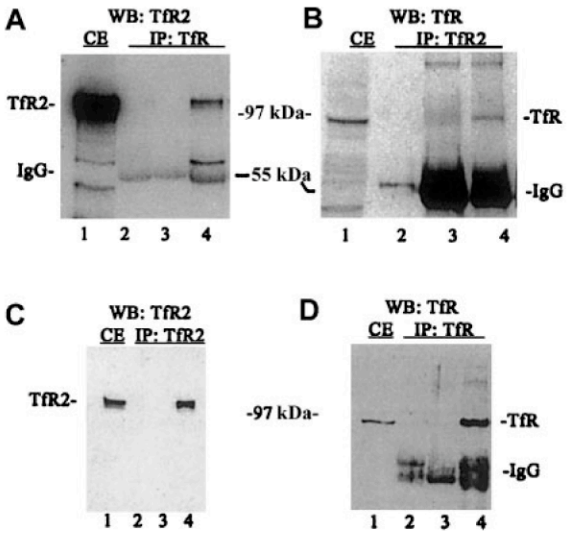

Figure 2. TfR and TfR2 are associated in vitro. Cell extracts from K562 cells were solubilized (1×10^7 cells/mL) as described in "Materials and methods," immunoprecipitated, subjected to SDS-PAGE, transferred to nitrocellulose, and immunodetected using TfR (WB:TfR) and TfR2 antibodies (WB:TfR2). (A) K562 cell extracts (50 mL) were immunoprecipitated with a sheep antihuman TfR antiserum and *S aureus* (IP:TfR), and detected by Western blotting using the mouse monoclonal antibody to human TfR2 (9F8 1C11) and an antimouse/HRP-conjugated secondary antibody. All blots were visualized by chemiluminescence (Pierce). Lanes are as follows: (1) K562 extract (25 mL); (2) *S aureus* and TfR antibody alone; (3) *S aureus* and K562 extract alone; and (4) *S aureus,* anti-TfR serum, and K562 extract. (B) K562 extract from 5×10^5 cells was immunoprecipitated with the monoclonal TfR2 antibody (9F8 1C11) and protein G–Sepharose (IP:TfR2) and detected with sheep anti-TfR serum and swine antisheep/HRP-conjugated secondary antibody on Western blots. Lanes are as follows: (1) K562 extract (25 mL); (2) protein G–Sepharose and TfR2 monoclonal antibody (9F8 1C11) only; (3) protein G–Sepharose and K562 extract (50 mL) only; and (4) protein G–Sepharose, TfR2 monoclonal antibody (9F8 1C11), and K562 extract (50 mL). (C) K562 extract (50 mL) immunoprecipitated with anti-TfR2 monoclonal antibody (9F8 1C11) (IP:TfR2) and immunodetected for TfR2 by Western blots. Lanes are as follows: (1) K562 extract (25 mL); (2) TfR2 monoclonal antibody (9F8 1C11) isolated with protein G–Sepharose; (3) K562 extract (50 mL) isolated with *S aureus* alone; and (4) TfR2 isolated from K562 extracts (50 mL) with anti-TfR2 monoclonal antibody (9F8 1C11) and protein G–Sepharose. (D) K562 extract (50 mL) immunoprecipitated with anti-TfR (IP:TfR) and Western blotted for TfR (WB:TfR). Lanes are as follows: (1) K562 extract (25 mL); (2) *S aureus* and anti-TfR serum only; (3) K562 extract (50 mL) incubated with *S aureus* only; and (4) K562 extract (50 mL) immunoprecipitated with anti-TfR serum and *S aureus*. IP indicates immunoprecipitated; WB, Western blot; and CE, cell extract.

immunoreactive bands (Figure 2A, lane 2 and 2B, lane 2, respectively). To measure the total amount of TfR2 and TfR that immunoprecipitated, a series of control blots were performed (Figure 2C-D). Immunoprecipitation with TfR2 antibody and *S aureus*, followed by immunodetection for TfR2, shows that TfR2 can be quantitatively precipitated with this antibody (Figure 2C, lanes 1,4). Similarly, TfR can be quantitatively precipitated from lysates (Figure 2D, lanes 1,4). These results indicate that that homodimer formation is strongly preferred.

We also tested to determine if the 2 receptors had to be expressed in the same cell in order to associate or if higher order complexes formed only after the cells were lysed. For these experiments, we transfected TRVb cells, a Chinese hamster ovary cell line lacking endogenous transferrin receptor.[19] A series of immunoprecipitations were carried out with TRVb cells stably transfected with TfR (TRVb1) or TfR2 (TRVb2) (Figure 3). When cell lysates from these 2 cell lines were mixed and immunoprecipitated with anti-TfR2, no TfR could be detected (Figure 3A). Similarly, immunoprecipitation of a mixture of cell lysates from the 2 cell lines with anti-TfR shows no detectable TfR2 in the immunoprecipitates (Figure 3B). These results indicate that the 2 homodimers generated in separate cell lines do not form higher order complexes after solubilization.

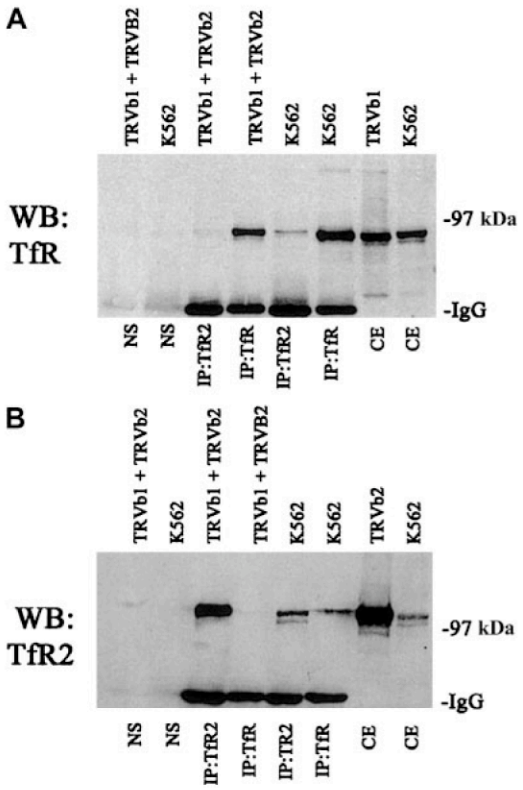

Figure 3. Specificity of interaction between TfR and TfR2. A series of control immunoprecipitations for TfR and TfR2 was performed. Fifty micrograms of extracts from K562 cells, TRVb cells transfected with a wild-type TfR plasmid (TRVb1), TRVb cells transfected with a wild-type TfR2 plasmid (TRVb2), and a mixture of TRVb1 and TRVb2 cells were immunoprecipitated using either the TfR mouse monoclonal antibody or the TfR2 mouse monoclonal antibody and *S aureus* precoated with an affinity-purified rabbit antimouse antibody (Jackson Immunolabs). Immunoprecipitates and 16.7 μg of cell extracts (equivalent to one third of the amount immunoprecipitated) were run on an 8% gel under denaturing and reducing conditions, transferred to nitrocellulose, and immunodetected for TfR or TfR2 (A and B, respectively). The legend above each blot indicates the cell lines in each lane and the legend below each blot indicates the treatment of each cell line and the antibodies used for the immunoprecipitations. NS indicates cell extracts combined only with precoated *S aureus*; CE, cell extracts only. These results indicate that anti-TfR cannot immunoprecipitate TfR2 by itself and vice versa.

Colocalization of TfR and TfR2 in K562 cells

Confocal microscopy was used to examine the intracellular locations of TfR and TfR2. K562 cells were fixed and incubated with either a sheep anti-TfR serum or the mouse anti-TfR2 antibody, followed by appropriate fluorescent secondary antibodies (Figure 4). Prior experiments (Figures 1-2) demonstrated that TfR and TfR2 are both expressed in erythroid and liver cell lines and that they can associate to form heterodimers; yet the extent to which these proteins share similar subcellular locations was unknown. Confocal images of stained cells demonstrate that TfR and TfR2 localize in overlapping subcellular compartments. In both nonpermeabilized cells (Figure 4A-C) and cells permeabilized with Triton X-100 (Figure 4D-E,K), TfR and TfR2 have similar localizations. Both receptors are expressed on the cell surface (Figure 4 H-I) and appear to colocalize (Figure 4A-C,H-I). Inside the cells, both TfR and TfR2 localize to punctate perinuclear compartments (Figure 4E-F, J-K). Previous results from our laboratory and others demonstrated that TfR localizes to perinuclear recycling endosomes,[20,21] which in combination with the present results suggests that TfR and TfR2 utilize the same endosomes and traffic together in K562 cells.

HFE and Tf do not prevent association between TfR and TfR2

Crystallographic studies of the HFE-TfR complex reveal that the HFE binding site on TfR comprises 2 helices on the outer edge of the helical domain.[22] In vitro studies using the ectodomains of TfR, HFE, and Tf suggest that HFE and Tf compete with each other for binding to TfR[23] and are consistent with the demonstration that site-directed mutagenesis of the HFE binding site on TfR affects Tf binding.[11] We wanted to test whether the TfR2 interaction site on TfR overlapped with the region on the TfR helical domain identified as the HFE and Tf binding site. Extracts of K562 cells were incubated in the presence of 100 μM soluble recombinant HFE,[10] and the amount of TfR2 associated with TfR was evaluated. At this concentration, HFE binds to TfR and competes with Tf binding. The extracts were immunoprecipitated with either anti-TfR2 and probed with anti-TfR or vice versa. No decrease in the TfR-TfR2 interaction was detected (Figure 5). Similar results were obtained upon addition of Tf (results not shown), suggesting that TfR and TfR2 do not interact with each other at the HFE-TfR interface.

TfR and TfR2 interaction under nonreducing conditions

Because TfR and TfR2 each contain cysteine residues that are used for intersubunit disulfide bonds, a possible mode of association between TfR and TfR2 is the formation of covalent, disulfide-linked heterodimers (Figure 6). To determine whether covalent TfR-TfR2 heterodimers can form, cell lysates from K562 and TRVb1 cells were examined under nonreducing conditions and TfR and TfR2 were immunodetected on Western blots. A single homodimer band will be seen at approximately 186 kDa and a monomeric band will be detected at approximately 93 kDa for TfR if the receptors interact yet do not form intersubunit disulfide bonds. The migration pattern of TfR2 under nonreducing conditions is more complicated because it migrates as a doublet under reducing conditions. If TfR and TfR2 form intersubunit disulfide bonds, then TfR should be detected as a doublet with the lower molecular mass at approximately 186 kDa and little or no

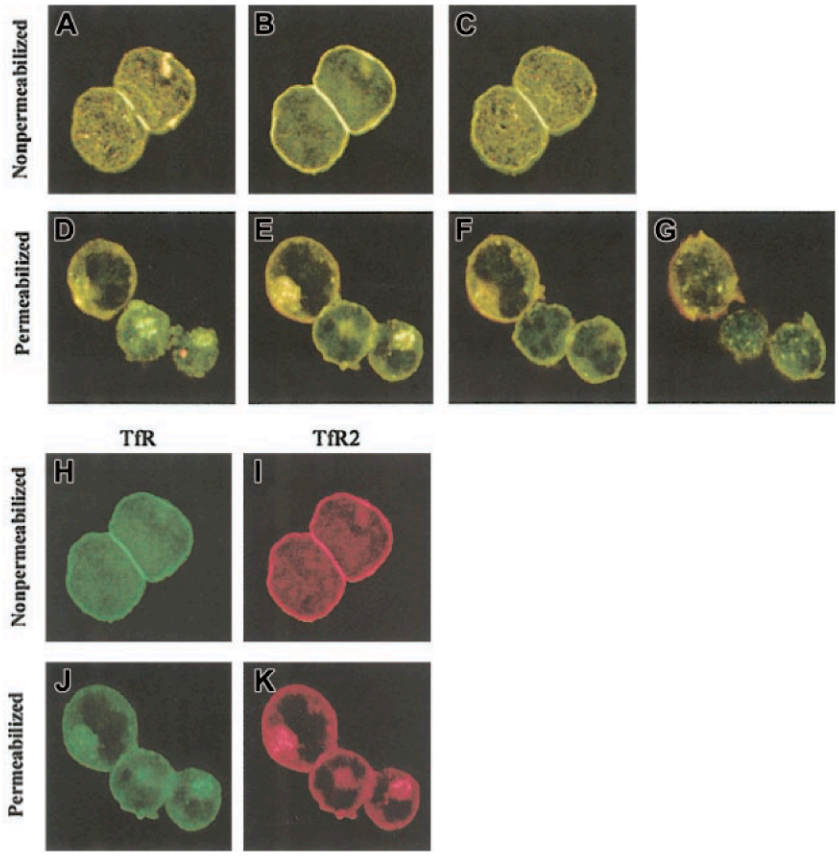

Figure 4. Colocalization of TfR and TfR2 in K562 cells. K562 cells were fixed and labeled with mouse anti-TfR2 monoclonal antibody (9F8 1C11) and sheep anti-TfR serum, followed by Alexa 594 antimouse (red) and Alexa 488 antisheep (green). Merged sections of nonpermeabilized cells are shown in panels A to C. Yellow indicates overlapping fluorescence. Sections are 2.0 μm apart. Panels H and I, respectively, show the separate TfR (green) and TfR2 (red) channels of panel B. Merged sections of permeabilized cells (D-G) also indicate colocalization in perinuclear compartments. Sections in panels D to G are 1.5 μm apart; panels J and K are separate TfR (green) and TfR2 (red) channels of image in panel E. Images were captured with a × 60 oil immersion lens as described in "Materials and methods."

monomer. The evidence supports this possibility. Under nonreducing conditions a doublet of the TfR is detected in K562 cell extracts. No such doublet is seen in TRVb1 cells expressing TfR only (Figure 6).

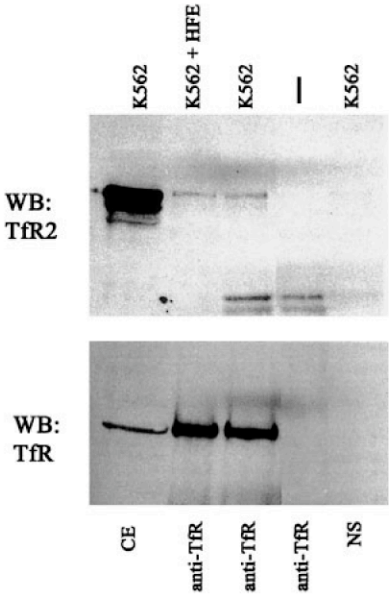

Figure 5. HFE does not alter TfR-TfR2 interaction. Cell extracts from K562 cells were incubated with 1 μM purified recombinant HFE for 60 minutes at 4°C (K562 + HFE) and immunoprecipitated using sheep anti-TfR serum and *S aureus* (IP:TfR). Immunoprecipitated proteins were subjected to SDS-PAGE on an 8% gel, transferred to nitrocellulose, and immunodetected for TfR2 (upper panel) (WB:TfR2) and TfR (lower panel) (WB:TfR). NS indicates background control using K562 cell extracts and *S aureus* without antibody; vertical dash, no cell extract with anti-TfR and *S aureus* only; and CE, cell extract.

Interaction of TfR and TfR2 in human liver tissue

Because TfR and TfR2 interact with each other in K562 cells we wanted to determine whether this interaction could be detected in the liver, the tissue that has the highest concentration of TfR2 mRNA. Western blots were used to evaluate the relative levels of TfR2 in K562 cells and liver tissue. TfR2 is much more abundant in liver compared with K562 cells. The opposite is true for TfR. TfR is barely detectable in liver and easily detected in K562 cells (Figure 7A). Similar to K562 cells, small but detectable amounts of TfR2 and TfR coprecipitate, indicating that the 2 receptors interact in liver as well as K562 cells but, again, to only a limited extent.

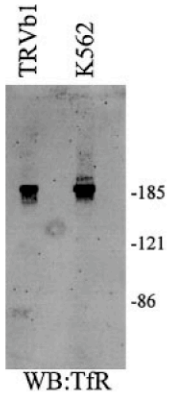

Figure 6. TfR and TfR2 under nonreducing conditions. Cell extracts (25 μg) from TfR-transfected TRVb cells (TRVb1) and K562 cells were separated on an 8% acrylamide gel under denaturing but nonreducing conditions, transferred to nitrocellulose, and Western blotted for TfR and TfR2. TfR homodimer is approximately 190 kDa, while the TfR2 homodimer is a doublet of approximately 200 and 210 kDa.

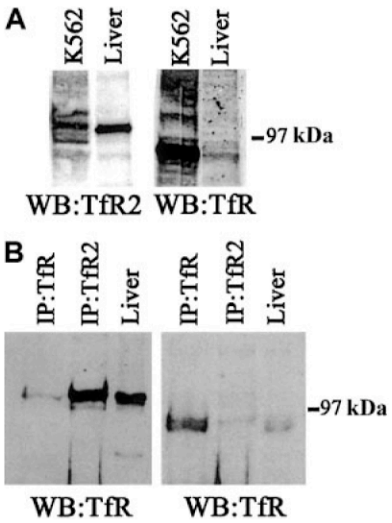

Figure 7. TfR and TfR2 protein expression in human liver. (A) To determine the relative levels of TfR and TfR2 protein in human liver tissue and K562 cells, 50 μg of cell extracts were Western blotted for either TfR (WB:TfR) or TfR2 (WB:TfR2). The panel on the left was developed using a mouse monoclonal antibody to human TfR2 (1:10 000), while the panel on the right was developed using a mouse monoclonal antibody to TfR (1:10 000). (B) To determine whether TfR and TfR2 interact in human liver, a series of immunoprecipitations for either TfR or TfR2, followed by immunoblotting for TfR or TfR2, was performed. Human liver extract (60 μg) was immunoprecipitated with either a sheep polyclonal antibody to TfR (1:100) and 30 μL of *S aureus* (IP:TfR) or with a mouse monoclonal antibody to TfR2 (1:120) and 30 μL of protein G–Sepharose (IP:TfR2), or the extract was loaded onto the gel (liver). Proteins were separated on an 8% acrylamide gel under denaturing and reducing conditions, transferred to nitrocellulose, and immunoblotted for either TfR (right panel) or TfR2 (left panel).

Discussion

Tf is the major iron transport protein in the blood and was originally thought to bind to and be taken up into cells via only a single receptor, TfR. Recently however, 2 more Tf binding receptors have been identified, TfR2[5,6] and the cubulin-megalin complex.[24] These 2 receptors for Tf are tissue specific, whereas TfR appears to be expressed at least at low levels ubiquitously. TfR2 is expressed mainly in the liver and erythropoietic cells, and the cubulin-megalin complex is localized in the kidneys and rat yolk sac.[24]

Each receptor presumably has a different function in the regulation of iron homeostasis in the body. TfR regulates the uptake of iron into cells and itself is regulated by intracellular iron concentrations and by the proliferation status of the cells. The cubulin-megalin complex appears to be essential in the scavenging of iron, which would otherwise be excreted by the kidneys. The function of TfR2 has not been elucidated to date. It likely plays a major role in iron homeostasis in the body because mutations in this gene result in a rare form of hereditary hemochromatosis with iron accumulation in the liver, heart, and pancreas and high levels of Tf iron saturation.[3]

The interactions between these 3 transferrin receptors have not been examined. There is probably no interaction between the cubulin-megalin complex and TfR. They are located in different regions of the cell: the cubulin-megalin complex apically oriented, and the TfR basolaterally oriented. Here we used a cell line that endogenously expresses both TfR and TfR2 in order to study their interaction. We found the highest levels of TfR2 protein present in K562 and HEL92 erythroleukemia cell lines, with lesser amounts in HepG2 and Huh7 liver cell lines, correlating with previous work

Table 1. TfR dimer interface residues and their TfR2 counterparts

TfR position	TfR residue	TfR2 residue	TfR2 position
182	Trp	Trp	192
183	Arg	Thr	193
185	Gln	Thr	196
312	Gly	Gly	334
313	Phe	Phe	335
314	Pro	Pro	336
315	Ser	Ser	337
316	Phe	Phe	338
317	Asn	Asn	339
320	Gln	Gln	342
321	Phe	Phe	343
322	Pro	Pro	344
400	Asp	Asp	424
402	Tyr	Tyr	426
449	*Ile*	*Leu*	472
466	Trp	Trp	489
469	Gly	Gly	492
470	Tyr	Tyr	493
471	Leu	Leu	494
472	Ser	Ser	495
473	Ser	Val*	496
474	Leu	Leu	497
476	Leu	Leu	499
477	Lys	Lys	500
637	Leu	Leu	669
638	*Ser*	*Thr*	670
639	Leu	Leu	671
641	Trp	Trp	673
667	Asp	Asp	699
668	Arg	Glu*	700
669	Phe	Arg*	701
672	*Lys*	*Arg*	704
673	Lys	Met*	705
676	Asp	Val	708
680	Arg	Arg	712
683	*Tyr*	*Phe*	715
684	*His*	*Tyr*	716
688	Pro	Gln*	720
689	Tyr	Tyr	721
691	Ser	Ser	723
692	Pro	Pro	724
693	Lys	Ala	725
733	Asn	Arg*	774
735	Leu	Leu	776
736	Ala	Ala	777
737	Leu	Leu	778
740	Trp	Trp	781
744	Gly	Gly	785
747	Asn	Asn	788
748	Ala	Ala	789
753	Val	Val	794
754	Trp	Trp	795
755	*Asp*	*Asn*	796
756	Ile	Ile	797
758	Asn	Asn	799
759	*Glu*	*Asn*	800
760	Phe	Phe	801

Residues in the TfR dimer interface were identified by contact analysis in CNS[25] of the unliganded TfR structure (1CX8.pdb)[26] using a probe radius of 1.4 Å and a distance cutoff of 4 Å. The interface is 70% identical between TfR and TfR2, consistent with the observation of TfR-TfR2 heterodimers. Nonconservative substitutions are underlined and semiconservative substitutions are italicized. Nonconservative substitutions with an asterisk could probably be accommodated in the dimer interface, as determined by inspection of the TfR structure. For example, the substitutions at TfR position 668 and 669 would disrupt a cation-π interaction between an arginine and a phenylalanine and replace it with a salt bridge between a glutamate and an arginine.

by Kawabata et al, which demonstrated high levels of TfR2 mRNA expression in erythroid precursors and liver.[5,14] In K562 cells, TfR2 levels are approximately 10 times lower than TfR levels; however, the 2 receptors have similar cellular distributions, with most of both receptors in the cell interior. Being 10 times more abundant and possessing a higher affinity for Tf, TfR is responsible for the majority of iron uptake in this cell line. However, TfR2 mRNA and protein levels are more abundant than TfR mRNA and protein levels in liver and immature erythroid precursors, suggesting that TfR2 protein predominates in these cells.[4,6]

We have demonstrated an interaction between TfR and TfR2. Studies using coprecipitation and nonreducing SDS-PAGE show that the transferrin receptors interact and form heterodimers, and this in vitro interaction is supported by the similar colocalization of TfR and TfR2 in vivo. On the cell surface both receptors appear diffuse and in similar locations, while on the cell interior both receptors colocalize to punctate vesicles, likely the recycling endosome. These results suggest that similar mechanisms are used in the internalization and trafficking of each receptor within the cell, even though the amino acid sequences of the cytoplasmic domains of each receptor share no similarity other than both containing tyrosine-based internalization motifs.

HFE and Tf do not prevent TfR-TfR2 association, suggesting TfR2 binds to TfR somewhere other than the common HFE and Tf binding site on TfR. Another possibility is that TfR and TfR2 formed mixed heterodimers. This suggestion is supported by the observation of the mixed covalent heterodimers and by the fact that many of the residues at the crystallographically determined TfR dimerization interface are conserved in TfR2 (Table 1).

How the interaction between these 2 transferrin receptors affects their function remains to be studied. The subunits of TfR and TfR2 do not interact equally well with each other. TfR and TfR2 preferentially form homodimers, and only a small percentage form heterodimers. From crystallographic studies, HFE interacts with TfR via a hydrophobic region on the ectodomain of the receptor, competing with Tf for binding to TfR.[9,23] Because TfR2 is not regulated in response to changes in cellular iron levels and does not interact with HFE, the TfR-TfR2 interaction could function as a potential mechanism to regulate iron uptake in unique ways, perhaps by utilizing signaling pathways. If this were the case, then the heterodimers could be potentially important in regulating signaling. Additional studies are required to fully understand the role of TfR2 and the relationship of TfR2 with TfR.

Acknowledgments

We would like to thank Dr Tim McGraw, Cornell Medical College for the TRVb and the TRVb1 cell lines; Drs Kawabata and Koeffler for the human TfR2 plasmid; Anthony P. West for the TfR2 used in the immunizations; Thomas O'Hare and Greg Wiens for critical comments on the manuscript; and Aeisha D. Robb and Marianne Wessling-Resnick for insightful discussions.

References

1. Aisen P, Enns C, Wessling-Resnick M. Chemistry and biology of eukaryotic iron metabolism. Int J Biochem Cell Biol. 2001;33:940-959.
2. Levy JE, Jin O, Fujiwara Y, Kuo F, Andrews NC. Transferrin receptor is necessary for development of erythrocytes and the nervous system. Nat Genet. 1999;21:396-399.
3. Camaschella C, Roetto A, Cali A, et al. The gene TFR2 is mutated in a new type of haemochromatosis mapping to 7q22. Nat Genet. 2000;25:14-15.
4. Kawabata H, Germain RS, Vuong PT, Nakamaki T, Said JW, Koeffler HP. Transferrin receptor 2-alpha supports cell growth both in iron-chelated cultured cells and in vivo. J Biol Chem. 2000;275:16618-16625.
5. Kawabata H, Yang R, Hirama T, et al. Molecular cloning of transferrin receptor 2: a new member of the transferrin receptor-like family. J Biol Chem. 1999;274:20826-20832.
6. Fleming RE, Migas MC, Holden CC, et al. Transferrin receptor 2: continued expression in mouse liver in the face of iron overload and in hereditary hemochromatosis. Proc Natl Acad Sci U S A. 2000;97:2214-2219.
7. Parkkila S, Waheed A, Britton RS, et al. Association of the transferrin receptor in human placenta with HFE, the protein defective in hereditary hemochromatosis. Proc Natl Acad Sci U S A. 1997;94:13198-13202.
8. Feder JN, Penny DM, Irrinki A, et al. The hemochromatosis gene product complexes with the transferrin receptor and lowers its affinity for ligand binding. Proc Natl Acad Sci U S A. 1998;95:1472-1477.
9. Lebron JA, Bennett MJ, Vaughn DE, et al. Crystal structure of the hemochromatosis protein HFE and characterization of its interaction with transferrin receptor. Cell. 1998;93:111-123.
10. Lebron JA, Bjorkman PJ. The transferrin receptor binding site on HFE, the class I MHC-related protein mutated in hereditary hemochromatosis. J Mol Biol. 1999;289:1109-1118.
11. West AP Jr, Giannetti AM, Herr AB, et al. Mutational analysis of the transferrin receptor reveals overlapping HFE and transferrin binding sites. J Mol Biol. 2001;313:385-397.
12. West AP Jr, Bennett MJ, Sellers VM, Andrews NC, Enns CA, Bjorkman PJ. Comparison of the interactions of transferrin receptor and transferrin receptor 2 with transferrin and the hereditary hemochromatosis protein HFE. J Biol Chem. 2000;275:38135-38138.
13. Gatter KC, Brown G, Trowbridge IS, Woolston R-E, Mason DY. Transferrin receptors in human tissues: their distribution and possible clinical relevance. J Clin Path. 1983:539-545.
14. Kawabata H, Germain RS, Ikezoe T, et al. Regulation of expression of murine transferrin receptor 2. Blood. 2001;98:1949-1954.
15. Sanchez LM, Lopez OC, Bjorkman PJ. Biochemical characterization and crystalization of human Zn-alpha2-glycoprotein, a soluble class I major histocompatibility complex homolog. Proc Natl Acad Sci U S A. 1997;94:4626-4630
16. Rutledge EA, Green FA, Enns CA. Generation of the soluble transferrin receptor requires cycling through an endosomal compartment. J Biol Chem. 1994;269:31864-31868.
17. Laemmli UK. Cleavage of structural proteins during the assembly of the head of bacteriophage T4. Nature. 1970;227:680-685.
18. Reckhow CL, Enns CA. Characterization of the transferrin receptor in tunicamycin-treated A431 cells. J Biol Chem. 1988;263:7297-7301.
19. McGraw T, Greenfield L, Maxfield FR. Functional expression of the human transferrin receptor cDNA in Chinese hamster ovary cells deficient in endogenous transferrin receptor. J Cell Biol. 1987;105:207-214.
20. Enns CA, Larrick JW, Suomalainen H, Schroder J, Sussman HH. Co-migration and internalization of transferrin and its receptor on K562 cells. J Cell Biol. 1983;97:579-585.
21. Yamashiro DJ, Tycko B, Fluss SR, Maxfield FR. Segregation of transferrin to a mildly acidic (pH 6.5) para-Golgi compartment in the recycling pathway. Cell. 1984;37:789-800.
22. Bennett MJ, Lebron JA, Bjorkman PJ. Crystal structure of the hereditary haemochromatosis protein HFE complexed with transferrin receptor. Nature. 2000;403:46-53.
23. Lebron JA, West AP Jr, Bjorkman PJ. The hemochromatosis protein HFE competes with transferrin for binding to the transferrin receptor. J Mol Biol. 1999;294:239-245.
24. Kozyraki R, Fyfe J, Verroust PJ, et al. Megalin-dependent cubilin-mediated endocytosis is a major pathway for the apical uptake of transferrin in polarized epithelia. Proc Natl Acad Sci U S A. 2001;98:12491-12496.
25. Brunger AT, Adams PD, Clore GM, et al. Crystallography & NMR system: a new software suite for macromolecular structure determination. Acta Crystallogr D Biol Crystallogr. 1998;54 (pt 5):905-921.
26. Lawrence CM, Ray S, Babyonyshev M, Galluser R, Borhani DW, Harrison SC. Crystal structure of the ectodomain of human transferrin receptor. Science. 1999;286:779-782.